

Advances in green synthesis for drug discovery

Edited by

Florent Allais, Simone Brogi, Veroniki P. Vidali and
Guillermo Raul Castro

Published in

Frontiers in Chemistry



FRONTIERS EBOOK COPYRIGHT STATEMENT

The copyright in the text of individual articles in this ebook is the property of their respective authors or their respective institutions or funders. The copyright in graphics and images within each article may be subject to copyright of other parties. In both cases this is subject to a license granted to Frontiers.

The compilation of articles constituting this ebook is the property of Frontiers.

Each article within this ebook, and the ebook itself, are published under the most recent version of the Creative Commons CC-BY licence. The version current at the date of publication of this ebook is CC-BY 4.0. If the CC-BY licence is updated, the licence granted by Frontiers is automatically updated to the new version.

When exercising any right under the CC-BY licence, Frontiers must be attributed as the original publisher of the article or ebook, as applicable.

Authors have the responsibility of ensuring that any graphics or other materials which are the property of others may be included in the CC-BY licence, but this should be checked before relying on the CC-BY licence to reproduce those materials. Any copyright notices relating to those materials must be complied with.

Copyright and source acknowledgement notices may not be removed and must be displayed in any copy, derivative work or partial copy which includes the elements in question.

All copyright, and all rights therein, are protected by national and international copyright laws. The above represents a summary only. For further information please read Frontiers' Conditions for Website Use and Copyright Statement, and the applicable CC-BY licence.

ISSN 1664-8714
ISBN 978-2-83251-934-9
DOI 10.3389/978-2-83251-934-9

About Frontiers

Frontiers is more than just an open access publisher of scholarly articles: it is a pioneering approach to the world of academia, radically improving the way scholarly research is managed. The grand vision of Frontiers is a world where all people have an equal opportunity to seek, share and generate knowledge. Frontiers provides immediate and permanent online open access to all its publications, but this alone is not enough to realize our grand goals.

Frontiers journal series

The Frontiers journal series is a multi-tier and interdisciplinary set of open-access, online journals, promising a paradigm shift from the current review, selection and dissemination processes in academic publishing. All Frontiers journals are driven by researchers for researchers; therefore, they constitute a service to the scholarly community. At the same time, the *Frontiers journal series* operates on a revolutionary invention, the tiered publishing system, initially addressing specific communities of scholars, and gradually climbing up to broader public understanding, thus serving the interests of the lay society, too.

Dedication to quality

Each Frontiers article is a landmark of the highest quality, thanks to genuinely collaborative interactions between authors and review editors, who include some of the world's best academicians. Research must be certified by peers before entering a stream of knowledge that may eventually reach the public - and shape society; therefore, Frontiers only applies the most rigorous and unbiased reviews. Frontiers revolutionizes research publishing by freely delivering the most outstanding research, evaluated with no bias from both the academic and social point of view. By applying the most advanced information technologies, Frontiers is catapulting scholarly publishing into a new generation.

What are Frontiers Research Topics?

Frontiers Research Topics are very popular trademarks of the *Frontiers journals series*: they are collections of at least ten articles, all centered on a particular subject. With their unique mix of varied contributions from Original Research to Review Articles, Frontiers Research Topics unify the most influential researchers, the latest key findings and historical advances in a hot research area.

Find out more on how to host your own Frontiers Research Topic or contribute to one as an author by contacting the Frontiers editorial office: frontiersin.org/about/contact

Advances in green synthesis for drug discovery

Topic editors

Florent Allais — AgroParisTech Institut des Sciences et Industries du Vivant et de L'environnement, France

Simone Brogi — University of Pisa, Italy

Veroniki P. Vidali — Institute of Nanoscience and Nanotechnology, National Centre of Scientific Research Demokritos, Greece

Guillermo Raul Castro — National Scientific and Technical Research Council (CONICET), Argentina

Citation

Allais, F., Brogi, S., Vidali, V. P., Castro, G. R., eds. (2023). *Advances in green synthesis for drug discovery*. Lausanne: Frontiers Media SA.
doi: 10.3389/978-2-83251-934-9

Table of contents

- 05 **Editorial: Advances in green synthesis for drug discovery**
Florent Allais, Simone Brogi, Guillermo Raul Castro and Veroniki P. Vidali
- 09 **Synthesis of *N*-Heteroarenemethyl Esters via C–C Bond Cleavage of Acyl Cyanides Under Transition Metal-Free Conditions**
Miao Lai, Fangyao Su, Jingyi Hu, Mengzhuo Wang, Mingqin Zhao and Ganlin Zhang
- 17 **Facile and Sustainable Synthesis of Commendamide and its Analogues**
Rosaria Villano, Francesco Tinto and Vincenzo Di Marzo
- 24 **Pd@Py₂PZ@MSN as a Novel and Efficient Catalyst for C–C Bond Formation Reactions**
Mohammad Hosein Sayahi, Mansoureh Toosibashi, Mehdi Bahmaei, Hosein Lijan, Leila Ma'Mani, Mohammad Mahdavi and Saeed Bahadorikhalili
- 33 **A Novel Antimalarial Metabolite in Erythrocyte From the Hydroxylation of Dihydroartemisinin by *Cunninghamella elegans***
Yue Bai, Yifan Zhao, Xinna Gao, Dong Zhang, Yue Ma, Lan Yang and Peng Sun
- 48 **Copper-Promoted Hiyama Cross-Coupling of Arylsilanes With Thiuram Reagents: A Facile Synthesis of Aryl Dithiocarbamates**
Yiying Wang, Hongtao Shen, Jianhua Qiu, Mengqi Chen, Weimin Song, Mingqin Zhao, Longfei Wang, Feng Bai, Hongxia Wang and Zhiyong Wu
- 59 **Pyrene Functionalized Highly Reduced Graphene Oxide-palladium Nanocomposite: A Novel Catalyst for the Mizoroki-Heck Reaction in Water**
Mujeeb Khan, Muhammad Ashraf, Mohammed Rafi Shaik, Syed Farooq Adil, Mohammad Shahidul Islam, Mufsir Kuniyil, Merajuddin Khan, Mohammad Rafe Hatshan, Riyadh H. Alshammari, Mohammed Rafiq H. Siddiqui and Muhammad Nawaz Tahir
- 72 **Levoglucosenone: Bio-Based Platform for Drug Discovery**
Jason E. Camp and Ben W. Greatrex
- 81 **Enzymatic Active Release of Violacein Present in Nanostructured Lipid Carrier by Lipase Encapsulated in 3D-Bioprinted Chitosan-Hydroxypropyl Methylcellulose Matrix With Anticancer Activity**
Ignacio Rivero Berti, Boris E. Rodenak-Kladniew, Sergio F. Katz, Eva Carolina Arrua, Vera A. Alvarez, Nelson Duran and Guillermo R. Castro

- 94 **Synthesis, bioactivity, and molecular docking of novel arylpiperazine derivatives as potential AR antagonists**
Yueheng Qi, Hong Chen, Shijin Chen, Jianliang Shen and Jingguo Li
- 106 **Advances in Research at Synthesis Process Optimization and Quality Standard Improvement of *O*-desmethylvenlafaxine Succinate**
Shiwei Yang, Shiyun Chen, Cheng Wang, Shibo Zhang, Shuaifei Li, Xinsong Yuan, Fuyun Peng and Yong He
- 117 **The green chemistry of chalcones: Valuable sources of privileged core structures for drug discovery**
Ludovica Marotta, Sara Rossi, Roberta Ibba, Simone Brogi, Vincenzo Calderone, Stefania Butini, Giuseppe Campiani and Sandra Gemma



OPEN ACCESS

EDITED AND REVIEWED BY
James Clark,
University of York, United Kingdom

*CORRESPONDENCE

Florent Allais,
✉ florent.allais@agroparistech.fr
Simone Brogi,
✉ simone.brogi@unipi.it
Guillermo Raul Castro,
✉ grcastro@gmail.com
Veroniki P. Vidali,
✉ v.vidali@inn.demokritos.gr

SPECIALTY SECTION

This article was submitted to Green and Sustainable Chemistry, a section of the journal Frontiers in Chemistry

RECEIVED 15 February 2023

ACCEPTED 23 February 2023

PUBLISHED 02 March 2023

CITATION

Allais F, Brogi S, Castro GR and Vidali VP (2023), Editorial: Advances in green synthesis for drug discovery. *Front. Chem.* 11:1166887. doi: 10.3389/fchem.2023.1166887

COPYRIGHT

© 2023 Allais, Brogi, Castro and Vidali. This is an open-access article distributed under the terms of the [Creative Commons Attribution License \(CC BY\)](#). The use, distribution or reproduction in other forums is permitted, provided the original author(s) and the copyright owner(s) are credited and that the original publication in this journal is cited, in accordance with accepted academic practice. No use, distribution or reproduction is permitted which does not comply with these terms.

Editorial: Advances in green synthesis for drug discovery

Florent Allais^{1*}, Simone Brogi^{2*}, Guillermo Raul Castro^{3,4*} and Veroniki P. Vidali^{5*}

¹URD Agro-Biotechnologies Industrielles (ABI), CEBB, AgroParisTech, Pomacle, France, ²Department of Pharmacy, University of Pisa, Pisa, Italy, ³Nanomedicine Research Unit (Nanomed), Center for Natural and Human Sciences, Federal University of ABC (UFABC), Santo André, Brazil, ⁴Max Planck Laboratory for Structural Biology, Chemistry and Molecular Biophysics of Rosario (MPLbioR UNR-MPLbpC), Partner Laboratory of the Max Planck Institute for Biophysical Chemistry (MPLbpC MPG), Universidad Nacional de Rosario—CONICET, Rosario, Argentina, ⁵Institute of Nanoscience and Nanotechnology, National Centre for Scientific Research “Demokritos”, Athens, Greece

KEYWORDS

green chemistry, drug discovery, synthetic approaches, green solvents, green reagents, enzymes for the synthesis of bioactive compounds

Editorial on the Research Topic

Advances in green synthesis for drug discovery

In July 2021 we announced a Frontiers Research Topic, hosted by Frontiers in Chemistry, entitled *Advances in green synthesis for drug discovery*, as a part of the Green and Sustainable Chemistry section of the journal. The topic related to the green synthesis methods aimed to highlight novel environmentally safe approaches for synthesizing novel chemical entities with importance in pharmaceutical and pharmacological fields. Due to the growing population and damage from industrial pharmaceutical manufacture, it is well proved that the development of new and improved pharmaceuticals comes with a substantial environmental cost. As a result, one of the most popular study fields at every stage of the drug discovery process is the creation of environmentally friendly technologies. Even while there is opposition to changing the established procedures, the financial benefits that eco-friendly practices provide might spur development in this direction. This means that research in this field still has a lot to offer as the demand for ecologically friendly approaches rises. Green chemistry is a useful instrument that is becoming more significant since drug development raises global living standards. Therefore, this Research Topic focuses on all chemical aspects of the development of bioactive molecules based on green chemistry strategies and represents a practical manual for scientists that work on this area. Due to the factors mentioned above, this Research Topic caught the interest of researchers, receiving a significant number of submissions, with nine original research papers and two reviews published.

Considering the original research articles, [Lai et al.](#) reported a convenient method for the synthesis of *N*-heteroaryl esters using *N*-heteroaryl methanols and acyl cyanides through the cleavage of the C–C bond, excluding the use of any transition metal. In fact, the usage of Na₂CO₃/15-crown-5 couple allowed preparing different *N*-heteroaryl esters, with great efficiency. Notably, *N*-heteroaryl esters, such as furans, pyridines, pyrazines, quinolines, and thiophenes, constitute vital structures in pharmaceuticals, dyes, flavors, or natural products. The protocol, described in this work, is operationally

straightforward and environmentally friendly, only with the production of cyanides as byproducts.

In a fascinating paper, [Sayahi et al.](#) exploited the Pd@Py₂PZ@MSN as a new and effective catalyst to form C-C bond. In particular, in the described procedure, the authors immobilized palladium onto dipyrro (3,2-*a*:2',3'-*c*) phenazine (Py₂PZ)-modified mesoporous silica nanoparticles (MSNs), led to the generation of a novel catalyst. A simple procedure was used to create the Py₂PZ ligand from the reaction of the raw materials 1,10-phenanthroline-5,6-dione and 3,4-diaminobenzoic acid. The resulting compound was employed for functionalizing MSNs, modifying their surface chemistry so that the palladium could be immobilized. Accordingly, the palladium-immobilized Py₂PZ-modified MSNs (Pd@Py₂PZ@MSNs) were synthesized and characterized using different methods, and their activity and efficiency were studied in C-C bond formation reactions. Particularly, the results were favorable in aqueous medium, and significant yields of desired compounds were achieved. After ten consecutive runs, the catalyst also displayed outstanding reusability and no discernible loss of activity.

[Bai et al.](#) used a biosynthetic method for generating novel antimalarial metabolites into the erythrocytes by hydroxylation of the well-known drug dihydroartemisinin (DHA) performed by the organism *Cunninghamella elegans* CICC-40250. The analysis of the resultant compounds and comparison with DHA metabolites in erythrocytes were conducted. The authors using UPLC-MS detected nine DHA derivatives (**M1-M9**) obtained by means of microbial transformation, and some of them such as 7-hydroxydihydroartemisinin (**M1**), 1-deoxydihydroartemisinin (**M8**), and 1-deoxyartemisinin (**M9**) were extracted. These substances were also present in erythrocytes. In order to describe and characterize the substance **M1**, the authors employed X-ray single-crystal diffraction. Furthermore, **M1** showed an interesting *in vitro* antimalarial activity against the *Plasmodium* strain Pf3D7 (IC₅₀ = 133 nM). Remarkably, the presented work represents the first effort to isolate and characterize the DHA metabolites in erythrocytes through microbial transformation. Accordingly, using environmentally friendly microbial transformation, it is now possible to produce antimalarial drugs as a result of the discovery and synthesis of these compounds.

In another interesting research article, [Villano et al.](#) described a simple and adaptable methodology for synthesizing the gut microbiota-derived bioactive metabolite, commendamide (*N*-(3-hydroxypalmitoyl)-glycine) and its derivatives. This substance shares structural similarities with long-chain *N*-acyl-amino acids from the endocannabinoidome, a complicated lipid signaling system that plays significant functions in mammals by, among other things, activating G-protein-coupled receptors (GPCRs) (GPCR G2A/132). Easily available reagents, simple workups, non-halogenated solvents, and small amounts of organic solvents were used to synthesize commendamide in an environmentally friendly and economically feasible manner. Notably, the usage of column chromatography for purifying synthetic intermediate derivatives was moreover frequently avoided due to the high yields seen in several reaction stages. The same synthetic route was also effectively employed for synthesizing deuterated commendamide and an additional

secondary commendamide-like metabolite, thus demonstrating the usefulness of the novel synthetic strategy described in the mentioned paper.

[Yang et al.](#) described a synthetic protocol to efficiently produce *O*-desmethylvenlafaxine (ODV), the main active metabolite of venlafaxine, a serotonin-norepinephrine reuptake inhibitor (SNRI), which has been marketed for treating mild/severe depression, anxiety, and many different mental diseases, and *O*-desmethylvenlafaxine succinate monohydrate (DVS) in a significant yield and high purity. The five-step synthetic approach was developed using, as the starting material, *p*-hydroxybenzene acetonitrile, followed by condensation of cyclohexanone, deprotection of the phenolic hydroxyl group, cyano reduction, dimethylation, and production of succinic acid salts. The route involved high-yielding steps with low genotoxic impurities (GIs), the use of cheap reagents and solvents, and cost-effective purification procedures. ODV was prepared with 99.92% purity, and DVS was obtained in 71.09% overall yield. According to XRD powder diffraction, the crystalline form of DVS exhibited distinctive peaks at 5, 10, 21, and 26 min. Remarkably, when compared to traditional synthesis methods, the suggested strategy demonstrated an innovative, environmentally friendly method that ensured a great total yield with minimal environmental impact and remarkable residual standards for GIs, improving the safety of the drug.

According to [Wang et al.](#), copper fluoride facilitates a simple Hiyama cross-coupling reaction between arylsilanes and thiuram derivatives (tetraalkylthiuram disulfides (TATD) or tetraalkylthiuram monosulfide (TMTM)). This synthetic procedure is a useful option to generate *S*-aryl dithiocarbamates in good yields, showing limited toxic and easily accessible substrates, low-cost promoter, and straightforward performance. The method on the cross-coupling of arylsilanes with TATD or TMTM enhanced by copper allowed for the production of the significant *S*-aryl dithiocarbamates in yields ranging from moderate to good. This simple method allowed for practical and friendly reaction conditions, greatly enhancing functional group compatibility, increasing the range of substrates, and stressing the synthetic use of complicated compounds. The suggested method can provide a strategy to expedite synthesis of *S*-aryl dithiocarbamates from affordable and stable substrates as well as a fresh illustration of how to use Hiyama cross-coupling to synthesize pharmacologically intriguing compounds.

The potential application of a new catalyst to carry out the reaction of Mizoroki-Heck in aqueous medium was discussed by [Khan et al.](#) They specifically applied the aforementioned method to functionalize pyrene derivatives. Considering that it is difficult to successfully carry out Mizoroki-Heck cross-coupling reactions in water using effective heterogeneous catalysts to produce C-C bonds, Khan and coworkers were able to catalyze, in water, Mizoroki-Heck cross-coupling reactions using a highly reduced graphene oxide (HRG) immobilized palladium nanoparticle (Pd-NPs)-based catalyst (HRG-Py-Pd). Amino pyrene was employed during the catalyst's preparation as a functionalized ligand that provided appropriate binding sites for the efficient and uniform nucleation of Pd-NPs on the surface of HRG. As a result, the catalyst's physical stability and water dispersibility were considerably enhanced. Accordingly, the Mizoroki-Heck cross-coupling reactions of several aryl halides with acrylic acid in a water solution were

used to examine the catalytic capabilities of HRG-Py-Pd. Likewise, HRG-Py-catalytic Pd's effectiveness was compared to that of its non-functionalized counterparts, HRG-Pd and pure Pd-NPs. The coupling reaction of 4-bromoanisole and acrylic acid in a water solution was accomplished employing the HRG-Py-Pd nanocatalyst in a relatively small time (3 h), using a limited amount of the catalyst (3 mg). In contrast, pure Pd-NPs provided lesser conversion (92%) considering the identical reaction, which necessitated a lengthy period of time to react and a significant quantity of catalyst (5.3 mg). When 3 mg of Pd-NPs were utilized that was adequate to induce a 99% conversion for HRG-Py-Pd, the conversion was further reduced to barely 40%. HRG-Pd, however, was unsuccessful and failed to produce any conversion, even when a large amount of catalyst was used, and the reaction period was prolonged. The accumulation of Pd-NPs, which decreased the catalyst's capacity to disperse in water, is what prevents the HRG-Pd from promoting coupling processes. Because of the smart functionalization, HRG-Py-Pd has high aquatic stability, making it possible to undertake various organic reactions in water that would not have been conceivable otherwise.

Rivero Berti et al. reported the production, purification, and encapsulation of Violacein in a nanostructured lipid carrier (NLC). Considering that Violacein, a purple water-insoluble pigment produced by *Chromobacterium violaceum* and other microbes, showed an interesting pharmacological profile, also including anticancer action, the proposed approach is of extreme utility for the delivery of this water-insoluble compound. The NLC is constituted by the solid lipid myristyl myristate (a capric- and caprylic-acid-based oily lipid combination), and the P188, a surfactant poloxamer. To generate an active release system, inactive lipase from *Rhizomucor miehei* was added to NLC-Violacein. Finally, the printing Violacein encapsulation efficiency exceeded 90%. At pH = 7.4, the mesh containing NLC-lipase demonstrated a kinetic release of the biodye that was 20% faster than that without the enzyme. At pH = 5.0, when the lipase is not active, both Violacein kinetic releases showed patterns that were comparable. In addition to the biologically synergistic actions of Violacein and lipase reported, cytotoxic experiments employing the cancer cells A549 and HCT-116 demonstrated strong antitumor action of the developed complex.

Qi et al. reported a straightforward synthesis of novel androgen receptor (AR) antagonists potentially useful in prostate cancer. The use of AR-targeted therapeutics can block androgen and slow the growth of cancer cells, but they could also lead to severe resistance issues. In order to develop new AR antagonists, 22 different kinds of arylpiperazine derivatives were developed. Among these compounds, some not only exhibited strong antagonistic activity (>55% inhibition) and binding affinities ($IC_{50} < 3 \mu M$) to AR but also exhibited a significant inhibitory activity toward the LNCaP cell line than the PC-3 cell line. Interestingly, compound 21 showed the best antagonistic potency (76.2% inhibition) and binding affinity to AR ($IC_{50} = 0.65 \mu M$). The computational investigation highlighted the possible binding mode of these derivatives within the AR binding site. Overall, the findings offered experimental strategies to develop new arylpiperazine containing-compounds that are effective AR antagonists.

Regarding the review articles, two papers have been published in the Research Topic. The first work was focused on the green chemistry of chalcones, a useful source of privileged core

structures for drug discovery, while the second reports the attempts to obtain levoglucosone (LGO) through a bio-based platform with implications in drug discovery.

Marotta et al. focused their review of the literature on the sustainable usage of sources, which is crucial in many industrial sectors such as the pharmaceutical industry. However, the issue of sustainability must be taken into account during the entire process of the drug discovery trajectory, not just during the production phase. The efficiency and speed of a more sustainable drug discovery pipeline are being boosted by the ongoing advancements in the disciplines of green chemistry and the application of artificial intelligence (AI). In this context, the authors reviewed the most recent environmentally friendly and sustainable synthetic methods for creating and derivatizing chalcones, a crucial class of privileged structures and building blocks for the generation of novel molecules with interesting pharmacological profiles. In order to filter the results using the term "green chemistry," the word "chalcone" was used as a keyword in the SciFinder database for the literature search (2017–2022), and the keywords "chalcone" and "green" were used in the Reaxys database. Particularly, in the past few years, chalcones have been employed to develop different biologically active heterocyclic scaffolds, enabling more sustainable access to a wider range of scaffolds. The most appealing procedures for derivatizing and preparing chalcone derivatives are flow chemistry and biocatalysis, which have considerable potential. Another crucial element is the use of AI to prioritize the synthesis of particular molecules. Based on the cases reported in this review and the advances in computer-aided techniques expected in the next decade, the authors anticipate that *in silico* methods will be employed to synthesize focused chemical libraries, as in the cases of chalcone-based compounds presented. This will hasten the drug discovery process, increase environmental awareness, and decrease the requirement for experimental testing.

The bio-privileged LGO compound, which can be manufactured on a massive scale from waste biomass, was studied by Camp and Greatrex. This chiral building block was employed to synthesize previously challenging building blocks including enantiopure butenolides, dihydropyrans, modified cyclopropanes, deoxy-sugars, and ribonolactones by well-known chemical methods. LGO is a great starting point for synthesizing biologically active molecules, such as those with antiinflammatory, anticancer, and antimicrobial properties. As a result, it is anticipated that the creation of reactions for the LGO ring-system and its widespread availability would open up more chances to access both established and novel bioactive chemical entities. This review is focused on the conversion of LGO to molecules with pharmacological potential, and provides upcoming research ways linked to the mentioned compound.

In conclusion, we would like to express our gratitude to all of the authors and co-authors for their significant contributions to this Research Topic in Frontiers in Chemistry, to all of the reviewers for their insightful work in assessing the presented papers, and to the editorial staff of Frontiers for the support. The success of this Research Topic was greatly reliant on all of these collective efforts, seen as a whole. We anticipate that this subject will aid green synthesis in drug development progress, and we hope that it will serve as an educational and inspirational tool for researchers and students. The following URL provides free access to the

mentioned Research Topic <https://www.frontiersin.org/research-topics/24085/advances-in-green-synthesis-for-drug-discovery>.

Author contributions

All authors listed have made a substantial, direct, and intellectual contribution to the work, and approved it for publication.

Acknowledgments

The authors want to thank all the contributors to the Research Topic, reviewers, and the Editorial Office of Frontiers in Chemistry for the helpful advice during the management of the submitted manuscripts.

Conflict of interest

The authors declare that the research was conducted in the absence of any commercial or financial relationships that could be construed as a potential conflict of interest.

Publisher's note

All claims expressed in this article are solely those of the authors and do not necessarily represent those of their affiliated organizations, or those of the publisher, the editors and the reviewers. Any product that may be evaluated in this article, or claim that may be made by its manufacturer, is not guaranteed or endorsed by the publisher.



Synthesis of *N*-Heteroarenemethyl Esters via C–C Bond Cleavage of Acyl Cyanides Under Transition Metal-Free Conditions

Miao Lai[†], Fangyao Su[†], Jingyi Hu, Mengzhuo Wang, Mingqin Zhao* and Ganlin Zhang

Flavors and Fragrance Engineering and Technology Research Center of Henan Province, College of Tobacco Science, Henan Agricultural University, Zhengzhou, China

OPEN ACCESS

Edited by:

Florent Allais,
AgroParisTech Institut des Sciences et
Industries du Vivant et de
L'Environnement, France

Reviewed by:

Muhammet Uyanik,
Nagoya University, Japan
Michal Szostak,
The State University of New Jersey,
United States

*Correspondence:

Mingqin Zhao
zhaomingqin@126.com

[†]These authors have contributed
equally to this work

Specialty section:

This article was submitted to
Organic Chemistry,
a section of the journal
Frontiers in Chemistry

Received: 26 November 2021

Accepted: 15 December 2021

Published: 27 January 2022

Citation:

Lai M, Su F, Hu J, Wang M, Zhao M
and Zhang G (2022) Synthesis of *N*-
Heteroarenemethyl Esters via C–C
Bond Cleavage of Acyl Cyanides
Under Transition Metal-
Free Conditions.
Front. Chem. 9:822625.
doi: 10.3389/fchem.2021.822625

A practical method to synthesize *N*-heteroaryl esters from *N*-heteroaryl methanols with acyl cyanides via C–C bond cleavage without using any transition metal is demonstrated here. The use of Na₂CO₃/15-crown-5 couple enables access to a series of *N*-heteroaryl esters in high efficiency. This protocol is operationally simple and highly environmentally benign producing only cyanides as byproducts.

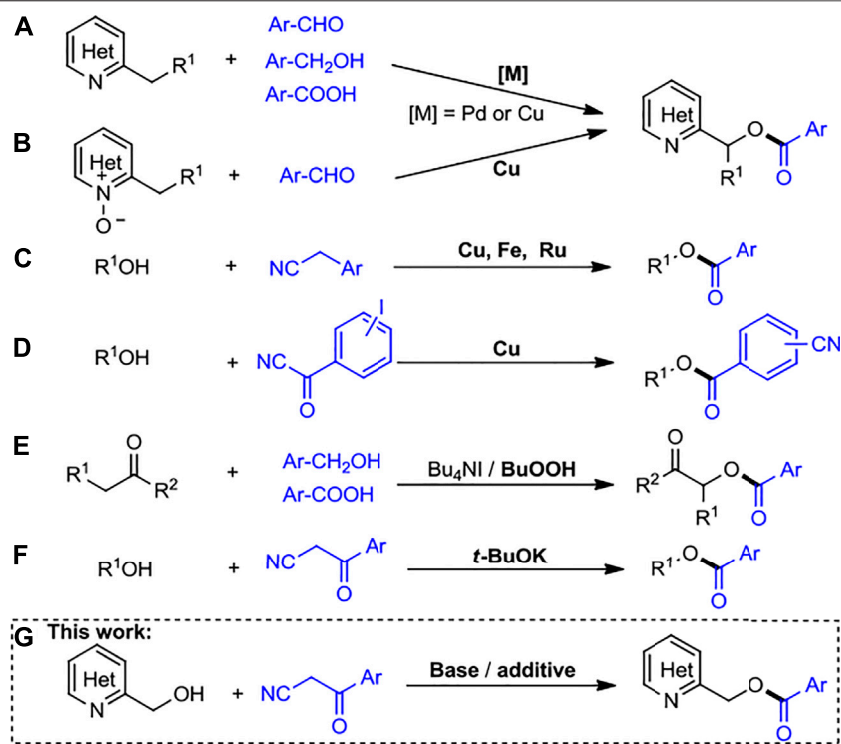
Keywords: *N*-heteroaryl esters, C–C bond cleavage, acyl cyanides, transition-metal free synthesis, *N*-heteroaryl methanols

INTRODUCTION

Heteroaryl esters and their derivatives could serve as interesting building blocks for the preparation of various functionalized products including bioactive natural products, pharmaceuticals, dyes, and flavors (Otera, 2010; Trotier Faurion et al., 2013; Armani et al., 2014; Liu B. et al., 2015; Xu et al., 2018; Bayout et al., 2020; Xu et al., 2022). Therefore, methodologies for the synthesis of these molecular architectures have experienced huge developments in recent years. The conventional syntheses include interesterification and oxidative carbonylation of ethers (Zhao et al., 2014; Lu et al., 2015), and the reactions of alcohols with methanol (Zhang and Wang, 2019), carboxylic acids (Teruaki et al., 2003; Saeed et al., 2008), aldehydes (Tang et al., 2014; Huang et al., 2016; Chun and Chung, 2017), ketones (Huang et al., 2014; Rammurthy et al., 2021), aliphatic amides (Hie et al., 2016; Bourne-Branchu et al., 2017), carbonates (Chen et al., 2014), and acid halides (Tamaddon et al., 2005; Akhlaghinia et al., 2010), respectively. In the last decade, direct activation and functionalization of the C–H bond has emerged as a powerful method in the field of organic synthesis and witnessed significant progress (McMurray et al., 2011; Huang et al., 2012; Wencel-Delord and Glorius, 2013; Chen et al., 2015; Liu C. et al., 2015; Dong et al., 2017). For example, successful benzylic C (sp³)-H acyloxylations of alkyl *N*-heteroarenes were achieved using simple aldehydes and acids via a copper or palladium catalysis (Scheme 1A) (Jiang et al., 2010; Chen et al., 2018; Cheng et al., 2019). Moreover, Soulé and coworkers achieved oxidative esterification of aldehydes with prefunctionalized 2-alkylheterocycle *N*-oxides via copper catalysis (Scheme 1B) (Wang et al., 2017).

In recent years, the process of carbon–carbon (C–C) bond cleavage of ketones under transition metal (Fe, Cu, or Ru) catalysis has provided various ester compounds (Yan et al., 2014; Huang et al., 2016; Arzumanyan, 2017).

Recently, a simple and direct aerobic oxidative esterification reaction of arylacetoneitriles with alcohols/phenols is achieved in the presence of a copper salt and molecular oxygen (Dong et al., 2021). On the other hand, Song and Plietker groups reported aerobic oxidative C–CN bond cleavage of arylacetoneitriles leading to various esters with catalysis of Fe and Ru, respectively (Scheme 1C)



SCHEME 1 | Strategies toward the synthesis of esterification products.

(Kong et al., 2016; Eisele et al., 2019). In general, ester compounds could be achieved using acylcyanides as acylating agents. Cu-catalyzed esterification using acyl cyanides with alcohols to yield the corresponding cyano-substituted esters is also reported (**Scheme 1D**) (Chen et al., 2020).

Furthermore, esterification reactions could proceed using photochemical strategies, in which reaction mechanisms involve mainly single electron transfer, energy transfer, or other radical procedures (Deng et al., 2021). A novel and metal-free method for the synthesis of α -ketoesters from β -ketonitriles and alcohols was reported, but under visible light irradiation conditions (Xu et al., 2018). Besides, the acyloxycarbonyl compounds could be obtained by TBAI-catalyzed acyloxylation of ketones (Uyanik et al., 2011; Guo et al., 2014), which the excess TBHP was required for the reaction process (**Scheme 1E**). Very recently, Subaramanian et al. reported *t*-BuOK catalyzed esterification using acyl cyanides with alcohols (**Scheme 1F**); however, their applicability was limited to *N*-heteroaryl methanols (Subaramanian et al., 2020). In addition, transition metal-free activation of amides by cleavage of C–N bond to obtain the aryl esters is well known (Li et al., 2018; Li and Szostak, 2020). Therefore, these reported esterification protocols involve the metal catalysts, lack of step efficiency, conditions of light irradiation, limited substrate scope of *N*-heterocyclic compounds, and need of oxidants. In our continuous effort in the construction of *N*-heteroaryl compounds (Lai et al., 2018; Zhai et al., 2018), we disclose herein an efficient and new protocol for the base-promoted

esterification of *N*-heteroaryl methanols via C–C bond cleavage of arylacetone nitriles acyl cyanides as acylating sources (**Scheme 1G**). The present protocol is simple to handle and does not involve any metal catalyst detrimental to environmental safety.

RESULT AND DISCUSSION

Our initial optimization using 2-pyrazinylmethanol **1a** and benzoylacetonitrile **2a** as the model substrates revealed that the reaction proceeded as anticipated with 1 equiv of *t*-BuOK in toluene according to the reported conditions (Roy et al., 2019; Subaramanian et al., 2020), affording the desired product **3a** in 10% yield (**Table 1**, entry 1). No product was detected in the absence of base (**Table 1**, entry 2), which suggests that it played a crucial role. Further screening of other bases indicated that Na_2CO_3 was obviously superior to the others, providing the desired product **3a** in 25% isolated yield (**Table 1**, entries 3–9 vs. entry 1). Interestingly, an improved yield (61%) was obtained when the reaction was conducted in the presence of 15-crown-5 (**Table 1**, entry 10). The role of crown ether in the reaction is increasing the solubility of base in solvent and known to be effective for trapping the potassium and sodium ions (Liotta et al., 1974; Lutz et al., 1988; Hay et al., 1993; Reuter et al., 1999). Subsequently, the evaluation of additives was conducted, and the results indicated that none of the screened additives (PPh_3 , 1,10-Phen, and TMEDA)

TABLE 1 | Optimization of reaction conditions^a.

Entry	Base	Additive	Solvent	T (°C)	Yields of 3a (%) ^b
1	<i>t</i> -BuOK	-	Toluene	140	10
2	-	-	Toluene	140	0
3	KOH	-	Toluene	140	11
4	K ₂ CO ₃	-	Toluene	140	12
5	KHMDS	-	Toluene	140	10
6	NaOH	-	Toluene	140	18
7	<i>t</i> -BuONa	-	Toluene	140	16
8	NaOAc	-	Toluene	140	15
9	Na ₂ CO ₃	-	Toluene	140	25
10	Na ₂ CO ₃	15-Crown-5	Toluene	140	61
11	Na ₂ CO ₃	PPh ₃	Toluene	140	32
12	Na ₂ CO ₃	1,10-Phen	Toluene	140	29
13	Na ₂ CO ₃	TMEDA	Toluene	140	30
14	Na ₂ CO ₃	15-Crown-5	1,4-Dioxane	140	40
15	Na ₂ CO ₃	15-Crown-5	DMF	140	Trace
16	Na ₂ CO ₃	15-Crown-5	DMSO	140	42
17	Na ₂ CO ₃	15-Crown-5	DCE	140	0
18	Na ₂ CO ₃	15-Crown-5	THF	140	41
19	Na ₂ CO ₃	15-Crown-5	Toluene	120	50
20	Na ₂ CO ₃	15-Crown-5	Toluene	150	62
21 ^c	Na ₂ CO ₃	15-Crown-5	Toluene	140	56
22^d	Na₂CO₃	15-Crown-5	Toluene	140	85
23 ^{d,e}	Na ₂ CO ₃	15-Crown-5	Toluene	140	83
24 ^{d,f}	Na ₂ CO ₃	15-Crown-5	Toluene	140	69
25 ^{d,g}	Na ₂ CO ₃	15-Crown-5	Toluene	140	81

^aNote. 2-Pyrazinylmethanol **1a** (0.2 mmol), Benzoylacetonitrile **2a** (0.2 mmol), base (1.0 eq), additive (1.0 eq), and toluene (1 ml) for 24 h, under N₂ atmosphere.

^bIsolated yields.

^c1a/2a ratio = 0.2/0.5.

^d1a/2a ratio = 0.5/0.2.

^eAdditive (1.5 eq) was used.

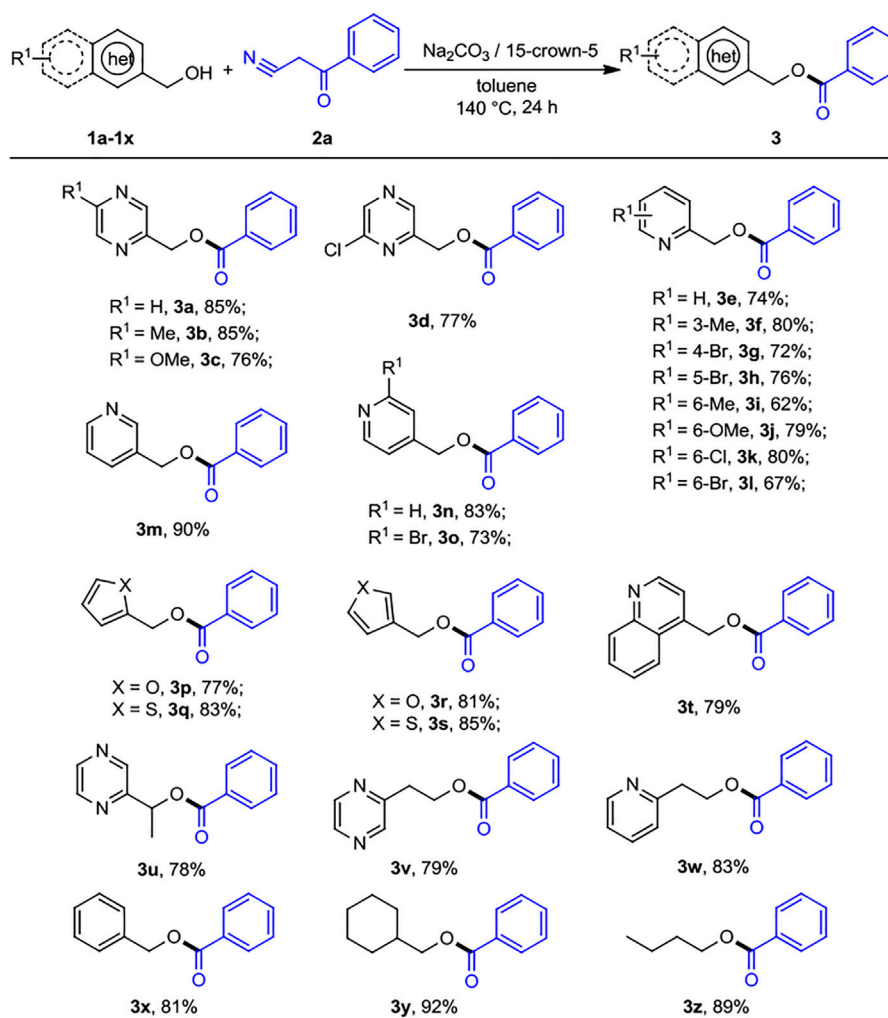
^fAdditive (0.5 eq) was used.

^g48 h.

benefited the outcome (29%–32%, **Table 1**, entries 11–13 vs. 10). Thus, 15-crown-5 was selected as the additive to assess the effect of solvents, including 1,4-dioxane, DMF, DMSO, DCE, and THF (**Table 1**, entries 14–18). All of the attempts did not show any improvement on the reaction yield compared with toluene (**Table 1**, entry 10). Then, we explored the other reaction parameters including the reaction temperature, the mol ratio of **1a** and **2a**, and the amount of additive. The yield was not much improved compared with the yield of 140°C (51%) when the reaction was conducted at 150°C (62%, **Table 1**, entry 20 vs. 10). Therefore, the reaction temperature remains unchanged. Gratifyingly, when the mole ratio of **1a** and **2a** was modified from 1:1 to 2.5:1, the reaction provided the best yield (85%) of **3a** (**Table 1**, entry 22 vs. entry 10). Then, the effect of the amount of additive and reaction time was examined; unfortunately, no better results were obtained (**Table 1**, entries 23–25). Finally, the optimal reaction conditions were identified as follows: The mixture of **1a**

(0.5 mmol), **2a** (0.2 mmol), Na₂CO₃ (0.2 mmol), and 15-crown-5 (0.2 mmol) was stirred in toluene at 140°C under N₂ atmosphere for 24 h.

With the optimized reaction conditions in hand, we next sought to generalize the protocol on a range of diverse substrates. As shown in **Scheme 2**, various commercially available *N*-heteroaryl methanols and benzoylacetonitrile were exposed to the standard reaction conditions, and the desired heteroarenemethyl benzoates were successfully afforded with good yields. Initially, pyrazinylmethanol was substituted by an electron-donating group such as Me– or MeO–, and we obtained the desired products with moderate to good yields (**3b**, 85%) and (**3c**, 76%), respectively, while, the electron-withdrawing substituent Cl– also gave the corresponding ester **3d** at a moderate yield of 77%. 2-pyridinylmethanols with 3-methyl, 6-methyl, 6-methoxy, 4-Br, 5-Br, 6-Cl, and 6-Br groups were converted to the corresponding products with lower yields (**3e–3l**, 62%–80% yields). It was worth mentioning that the yields were slightly

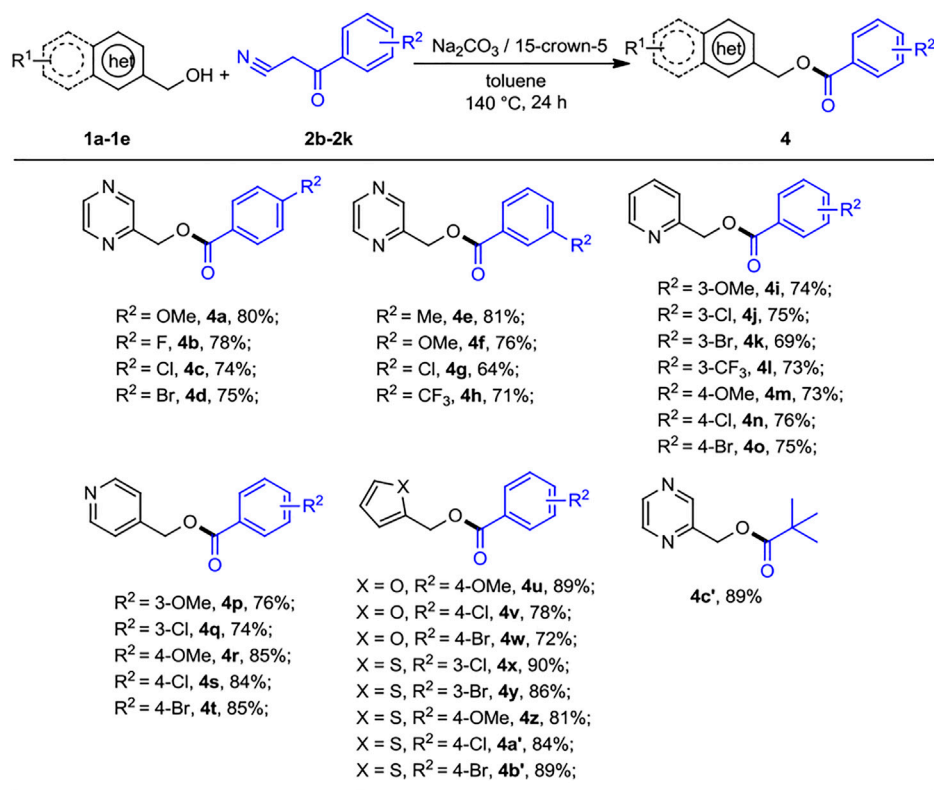


SCHEME 2 | Substrate scope of heteroaryl methanols for the acylation reactions. ^{a,b}Reaction conditions: ^aheteroaryl methanols 1 (0.5 mmol), benzoylacetonitrile 2 (0.2 mmol), Na_2CO_3 (0.2 mmol), 15-crown-5 (0.2 mmol), and toluene (1 ml) at 140°C for 24 h, under N_2 atmosphere. ^bIsolated yields.

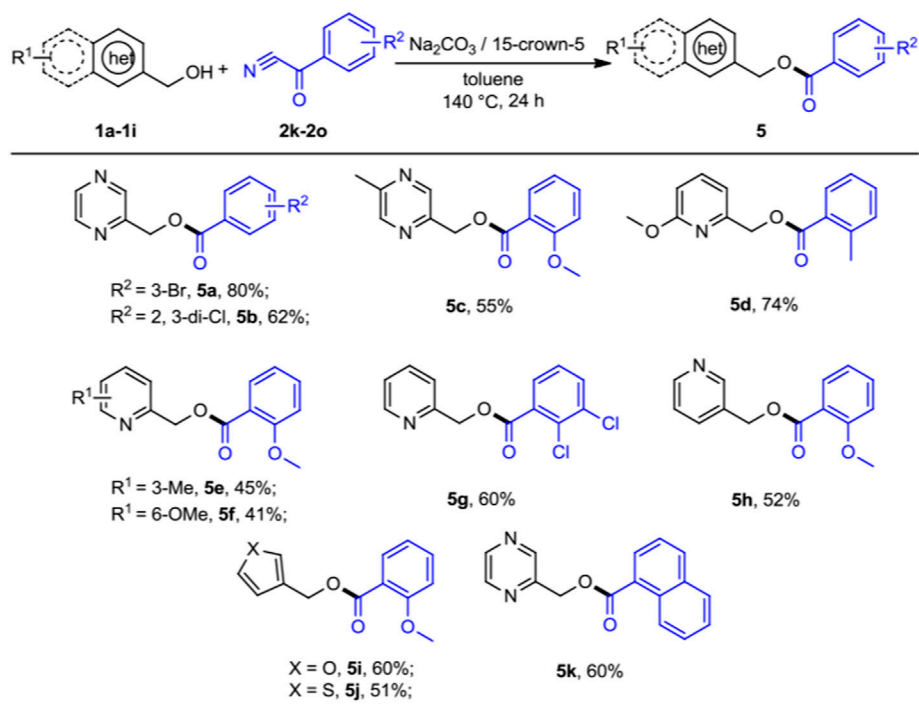
decreased by the presence of different substituents on the 2-pyridinylmethanols. However, 3- and 4-pyridinylmethanol exhibited good reactivity obtaining the esterification products **3m** and **3n** in 90% and 83% yield, respectively. 4-Pyridinylmethanol bearing electron-withdrawing substituent (2-Br) revealed the lower yield of desired product (**3o**, 73%). The reactions of benzoylacetonitrile with furanmethanols, thiophenemethanols, and 4-quinolylmethanol also smoothly afforded the corresponding products **3p–3t** in yields of 77%–85%. As we expected, both α -methyl-2-pyrazinemethanol, 2-pyrazinylethyl alcohol, and 2-pyridinylethyl alcohol worked well to give the corresponding products **3u–3w** in 78%–83% yield. Interestingly, simple alcohols such as benzyl and aliphatic (**1v–1y**) could be used as substrates under the present conditions, and the desired products (**3x–3z**) were obtained at the yields of 81%, 92%, and 88%, respectively. The results indicated that the simple

unhindered aliphatic alcohols show the excellent nucleophilic activity.

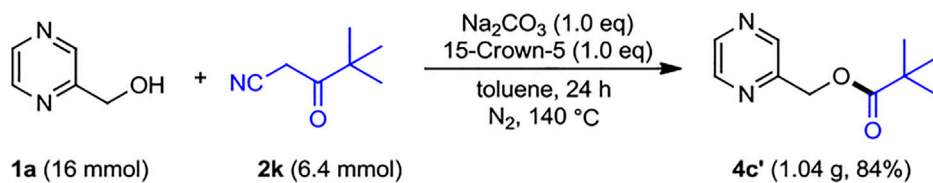
Next, the scope of the reaction was evaluated on various benzoylacetonitrile derivatives under the optimized reaction conditions, and the results are summarized in **Scheme 3**. Benzoylacetonitrile containing electron-donating groups methoxy (**2b**, **2g**) and methyl (**2f**) were successfully transformed to the corresponding esters to give the products (**4a**, **4e**, and **4f**) at good yields of 76%–81%. Slight lower yields were obtained when electron-withdrawing groups 4-F, 4-Cl, 4-Br, 3-Cl, and 3- CF_3 substituted benzoylacetonitriles with 2-pyrazinylmethanol were subjected to this transformation (**4b–4d**, **4g–4h**, 64%–78% yields). Interestingly, 2- and 4-pyridinylmethanol bearing the OMe group and halogen atom (Cl, Br, and CF_3) at the *para* or *meta* position are well tolerated, as the products of pyridin-2-ylmethyl and -4-ylmethyl substituted benzoates, **4i–4t** were obtained in 73%–85%



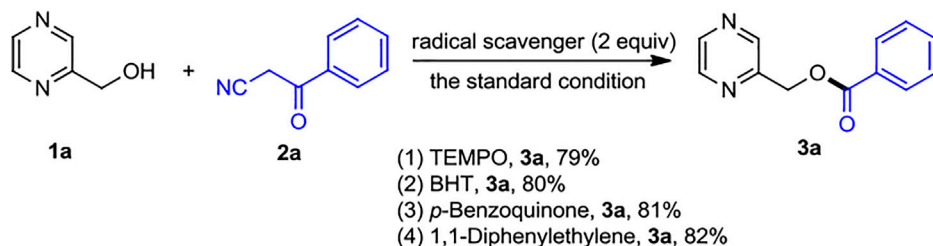
SCHEME 3 | Substrate scope of benzoylacetonitriles for the acylation reactions. ^{a,b}Reaction conditions: ^aheteroaryl methanols 1 (0.5 mmol), benzoylacetonitrile derivatives 2 (0.2 mmol), Na_2CO_3 (0.2 mmol), 15-crown-5 (0.2 mmol), and toluene (1 ml) at 140 °C for 24 h, under N_2 atmosphere. ^bIsolated yields.



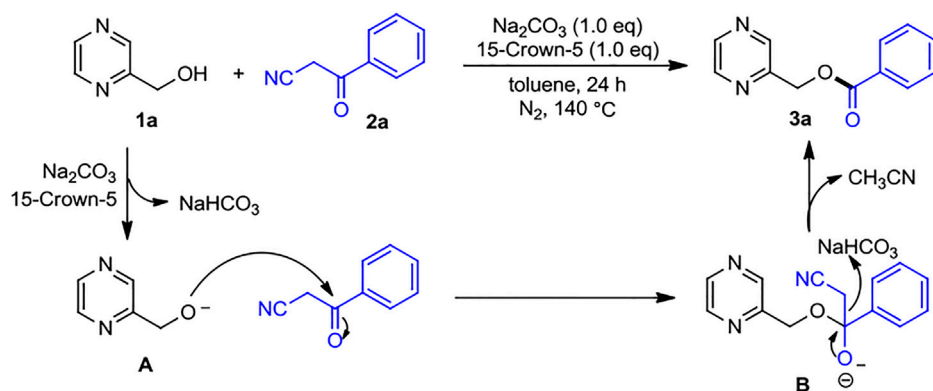
SCHEME 4 | Substrate scope of benzoyl cyanides for the acylation reactions. ^{a,b}Reaction conditions: ^aheteroaryl methanols 1 (0.5 mmol), benzoyl cyanides 2 (0.2 mmol), Na_2CO_3 (0.2 mmol), 15-crown-5 (0.2 mmol), and toluene (1 ml) at 140 °C for 24 h, under N_2 atmosphere. ^bIsolated yields.



SCHEME 5 | Gram-scale reaction of 1a and 2k.



SCHEME 6 | Mechanistic experiments.



SCHEME 7 | Plausible reaction mechanism.

yields. The reactions of benzoylacetonitriles substituted at the *para* or *meta* position by various groups (OMe, Cl, and Br) with 2-furanmethanol and 2-thiophenemethanol underwent a smooth reaction to provide the products **4u–4b'** in good to excellent yields. Moreover, pyvaolylacetonitrile displayed the good reactivity, as **4c'** was isolated in 89% yield.

Finally, we also briefly set out to evaluate the scope of aryl cyanides (Scheme 4). As expected, these reactions proceeded smoothly when 2-pyrazinylmethanol and pyridinylmethanols with benzoyl cyanides served as the substrates, leading the corresponding products **5a–5h** in moderate to good yields (41%–80%). 3-furanmethanol and 3-thiophenemethanol could undergo the expected acylation with 2-methoxy- α -oxo-benzeneacetonitrile (**2m**) in moderate yields (**5i–5j**, 51%–60%). We were pleased to observe that α -oxo-1-naphthaleneacetonitrile was readily reacted with **1a** in moderate yield (**5k**, 60%). It was satisfying to discover that the protocol was amenable for most benzoyl cyanides substrates, which

is different from the work of Subaramannian et al. involving the single-electron transfer (SET) in the catalytic transformation (Subaramanian et al., 2020). This was probably because the nature of reaction mechanism of these two methods is distinct.

The gram-scale reaction of **1a** (16 mmol, 1.761 g) and **2k** (6.4 mmol, 0.801 g) was carried out to demonstrate the practicability of this protocol, which could give the desired product **4c'** in 84% yield (Scheme 5). As shown in Scheme 6, radical trapping experiments were performed through the addition of TEMPO, BHT, *p*-benzoquinone, and 1,1-diphenylethylene to the reaction system in the standard conditions, and the formation of **3a** was not suppressed. These results inferred that this transformation did not occur *via* a radical mechanism.

A tentative mechanism was proposed and is shown in Scheme 7 on the basis of the results presented above and previous reports (Xie et al., 2014; Kong et al., 2016). The reaction initiated with Na_2CO_3 associated with 15-crown-5

induced deprotonation of 2-pyrazinylmethanol **1a** to form 2-pyrazinyl alkoxy anion **A**. Then anion **A** undergoes a nucleophilic attack to the carbonyl group of benzoylacetonitrile **2a** and affords intermediate **B**. Moreover, by abstracting a proton from the *in situ* formed NaHCO₃, the thermodynamic favorable C–C bond cleavage of **B** would provide the desired product **3a**, in which the side product CH₃CN is released.

CONCLUSION

In summary, Na₂CO₃/15-crown-5 couple-mediated direct acylation of *N*-heteroaryl methanols with acyl cyanides *via* C–C bond cleavage is reported. This new synthetic protocol proceeds under metal-free conditions and offers broad substrate scope in high efficiency. A variety of *N*-heteroaryl esters including pyrazines, pyridines, quinolines, furans, and thiophenes, which are key molecules in pharmaceuticals, natural products, dyes, or flavors, have thus been efficiently synthesized with good yields.

REFERENCES

- Akhlaghinia, B., Safaei, E., and Larki, P. (2010). Chemoselective Protocol for O-Acylation with a New Catalyst. *Trends Org. Chem.* 14, 93–106. doi:10.1039/toc100814a
- Armani, E., Amari, G., Rizzi, A., Fanti, R. D., Ghidini, E., Capaldi, C., et al. (2014). Novel Class of Benzoic Acid Ester Derivatives as Potent PDE4 Inhibitors for Inhaled Administration in the Treatment of Respiratory Diseases. *J. Med. Chem.* 57, 793–816. doi:10.1021/jm401549m
- Arzumanyan, A. V. (2017). Iron-catalyzed C C Bond Activation/C O Bond Formation: Direct Conversion of Ketones to Esters. *Tetrahedron Lett.* 58, 4667–4671. doi:10.1016/j.tetlet.2017.10.068
- Balalaie, S., Mahdidoust, M., and Eshaghi-Najafabadi, R. (2008). ChemInform Abstract: 2-Ih-Benzotriazole-1-Yl-1,1,3,3-Tetramethyluronium Tetrafluoroborate (TBTU) as an Efficient Coupling Reagent for the Esterification of Carboxylic Acids with Alcohols and Phenols at Room Temperature. *ChemInform* 39, 1141–1144. doi:10.1002/chin.200839075
- Bayout, I., Bouzemi, N., Guo, N., Mao, X., Serra, S., Riva, S., et al. (2020). Natural Flavor Ester Synthesis Catalyzed by Lipases. *Flavour Fragr J.* 35, 209–218. doi:10.1002/ffj.3554
- Bourne-Branchu, Y., Gosmini, C., and Danoun, G. (2017). Cobalt-Catalyzed Esterification of Amides. *Chem. Eur. J.* 23, 10043–10047. doi:10.1002/chem.201702608
- Chen, X., Liu, M., Liu, Y., Chen, Y., Au, C.-T., and Yin, S.-F. (2018). Copper-Catalyzed Esterification of *N*-Heteroaryl Methanes by Oxidative Dehydrogenation. *Asian J. Org. Chem.* 7, 1825–1829. doi:10.1002/ajoc.201800421
- Chen, Z., Wang, B., Zhang, J., Yu, W., Liu, Z., and Zhang, Y. (2015). Transition Metal-Catalyzed C-H Bond Functionalizations by the Use of Diverse Directing Groups. *Org. Chem. Front.* 2, 1107–1295. doi:10.1039/c5qo00004a
- Chen, Z., Wen, X., Zheng, W., He, R., Chen, D., Cao, D., et al. (2020). Acyl Cyanides as Bifunctional Reagent: Application in Copper-Catalyzed Cyanoamidation and Cyanoesterification Reaction. *J. Org. Chem.* 85, 5691–5701. doi:10.1021/acs.joc.9b03500
- Cheng, L., Sun, Y., Wang, W., Yao, C., and Li, T.-J. (2019). Ligand-Free Copper(I)-Catalyzed Benzylic Acyloxylation of 2-Alkylpyridines under Aerobic Conditions. *J. Org. Chem.* 84, 3074–3082. doi:10.1021/acs.joc.8b02794
- Chun, S., and Chung, Y. K. (2017). Transition-Metal-Free Poly(thiazolium) Iodide/1,8-Diazabicyclo[5.4.0]undec-7-ene/Phenazine-Catalyzed Esterification of Aldehydes with Alcohols. *Org. Lett.* 19, 3787–3790. doi:10.1021/acs.orglett.7b01617
- Deng, Y., Yang, T., Wang, H., Yang, C., Cheng, L., Yin, S.-F., et al. (2021). Recent Progress on Photocatalytic Synthesis of Ester Derivatives and Reaction Mechanisms. *Top. Curr. Chem. (Z)* 379, 42–94. doi:10.1007/s41061-021-00355-5
- Dong, D.-Q., Zhang, H., and Wang, Z.-L. (2017). Synthesis of Benzyl Esters from the Commercially Available Alcohols Catalyzed by TBAI *via* C(sp³)-H Bond Functionalization. *RSC Adv.* 7, 3780–3782. doi:10.1039/C6RA26387A
- Dong, J., Chen, X., Ji, F., Liu, L., Su, L., Mo, M., et al. (2021). Copper-mediated Simple and Direct Aerobic Oxidative Esterification of Arylacetonitriles with Alcohols/phenols. *Appl. Organomet. Chem.* 35, 6073–6083. doi:10.1002/aoc.6073
- Eisele, P., Bauder, M., Hsu, S. F., and Plietker, B. (2019). A Cyanide-Free Synthesis of Acylcyanides through Ru-Catalyzed C(sp³)-H-Oxidation of Benzylic Nitriles. *ChemistryOpen* 8, 689–691. doi:10.1002/open.201900130
- Guo, C., Xu, C., Zhang, N.-N., Li, X.-j., Ge, Y.-q., and Diao, P.-h. (2018). Visible Light Promotes Decyanation Esterification Reaction of β -Ketonitriles with Dioxxygen and Alcohols to α -Ketoesters. *Synlett* 29, 1065–1070. doi:10.1055/s-0036-1591943
- Guo, S., Yu, J.-T., Dai, Q., Yang, H., and Cheng, J. (2014). The Bu₄NI-Catalyzed Alfa-Acyloxylation of Ketones with Benzylic Alcohols. *Chem. Commun.* 50, 6240–6242. doi:10.1039/C4CC01652A
- Hay, B. P., Rustad, J. R., and Hostetler, C. J. (1993). Quantitative Structure-Stability Relationship for Potassium Ion Complexation by crown Ethers. A Molecular Mechanics and Ab Initio Study. *J. Am. Chem. Soc.* 115, 11158–11164. doi:10.1021/ja00077a013
- Hie, L., Baker, E. L., Anthony, S. M., Desrosiers, J.-N., Senanayake, C., and Garg, N. K. (2016). Nickel-Catalyzed Esterification of Aliphatic Amides. *Angew. Chem. Int. Ed. Angew. Chem.* 55, 15129–15132. doi:10.1002/anie.201607856
- Huang, X., Li, X., Zou, M., Song, S., Tang, C., Yuan, Y., et al. (2014). From Ketones to Esters by a Cu-Catalyzed Highly Selective C(CO)-C(alkyl) Bond Cleavage: Aerobic Oxidation and Oxygenation with Air. *J. Am. Chem. Soc.* 136, 14858–14865. doi:10.1021/ja5073004
- Huang, Z., Huang, X., Li, B., Mou, C., Yang, S., Song, B.-A., et al. (2016). Access to P-Stereogenic Phosphinates *via* N-Heterocyclic Carbene-Catalyzed Desymmetrization of Bisphenols. *J. Am. Chem. Soc.* 138, 7524–7527. doi:10.1021/jacs.6b04624
- Jiang, H., Chen, H., Wang, A., and Liu, X. (2010). Palladium-catalyzed Acetoxylation of Sp³ C-H Bonds Using Molecular Oxygen. *Chem. Commun.* 46, 7259–7261. doi:10.1039/c0cc00841a

DATA AVAILABILITY STATEMENT

The original contributions presented in the study are included in the article/**Supplementary Material**. Further inquiries can be directed to the corresponding author.

AUTHOR CONTRIBUTIONS

ML and MZ contributed to the conception and design of the study. The synthetic work and data collection were carried out by FS, MW, and GZ. JH contributed to the article revision. All authors read and approved the submitted version.

SUPPLEMENTARY MATERIAL

The Supplementary Material for this article can be found online at: <https://www.frontiersin.org/articles/10.3389/fchem.2021.822625/full#supplementary-material>

- Kong, W., Li, B., Xu, X., and Song, Q. (2016). Fe-Catalyzed Aerobic Oxidative C-CN Bond Cleavage of Arylacetonitriles Leading to Various Esters. *J. Org. Chem.* 81, 8436–8443. doi:10.1021/acs.joc.6b01594
- Lai, M., Zhai, K., Cheng, C., Wu, Z., and Zhao, M. (2018). Direct Thiolation of Aza-Heteroaromatic N-Oxides with Disulfides via Copper-Catalyzed Regioselective C-H Bond Activation. *Org. Chem. Front.* 5, 2986–2991. doi:10.1039/C8QO00840J
- Li, G., Lei, P., and Szostak, M. (2018). Transition-Metal-Free Esterification of Amides via Selective N-C Cleavage under Mild Conditions. *Org. Lett.* 20, 5622–5625. doi:10.1021/acs.orglett.8b02323
- Li, G., and Szostak, M. (2020). Transition-Metal-Free Activation of Amides by N-C Bond Cleavage. *Chem. Rec.* 20, 649–659. doi:10.1002/tcr.201900072
- Liotta, C. L., Harris, H. P., McDermott, M., Gonzalez, T., and Smith, K. (1974). Chemistry of "naked" Anions II. Reactions of the 18-crown-6 Complex of Potassium Acetate with Organic Substrates in Aprotic Organic Solvents. *Tetrahedron Lett.* 15, 2417–2420. doi:10.1016/S0040-4039(01)92273-7
- Liu, B., Hu, F., and Shi, B.-F. (2015a). Recent Advances on Ester Synthesis via Transition-Metal Catalyzed C-H Functionalization. *ACS Catal.* 5, 1863–1881. doi:10.1021/acscatal.5b00050
- Liu, C., Yuan, J., Gao, M., Tang, S., Li, W., Shi, R., et al. (2015b). Oxidative Coupling between Two Hydrocarbons: an Update of Recent C-H Functionalizations. *Chem. Rev.* 115, 12138–12204. doi:10.1021/cr500431s
- Lu, P., Hou, T., Gu, X., and Li, P. (2015). Visible-Light-Promoted Conversion of Alkyl Benzyl Ether to Alkyl Ester or Alcohol via O- α -Sp³ C-H Cleavage. *Org. Lett.* 17, 1954–1957. doi:10.1021/acs.orglett.5b00663
- Lutz, H. D., Jung, M., and Beckenkamp, K. (1988). Nature of the strong Basicity of Superbases, Unsolvated Hydroxide Ions? *J. Mol. Struct.* 175, 257–261. doi:10.1016/S0022-2860(98)80085-9
- McMurray, L., O'Hara, F., and Gaunt, M. J. (2011). Recent Developments in Natural Product Synthesis Using Metal-Catalyzed C-H Bond Functionalisation. *Chem. Soc. Rev.* 40, 1885–1898. doi:10.1039/c1cs15013h
- Mukaiyama, T., Kikuchi, W., and Shintou, T. (2003). Preparation of Various Carboxylic Acid Esters from Bulky Alcohols and Carboxylic Acids by a New Type Oxidation-Reduction Condensation Using 2,6-Dimethyl-1,4-Benzoquinone. *Chem. Lett.* 32, 300–301. doi:10.1246/cl.2003.300
- Otera, J. (2010). *Esterification: Methods, Reactions, and Applications*. Weinheim: Wiley VCH.
- Rammurthy, B., Peraka, S., Vasu, A., Krishna Sai, G., Divya Rohini, Y., and Narender, N. (2021). Metal-free Catalytic Esterification of Aryl Alkyl Ketones with Alcohols via Free-radical Mediated C(sp³)-H Bond Oxygenation. *Asian J. Org. Chem.* 10, 594–601. doi:10.1002/ajoc.202000691
- Reuter, C., Wienand, W., Hübner, G. M., Seel, C., and Vögtle, F. (1999). High-Yield Synthesis of Ester, Carbonate, and Acetal Rotaxanes by Anion Template Assistance and Their Hydrolytic Dethreading. *Chem. Eur. J.* 5, 2692–2697. doi:10.1002/(SICI)1521-3765(19990903)5:9<2692:AID-CHEM2692>3.0.CO;2-F
- Roy, B. C., Ansari, I. A., Samim, S. A., and Kundu, S. (2019). Base-Promoted α -Alkylation of Arylacetonitriles with Alcohols. *Chem. Asian J.* 14, 2215–2219. doi:10.1002/asia.201900285
- Subramanian, M., Ramar, P. M., Rana, J., Gupta, V. K., and Balaraman, E. (2020). Catalytic Conversion of Ketones to Esters via C(O)-C Bond Cleavage under Transition-Metal Free Conditions. *Chem. Commun.* 56, 8143–8146. doi:10.1039/d0cc03312j
- Tamaddon, F., Amrollahi, M. A., and Sharafat, L. (2005). A green Protocol for Chemoselective O-Acylation in the Presence of Zinc Oxide as a Heterogeneous, Reusable and Eco-Friendly Catalyst. *Tetrahedron Lett.* 46, 7841–7844. doi:10.1016/j.tetlet.2005.09.005
- Tang, S., Yuan, J., Liu, C., and Lei, A. (2014). Direct Oxidative Esterification of Alcohols. *Dalton Trans.* 43, 13460–13470. doi:10.1039/c4dt01133c
- Trotier-Faurion, A., D  zard, S., Taran, F., Valayannopoulos, V., de Lonlay, P., and Mabondzo, A. (2013). Synthesis and Biological Evaluation of New Creatine Fatty Esters Revealed Dodecyl Creatine Ester as a Promising Drug Candidate for the Treatment of the Creatine Transporter Deficiency. *J. Med. Chem.* 56, 5173–5181. doi:10.1021/jm400545n
- Uyanik, M., Suzuki, D., Yasui, T., and Ishihara, K. (2011). *In Situ* Generated (Hypo) Iodite Catalysts for the Direct α -Oxyacylation of Carbonyl Compounds with Carboxylic Acids. *Angew. Chem. Int. Ed.* 50, 5331–5334. doi:10.1002/anie.201101522
- Wang, C.-S., Roisnel, T., Dixneuf, P. H., and Sou  l  , J.-F. (2017). Synthesis of 2-Pyridinemethyl Ester Derivatives from Aldehydes and 2-Alkylheterocycle N-Oxides via Copper-Catalyzed Tandem Oxidative Coupling-Rearrangement. *Org. Lett.* 19, 6720–6723. doi:10.1021/acs.orglett.7b03446
- Wencel-Delord, J., and Glorius, F. (2013). C-H Bond Activation Enables the Rapid Construction and Late-Stage Diversification of Functional Molecules. *Nat. Chem.* 5, 369–375. doi:10.1038/nchem.1607
- Xie, F., Yan, F., Chen, M., and Zhang, M. (2014). Base-catalyzed Retro-Claisen Condensation: a Convenient Esterification of Alcohols via C-C Bond Cleavage of Ketones to Afford Acylating Sources. *RSC Adv.* 4, 29502–29508. doi:10.1039/c4ra04618h
- Xu, Y., Zhao, J., Liu, X., Zhang, C., Zhao, Z., Li, X., et al. (2022). Flavor Mystery of Chinese Traditional Fermented Baijiu: The Great Contribution of Ester Compounds. *Food Chem.* 369, 130920–130932. doi:10.1016/j.foodchem.2021.130920
- Yan, F.-X., Zhang, M., Wang, X.-T., Xie, F., Chen, M.-M., and Jiang, H. (2014). Efficient Ruthenium-Catalyzed α -alkylation of Ketones Using Pyridyl Methanols. *Tetrahedron* 70, 1193–1198. doi:10.1016/j.tet.2013.12.065
- Yasin, F. M., Boulos, R. A., Hong, B. Y., Cornejo, A., Iyer, K. S., Gao, L., et al. (2012). Microfluidic Size Selective Growth of Palladium Nano-Particles on Carbon Nano-Onions. *Chem. Commun.* 48, 10102–10206. doi:10.1039/c2cc35017c
- Zeng, R., Sheng, H., Zhang, Y., Feng, Y., Chen, Z., Wang, J., et al. (2014). Heterobimetallic Dinuclear Lanthanide Alkoxide Complexes as Acid-Base Difunctional Catalysts for Transesterification. *J. Org. Chem.* 79, 9246–9252. doi:10.1021/jo5016536
- Zhai, K., Lai, M., Wu, Z., Zhao, M., Jing, Y., and Liu, P. (2018). Synthesis and Initial thermal Behavior Investigation of 2-alkenyl Substituted Pyrazine N-Oxides. *Catal. Commun.* 116, 20–26. doi:10.1016/j.catcom.2018.07.017
- Zhang, C., and Wang, Y. (2019). Chloride-Induced Highly Active Au Catalyst for Methyl Esterification of Alcohols. *Chin. J. Chem.* 37, 249–254. doi:10.1002/cjoc.201800374
- Zhao, J., Fang, H., Zhou, W., Han, J., and Pan, Y. (2014). Iron-Catalyzed Cross-Dehydrogenative Coupling Esterification of Unactive C(sp³)-H Bonds with Carboxylic Acids for the Synthesis of α -Acyloxy Ethers. *J. Org. Chem.* 79, 3847–3855. doi:10.1021/jo500192h

Conflict of Interest: The authors declare that the research was conducted in the absence of any commercial or financial relationships that could be construed as a potential conflict of interest.

Publisher's Note: All claims expressed in this article are solely those of the authors and do not necessarily represent those of their affiliated organizations, or those of the publisher, the editors, and the reviewers. Any product that may be evaluated in this article, or claim that may be made by its manufacturer, is not guaranteed or endorsed by the publisher.

Copyright    2022 Lai, Su, Hu, Wang, Zhao and Zhang. This is an open-access article distributed under the terms of the Creative Commons Attribution License (CC BY). The use, distribution or reproduction in other forums is permitted, provided the original author(s) and the copyright owner(s) are credited and that the original publication in this journal is cited, in accordance with accepted academic practice. No use, distribution or reproduction is permitted which does not comply with these terms.



Facile and Sustainable Synthesis of Commendamide and its Analogues

Rosaria Villano^{1*}, Francesco Tinto² and Vincenzo Di Marzo^{1,3}

¹Istituto di Chimica Biomolecolare, Pozzuoli, Italy, ²Département de Médecine, Faculté de Médecine, Centre de Recherche de l'Institut Universitaire de Cardiologie et de Pneumologie de Québec, Université Laval, Québec City, QC, Canada, ³Canada Excellence Research Chair on the Microbiome-Endocannabinoidome Axis in Metabolic Health, Faculty of Medicine and Faculty of Agricultural and Food Sciences, Centre NUTRISS, Centre de Recherche de l'Institut de Cardiologie et Pneumologie de l'Université et Institut sur la Nutrition et les Aliments Fonctionnels, Université Laval, Québec City, QC, Canada

Commendamide, or N-(3-hydroxypalmitoyl)-glycine **1a**, is a gut microbiota-derived bioactive metabolite, structurally similar to long-chain N-acyl-amino acids which belong to the complex lipid signaling system known as endocannabinoidome and play important roles in mammals through activation of, *inter alia*, G-protein-coupled receptors (GPCRs). In this work, we describe a simple, green and economic method for the preparation of commendamide **1a**, a GPCR G2A/132 agonist. The developed protocol is general and could also be applied to the synthesis of deuterated commendamide **1b**, as well as to other minor microbiota-derived metabolites, such as the analog **2**.

Keywords: commendamide, microbiota, endocannabinoidome, green chemistry, organic synthesis, drug discovery

OPEN ACCESS

Edited by:

Guillermo Raul Castro,
Consejo Nacional de Investigaciones
Científicas y Técnicas (CONICET),
Argentina

Reviewed by:

George Kokotos,
National and Kapodistrian University of
Athens, Greece
Luke Hunter,
University of New South Wales,
Australia

*Correspondence:

Rosaria Villano
rosaria.villano@icb.cnr.it

Specialty section:

This article was submitted to
Green and Sustainable Chemistry,
a section of the journal
Frontiers in Chemistry

Received: 20 January 2022

Accepted: 08 February 2022

Published: 01 March 2022

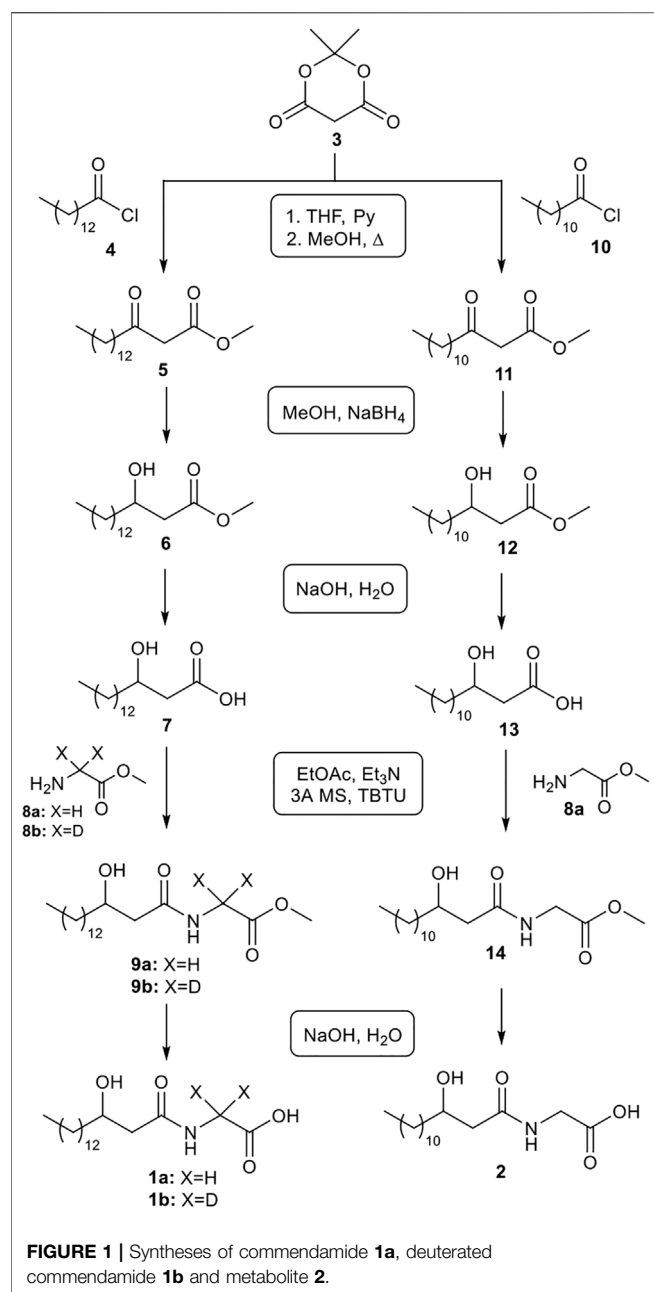
Citation:

Villano R, Tinto F and Di Marzo V (2022)
Facile and Sustainable Synthesis of
Commendamide and its Analogues.
Front. Chem. 10:858854.
doi: 10.3389/fchem.2022.858854

INTRODUCTION

The gut microbiota has proven to be an important source of bioactive metabolites (McNeil, 1984; De Vadder et al., 2014; Vernocchi et al., 2016; Postler and Ghosh, 2017), which are often able to interact with host receptors thanks to their structural similarity with endogenous signal molecules, such as those belonging to the endocannabinoidome (Iannotti and Di Marzo, 2021). This host signaling system includes hundreds of endocannabinoid-like long chain fatty acid-derived amides and esters, which signal at G-protein-coupled receptors (including the cannabinoid receptors), ligand-activated ion channels and peroxisome proliferator-activated receptors (PPARs) (Di Marzo, 2018). Gut microbiota metabolites can therefore act as highly specific modulators of important host functions and are very often well tolerated because biosynthesized by bacteria that live in symbiosis with the host. These aspects make bacterial endocannabinoidome-mimic molecules very promising candidates for the development of new drugs (Saha et al., 2016; Iannotti and Di Marzo, 2021).

In 2015, the discovery and structural identification of commendamide (Cohen et al., 2015) among the gut microbiota-derived metabolites aroused considerable interest due to its structure that is very similar to long-chain N-acyl-amino acids [such as N-oleoyl-glycine (Donvito et al., 2018)], which in the host signal through GPCRs (Cohen et al., 2017) and PPAR α (Donvito et al., 2018). In a very inspiring study (Cohen et al., 2015), Cohen et al. showed that commendamide was indeed able to interact with GPCRs by acting as an agonist of the GPCR G2A/132 receptor, implicated in autoimmunity and atherosclerosis. These interesting structural properties, its biogenic origin and bioactivity (Cohen et al., 2015; Lynch et al., 2017; Lynch et al., 2019; Piscotta et al., 2021), but also the presence of an N-(3-hydroxyacyl)amino acid scaffold, which is a structural motif found in many other interesting bioactive products (Morishita et al., 1997; Nemoto et al., 1998; Fuqua and Greenberg, 2002; Grandclément et al., 2016; Lynch et al., 2019), make of commendamide, a metabolite at the cross-road of gut microbiota and host signaling, an exceptionally attractive target for chemical synthesis.



Organic synthesis represents a powerful tool to conclusively confirm NMR and MS-based structure elucidation, and to produce greater amounts of the product, to be tested *in vitro* and *in vivo* (Nicolaou, 2014). Therefore, the elaboration of simple and effective synthetic protocols is very important; in addition, the development of versatile and general methodologies, which can also be used for the synthesis of the products in deuterated form (necessary for the development of LC-MS quantitative analysis methods) or to introduce structural modifications to the initial target molecule (for SAR studies) is highly desirable.

In the last decades, green chemistry (Horváth and Anastas, 2007; Li and Trost, 2008) has given impetus to a new generation of chemical syntheses through the creation of innovative reaction

methodologies that can maximize the desired products and minimize waste, but also by identifying new synthetic sequences and equipments that can simplify the experimental procedures and replace old and often unsustainable protocols. These green syntheses, by employing more eco-friendly reaction conditions, represent a powerful tool in modern drug discovery programs.

Here, an easy and versatile methodology for the synthesis of the commendamide **1a** is reported. This synthetic sequence (Figure 1) is characterized by the use of simple workups, readily available reagents, no halogenated solvent (for reaction, workup and purification) and minimal volumes of organic solvents. Furthermore, the high yields observed in many reaction steps often rendered unnecessary the use of column chromatography for the purification of synthetic intermediates. The same synthetic sequence was also successfully applied to the synthesis of deuterated commendamide **1b** and another minor commendamide-like metabolite **2**, with a poorly studied bioactivity, thus demonstrating the generality of the novel synthetic route presented here.

METHODS

General

All reagents and solvents were purchased from Merck-SigmaAldrich and used as received. Reactions were monitored by thin layer chromatography (TLC) on Merck silica gel plates (0.25 mm) and visualized by UV light at 254 nm and cerium sulfate reagent. ¹H NMR and ¹³C NMR spectra were recorded on a Bruker Avance-400 and on a Bruker DRX 600 equipped with an inverse TCI CryoProbe at room temperature in CDCl₃ or CD₃OD. Chemical shifts are reported in ppm, multiplicities are indicated by s (singlet), d (doublet), t (triplet), q (quartet), m (multiplet) and br (broad). Coupling constants (J) are reported in Hz. Yields are given for isolated products showing one spot on a TLC plate and no impurities detectable in the NMR spectrum.

Synthetic Procedures and Characterization of Products

Methyl 3-oxohexadecanoate (5): Pyridine (2 eq, 2.0 mmol) was added to a solution of Meldrum's acid (**3**; 1 eq, 1.0 mmol) in THF (0.7 ml) at room-temperature. The reaction was cooled at 0°C and myristoyl chloride (**4**, 1.2 eq, 1.2 mmol) was portion-wise added to the solution. The reaction was warmed to rt and stirred overnight. After adding 1N HCl_{aq} to pH 2, the phases were separated and the H₂O phase was extracted with EtOAc (3 × 2 ml). The combined organic layers were dried over Na₂SO₄. After evaporation of the solvent, the crude product was dissolved in MeOH (5 ml) and the reaction solution was mildly refluxed for 3 h by using a waterless air condenser (Asynt CondensSyn). After cooling to room temperature, the solvent was removed by reduced pressure and the crude product **5** was used directly without any further purification.

Methyl 3-hydroxyhexadecanoate (6): A solution of the product **5** in MeOH (1 ml) was prepared in a vial. The reaction was cooled

at 0°C and NaBH₄ (1 eq, 1.0 mmol) was added slowly; the reaction was stirred at 0°C for 30 min and, after adding 1N HCl_{aq} to pH 7, the reaction was warmed to rt. H₂O (2 ml) and EtOAc (2 ml) were added to the reaction mixture, the phases were separated and the H₂O phase was extracted with EtOAc (2 × 2 ml). The combined organic layers were dried over Na₂SO₄. After evaporation of the solvent, the crude product was purified by silica gel chromatography using a light petroleum ether/EtOAc 6/1 to give the product **6** (0.9 mmol, 90% yield from **3**). The spectroscopic data of **6** matched the ones reported in the literature (Jakob et al., 1996). ¹H-NMR (CDCl₃) δ 4.00 (m, 1H), 3.71 (s, 3H), 2.51 (dd, J = 3 Hz, 16.4 Hz, 1H), 2.40 (dd, J = 9.1 Hz, 16.4 Hz, 1H), 1.52–1.27 (m, 24H), 0.87 (t, J = 6.8 Hz, 3H). ¹³C-NMR (CDCl₃) δ 173.5, 68.0, 51.7, 41.1, 36.5, 31.9, 29.7, 29.6, 29.5, 29.3, 25.5, 22.7, 14.1 (some signals were overlapped).

3-Hydroxyhexadecanoic acid (7): 1N NaOH_{aq} (10 eq, 2.5 mmol) was added to a solution of **6** (0.25 mmol) in THF (0.1 ml) at 0°C. The reaction was stirred at 0°C for 30 min and then 2 h at rt. After adding 1N HCl to pH 2, the phases were separated and the H₂O phase was extracted with EtOAc (3 × 2 ml). The combined organic layers were dried over Na₂SO₄ and the solvent was removed by reduced pressure to afford β-hydroxy-acid **7** as a colorless solid (0.22 mmol, 88% yield). The spectroscopic data of **7** matched the ones reported in the literature (Bourboulia et al., 2019). ¹H-NMR (CDCl₃) δ 4.02 (m, 1H), 2.58 (dd, J = 3.0, 16.6 Hz, 1H), 2.47 (dd, J = 9.0, 16.6 Hz, 1H), 1.57–1.25 (m, 24H), 0.88 (t, J = 6.8 Hz, 3H). ¹³C-NMR (CDCl₃) δ 176.0, 68.0, 40.7, 36.5, 31.9, 29.7, 29.6, 29.57, 29.54, 29.5, 29.3, 25.4, 22.7, 14.1.

Methyl (3-hydroxyhexadecanoyl)glycinate (9a): The β-hydroxy-acid **7** (0.22 mmol) was dissolved in EtOAc (2 ml). 3 Å MS (400 mg), Et₃N (3 eq, 0.66 mmol) and TBTU (1 eq, 0.22 mmol) were added and the reaction mixture was stirred at rt for 1 h. Then **8a** (Wang et al., 2009) (2.5 eq, 0.55 mmol) was added and the reaction was kept stirring overnight. The reaction mixture was diluted by adding 3 ml of H₂O; the phases were separated and the H₂O phase was extracted with EtOAc (3 × 2 ml). The collected organic layer was dried over Na₂SO₄ and concentrated. The residue was purified by flash chromatography using a light petroleum ether/ethyl acetate 7/3 to give **9a** (0.16 mmol, 73% yield). The spectroscopic data of **9a** matched the ones reported in the literature (Nemoto et al., 1998). ¹H-NMR (CDCl₃) δ 6.50 (bs, NH, 1H), 4.07 (dd, J = 5.4, 13.1 Hz, 1H), 4.03 (dd, J = 5.3, 13.1 Hz, 1H), 4.02 (m, 1H), 3.78 (s, 3H), 2.84 (bs, OH, 1H), 2.46 (dd, J = 2.5, 15.1 Hz, 1H), 2.35 (dd, J = 9.1, 15.1 Hz, 1H), 1.58–1.27 (m, 24H), 0.90 (t, J = 6.8 Hz, 3H). ¹³C-NMR (CDCl₃) δ 172.9, 170.5, 68.8, 52.5, 42.7, 41.2, 36.8, 31.9, 29.7, 29.65, 29.58, 29.56, 29.5, 29.3, 25.5, 22.7, 14.1.

Methyl (3-hydroxyhexadecanoyl)glycinate-d₂ (9b) was synthesized according to the same protocol as described for **9a**, by using **8b** (Wang et al., 2009) instead of **8a**, with 75% yield. ¹H-NMR (CDCl₃) δ 6.43 (bs, NH, 1H), 4.02 (m, 1H), 3.78 (s, 3H), 2.84 (bs, OH, 1H), 2.46 (dd, J = 2.5, 15.1 Hz, 1H), 2.34 (dd, J = 9.1, 15.1 Hz, 1H), 1.58–1.27 (m, 24H), 0.90 (t, J = 6.8 Hz, 3H). ¹³C-NMR (CDCl₃) δ 172.8, 170.5, 68.7, 52.5, 42.7, 36.9, 31.9, 29.7, 29.66, 29.65, 29.58, 29.5, 29.3, 25.5, 22.7, 14.1.

Commendamide or N-(3-hydroxypalmitoyl)-glycine (1a): 1N NaOH_{aq} (10 eq, 1.3 mmol) was added to a solution of **9a**

(0.13 mmol) in THF (0.1 ml) at 0°C. The reaction was stirred at 0°C for 30 min and then 3 h at rt. After adding 1N HCl to pH 2, the formation of a solid was observed. The solid product was collected by filtration and washed with H₂O (2 × 1 ml) and then Etp/EtOAc 8/2 (3 × 1 ml) to give **1a** as a colorless solid (90% yield). Spectral data are consistent with a previous literature report (Cohen et al., 2015). ¹H-NMR (CD₃OD) δ 3.99 (m, 1H), 3.93 (ABq, J = 17.8 Hz, 2H), 2.41 (dd, J = 5.0, 14.3 Hz, 1H), 2.37 (dd, J = 7.7, 14.3 Hz, 1H), 1.52–1.31 (m, 24H), 0.92 (t, J = 6.8 Hz, 3H). ¹³C-NMR (CDCl₃) δ 173.3, 171.7, 68.3, 43.2, 40.4, 36.7, 31.7, 29.4, 29.3, 29.2, 29.1, 25.2, 22.3, 13.0.

Commendamide-d₂ or N-(3-hydroxypalmitoyl)-glycine-d₂ (1b) was synthesized based on the same protocol as described for **1a**, by using **9b** instead of **9a**, with 92% yield. ¹H-NMR (CD₃OD) δ 3.99 (m, 1H), 2.41 (dd, J = 5.0, 14.3 Hz, 1H), 2.37 (dd, J = 7.7, 14.3 Hz, 1H), 1.53–1.31 (m, 24H), 0.92 (t, J = 6.8 Hz, 3H). ¹³C-NMR (CDCl₃) δ 173.3, 171.7, 68.3, 43.2, 36.7, 31.7, 29.4, 29.3, 29.2, 29.1, 25.2, 22.3, 13.0.

Methyl 3-oxotetradecanoate (11): Pyridine (2 eq, 2.0 mmol) was added to a solution of Meldrum's acid (**3**; 1 eq, 1.0 mmol) in THF (0.7 ml) at room-temperature. The reaction was cooled at 0°C and lauroyl chloride (**10**, 1.2 eq, 1.2 mmol) was portion-wise added to the solution. The reaction was warmed to rt and stirred overnight. After adding 1N HCl_{aq} to pH 2, the phases were separated and the H₂O phase was extracted with EtOAc (3 × 2 ml). The combined organic layers were dried over Na₂SO₄. After evaporation of the solvent, the crude product was dissolved in MeOH (5 ml) and the reaction solution was mildly refluxed for 3 h by using a waterless air condenser (Asynt CondensSyn). After cooling to room temperature, the solvent was removed by reduced pressure and the crude product **11** was used directly without any further purification.

Methyl 3-hydroxytetradecanoate (12): A solution of the crude product **11** in MeOH (1 ml) was prepared in a vial. The reaction was cooled at 0°C and NaBH₄ (1 eq, 1.0 mmol) was added slowly; the reaction was stirred at 0°C for 30 min and, after adding 1N HCl_{aq} to pH 7, the reaction was warmed to rt. H₂O (2 ml) and EtOAc (2 ml) were added to the reaction mixture, the phases were separated and the H₂O phase was extracted with EtOAc (2 × 2 ml). The combined organic layers were dried over Na₂SO₄. After evaporation of the solvent, the crude was purified by silica gel chromatography using a light petroleum ether/EtOAc 6/1 to give the product **12** (0.75 mmol, 75% yield from **3**). The spectroscopic data of **12** matched the ones reported in the literature (Hon et al., 2007). ¹H-NMR (CDCl₃) δ 4.02 (m, 1H), 3.73 (s, 3H), 2.53 (dd, J = 3 Hz, 16.4 Hz, 1H), 2.43 (dd, J = 9.1 Hz, 16.4 Hz, 1H), 1.57–1.29 (m, 20H), 0.90 (t, J = 6.8 Hz, 3H). ¹³C-NMR (CDCl₃) δ 173.5, 68.1, 51.7, 41.1, 36.5, 31.9, 29.7, 29.6, 29.5, 29.4, 29.3, 25.5, 22.7, 14.1.

3-Hydroxytetradecanoic acid (13): 1N NaOH_{aq} (10 eq, 7.5 mmol) was added to a solution of **12** (0.75 mmol) in THF (0.1 ml) at 0°C. The reaction was stirred at 0°C for 30 min and then 2 h at rt. After adding 1N HCl to pH 2, the phases were separated and the H₂O phase was extracted with EtOAc (3 × 2 ml). The combined organic layers were dried over Na₂SO₄ and the solvent was removed by reduced pressure to afford β-hydroxy-acid **13** as a colorless solid (0.67 mmol, 89% yield).

The spectroscopic data of **13** matched the ones reported in the literature (Fukuchi et al., 1992). $^1\text{H-NMR}$ (CDCl_3) δ 4.06 (m, 1H), 2.61 (dd, $J = 3.1, 16.6$ Hz, 1H), 2.51 (dd, $J = 8.8, 16.6$ Hz, 1H), 1.58–1.27 (m, 20H), 0.91 (t, $J = 6.8$ Hz, 3H). $^{13}\text{C-NMR}$ (CDCl_3) δ 176.0, 68.0, 40.7, 36.5, 31.9, 29.7, 29.6, 29.5 (some signals were overlapped), 29.3, 25.4, 22.7, 14.1.

Methyl (3-hydroxytetradecanoyl)glycinate (14): The β -hydroxy-acid **13** (0.67 mmol) was dissolved in EtOAc (6 ml). 3A MS (1 g), Et_3N (3 eq, 2.0 mmol) and TBTU (1 eq, 0.67 mmol) were added and the reaction was stirred at rt for 1 h. Then **8a** (Wang et al., 2009) (2.5 eq, 1.7 mmol) was added and the reaction was kept stirring overnight. The reaction mixture was diluted by adding 6 ml of H_2O ; the phases were separated and the H_2O phase was extracted with EtOAc (3×4 ml). The collected organic layer was dried over Na_2SO_4 and concentrated. The residue was purified by flash chromatography using a light petroleum ether/ethyl acetate 7/3 to give **14** (0.47 mmol, 70% yield). $^1\text{H-NMR}$ (CDCl_3) δ 6.40 (bs, NH, 1H), 4.11 (dd, $J = 5.4, 18.3$ Hz, 1H), 4.05 (dd, $J = 5.4, 18.3$ Hz, 1H), 4.02 (m, 1H), 3.79 (s, 3H), 2.88 (bs, OH, 1H), 2.46 (dd, $J = 2.6, 15.1$ Hz, 1H), 2.34 (dd, $J = 9.1, 15.1$ Hz, 1H), 1.58–1.27 (m, 20H), 0.90 (t, $J = 6.5$ Hz, 3H). $^{13}\text{C-NMR}$ (CDCl_3) δ 172.7, 170.5, 68.7, 52.5, 42.7, 41.1, 36.8, 31.9, 29.65, 29.63, 29.58, 29.5, 29.3, 25.5, 22.7, 14.1.

3-Hydroxytetradecanoyl-glycine (2): 1N NaOH aq (10 eq, 4.7 mmol) was added to a solution of **14** (0.47 mmol) in THF (0.1 ml) at 0°C . The reaction was stirred at 0°C for 30 min and then 3 h at rt. After adding 1N HCl to pH 2, the formation of a solid was observed. The solid product was collected by filtration and washed with H_2O (2×2 ml) and then Etp/EtOAc 8/2 (3×2 ml) to give **2** as a colourless solid with 89% yield (0.42 mmol). This spectral data is consistent with a previous literature report (Morishita et al., 1997; Cohen et al., 2015). $^1\text{H-NMR}$ (CD_3OD) δ 3.99 (m, 1H), 3.94 (ABq, $J = 17.8$ Hz, 2H), 2.41 (dd, $J = 5.0, 14.3$ Hz, 1H), 2.37 (dd, $J = 7.7, 14.3$ Hz, 1H), 1.53–1.31 (m, 20H), 0.92 (t, $J = 6.8$ Hz, 3H). $^{13}\text{C-NMR}$ (CDCl_3) δ 173.3, 171.7, 68.3, 43.2, 40.3, 36.7, 31.7, 29.4, 29.35, 29.34, 29.3 (some signals were overlapped), 29.1, 25.2, 22.3, 13.0.

RESULTS AND DISCUSSION

As delineated in **Figure 1**, 3-hydroxypalmitic acid **7** was the key intermediate for the production of commendamide **1a**. Several methods for the synthesis of 3-hydroxy carboxylic acids are reported in the literature and they mainly use the Reformatsky reaction (Gawrorisk, 1984) or the reduction of β -ketoesters obtained by acylation of Meldrum's acid (Oikawa et al., 1978; Hodgkinson et al., 2011; Brinkerhoff et al., 2014; Brosge et al., 2021) or γ -alkylation of acetoacetate (Smith et al., 2009). Here, we started from the reaction between the commercially available Meldrum's acid **3** and myristoyl chloride **4**. Unlike the protocols reported in literature, this C-acylation was carried out in a minimal volume of THF (workup with EtOAc) instead of classical CH_2Cl_2 , without any reduction in the efficiency of the reaction. Because the acyl Meldrum's acid derivatives are decomposed by column chromatography, the crude product was used without any further purification and directly

converted to methyl 3-oxohexadecanoate **5** by alcoholysis with methanol. This reaction was performed at $72\text{--}75^\circ\text{C}$, by classical heating (3 h) in the presence of a waterless air condenser (Asynt CondensSyn)¹, an eco-friendly equipment that reduces water waste. The crude β -ketoester **5** was swiftly converted into β -hydroxy-ester **6** by reduction with NaBH_4 in MeOH (30min/ 0°C) and the product **6** was easily isolated by column chromatography (90% yield from **3**, after 3 reaction steps). Saponification of the methyl ester group with NaOH in water gave the corresponding β -hydroxy-acid **7** as a colorless solid in 88% yield. In order to increase the solubility of product **6** and improve the efficiency of the reaction, a small volume (100 μL) of THF was also added as co-solvent. TBTU-mediated coupling of **7** with glycine methyl ester hydrochloride **8a** [prepared according to the literature (Wang et al., 2009)], in the presence of Et_3N and 3 Å MS provided the glycinate **9a** with an interesting yield (73%) after purification by flash chromatography. Finally, commendamide **1a** was obtained as a colourless solid by saponification of the derivative **9a** and, after crystallization, was collected by filtration (total yield 52% from **3**).

The synthesis of commendamide was reported by Cohen in 2015 (Cohen et al., 2015). In this case the racemic product was prepared by a coupling reaction between 3-hydroxy-palmitic acid and glycine promoted by PyBOP and Cl-HOBt. Unfortunately, the article does not provide sufficient synthetic details and the final product was obtained in very small amount (less than 6% of yield).

The synthetic sequence from **3** to **1a** was rather concise (6 steps) and all reactions gave the corresponding products with good yields, without formation of side-products. All reactions of this sequence were not very water-sensitive, so they did not need to be carried out under an inert atmosphere, nor did they require the use of anhydrous reagents, solvents, glassware, and equipments. Furthermore, most of the reactions were realized at room temperature, while low temperatures (0°C) and high temperatures (75°C) were used only in a few steps for very limited times. In addition, all workups were very simple and column chromatography was performed only for the purification of two synthetic intermediates, since the other products were used in crude form or after purification by crystallization and filtration, with a significant and beneficial reduction in the amount of solvent and energy needed for the separation and purification of intermediates. Finally, this synthetic sequence was readily scalable (up to 5 mmol) without substantial change in efficiency.

The same synthetic protocol was also applied to the synthesis of deuterated commendamide **1b** (**Figure 1**); in this case, deuterated glycine methyl ester hydrochloride **8b** [prepared according to the literature (Wang et al., 2009)], was used in the coupling reaction with 3-hydroxypalmitic acid **7**. Deuterated commendamide **1b** was synthesized with a total yield of 55% from **3**.

To further explore the synthetic value of this strategy, we extended it to the synthesis of another poorly studied gut-

¹<http://www.asynt.com/product/asyntcondensyn-air-condenser/>

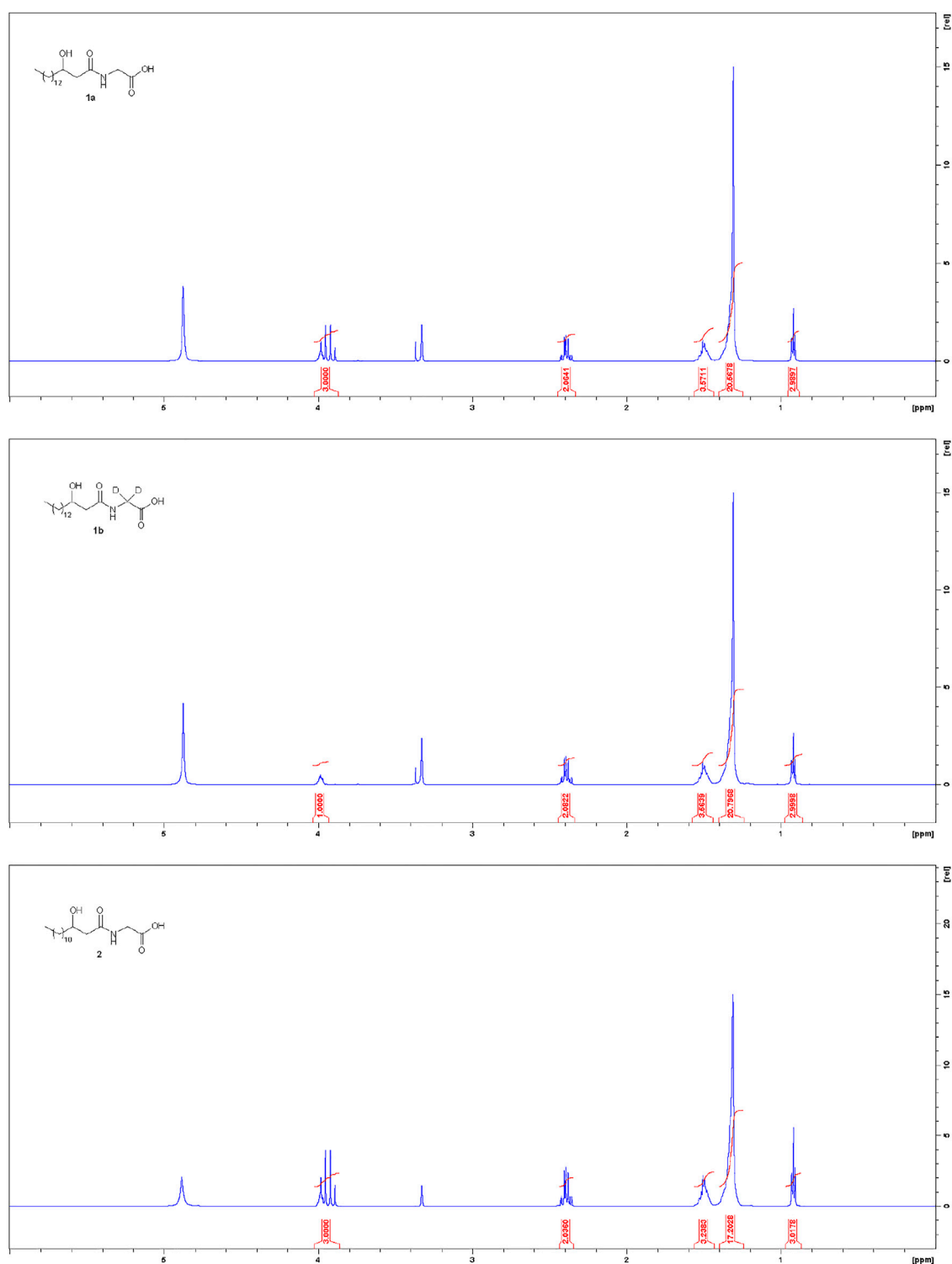


FIGURE 2 | ^1H NMR spectra (600MHz, CD_3OD) of synthetic products **1a**, **1b** and **2**.

microbiota metabolite, that is the commendamide analog **2** (Figure 1). In this case, C-acylation of the Meldrum's acid **3** was performed with lauroyl chloride **10**, then the alcoholysis with

MeOH, followed by reduction with NaBH_4 and saponification gave β -hydroxy-myristic acid **13**. Finally, TBTU-mediated coupling of **13** with glycine methyl ester hydrochloride **8a**

followed by saponification produced the derivative **2** with 42% overall yield from **3**, which is higher than that reported in the literature by using a different synthetic protocol (Venkateswaran et al., 2016).

The possibility to apply the same synthetic sequence for the production of several products with a 3-hydroxyacyl glycine scaffold (highly pure **1a**, **1b** and **2**, **Figure 2**) confirmed the generality and versatility of the developed strategy.

CONCLUSION

In conclusion, a practical and “green” procedure for the synthesis of commendamide and its analogues was developed. This procedure involved a total of six steps to obtain highly pure N-(3-hydroxyacyl) glycines (**Figure 2**) from the commercially available Meldrum’s acid and acyl-chloride. Key advantages are that all reactions of this synthetic sequence gave the corresponding products with high yields, without formation of side-products, and only two column chromatographic purifications were needed with a beneficial reduction in the amount of solvent and energy needed for separation and purification; furthermore, all reactions were not very water-sensitive, so they did not need to be carried out under an inert atmosphere, and they did not require the use of anhydrous reagents/solvents/glassware.

The possibility to apply the same synthetic sequence for the production of several products with a 3-hydroxyacyl glycine scaffold (**1a**, **1b** and **2**) confirmed the generality and versatility of the developed strategy. Given the simplicity and high efficiency of this synthetic sequence, the extension of this methodology toward the synthesis of other gut microbiota-derived commendamide-like metabolites (Cohen et al., 2017) for biological evaluation, *in vitro* and *in vivo*, are underway in our laboratory. Finally, the separation of the single enantiomers by chiral HPLC will allow to test their individual biological activities and evaluate any differences between the stereoisomers (in

addition to the biological tests performed on the racemic products).

DATA AVAILABILITY STATEMENT

The original contributions presented in the study are included in the article, further inquiries can be directed to the corresponding author.

AUTHOR CONTRIBUTIONS

RV and VD designed research; RV and FT performed research; VD supervised the project and provided funding acquisition; RV wrote the original draft; VD reviewed and edited the manuscript. RV, FT, and VD discussed the results and commented on the manuscript. All authors read and approved the final manuscript.

FUNDING

FT was supported by a post-doctoral fellowship from the UMI MicroMeNu.

ACKNOWLEDGMENTS

The financial support from MUR PRIN 2017XC73BW_002—CUP B84I19002450001 and Unité Mixte Internationale (UMI) for Chemical and Biomolecular Research on the Microbiome and its impact on Metabolic Health and Nutrition (MicroMeNu), which is partly funded by the Sentinelle Nord project, supported by the Apogée (Canada First) programme from the Federal Tri-Agency of Canada, is acknowledged.

REFERENCES

- Bourboulia, A., Limnios, D., Kokotou, M. G., Mountanea, O. G., and Kokotos, G. (2019). Enantioselective Organocatalysis-Based Synthesis of 3-Hydroxy Fatty Acids and Fatty γ -Lactones. *Molecules* 24, 2081. doi:10.3390/molecules24112081
- Brinkerhoff, R. C., Tarazona, H. F., de Oliveira, P. M., Flores, D. C., Montes D’Oca, C. D. R., Russowsky, D., et al. (2014). Synthesis of β -ketoesters from Renewable Resources and Meldrum’s Acid. *RSC Adv.* 4, 49556–49559. doi:10.1039/c4ra08986c
- Brosge, F., Singh, P., Almqvist, F., and Bolm, C. (2021). Selected Applications of Meldrum’s Acid - a Tutorial. *Org. Biomol. Chem.* 19, 5014–5027. doi:10.1039/d1ob00395j
- Cohen, L. J., Esterhazy, D., Kim, S.-H., Lemetre, C., Aguilar, R. R., Gordon, E. A., et al. (2017). Commensal Bacteria Make GPCR Ligands that Mimic Human Signalling Molecules. *Nature* 549, 48–53. doi:10.1038/nature23874
- Cohen, L. J., Kang, H.-S., Chu, J., Huang, Y.-H., Gordon, E. A., Reddy, B. V. B., et al. (2015). Functional Metagenomic Discovery of Bacterial Effectors in the Human Microbiome and Isolation of Commendamides, a GPCR G2A/132 Agonist. *Proc. Natl. Acad. Sci. USA* 112, E4825–E4834. doi:10.1073/pnas.1508737112
- De Vadder, F., Kovatcheva-Datchary, P., Goncalves, D., Vinera, J., Zitoun, C., Duchamp, A., et al. (2014). Microbiota-generated Metabolites Promote
- Metabolic Benefits via Gut-Brain Neural Circuits. *Cell* 156, 84–96. doi:10.1016/j.cell.2013.12.016
- Di Marzo, V. (2018). New Approaches and Challenges to Targeting the Endocannabinoid System. *Nat. Rev. Drug Discov.* 17, 623–639. doi:10.1038/nrd.2018.115
- Donvito, G., Piscitelli, F., Muldoon, P., Jackson, A., Vitale, R. M., D’Aniello, E., et al. (2019). N-Oleoyl-glycine Reduces Nicotine Reward and Withdrawal in Mice. *Neuropharmacology* 148, 320–331. doi:10.1016/j.neuropharm.2018.03.020
- Fukuchi, N., Isogai, A., Nakayama, J., Takayama, S., Yamashita, S., Suyama, K., et al. (1992). Isolation and Structural Elucidation of Syringostatin, Phytotoxins Produced by *Pseudomonas syringae* P. Syringae Lilac Isolate. *J. Chem. Soc. Perkin Trans. 1*, 875–880. doi:10.1039/P19920000875
- Fuqua, C., and Greenberg, E. P. (2002). Listening in on Bacteria: Acyl-Homoserine Lactone Signalling. *Nat. Rev. Mol. Cell Biol.* 3, 685–695. doi:10.1038/nrm907
- Gawrorisk, J. K. (1984). Tandem Reformatsky Reactions of 2-bromopropionates in the Presence of Chlorotrimethylsilane. *Tetrahedron Lett.* 25, 2605–2608. doi:10.1016/S0040-4039(01)81242-9
- Grandclément, C., Tannières, M., Moréra, S., Dessaux, Y., and Faure, D. (2016). Quorum quenching: Role in Nature and Applied Developments. *FEMS Microbiol. Rev.* 40, 86–116. doi:10.1093/femsrev/fuv038
- Hodgkinson, J. T., Galloway, W. R. J. D., Casoli, M., Keane, H., Su, X., Salmond, G. P. C., et al. (2011). Robust Routes for the Synthesis of N-Acylated-L-Homoserine

- Lactone (AHL) Quorum Sensing Molecules with High Levels of Enantiomeric Purity. *Tetrahedron Lett.* 52, 3291–3294. doi:10.1016/j.tetlet.2011.04.059
- Hon, Y. S., Hsieh, C. H., and Chen, H. F. (2007). Dibromomethane as One-Carbon Source in Organic Synthesis: Formal Total Synthesis of (±)-Nephrosteranic Acid. *Synth. Commun.* 37, 1635–1651. doi:10.1080/00397910701263767
- Horváth, I. T., and Anastas, P. T. (2007). Innovations and Green Chemistry. *Chem. Rev.* 107, 2169–2173. doi:10.1021/cr078380v
- Iannotti, F. A., and Di Marzo, V. (2021). The Gut Microbiome, Endocannabinoids and Metabolic Disorders. *J. Endocrinol.* 248, R83–R97. doi:10.1530/JOE-20-0444
- Jakob, B., Voss, G., and Gerlach, H. (1996). Synthesis of (S)- and (R)-3-Hydroxyhexadecanoic Acid. *Tetrahedron: Asymmetry* 7, 3255–3262. doi:10.1016/0957-4166(96)00426-0
- Li, C.-J., and Trost, B. M. (2008). Green Chemistry for Chemical Synthesis. *Proc. Natl. Acad. Sci.* 105, 13197–13202. doi:10.1073/pnas.0804348105
- Lynch, A., Crowley, E., Casey, E., Cano, R., Shanahan, R., McGlacken, G., et al. (2017). The Bacteroidales Produce an N-Acylated Derivative of glycine with Both Cholesterol-Solubilising and Hemolytic Activity. *Sci. Rep.* 7, 13270–13280. doi:10.1038/s41598-017-13774-6
- Lynch, A., Tammireddy, S. R., Doherty, M. K., Whitfield, P. D., and Clarke, D. J. (2019). The glycine Lipids of Bacteroides Thetaiotaomicron Are Important for Fitness during Growth *In Vivo* and *In Vitro*. *Appl. Environ. Microbiol.* 85, e02157. doi:10.1128/AEM.02157-18
- McNeil, N. I. (1984). The Contribution of the Large Intestine to Energy Supplies in Man. *Am. J. Clin. Nutr.* 39, 338–342. doi:10.1093/ajcn/39.2.338
- Morishita, T., Sato, A., Hisamoto, M., Oda, T., Matsuda, K., Ishii, A., et al. (1997). N-type Calcium Channel Blockers from a marine Bacterium, *Cytophaga* Sp. SANK 71996. *J. Antibiot.* 50, 457–468. doi:10.7164/antibiotics.50.457
- Nemoto, T., Ojika, M., Takahata, Y., Andoh, T., and Sakagami, Y. (1998). Structures of Topostins, DNA Topoisomerase I Inhibitors of Bacterial Origin. *Tetrahedron* 54, 2683–2690. doi:10.1016/S0040-4020(98)83004-4
- Nicolaou, K. C. (2014). Organic Synthesis: the Art and Science of Replicating the Molecules of Living Nature and Creating Others like Them in the Laboratory. *Proc. R. Soc. A.* 470, 20130690. doi:10.1098/rspa.2013.0690
- Oikawa, Y., Sugano, K., and Yonemitsu, O. (1978). Meldrum's Acid in Organic Synthesis. 2. A General and Versatile Synthesis of .beta.-keto Esters. *J. Org. Chem.* 43, 2087–2088. doi:10.1021/jo00404a066
- Piscotta, F. J., Whitfield, S. T., Nakashige, T. G., Estrela, A. B., Ali, T., and Brady, S. F. (2021). Multiplexed Functional Metagenomic Analysis of the Infant Microbiome Identifies Effectors of NF-Kb, Autophagy, and Cellular Redox State. *Cel. Rep.* 36, 109746. doi:10.1016/j.celrep.2021.109746
- Postler, T. S., and Ghosh, S. (2017). Understanding the Holobiont: How Microbial Metabolites Affect Human Health and Shape the Immune System. *Cel. Metab.* 26, 110–130. doi:10.1016/j.cmet.2017.05.008
- Saha, S., Rajpal, D. K., and Brown, J. R. (2016). Human Microbial Metabolites as a Source of New Drugs. *Drug Discov. Today* 21, 692–698. doi:10.1016/j.drudis.2016.02.009
- Smith, J. W., Romo, D., Ma, G., and Zancanella, M. (2009). *Beta-lactone Compounds*. US 2009/0124681 A1.
- Venkateswaran, A., Raman, B., Swanson, P., and Lewer, P. (2016). *Heterologous Expression of glycine N-Acyltransferase Proteins*. WO 2016/049487 A1. Indianapolis IN: WIPO.
- Vernocchi, P., Del Chierico, F., and Putignani, L. (2016). Gut Microbiota Profiling: Metabolomics Based Approach to Unravel Compounds Affecting Human Health. *Front. Microbiol.* 7, 1–21. doi:10.3389/fmicb.2016.01144
- Wang, M., Opare, P., and Boddy, C. N. (2009). Polyketide Synthase Thioesterases Catalyze Rapid Hydrolysis of Peptidyl Thioesters. *Bioorg. Med. Chem. Lett.* 19, 1413–1415. doi:10.1016/j.bmcl.2009.01.040

Conflict of Interest: The authors declare that the research was conducted in the absence of any commercial or financial relationships that could be construed as a potential conflict of interest.

Publisher's Note: All claims expressed in this article are solely those of the authors and do not necessarily represent those of their affiliated organizations, or those of the publisher, the editors and the reviewers. Any product that may be evaluated in this article, or claim that may be made by its manufacturer, is not guaranteed or endorsed by the publisher.

Copyright © 2022 Villano, Tinto and Di Marzo. This is an open-access article distributed under the terms of the Creative Commons Attribution License (CC BY). The use, distribution or reproduction in other forums is permitted, provided the original author(s) and the copyright owner(s) are credited and that the original publication in this journal is cited, in accordance with accepted academic practice. No use, distribution or reproduction is permitted which does not comply with these terms.



Pd@Py₂PZ@MSN as a Novel and Efficient Catalyst for C–C Bond Formation Reactions

Mohammad Hosein Sayahi^{1*}, Mansoureh Toosibashi², Mehdi Bahmaei¹, Hosein Lijan², Leila Ma'Mani³, Mohammad Mahdavi⁴ and Saeed Bahadorikhalili^{5*}

¹Department of Chemistry, Payame Noor University (PNU), Tehran, Iran, ²School of Chemistry, College of Science, University of Tehran, Tehran, Iran, ³Department of Nanotechnology, Agricultural Biotechnology Research Institute of Iran (ABRII), Agricultural Research Education and Extension Organization (AREEO), Karaj, Iran, ⁴Endocrinology and Metabolism Research Center, Endocrinology and Metabolism Clinical Sciences Institute, Tehran University of Medical Sciences, Tehran, Iran, ⁵Department of Electronic Engineering, Universitat Rovira i Virgili, Tarragona, Spain

OPEN ACCESS

Edited by:

Veroniki P. Vidali,
National Centre of Scientific Research
Demokritos, Greece

Reviewed by:

R. K. Sharma,
University of Delhi, India
Naeimeh Bahri-Laleh,
Iran Polymer and Petrochemical
Institute, Iran

*Correspondence:

Mohammad Hosein Sayahi
sayahymh@pnu.ac.ir
Saeed Bahadorikhalili
saeed.bahadorikhalili@urv.cat

Specialty section:

This article was submitted to
Organic Chemistry,
a section of the journal
Frontiers in Chemistry

Received: 17 December 2021

Accepted: 08 March 2022

Published: 31 March 2022

Citation:

Sayahi MH, Toosibashi M, Bahmaei M, Lijan H, Ma'Mani L, Mahdavi M and Bahadorikhalili S (2022) Pd@Py₂PZ@MSN as a Novel and Efficient Catalyst for C–C Bond Formation Reactions. *Front. Chem.* 10:838294. doi: 10.3389/fchem.2022.838294

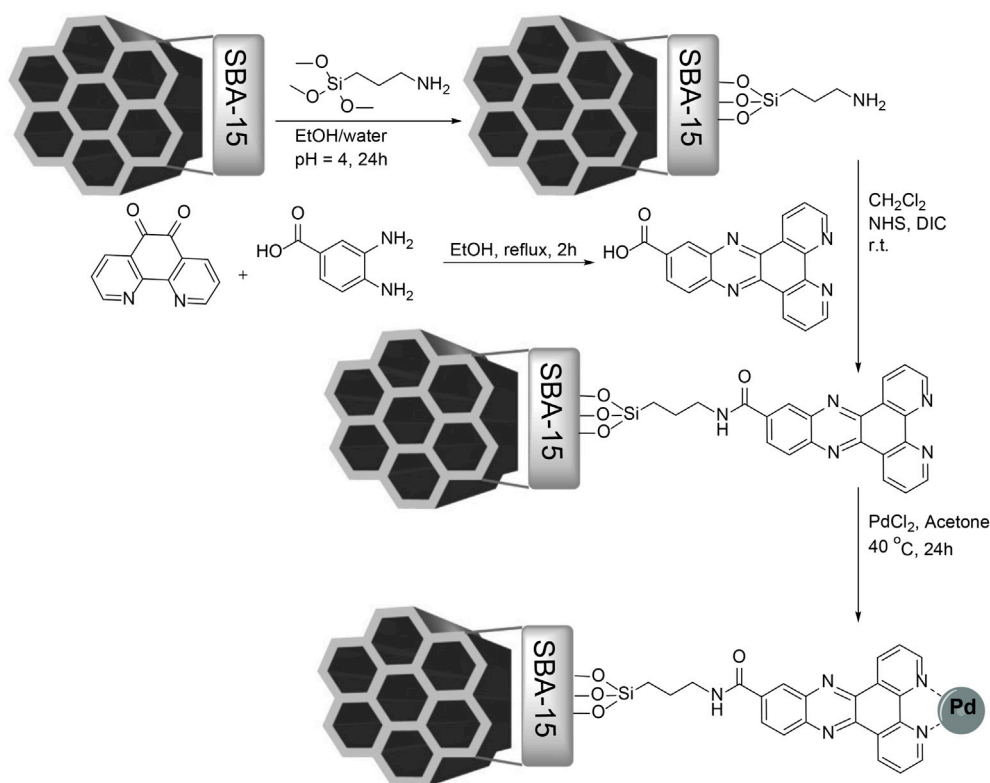
In this study, a novel catalyst is introduced based on the immobilization of palladium onto dipyrrodo (3,2-*a*:2',3'-*c*) phenazine–modified mesoporous silica nanoparticles. The dipyrrodo (3,2-*a*:2',3'-*c*) phenazine (Py₂PZ) ligand is synthesized in a simple method from the reaction of 1,10-phenanthroline-5,6-dione and 3,4-diaminobenzoic acid as starting materials. The ligand is used to functionalize mesoporous silica nanoparticles (MSNs) and modify their surface chemistry for the immobilization of palladium. The palladium-immobilized dipyrrodo (3,2-*a*:2',3'-*c*) phenazine–modified mesoporous silica nanoparticles (Pd@Py₂PZ@MSNs) are synthesized and characterized by several characterization techniques, including TEM, SEM, FT-IR, TGA, ICP, XRD, and EDS analyses. After the careful characterization of Pd@Py₂PZ@MSNs, the activity and efficiency of this catalyst is examined in carbon–carbon bond formation reactions. The results are advantageous in water and the products are obtained in high isolated yields. In addition, the catalyst showed very good reusability and did not show significant loss in activity after 10 sequential runs.

Keywords: palladium catalyst, immobilized catalyst, mesoporous silica nanoparticles, Heck reaction, Suzuki reaction

INTRODUCTION

Carbon–carbon bond formation reactions, especially palladium-catalyzed ones, are significant reactions in organic chemistry. Among all the palladium-catalyzed carbon–carbon bond formation reactions, Heck and Suzuki reactions have attracted interests due to their high applications in various organic syntheses (Bahadorikhalili and Mahdavi, 2018; Christoffel and Ward, 2018; Mpungose et al., 2018; González-Sebastián and Morales-Morales, 2019; Sherwood et al., 2019; Tashrifi et al., 2019; Easson et al., 2020; Fusini et al., 2020). Regarding the unique advantages of Heck and Suzuki reactions, these reactions are used for the synthesis of several compounds with complex chemical structures (Bahadorikhalili et al., 2018a; Bahadorikhalili et al., 2020; Reza Hajipour and Khorsandi, 2020; Yao et al., 2020; Zhou et al., 2020). Therefore, several efforts have been focused on the introduction of novel catalysts with improved characteristics (Hajipour et al., 2018; Ma et al., 2018).

An interesting approach for designing novel catalysts for Heck and Suzuki reactions is the immobilization of palladium onto modified nanoparticles. This method enables both the advantages



SCHEME 1 | Synthesis of the Pd@Py₂PZ@MSN catalyst.

of homogenous and heterogenous catalysts. Several nanoparticles including nanosilica (Isfahani et al., 2013; Khalafi-Nezhad and Panahi, 2014), nitrogen-rich polymers (Targhan et al., 2020), chitosan (Kumari et al., 2017), magnetic iron oxide (Bahadorikhalili et al., 2015; Ma'mani et al., 2014), and graphene oxide (Kumari et al., 2019) have been used as a support for palladium catalysts. Mesoporous silica nanoparticles (MSNs) are an interesting ordered porous material made of silica with high surface area and unique physical and chemical properties. MSNs are chemically and physically stable and are compatible with biological systems (Mehmood et al., 2017; Narayan et al., 2018; Jeelani et al., 2020). MSNs have been used in various applications, including catalysis (Bahadorikhalili et al., 2018b; Sayahi et al., 2020), drug delivery (Bharti et al., 2015; Moreira et al., 2016), tissue engineering (Rosenholm et al., 2016), and pollutant removal from air and solutions (Li et al., 2016; Gao et al., 2017; Zarandi, 2019). Based on the high surface area and stability and ease of functionalization of MSNs, this family of nanoporous materials has extensively been used as a support for catalysts in various reactions (Han et al., 2006; Lee et al., 2009; Sarkar et al., 2019; Xu et al., 2019).

In spite of many reports on the immobilization of the catalytic agents onto modified nanoparticles, several of them hold a number of disadvantages. It is critical to investigate this field and synthesize catalysts which are efficient and selective and, in an ideal case, have the possibility of use in green solvents. As an

interesting nanoparticle for the immobilization of the catalyst, MSNs are of high interest due to their advantages, including high surface area, high thermal stability, and high surface-active groups, which could be used for surface modifications. In this study, we introduce a novel palladium catalyst supported onto dipyrido (3,2-*a*:2',3'-*c*) phenazine-modified MSNs. The catalytic activity of Pd@Py₂PZ@MSNs is evaluated in Heck and Suzuki reactions. It should be noted that the palladium should be in the 0 oxidation state to catalyze the reaction (Zhang et al., 2006). Based on that, the catalyst should have been reduced to Pd (0) for efficiently catalyzing the reaction (Xiao et al., 2021).

RESULTS AND DISCUSSION

In this study, SBA-15 MSNs were synthesized using the hydrothermal method and modified by (3-aminopropyl) methoxysilane. Dipyrido (3,2-*a*:2',3'-*c*) phenazine (Py₂PZ) was synthesized in a one-step reaction between 3,4-diaminobenzoic acid and 1,10-phenanthroline-5,6-dione, which enables it to react with amine groups on the surface of MSNs *via* an amidation reaction to yield Py₂PZ@MSNs. The Pd@Py₂PZ@MSN catalyst was prepared using Py₂PZ@MSNs as a support, and it was fully characterized by various characterization techniques. The synthesis steps are presented in **Scheme 1**.

Electron microscopy images of the Pd@Py₂PZ@MSN catalyst are shown in **Figure 1**. The hexagonal meso-structure of the MSN

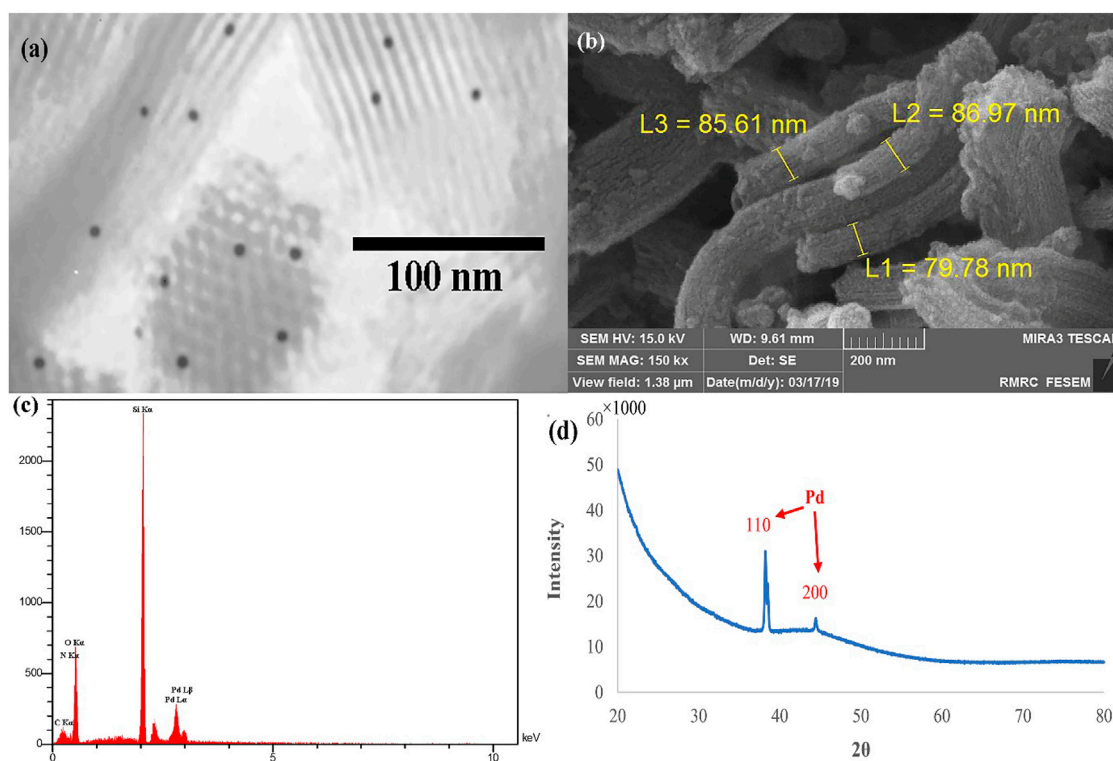


FIGURE 1 | (A) TEM; (B) SEM; (C) EDS; and (D) XRD results of the Pd@Py₂PZ@MSN catalyst.

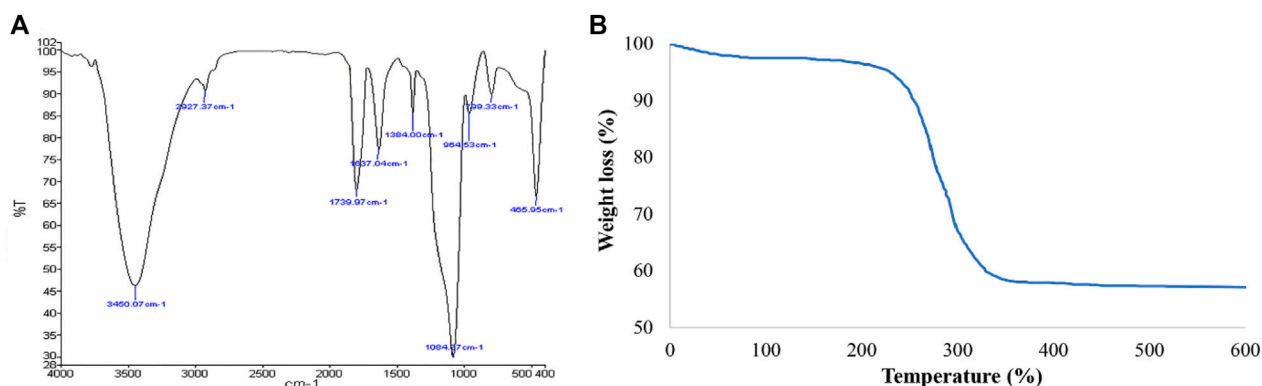


FIGURE 2 | (A) FT-IR; and (B) TGA results of the Pd@Py₂PZ@MSN catalyst.

backbone could be observed in the TEM image that Pd NPs appear as dark zones (**Figure 1A**). The rod-like structure of MSNs could clearly be observed in the SEM image (**Figure 1B**). In addition, the EDS analysis of the Pd@Py₂PZ@MSN catalyst confirms the presence of Pd in the structure of the catalyst (**Figure 1C**). As seen in **Figure 1D**, the XRD pattern of the Pd@Py₂PZ@MSN catalyst confirms that the crystallinity of the catalyst is similar to that of SBA-15 (Hu et al., 2016). In addition, the high-angle XRD confirms the presence of Pd NPs by two peaks of 110 and 200 planes at 2θ of 39.2 and 44.3°, respectively (**Figure 1D**).

To confirm the successful synthesis of Pd@Py₂PZ@MSNs, the FT-IR spectra of nanomaterials are compared (**Figure 2A**). In the FT-IR spectra of Pd@Py₂PZ@MSNs, a peak at 1084 cm⁻¹ represents Si–O vibrations in the structure of the catalyst. The hydroxyl groups of the catalyst could be observed at 3450 cm⁻¹, and the CH₂ stretching vibration is presented at 2927 cm⁻¹. The peak that appeared at 1739 cm⁻¹ is attributed to the C=O bond found in the ester moiety in the structure of the Pd@Py₂PZ@MSN catalyst.

The organic content in the structure of the catalyst was studied using TGA (**Figure 2B**). The TGA curve shows that the catalyst

TABLE 1 | Surface area and pore size results of MSN and the Pd@Py₂PZ@MSN catalyst.

	Surface area (m ² .g ⁻¹)	Pore width (nm)	Pore volume (cm ³ .g ⁻¹)
MSN	655.65	5.75	0.79
Pd@Py ₂ PZ@MSN	612.37	5.14	0.72

TABLE 2 | Optimization of the reaction of styrene and phenyl bromide in the presence of the Pd@Py₂PZ@MSN catalyst.

Entry	Solvent	Base (mol)	Catalyst (mol%)	Time (min)	Yield (%)
1	EtOH	TEA (1.5)	Pd@Py ₂ PZ@MSN (1.0)	120	61
2	MeOH	TEA (1.5)	Pd@Py ₂ PZ@MSN (1.0)	120	67
3	CH ₂ Cl ₂	TEA (1.5)	Pd@Py ₂ PZ@MSN (1.0)	120	47
4	DMF	TEA (1.5)	Pd@Py ₂ PZ@MSN (1.0)	120	59
5	H ₂ O	TEA (1.5)	Pd@Py ₂ PZ@MSN (1.0)	120	94
6	H ₂ O	NaOH (1.5)	Pd@Py ₂ PZ@MSN (1.0)	120	80
7	H ₂ O	KOH (1.5)	Pd@Py ₂ PZ@MSN (1.0)	120	87
8	H ₂ O	Pyridine (1.5)	Pd@Py ₂ PZ@MSN (1.0)	120	69
9	H ₂ O	K ₂ CO ₃	Pd@Py ₂ PZ@MSN (1.0)	120	77
10	H ₂ O	No base	Pd@Py ₂ PZ@MSN (1.0)	120	Trace
11	H ₂ O	TEA (0.5)	Pd@Py ₂ PZ@MSN (1.0)	120	55
12	H ₂ O	TEA (1.0)	Pd@Py ₂ PZ@MSN (1.0)	120	70
13	H ₂ O	TEA (2.0)	Pd@Py ₂ PZ@MSN (1.0)	120	94
14	H ₂ O	TEA (1.5)	Pd@Py ₂ PZ@MSN (0.5)	120	46
15	H ₂ O	TEA (1.5)	Pd@Py ₂ PZ@MSN (1.5)	120	94
16	H ₂ O	TEA (1.5)	Pd@Py ₂ PZ@MSN (1.0)	60	67
17	H ₂ O	TEA (1.5)	Pd@Py ₂ PZ@MSN (1.0)	150	94
18	H ₂ O	TEA (1.5)	Pd/C (1.0)	120	56
19	H ₂ O	TEA (1.5)	Pd(OAc) ₂ (1.0)	"	69
21	H ₂ O	TEA (1.5)	PdCl ₂ (1.0)	"	61
22	H ₂ O	TEA (1.5)	No catalyst	"	0

Reaction conditions: styrene (1 mmol); phenyl bromide (1 mmol); catalyst; solvent (5 ml); base; 25°C.

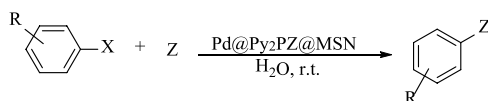
was thermally stable up to 250°C. A weight loss at the temperature of 250–350°C could be observed, which could be correlated to the degradation of organic moieties in the structure of the Pd@Py₂PZ@MSN catalyst. The palladium content in the structure of the catalyst was measured using ICP analysis. The results showed that the Pd content in the Pd@Py₂PZ@MSN catalyst was 0.12 mmol g⁻¹.

The surface area and pore size of the Pd@Py₂PZ@MSN catalyst were characterized using BET analysis and compared with those of MSNs. Based on the BET and nitrogen adsorption–desorption results, Py₂PZ@MSNs have a high surface area of 612.37 m² g⁻¹. In addition, the pore diameter and pore volume of the synthesized nanoporous support are 5.14 nm and 0.72 cm³ g⁻¹, respectively. The surface area, pore width, and pore volumes of MSNs are 655.37 m² g⁻¹, 5.75 nm, and 0.79 cm³ g⁻¹, respectively. The decrease in surface area, pore width, and pore volume of MSNs by the synthesis of the catalyst is expected, while functionalization of the nanoparticles leads to such changes. The surface area and pore size results of MSNs and the Pd@Py₂PZ@MSN catalyst are presented in **Table 1**.

After the characterization of the Pd@Py₂PZ@MSN catalyst, the efficiency of the catalyst was examined in carbon–carbon bond formation reactions. For this purpose, the Pd@Py₂PZ@MSN catalyst was used in Heck and Suzuki reactions. Initially, the optimal reaction conditions were evaluated by performing the reaction under different reaction conditions including various

solvents, bases, catalysts, and times of the reactions. To this end, the reaction of styrene and phenyl bromide was selected as a model reaction. The optimization results are presented in **Table 2**. According to the results, the best solvent for the reaction is water. However, the yields of the product were less in other solvents. Therefore, water was selected as the best solvent for the reaction. In addition, the results showed that the best yield of the product is obtained when the reaction is performed in the presence of 1 mol% of the catalyst. It should be noted that the presence of a base is critical for reaction performance. Therefore, the reaction was performed in the presence of several bases such as triethyl amine (TEA), NaOH, KOH, and pyridine. The results showed that TEA was the best base for the reaction. To study the role of the Pd@Py₂PZ@MSN catalyst in the reaction, a blank run was performed by all the reaction components, except the catalyst. No product was obtained in the absence of the catalyst. Therefore, the optimized reaction conditions were selected to be water as the solvent and 1.5 equivalent of triethyl amine base in the presence of 1.0 mol% of the Pd@Py₂PZ@MSN catalyst.

To rule out the presence of leached and homogenous Pd in the reaction mixture, in a run, the reaction was performed under the optimal reaction condition. After 60 min, the conversion of the substrates to the product measured by GC was 67%. Then, the catalyst was separated from the reaction mixture, and the filtrate was stirred under the same conditions for more 60 min.

TABLE 3 | Scope and generality of the Pd@Py₂PZ@MSN catalyst in Heck and Suzuki reactions^a.

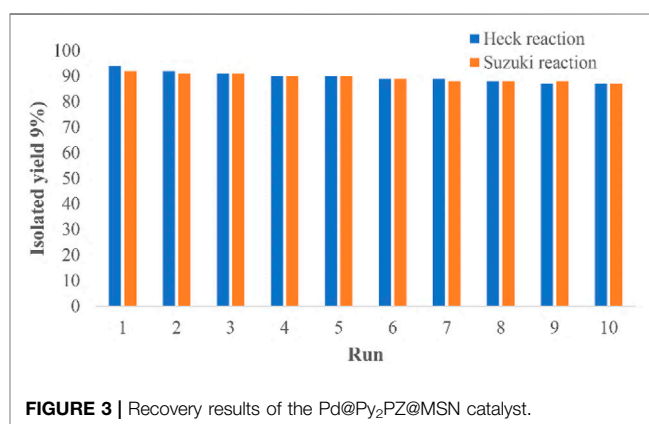
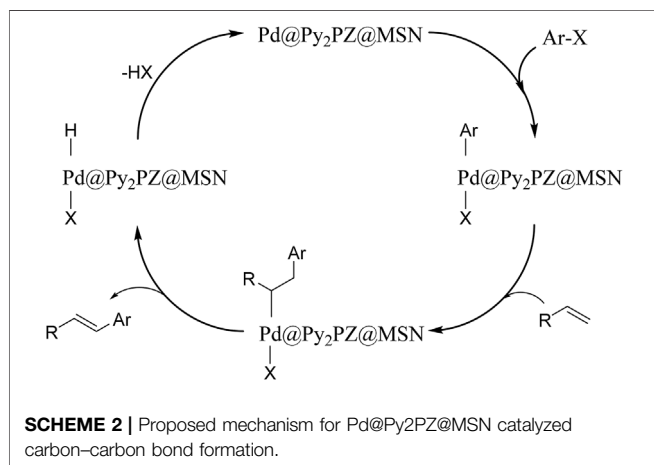
Entry	R	Z	X	Time (min)	Yield (%)	TON ^b	TOF ^c
1	H	Styrene	Br	120	94	9400	4700
2	H	Styrene	Cl	150	79	7900	3160
3	H	Styrene	I	120	96	9600	4800
4	4-Me	Styrene	Br	120	90	9000	4500
5	4-Me	Styrene	Cl	150	75	7500	3000
6	4-Me	Styrene	I	120	94	9400	4700
7	4-OMe	Styrene	Br	120	91	9100	4550
8	4-OMe	Styrene	I	120	93	9300	4650
9	4-NMe ₂	Styrene	Br	120	93	9300	4650
10	4-Cl	Styrene	Br	120	96	9600	4800
11	4-Cl	Styrene	Cl	150	70	8000	3200
12	4-CN	Styrene	Br	120	94	9400	4700
13	4-CN	Styrene	Cl	150	78	8800	3520
14	4-CHO	Styrene	Br	120	93	9300	4650
15	H	butyl acrylate	Br	120	96	9600	4800
16	H	butyl acrylate	Cl	150	82	8200	3280
17	H	butyl acrylate	I	90	96	9600	6400
18	4-Me	butyl acrylate	Br	120	89	8900	4450
19	4-Me	butyl acrylate	Cl	150	75	7500	3000
20	4-OMe	butyl acrylate	Br	120	91	9100	4550
21	4-OMe	butyl acrylate	Cl	150	76	7600	3040
22	4-CN	butyl acrylate	Br	120	94	9400	4700
23	4-CN	butyl acrylate	Cl	150	89	8900	3560
24	H	Ph(BOH) ₂	Br	120	92	9200	4600
25	H	Ph(BOH) ₂	I	150	97	9700	3880
26	4-Me	Ph(BOH) ₂	Br	120	88	8800	4400
27	4-Me	Ph(BOH) ₂	I	150	92	9200	3680
28	4-OMe	Ph(BOH) ₂	Br	120	84	8400	4200
29	4-Cl	Ph(BOH) ₂	Br	120	93	9300	4650
30	4-CN	Ph(BOH) ₂	Br	120	95	9500	4750
31	4-CN	Ph(BOH) ₂	I	150	99	9900	3960
32 ^d	H	Styrene	I	120	85	8500	4250
33 ^d	H	Ph(BOH) ₂	I	120	83	8300	4150

^aReaction conditions: styrene, butyl acrylate, or phenylboronic acid (1 mmol); phenyl halide (1 mmol); Pd@Py₂PZ@MSN catalyst (1 mol%); H₂O (5 ml); TEA (1.5 mmol); 25°C.

^bTON is calculated as the number of moles of the substrate converted to the product divided by the number moles of palladium catalyst.

^cTOF is defined as TON h⁻¹.

^dScale-up reactions: styrene or phenylboronic acid (10 mmol); phenyl bromide (10 mmol); Pd@Py₂PZ@MSN catalyst (1 mol%); H₂O (50 ml); TEA (15 mmol); 25°C.



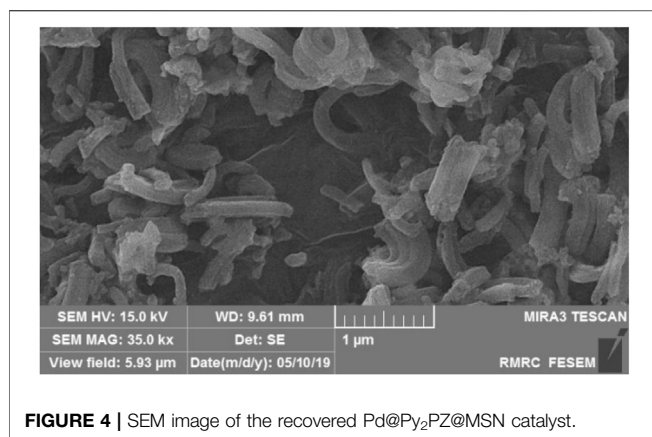


TABLE 4 | Surface area and pore size results of the recovered Pd@Py₂PZ@MSN catalyst.

Surface area (m ² .g ⁻¹)	Pore width (nm)	Pore volume (cm ³ .g ⁻¹)
607.21	5.09	0.70

The analysis of the product by GC showed that no more product has been obtained. These observations confirmed that the Pd catalyst worked in the heterogenous phase and the presence of the Pd@Py₂PZ@MSN catalyst was necessary for reaction performance.

Based on the optimized conditions, the scope and generality of the Pd@Py₂PZ@MSN catalyst were studied in Heck and Suzuki reactions. The structures and yields of the products are presented in **Table 3**. The high efficiency of the Pd@Py₂PZ@MSN catalyst in the mentioned reaction could clearly be observed. The catalyst is highly active in both Heck and Suzuki reactions, and advantageous results were obtained. All substrates with electron donating and electron withdrawing functionalities have given the desired products in high isolated yields. For example, entries 4–9, 18–22, and 26–28 with phenyl halides bearing electron-donating functionalities have provided the products in 84–93% yields. In addition, phenyl halides bearing electron-withdrawing functionalities (entries 10–14, 22–23, and 29–31) have successfully participated in the reaction and have given the products in 88–99% yields. In addition, a reaction was performed with 10 mmol of the substrates to evaluate the

possible scale up of the reaction. The results were advantageous, and high yields of the products were obtained in the scale-up reactions. To study the possibility of the use of the catalyst in industrial applications, scale-up reaction was performed under optimized conditions. The large-scale reaction of iodobenzene with styrene and phenylboronic acid has led to 85 and 83% yields, respectively.

A proposed mechanism was suggested, which is presented in **Scheme 2**. Based on the mechanism, the presence of the catalyst is critical for reaction performance. In the first step of the reaction, the catalyst activates the Ar–X bond, followed by the addition of the alkene. In the next step, the product is obtained, and the catalyst is ready for the next cycle of the reaction by the elimination of H–X.

A great advantage of the Pd@Py₂PZ@MSN catalyst is its reusability. For this purpose, the reaction was repeated for 10 sequential reactions, and the obtained results are presented in **Figure 3**. It could be seen that in both Heck and Suzuki reactions, no big loss in the activity of the catalyst is observed. It is significant to study the possible leaching of palladium from the catalyst. For studying the leaching of palladium from the Pd@Py₂PZ@MSN catalyst, a reaction was performed under the optimized reaction conditions. However, after 20 min when the reaction has not been completed, the catalyst was isolated from the reaction mixture. The reaction was continued without the catalyst for more than 3 h and based on GC analysis, no performance was observed in the reaction performance. In addition, the filtrate was studied by ICP, which did not show any leaching of palladium from the catalyst.

To show the structural stability of the catalyst during the reaction conditions, the catalyst was separated after the 5th reaction run and washed with water and ethanol. Then, the dried 5th re-used Pd@Py₂PZ@MSN catalyst was characterized by SEM and BET analysis. The results are presented in **Figure 4**; **Table 4**, respectively. Comparing the results of the recovered catalyst with the fresh ones confirm the good stability of the catalyst during the reactions.

To better study the activity of the catalyst, Pd@Py₂PZ@MSNs were compared with the previously reported catalysts. **Table 5** presents the catalysts, reaction conditions, and isolated yields of the reactions for the reaction of styrene and bromobenzene. According to the results, the best performance is observed for Pd@Py₂PZ@MSNs, and the reaction is performed under mild reaction conditions.

TABLE 5 | Comparison of the catalytic activity of Pd@Py₂PZ@MSN with the previously reported one.

Entry	Catalyst	Conditions	Time (h)	Yields ^a (%) ^{ref}
1	Pd/TiO ₂ NP	DMF, Et ₃ N, 140°C	10	93 Nasrollahzadeh et al. (2014)
2	Pd/SMNPs-DF	Solvent free, DABCO, 140°C	0.9	93 Zolfigol et al. (2014)
3	CO-NHC@MWCNTs	PEG, Li ₂ CO ₃ , 80°C	10	67 Hajipour and Khorsandi, (2016)
4	Pd/MPCS-TI	DMF/H ₂ O, Et ₃ N, 110°C	4	93 Movassagh and Rezaei, (2015)
5	Pd/BIP-silica-Fe ₂ O ₃	DMF, Et ₃ N, 100°C	3.5	82 Sobhani et al. (2015)
6	Pd/Guanidine/graphene	EtOH/H ₂ O, K ₂ CO ₃ , r.t.	2	92 Ma'mani et al. (2014)
7	This work	H ₂ O, TEA, 25°C	1	94

^aIsolated yields.

EXPERIMENTAL

General Remarks

All the chemicals, reagents, and solvents were purchased from Merck, Germany, and Sigma, Germany. TEM images were recorded using a CM 10 Philips instrument. ¹H (500 MHz) spectra were recorded using a Bruker Advance spectrometer in DMSO and d₆ solution with tetramethylsilane (TMS) as an internal standard. A TESCAN T3000 instrument was used to record the SEM images. An OPTIMA7300DV ICP analyzer was used for analyzing the palladium content of the catalyst. The FT-IR spectra were recorded on a Nicolet Magna FT-IR 550 spectrophotometer using potassium bromide disks. BET of the samples was analyzed using an ASAPTM micromeritics 2020 instrument. The particle size was measured using the HORIBA SZ100-Z DLS instrument. The thermogravimetric analyzer (TGA) at a heating rate of 10°C min^{−1} over the temperature range of 40–600°C under nitrogen atmosphere was used.

Synthesis of the Py₂PZ Ligand

1,10-phenanthroline-5,6-dione (1.05 g, 5 mmol) and 3,4-diaminobenzoic acid (0.76 g, 5 mmol) were dissolved in ethanol and refluxed for 2 h. The reaction progress was monitored by TLC monitoring. After the reaction was completed, the solvent was evaporated and the product was purified by recrystallization from ethanol.

Synthesis of the Pd@Py₂PZ@MSN Catalyst

SBA-15 was synthesized according to the previously reported method (Chaudhary and Sharma, 2017). A mixture containing MSNs (0.5 g) in ethanol/deionized water (1:2, 30 ml) and HCl (pH = 4) was prepared and sonicated for 30 min. A solution of (3-aminopropyl) methoxysilane (1 g) in ethanol (30 ml) was prepared and added drop-wise to the aforementioned mixture by vigorous stirring. The reaction mixture was stirred for 24 h, and then the product was separated by filtration and washed with deionized water and ethanol. The product was dried at 70°C in vacuum for 12 h to obtain amine-modified mesoporous SBA-15.

A mixture of amine-modified mesoporous SBA-15 (0.5 g) in dichloromethane (75 ml) was sonicated for 30 min. Then, dipyrdo (3,2-*a*:2',3'-*c*) phenazine-11-carboxylic acid (1.6 g, 5 mmol) in dichloromethane (25 ml) was added and 1-ethyl-3-(3-dimethylaminopropyl) carbodiimide (5 mmol, 1 eq) and *N*-hydroxysuccinimide (5.5 mmol, 1.1 eq) were added. The reaction mixture was stirred overnight at room temperature. The product was separated from the reaction mixture and washed with ethanol and dried for 12 h in a vacuum oven.

The solid support (0.5 g) was added to dry acetone and sonicated for 30 min. Then, PdCl₂ (1 mmol) was added, and the reaction mixture was stirred at 40°C under an inert atmosphere for 24 h. The Pd@Py₂PZ@MSN catalyst was separated from the reaction mixture by centrifugation, washed thoroughly with EtOH and diethyl ether, and dried under vacuum at room temperature for 12 h.

General Procedure for the Carbon–Carbon Bond Formation Reactions

Phenyl halide (1 mmol), alkene (1.1 mmol, in case of Heck reaction), phenylboronic acid (1.0 mmol, in case of Suzuki reaction), triethyl amine (1.5 mmol), and the Pd@Py₂PZ@MSN catalyst (1.0 mol%) were added into a flask containing H₂O (5 ml) and stirred at room temperature. When the TLC monitoring showed reaction completion, the catalyst was separated from the reaction mixture and washed with water and EtOH. The product was extracted with ethyl acetate. The organic phase was collected and dried over sodium sulfate. The solvent was evaporated, and the product was purified by column chromatography using *n*-hexane:ethyl acetate (6:1) as the eluent to obtain the pure product.

Recovery of the Nanocatalyst

The reaction of phenyl bromide (1 mmol) and styrene (1.1 mmol) was selected as a model reaction and was performed in the presence of the Pd@Py₂PZ@MSN catalyst under optimal reaction conditions. After the reaction was completed, the catalyst was separated from the reaction mixture and washed with water and used in the next reaction under the same conditions. The reactions were performed for 10 sequential runs.

CONCLUSION

In conclusion, Pd@Py₂PZ@MSN as a novel catalyst was designed, synthesized, and characterized based on the immobilization of palladium onto the modified SBA-15 MSNs. The catalyst was characterized using several methods, and the structure of the catalyst was confirmed. The activity of the Pd@Py₂PZ@MSN catalyst was evaluated in Heck and Suzuki reactions. The catalyst showed the best activity in water as the solvent in the presence of triethyl amine base. Several substrates with different functionalities were used and, in all cases, the desired compounds were synthesized in good isolated yields. As an advantage, the catalyst showed very good reusability after 10 sequential runs.

DATA AVAILABILITY STATEMENT

The raw data supporting the conclusions of this article will be made available by the authors, without undue reservation.

AUTHOR CONTRIBUTIONS

SB and MS defined the experiments. MT, MB, and HL ran the experiments and collected the data. MS, LM'M, and MM analyzed the data. SB prepared the manuscript.

REFERENCES

- Bahadorikhalili, S., Ma'mani, L., Mahdavi, H., and Shafiee, A. (2018b). Copper Supported β -cyclodextrin Functionalized PEGylated Mesoporous Silica Nanoparticle-graphene Oxide Hybrid: An Efficient and Recyclable Nano-Catalyst for Straightforward Synthesis of 2-arylbenzimidazoles and 1,2,3-triazoles. *Microporous Mesoporous Mater.* 262, 207–216. doi:10.1016/j.micromeso.2017.11.046
- Bahadorikhalili, S., and Mahdavi, H. (2018). Palladium Magnetic Nanoparticle-Polyethersulfone Composite Membrane as an Efficient and Versatile Catalytic Membrane Reactor. *Polym. Adv. Technol.* 29, 1138–1149. doi:10.1002/pat.4225
- Bahadorikhalili, S., Mahdavi, M., Ma'mani, L., Shafiee, A., Mahdavi, H., and Akbarzadeh, T. (2018a). Palladium Functionalized Phosphinite Polyethyleneimine Grafted Magnetic Silica Nanoparticles as an Efficient Catalyst for the Synthesis of Isoquinolino[1,2-B]quinazolin-8-Ones. *New J. Chem.* 42, 5499–5507. doi:10.1039/c7nj04837h
- Bahadorikhalili, S., Ma'mani, L., Mahdavi, H., and Shafiee, A. (2015). Palladium Catalyst Supported on PEGylated Imidazolium Based Phosphinite Ionic Liquid-Modified Magnetic Silica Core-Shell Nanoparticles: a Worthy and Highly Water-Dispersible Catalyst for Organic Reactions in Water. *RSC Adv.* 5, 71297–71305. doi:10.1039/c5ra12747e
- Bahadorikhalili, S., Ma'mani, L., Lijan, H., and Mahdavi, M. (2020). γ -Fe₂O₃@SiO₂(CH₂)₃-HPBM-Pd as a Versatile Boosted Nanocatalyst for CarbonCarbon Bond Formation. *Mater. Today Commun.* 26, 101913. doi:10.1016/j.mtcomm.2020.101913
- Bharti, C., Gulati, N., Nagaich, U., and Pal, A. (2015). Mesoporous Silica Nanoparticles in Target Drug Delivery System: A Review. *Int. J. Pharma Investig.* 5, 124. doi:10.4103/2230-973x.160844
- Chaudhary, V., and Sharma, S. (2017). An Overview of Ordered Mesoporous Material SBA-15: Synthesis, Functionalization and Application in Oxidation Reactions. *J. Porous Mater.* 24, 741–749. doi:10.1007/s10934-016-0311-z
- Christoffel, F., and Ward, T. R. (2018). Palladium-catalyzed Heck Cross-Coupling Reactions in Water: A Comprehensive Review. *Catal. Lett.* 148, 489–511. doi:10.1007/s10562-017-2285-0
- Easson, M. W., Jordan, J. H., Bland, J. M., Hinchliffe, D. J., and Condon, B. D. (2020). Application of Brown Cotton-Supported Palladium Nanoparticles in Suzuki-Miyaura Cross-Coupling Reactions. *ACS Appl. Nano Mater.* 3, 6304–6309. doi:10.1021/acsnm.0c01303
- Fusini, G., Rizzo, F., Angelici, G., Pitzalis, E., Evangelisti, C., and Carpita, A. (2020). Polyvinylpyridine-Supported Palladium Nanoparticles: An Efficient Catalyst for Suzuki-Miyaura Coupling Reactions. *Catalysts* 10, 330. doi:10.3390/catal10030330
- Gao, J., Lei, H., Han, Z., Shi, Q., Chen, Y., and Jiang, Y. (2017). Dopamine Functionalized Tannic-Acid-Templated Mesoporous Silica Nanoparticles as a New Sorbent for the Efficient Removal of Cu²⁺ from Aqueous Solution. *Sci. Rep.* 7, 45215. doi:10.1038/srep45215
- González-Sebastián, L., and Morales-Morales, D. (2019). Cross-coupling Reactions Catalysed by Palladium Pincer Complexes. A Review of Recent Advances. *J. Organomet. Chem.* 893, 39–51. doi:10.1016/j.jorganchem.2019.04.021
- Hajipour, A. R., and Khorsandi, Z. (2016). Multi Walled Carbon Nanotubes Supported N-Heterocyclic Carbene-Cobalt (II) as a Novel, Efficient and Inexpensive Catalyst for the Mizoroki-Heck Reaction. *Catal. Commun.* 77, 1–4. doi:10.1016/j.catcom.2015.12.027
- Hajipour, A. R., Sadeghi, A. R., and Khorsandi, Z. (2018). Pd Nanoparticles Immobilized on Magnetic Chitosan as a Novel Reusable Catalyst for green Heck and Suzuki Cross-coupling Reaction: In Water at Room Temperature. *Appl. Organometal Chem.* 32, e4112. doi:10.1002/aoc.4112
- Han, Y.-F., Chen, F., Zhong, Z., Ramesh, K., Chen, L., and Widjaja, E. (2006). Controlled Synthesis, Characterization, and Catalytic Properties of Mn₂O₃ and Mn₃O₄ Nanoparticles Supported on Mesoporous Silica SBA-15. *J. Phys. Chem. B* 110, 24450–24456. doi:10.1021/jp064941v
- Hu, G., Li, W., Xu, J., He, G., Ge, Y., Pan, Y., et al. (2016). Substantially Reduced Crystallization Temperature of SBA-15 Mesoporous Silica in NaNO₃ Molten Salt. *Mater. Lett.* 170, 179–182. doi:10.1016/j.matlet.2016.02.030
- Isfahani, A. L., Mohammadpoor-Baltork, I., Mirkhani, V., Khosropour, A. R., Moghadam, M., Tangestaninejad, S., et al. (2013). Palladium Nanoparticles Immobilized on Nano-Silica Triazine Dendritic Polymer (Pdn-pNSTDP): An Efficient and Reusable Catalyst for Suzuki-Miyaura Cross-Coupling and Heck Reactions. *Adv. Synth. Catal.* 355, 957–972. doi:10.1002/adsc.201200707
- Jeelani, P. G., Mulay, P., Venkat, R., and Ramalingam, C. (2020). Multifaceted Application of Silica Nanoparticles. A Review. *Silicon* 12, 1337–1354. doi:10.1007/s12633-019-00229-y
- Khalafi-Nezhad, A., and Panahi, F. (2014). Size-Controlled Synthesis of Palladium Nanoparticles on a Silica-Cyclodextrin Substrate: A Novel Palladium Catalyst System for the Heck Reaction in Water. *ACS Sustain. Chem. Eng.* 2, 1177–1186. doi:10.1021/sc5000122
- Kumari, S., Layek, S., and Pathak, D. D. (2017). Palladium Nanoparticles Immobilized on a Magnetic Chitosan-Anchored Schiff Base: Applications in Suzuki-Miyaura and Heck-Mizoroki Coupling Reactions. *New J. Chem.* 41, 5595–5604. doi:10.1039/C7NJ00283A
- Kumari, S., Mittal, A., Kumar, A., and Sharma, S. K. (2019). Palladium Nanoparticles Immobilized on Schiff Base-Functionalized Graphene-Oxide: Application in Carbon-Carbon Cross-Coupling Reactions. *ChemistrySelect* 4, 10828–10837. doi:10.1002/slct.201902242
- Lee, B., Ma, Z., Zhang, Z., Park, C., and Dai, S. (2009). Influences of Synthesis Conditions and Mesoporous Structures on the Gold Nanoparticles Supported on Mesoporous Silica Hosts. *Microporous Mesoporous Mater.* 122, 160–167. doi:10.1016/j.micromeso.2009.02.029
- Li, D., Egodawatte, S., Kaplan, D. I., Larsen, S. C., Serkiz, S. M., and Seaman, J. C. (2016). Functionalized Magnetic Mesoporous Silica Nanoparticles for U Removal from Low and High pH Groundwater. *J. Hazard. Mater.* 317, 494–502. doi:10.1016/j.jhazmat.2016.05.093
- Ma, R., Yang, P., and Bian, F. (2018). Magnetic Dendritic Polymer Nanocomposites as Supports for Palladium: a Highly Efficient and Reusable Catalyst for Mizoroki-Heck and Suzuki-Miyaura Coupling Reactions. *New J. Chem.* 42, 4748–4756. doi:10.1039/c7nj05014c
- Ma'mani, L., Miri, S., Mahdavi, M., Bahadorikhalili, S., Lotfi, E., Foroumadi, A., et al. (2014). Palladium Catalyst Supported on N-Aminoguanidine Functionalized Magnetic Graphene Oxide as a Robust Water-Tolerant and Versatile Nanocatalyst. *RSC Adv.* 4, 48613–48620. doi:10.1039/c4ra07130a
- Mehmood, A., Ghafar, H., Yaqoob, S., Gohar, U. F., and Ahmad, B. (2017). Mesoporous Silica Nanoparticles: a Review. *J. Dev. Drugs* 6, 1–14. doi:10.4172/2329-6631.1000174
- Moreira, A. F., Dias, D. R., and Correia, I. J. (2016). Stimuli-responsive Mesoporous Silica Nanoparticles for Cancer Therapy: A Review. *Microporous Mesoporous Mater.* 236, 141–157. doi:10.1016/j.micromeso.2016.08.038
- Movassagh, B., and Rezaei, N. (2015). A Magnetic Porous Chitosan-Based Palladium Catalyst: a green, Highly Efficient and Reusable Catalyst for Mizoroki-Heck Reaction in Aqueous media. *New J. Chem.* 39, 7988–7997. doi:10.1039/c5nj01337b
- Mpungose, P., Vundla, Z., Maguire, G., and Friedrich, H. (2018). The Current Status of Heterogeneous Palladium Catalysed Heck and Suzuki Cross-Coupling Reactions. *Molecules* 23, 1676. doi:10.3390/molecules23071676
- Narayan, R., Nayak, U., Raichur, A., and Garg, S. (2018). Mesoporous Silica Nanoparticles: A Comprehensive Review on Synthesis and Recent Advances. *Pharmaceutics* 10, 118. doi:10.3390/pharmaceutics10030118
- Nasrollahzadeh, M., Azarian, A., Ehsani, A., and Khalaj, M. (2014). Preparation, Optical Properties and Catalytic Activity of TiO₂ @Pd Nanoparticles as Heterogeneous and Reusable Catalysts for Ligand-free Heck Coupling Reaction. *J. Mol. Catal. A: Chem.* 394, 205–210. doi:10.1016/j.molcata.2014.06.033
- Reza Hajipour, A., and Khorsandi, Z. (2020). Asymmetric Intermolecular Heck Reaction of Aryl Halides by Pd-Histidine Organocatalysts. *Mod. Chem.* 8, 18. doi:10.11648/j.mc.20200802.11
- Rosenholm, J. M., Zhang, J., Linden, M., and Sahlgren, C. (2016). Mesoporous Silica Nanoparticles in Tissue Engineering - a Perspective. *Nanomedicine* 11, 391–402. doi:10.2217/nnm.15.212
- Sarkar, C., Pendem, S., Shrotri, A., Dao, D. Q., Pham Thi Mai, P., Nguyen Ngoc, T., et al. (2019). Interface Engineering of Graphene-Supported Cu Nanoparticles Encapsulated by Mesoporous Silica for Size-dependent Catalytic Oxidative Coupling of Aromatic Amines. *ACS Appl. Mater. Inter.* 11, 11722–11735. doi:10.1021/acsmi.8b18675
- Sayahi, M. H., Bahadorikhalili, S., Saghanzad, S. J., Miller, M. A., and Mahdavi, M. (2020). Sulfonic Acid-Functionalized Poly(4-Styrenesulfonic Acid)

- Mesoporous Graphene Oxide Hybrid for One-Pot Preparation of Coumarin-Based Pyrido[2,3-D]pyrimidine-Dione Derivatives. *Res. Chem. Intermed* 46, 491–507. doi:10.1007/s11164-019-03962-6
- Sherwood, J., Clark, J. H., Fairlamb, I. J. S., and Slattery, J. M. (2019). Solvent Effects in Palladium Catalysed Cross-Coupling Reactions. *Green. Chem.* 21, 2164–2213. doi:10.1039/c9gc00617f
- Sobhani, S., Zeraatkar, Z., and Zarifi, F. (2015). Pd Complex of an NNN Pincer Ligand Supported on γ -Fe₂O₃@SiO₂ Magnetic Nanoparticles: a New Catalyst for Heck, Suzuki and Sonogashira Coupling Reactions. *New J. Chem.* 39, 7076–7085. doi:10.1039/c5nj00344j
- Targhan, H., Hassanpour, A., Sohrabnezhad, S., and Bahrami, K. (2020). Palladium Nanoparticles Immobilized with Polymer Containing Nitrogen-Based Ligand: A Highly Efficient Catalyst for Suzuki-Miyaura and Mizoroki-Heck Coupling Reactions. *Catal. Lett.* 150, 660–673. doi:10.1007/s10562-019-02981-7
- Tashrfi, Z., Bahadorikhalili, S., Lijan, H., Ansari, S., Hamedifar, H., and Mahdavi, M. (2019). Synthesis and Characterization of γ -Fe₂O₃@SiO₂-(CH₂)₃-PDTC-Pd Magnetic Nanoparticles: a New and Highly Active Catalyst for the Heck/Sonogashira Coupling Reactions. *New J. Chem.* 43, 8930–8938. doi:10.1039/c9nj01562k
- Xiao, J., Zhang, H., Ejike, A. C., Wang, L., Tao, M., and Zhang, W. (2021). Phenanthroline Functionalized Polyacrylonitrile Fiber with Pd(0) Nanoparticles as a Highly Active Catalyst for the Heck Reaction. *Reactive Funct. Polym.* 161, 104843. doi:10.1016/j.reactfunctpolym.2021.104843
- Xu, J., Qu, Z., Wang, Y., and Huang, B. (2019). HCHO Oxidation over Highly Dispersed Au Nanoparticles Supported on Mesoporous Silica with superior Activity and Stability. *Catal. Today* 327, 210–219. doi:10.1016/j.cattod.2018.04.051
- Yao, T., Zhang, F., Zhang, J., and Liu, L. (2020). Palladium-Catalyzed Intermolecular Heck-type Dearomative [4 + 2] Annulation of 2H-Isoindole Derivatives with Internal Alkynes. *Org. Lett.* 22, 5063–5067. doi:10.1021/acs.orglett.0c01643
- Zarandi, A. F. (2019). Air Pollution Method: A New Method Based on Ionic Liquid Passed on Mesoporous Silica Nanoparticles for Removal of Manganese Dust in the Workplace Air. *Anal. Methods Environ. Chem. J.* 2, 5–14. doi:10.24200/amecj.v2.i01.52
- Zhang, Z., Zha, Z., Gan, C., Pan, C., Zhou, Y., Wang, Z., et al. (2006). Catalysis and Regioselectivity of the Aqueous Heck Reaction by Pd(0) Nanoparticles under Ultrasonic Irradiation. *J. Org. Chem.* 71 (11), 4339–4342. doi:10.1021/jo060372b
- Zhou, B., Wang, H., Cao, Z. Y., Zhu, J. W., Liang, R. X., Hong, X., et al. (2020). Dearomative 1,4-difunctionalization of Naphthalenes via Palladium-Catalyzed Tandem Heck/Suzuki Coupling Reaction. *Nat. Commun.* 11, 4380. doi:10.1038/s41467-020-18137-w
- Zolfigol, M. A., Azadbakht, T., Khakyzadeh, V., Nejatyami, R., and Perrin, D. M. (2014). C(sp²)-C(sp²) Cross Coupling Reactions Catalyzed by an Active and Highly Stable Magnetically Separable Pd-Nanocatalyst in Aqueous media. *RSC Adv.* 4, 40036–40042. doi:10.1039/c4ra06097k

Conflict of Interest: The authors declare that the research was conducted in the absence of any commercial or financial relationships that could be construed as a potential conflict of interest.

Publisher's Note: All claims expressed in this article are solely those of the authors and do not necessarily represent those of their affiliated organizations, or those of the publisher, the editors, and the reviewers. Any product that may be evaluated in this article, or claim that may be made by its manufacturer, is not guaranteed or endorsed by the publisher.

Copyright © 2022 Sayahi, Toosibashi, Bahmaei, Lijan, Ma'Mani, Mahdavi and Bahadorikhalili. This is an open-access article distributed under the terms of the Creative Commons Attribution License (CC BY). The use, distribution or reproduction in other forums is permitted, provided the original author(s) and the copyright owner(s) are credited and that the original publication in this journal is cited, in accordance with accepted academic practice. No use, distribution or reproduction is permitted which does not comply with these terms.



A Novel Antimalarial Metabolite in Erythrocyte From the Hydroxylation of Dihydroartemisinin by *Cunninghamella elegans*

Yue Bai[†], Yifan Zhao[†], Xinna Gao, Dong Zhang, Yue Ma*, Lan Yang* and Peng Sun*

Institute of Chinese Materia Medica, Artemisinin Research Center, Academy of Chinese Medical Sciences, Beijing, China

OPEN ACCESS

Edited by:

Veroniki P. Vidali,
National Centre of Scientific Research
Demokritos, Greece

Reviewed by:

Guillermo R. Labadie,
National University of Rosario,
Argentina
Junmin Zhang,
Lanzhou University, China

*Correspondence:

Yue Ma
yma@icmm.ac.cn
Lan Yang
lyang@icmm.ac.cn
Peng Sun
psun@icmm.ac.cn

[†]These two authors contributed
equally to this work

Specialty section:

This article was submitted to
Green and Sustainable Chemistry,
a section of the journal
Frontiers in Chemistry

Received: 07 January 2022

Accepted: 22 March 2022

Published: 26 April 2022

Citation:

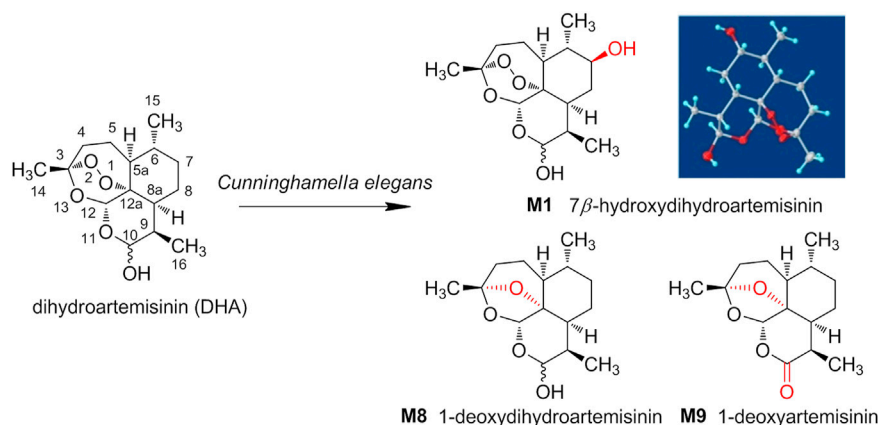
Bai Y, Zhao Y, Gao X, Zhang D, Ma Y,
Yang L and Sun P (2022) A Novel
Antimalarial Metabolite in Erythrocyte
From the Hydroxylation of
Dihydroartemisinin by
Cunninghamella elegans.
Front. Chem. 10:850133.
doi: 10.3389/fchem.2022.850133

Dihydroartemisinin (DHA) is a sesquiterpene endoperoxide with prominent antimalarial efficacy, which was discovered by Professor Youyou Tu through the reduction of artemisinin in the 1970s. It is always a challenging work for scientists to investigate the metabolites of DHA in the red blood cells due to the complicated matrix background. As a bottleneck, the investigation of metabolites, especially exploring the pharmacodynamic material in the red blood cell, is necessary and significant for metabolism research of antimalarial agent. Recently, microbial transformation provides a green and economical means for mimicking mammal metabolism and synthesis active metabolites, based on which is one efficient route for drug discovery. In this study, a strain from *Cunninghamella* was employed as an efficient tool to explore active metabolites of DHA in erythrocyte. Microbial transformation products of DHA by *Cunninghamella elegans* CICC 40250 were detected and analyzed by ultra-performance liquid chromatography (UPLC)-electrospray ionization (ESI)-quadrupole time-of-flight (Q-TOF)-mass spectrometry (MS^E), and the main products were isolated and identified. The antimalarial activity of the isolated products was also screened *in vitro*. Totally, nine products were discovered through UPLC-ESI-QTOF-MS^E, and three main products with novel chemical structures were isolated for the first time, which were also detected in red blood cells as the metabolites of DHA. After evaluation, 7 β -hydroxydihydroartemisinin (**M1**) exhibited a good antimalarial activity with an IC₅₀ value of 133 nM against *Plasmodium falciparum* (Pf.) 3D7. The structure and stereo-configuration of novel compound **M1** were validated via X-ray single crystal diffraction. Microbial transformation was firstly employed as the appropriate model for metabolic simulation in erythrocyte of DHA. Three novel metabolites in erythrocyte were obtained for the first time through our microbial model, and one of which was found to show moderate antimalarial activity. This work provided a new research foundation for antimalarial drug discovery.

Keywords: dihydroartemisinin, microbial transformation, active metabolites in erythrocyte, hydroxylation, antimalarial activity

INTRODUCTION

Dihydroartemisinin (DHA), a famous derivative of artemisinin (Qinghaosu, ART) through C-10 reduction of lactone carbonyl by sodium borohydride, was discovered by Youyou Tu in 1973 (Tu, 2009; Tu, 2016). Owing to their excellent antimalarial activity compared to artemisinin, DHA and its derivatives have been employed as the first-line drugs to treat malarial for several decades (World



SCHEME 1 | The structures of dihydroartemisinin (DHA) and its derivatives from *Cunninghamella elegans*.

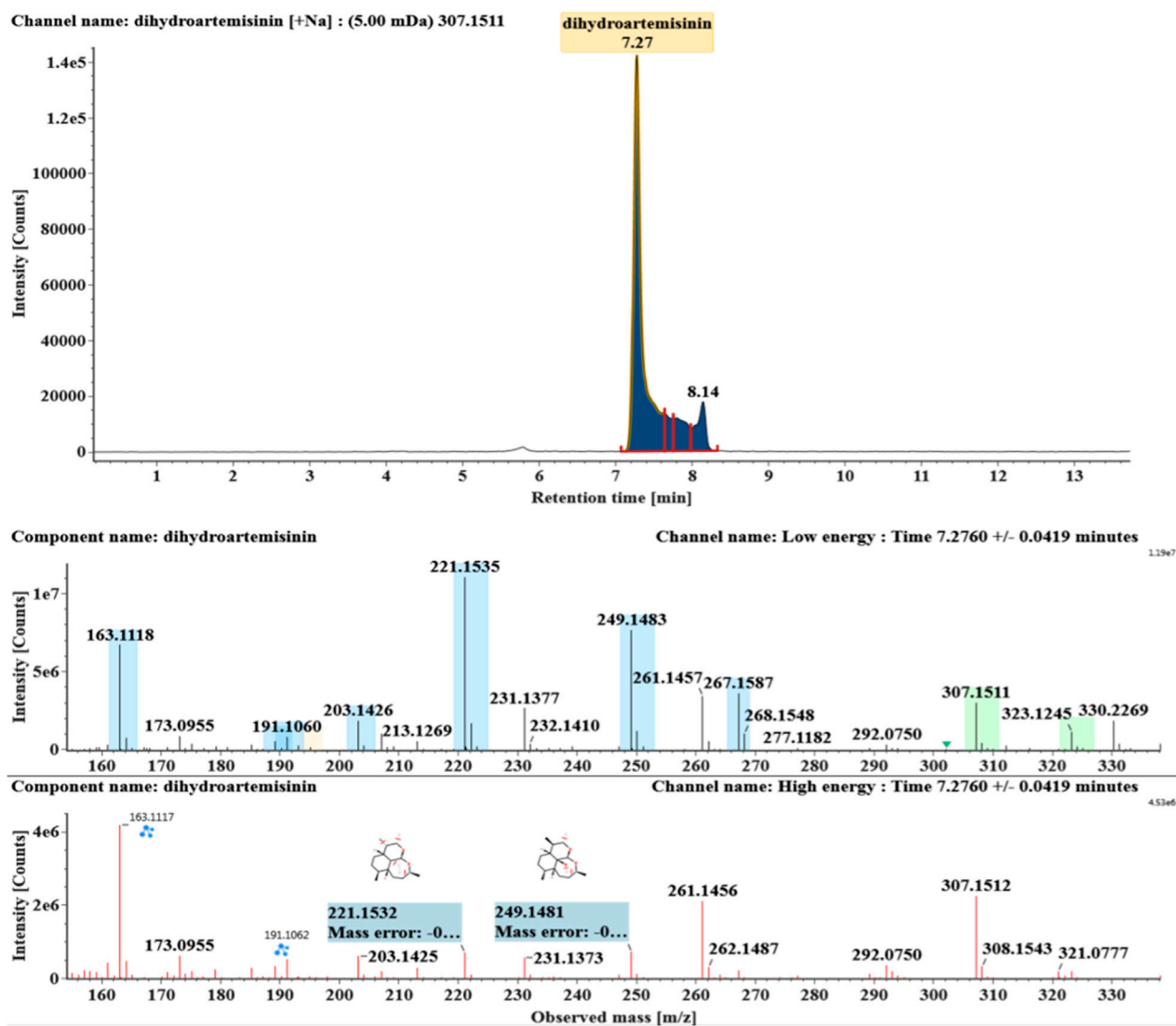
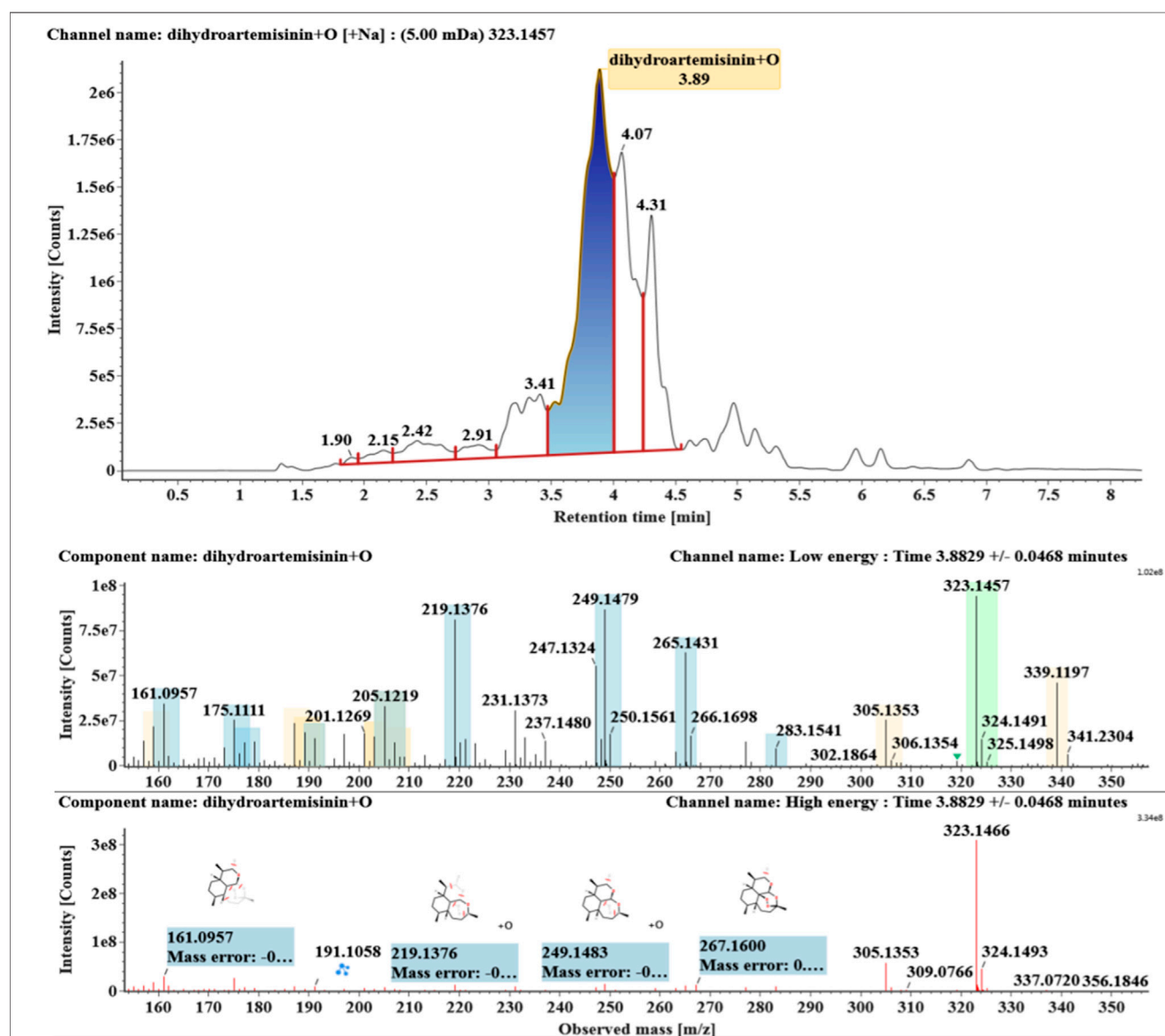
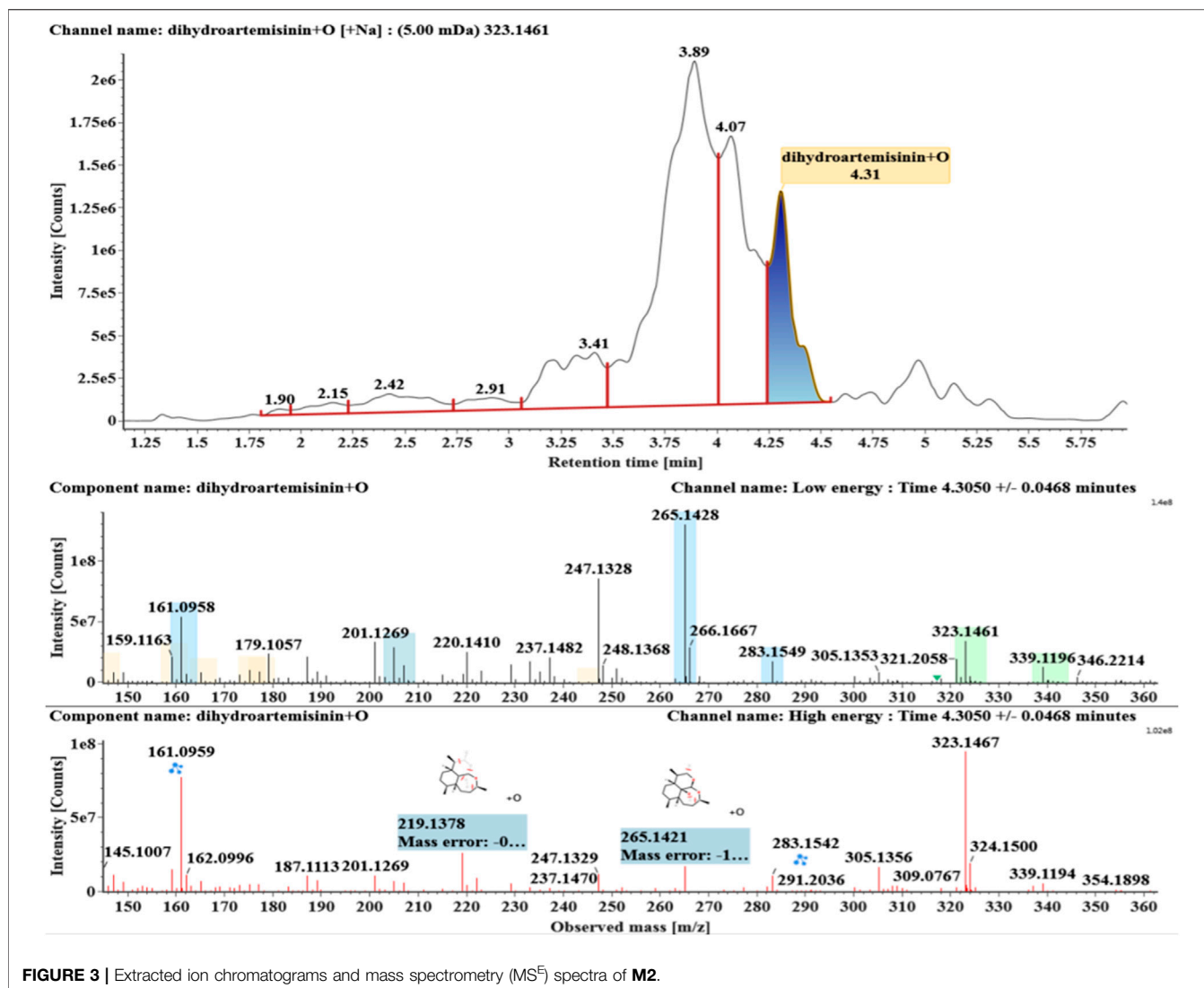


FIGURE 1 | Extracted ion chromatograms and mass spectrometry (MS^E) spectra of DHA.

TABLE 1 | Summary of microbial transformation products of dihydroartemisinin.

No	Component	Formula	Observed m/z	RT (min)	Major fragments	Response
M1	DHA + O	$C_{15}H_{24}O_6+Na^+$	323.1457	3.89	323, 283, 265, 249, 247, 231, 219	1709644
M2	DHA + O	$C_{15}H_{24}O_6+Na^+$	323.1461	4.31	339, 323, 283, 265, 247, 237, 219	613851
M3	DHA + O	$C_{15}H_{24}O_6+Na^+$	323.1455	4.97	339, 323, 283, 265, 247, 219	267107
M4	DHA + O	$C_{15}H_{24}O_6+Na^+$	323.1450	5.14	323, 283, 265, 247, 219	121182
M5	DHA + O-H ₂	$C_{15}H_{22}O_6+Na^+$	321.1294	4.17	321, 267, 249, 231, 221, 203	3365
M6	DHA + O-H ₂ O	$C_{15}H_{22}O_5+H^+$	283.1554	3.41	283, 265, 247, 237, 219, 201	333881
M7	DHA + O-H ₂ O	$C_{15}H_{22}O_5+H^+$	283.1554	4.42	283, 265, 237, 225, 219, 201	220113
M8	DHA-O	$C_{15}H_{24}O_4+Na^+$	291.1564	7.16	291, 269, 251, 233, 223, 205, 187	926704
M9	DHA-H ₂ O	$C_{15}H_{22}O_4+H^+$	267.1589	8.65	289, 267, 249, 231, 221, 203, 185	751976

**FIGURE 2** | Extracted ion chromatograms and mass spectrometry (MS^E) spectra of **M1**.



Health Organization, 2020). Apart from the application in malarial treatment, DHA was also found to exhibit a broad scope of biological activities, including anti-inflammatory, antitumor, antiviral, and immunoregulatory activities (Wang et al., 2018; Li et al., 2019; Zhang et al., 2020). Given the promising therapeutic potential in clinical, the metabolic study of DHA in the body is of great interest to researchers. Although considerable efforts have been devoted to the research on the disposal process of DHA, and a series of metabolites in body have been identified, the study on the metabolites of DHA in erythrocytes remains rarely involved but challenging. Indeed, the exploration of active metabolites in erythrocyte is of considerable important for antimalarial drug because red blood cells are the actual sites where the plasmodium lives and the drug works. Followed by Prof. Tu, our team has been engaged in the metabolism study of ART, DHA, and its derivatives in the last few years (Tu, 2011; Yang and Zhang, 2017; Ma et al., 2019a; Ma et al., 2019b; Bai et al., 2019; Zhao et al., 2021).

Recently, the microbial transformation has become an efficient tool for metabolic simulations of drugs (Parshikov et al., 2004). It exhibited good function for molecular modification and synthesis active metabolites environmental friendly and cheaper cost. Filamentous fungi, which share the similar cytochrome P450 enzymes with human, have been proved to possess the ability to mimic the metabolic process in body (Asha and Vidyavathi, 2009). To get some insight of the *in vivo* process of DHA, some projects have been conducted through filamentous fungi-mediated strategy, and six derivatives of DHA including 14-hydroxymethyl dihydroartemisinin (Hu et al., 1991), 9 α -hydroxyartemethin-I (Han and Lee, 2016), 3 α -hydroxydeoxydihydroartemisinin, 8 α -hydroxydeoxyartemisinin, deoxyarte-misinin, and 9 α -hydroxydihydroartemisinin (Wang et al., 2013) have been obtained. Unfortunately, there are no scientific results to validate whether these compounds are consistent with mammalian metabolites. The inhibitory efficiency on plasmodium of these compounds has never been studied.

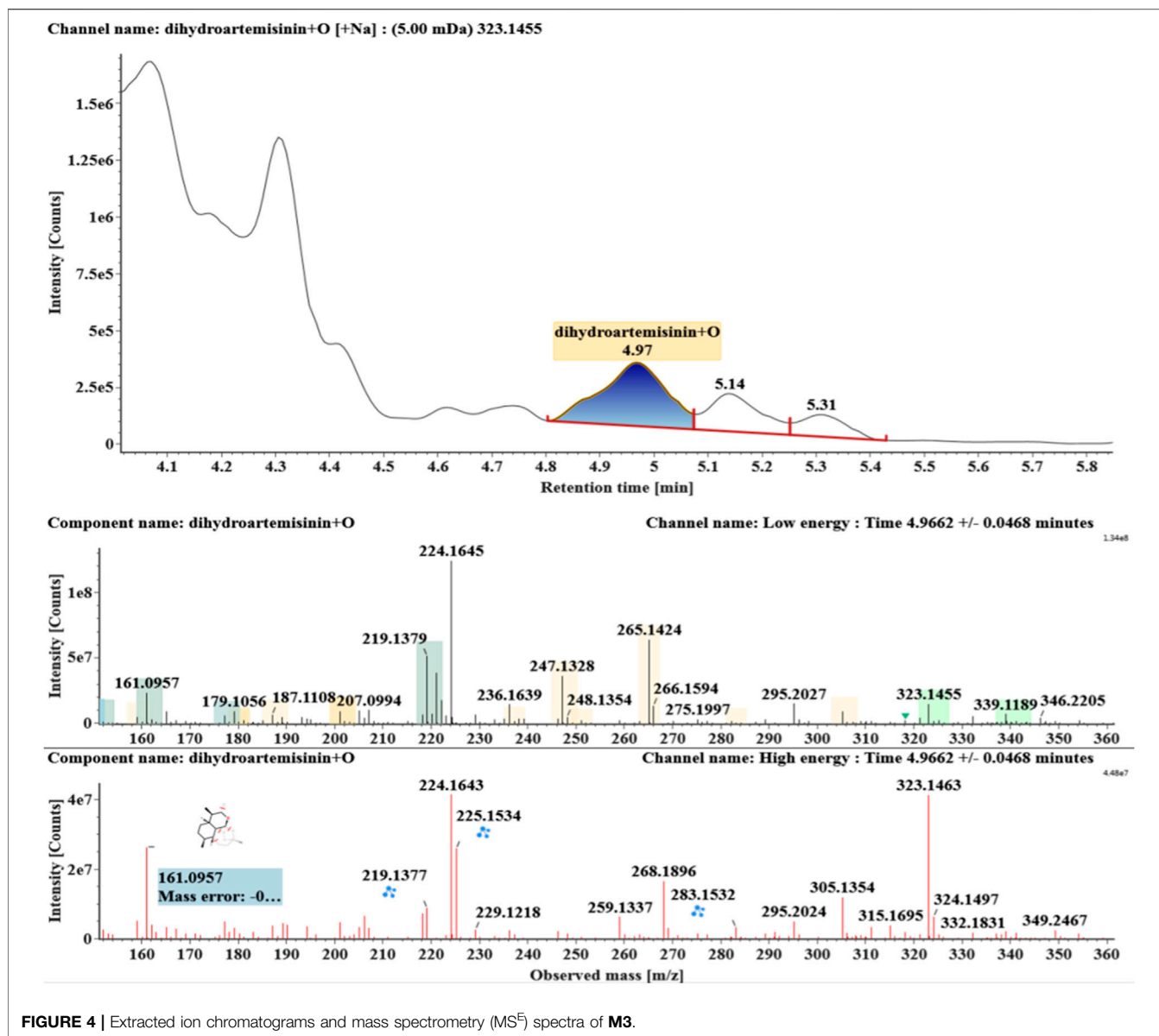


FIGURE 4 | Extracted ion chromatograms and mass spectrometry (MS^E) spectra of M3.

Herein, the metabolic study of DHA was performed employing *Cunninghamella elegans* (*C. elegans*) CICC 40250, and the products were analyzed and compared with the metabolites of DHA in erythrocytes. As a result, from microbial transformation, a total of nine DHA derivatives (M1–M9) were detected by UPLC-MS and three were isolated, including 7 β -hydroxydihydroartemisinin (M1), 1-deoxydihydroartemisinin (M8), and 1-deoxyartemisinin (M9). The three gained products were also identified in erythrocytes. The structure and stereo-configuration of the novel product (M1) were validated via X-ray single crystal diffraction, and reported here for the first time. Moreover, M1 was also proven to exhibit *in vitro* antimalarial activity against Pf 3D7, with an IC₅₀ value of 133 nM. As well as we know, this is the first attempt to isolate and identify the metabolites of DHA in red blood cells via microbial transformation. The discovery and synthesis of antimalarial

products provide the possibility for further drug development by eco-friendly microbial transformation. The structures of DHA and its derivatives from *C. elegans* were shown in Scheme 1.

MATERIALS AND METHODS

Materials and Reagents

DHA was obtained from the Kunming Pharmaceutical Group (Chongqing, China, batch number C00220160402). The compound had purity $\geq 99\%$. Methanol, acetonitrile, and formic acid were HPLC grade and purchased from Fisher (Geel, Belgium). Other chemicals in this work were of analytical grade and purchased from Beijing Chemical Works (Beijing, China). Silicone filler, silica gel GF₂₅₄ thin layer plates, and silica gel GF₂₅₄ thin layer preparation plates were purchased

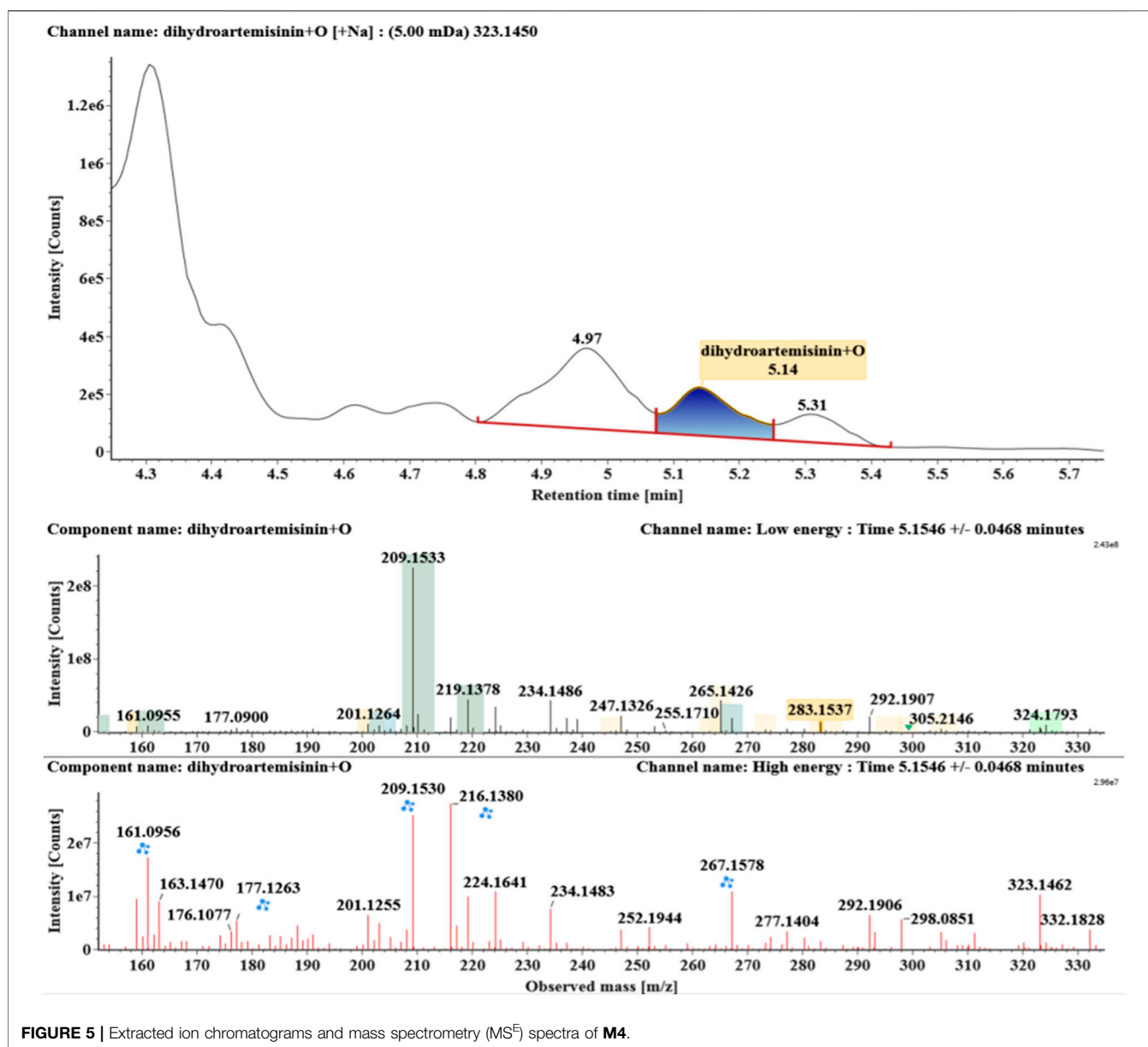


FIGURE 5 | Extracted ion chromatograms and mass spectrometry (MS^E) spectra of M4.

from Qingdao Marine Chemical Group Corporation (Qingdao, China). Silica gel (200–300 mesh, Qingdao Marine Chemical Group Corporation, Qingdao, China), Silica Flash Column 330 g, and Chormatorex (FujiSilysia Chemical, Japan) were used for column chromatography. Water was prepared using a Milli-Q system operating at 18.2 MΩ (Millipore, Bedford, MA, United States). All other chemicals used were purchased from Fisher Scientific or Beijing Chemical Works, and were of the highest purity available.

The UPLC-ESI-Q-TOF-MS^E system consisted of a Waters ACQUITY I-class UPLC and Xevo G2-XS Q-TOF Mass Spectrometer (Waters, Manchester, United Kingdom). ¹H (600 MHz), ¹³C (150 MHz), and NMR spectra were recorded on a Bruker AV 600 spectrometer (Bruker Corporation, Fallanden, Switzerland) with TMS as an internal reference.

X-ray diffraction experiments were performed using a Bruker D8 venture diffractometer with Cu Kα radiation. (Crystals of metabolites were obtained from EtOAc and acetone by slow evaporation of solvent at room temperature.)

Microorganism and Biotransformation Procedure

C. elegans CICC 40250 (MT1) was obtained from the China Center of Industrial Culture Collection (Beijing, China). Culture and biotransformation experiments were conducted in a medium composed of 20 g Sabouraud dextrose broth (Oxoid, Basingstoke, United Kingdom), 10 g peptone (Solarbio, Beijing, China), 15 g sucrose (Solarbio, Beijing, China), and 1,000 ml deionized water.

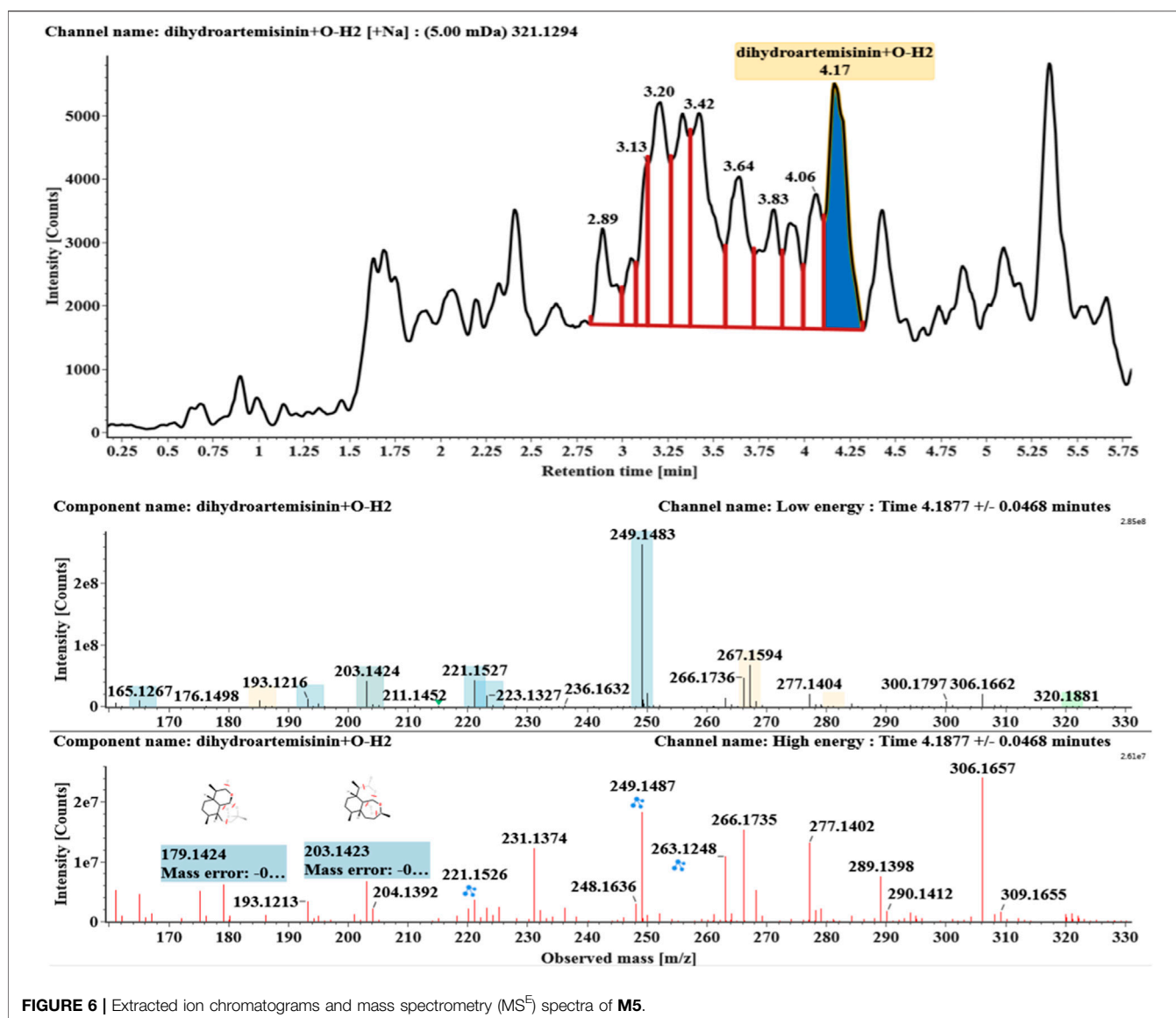


FIGURE 6 | Extracted ion chromatograms and mass spectrometry (MS^E) spectra of M5.

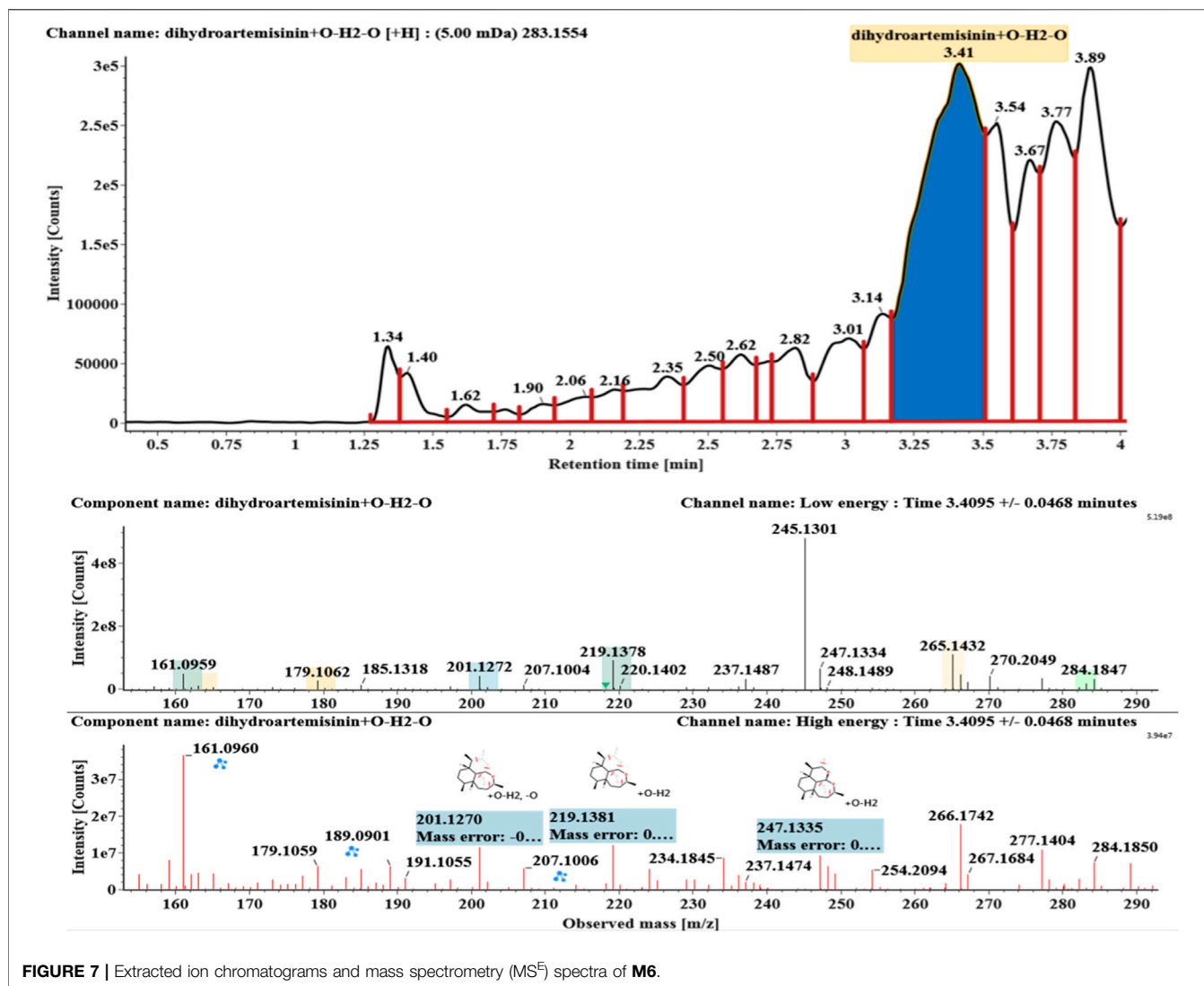
Two-stage fermentation was employed in this study (Zhan et al., 2017). The substrate was dissolved in MeOH at a concentration of 25 mg/ml, and 2 ml of the solution was added into each flask after the second fermentation stage, producing a DHA concentration of 0.5 mg/ml. Cultures were incubated at 28°C and shaken at 180 rpm for 14 days. Mycelia and broth were then separated by filtration. The filtrate was extracted with EtOAc (1:1, v/v) three times, and the extract was evaporated under vacuum to produce a brown residue.

UPLC-MS^E Conditions and Data Processing

The UPLC-ESI-QTOF-MS^E system consisted of a Waters ACQUITY I-class UPLC and Xevo G2-XS Q-TOF mass spectrometer equipped with electrospray ionization (ESI) source. Chromatographic separation was achieved using an

ACQUITY UPLC BEH C18 (2.1 mm × 100 mm, 1.7 μm, Waters). The mobile phase consisted of solvent A (H₂O containing 0.1% formic acid, v/v) and solvent B (acetonitrile containing 0.1% formic acid, v/v). The gradient program for biosamples included three segments: 5–100% B from 0 to 15 min; followed by 100–5% B from 15 to 17 min; and a post-run of 3 min for column equilibration. The flow rate was 0.4 ml/min, and the temperature was 30°C throughout the analysis.

The MS was operated in positive ionization mode across a scan range of m/z 50 to 1,000, with a scan time of 0.2 s. Source parameters: source temperature 150°C, cone gas 50 L/h, desolvations temperature 450°C, and desolvation gas flow 800 L/h. Argon (99.95%) was used for collision-induced dissociation, and N₂ was used as the drift gas. The low collision energy was set to 6 eV, and the high collision energy was ramped from 12 to 25 eV. MSE analysis was employed for simultaneous acquisition of the exact mass of small molecules at high and low collision energies.



All data processing was performed using UNIFI 1.9 (Waters, Manchester, United Kingdom). Components were identified using the following 3D peak detection features: low-energy limits of 150 and high-energy limits of 20, isotope clustering, and high-to-low energy association within a 0.5 fraction of the chromatographic and drift peak width, with a mass accuracy of ± 2 mDa. The maximum number of allowed fragment ions per match was set to 10.

Extraction and Isolation of Transformed Products

Scale-up fermentations were also carried out according to the standard two-stage procedure. Under the same temperature-controlled shaking conditions, each 2000 ml flask contained 500 ml Sabouraud glucose liquid medium, and DHA (6 g) was dissolved in MeOH at a concentration of 25 mg/ml and evenly distributed in all flasks. After incubation for 14 days, mycelia and broth were separated by filtration. The filtrate was extracted with

EtOAc (1:1, v/v) three times, and the extract was evaporated under vacuum to produce a brown residue. The EtOAc extract was fractionated by a Silica Flash Column using a gradient solvent system of petroleum ether-EtOAc to afford 43 fractions (Fr. 1-Fr. 43) according to TLC analysis.

Fr. 15 (0.5 g) was subjected to a Chromatorex column and eluted with a gradient solvent system of petroleum ether-EtOAc to afford compound **M1** (100 mg). Fr. 30 was separated by recrystallization to obtain compound **M9** (20 mg). Fr. 40 (1 g) was separated over a CHORMATOREX column and eluted with a gradient solvent system of petroleum ether-acetone to give 14 subfractions. Fr. 40-2 was subjected to thin layer preparation plates to obtain compound **M8** (80 mg).

Evaluation of Antimalarial Activity

Compounds **M1**, **M8**, and **M9** were diluted in DMSO and examined for antimalarial activity *in vitro* against the *Pf*. 3D7 clone. Artemisinin was used as a positive control drug. Inhibition of plasmodium proliferation by different concentrations of

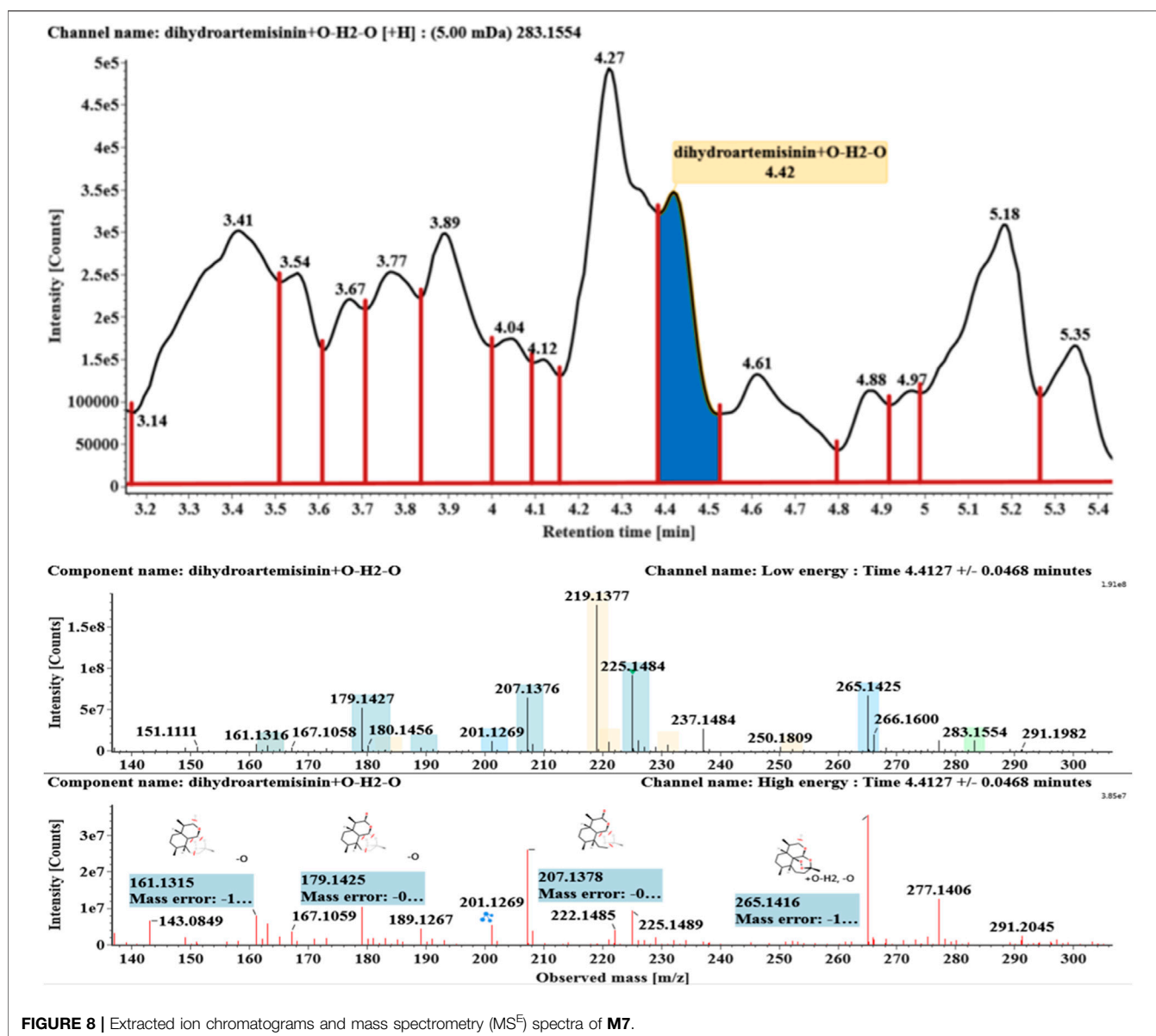


FIGURE 8 | Extracted ion chromatograms and mass spectrometry (MS^E) spectra of M7.

transformed products was determined according to a certain formula, and the *in vitro* antimalarial activity of the drug was evaluated with the IC_{50} .

RESULTS

Analysis of the Microbial Transformation DHA Products From *C. elegans* 40250

The microbial transformation products were identified with UNIFI platform based on chromatographic and mass spectral characteristics provided by reference substances DHA, such as retention time, exact mass, quasi-molecular ions, in-source fragments, characteristic fragments. A total of nine products were found from *C. elegans* 40250, classified into hydroxylated DHAs (DHA + O), hydroxylated and dehydrogenated DHAs

(DHA + O-H2), hydroxylated and dehydrated DHAs (DHA + O-H2-O), deoxygenated DHA (DHA-O), and dehydrated DHA (DHA-H2-O). All identified products were listed in Table 1. Extracted ion chromatograms and MS^E spectra of DHA biotransformation products were shown in Figure 1. Also extracted ion chromatograms and MS^E spectra of its products were shown in Figures 2–10, respectively. The response strength of nine products, which could partly estimate the transform yield of compounds, is shown in Supplementary Figure S1.

DHA, the reference substance, was eluted at 7.27 min. Its molecular ion $[M + Na]^+$ was observed at m/z 307.1509. The fragment ions at m/z 267.1590 and 249.1485 were generated by the successive loss of water from m/z 307.1509. The fragment ions at m/z 221.1538 represented the loss of $HCOOH$ from m/z 267.1590. The fragment ions at m/z 203.1432 resulted from the loss of water from m/z 221.1538. Extracted ion

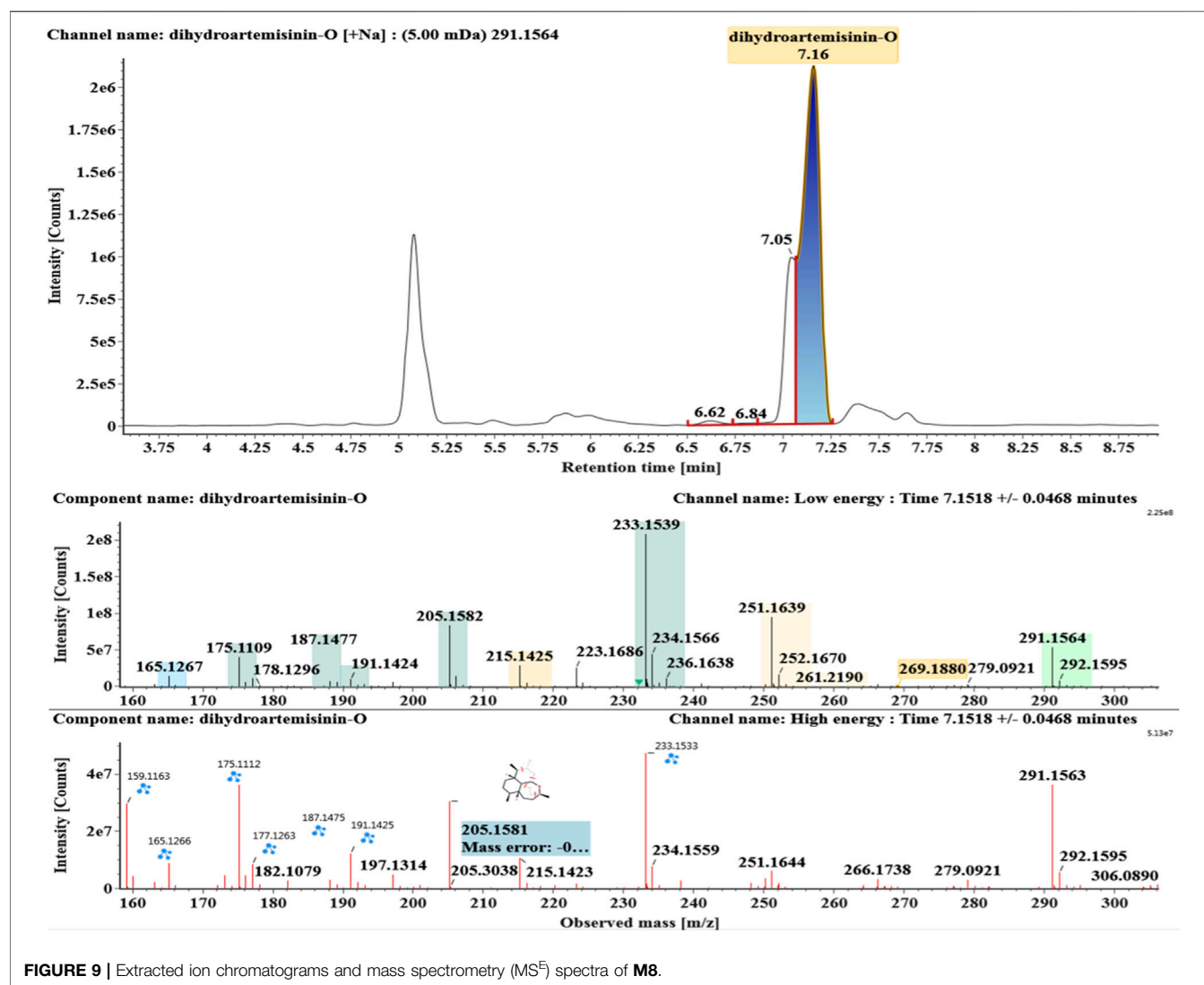


FIGURE 9 | Extracted ion chromatograms and mass spectrometry (MS^E) spectra of **M8**.

chromatograms and mass spectrometry (MS^E) spectra of DHA were shown in **Figure 1**.

Hydroxylated DHAs (DHA + O, **M1-M4**) were detected at 3.89, 4.31, 4.97, and 5.14 min. Their molecular ions $[M + Na]^+$ were observed at m/z 323.1457, 323.1461, 323.1455, and 323.1450, respectively. They exhibited the same fragment ions. The fragment ions at m/z 283, 265, and 247 were generated by the successive loss of water from m/z 323. The fragment ions at m/z 219 represented the loss of $HCOOH$ from m/z 265. The fragment ions at m/z 201 resulted from the loss of water from m/z 219. Extracted ion chromatograms and mass spectrometry (MS^E) spectra of **M1-M4** were shown in **Figures 2–5**, respectively.

Hydroxylated and dehydrogenated DHA (DHA + O- H_2 , **M5**) was detected at 4.17 min. Its molecular ion $[M + Na]^+$ was observed at m/z 321.1294. The fragment ions at m/z 249 and 231 were generated by the successive loss of water from m/z 267. The fragment ions at m/z 221 represented the loss of $HCOOH$ from m/z 267 or the loss of CO from m/z 249. The fragment ions at m/z 203 resulted from the loss of water from m/z 221. Extracted

ion chromatograms and mass spectrometry (MS^E) spectra of **M5** were shown in **Figure 6**.

Hydroxylated and dehydrated DHAs (DHA + O- H_2O , **M6-M7**) were detected at 3.41 and 4.42 min, respectively. The molecular ions $[M + H]^+$ were observed at m/z 283.1554. Consistent with DHA, these products showed a series of fragment ions resulting from the loss of H_2O , CO , or $HCOOH$, such as m/z 265, 247, 237, 219, and 201. The fragment ions at m/z 265 and 247 were generated by the successive loss of water from m/z 283. The fragment ions at m/z 237 represented the loss of CO from m/z 265. Extracted ion chromatograms and mass spectrometry (MS^E) spectra of **M6** and **M7** were shown in **Figures 6–8**, respectively.

Deoxygenated DHA (DHA-O, **M8**) and dehydrated DHA (DHA- H_2O , **M9**) were detected at 7.16 and 8.65 min, respectively. Their molecular ions $[M + Na]^+$ were observed at m/z 291.1564 and m/z 289.1405, respectively. They showed similar fragment ions except with a 2 Da (a hydrogen atom) mass shift, such as m/z 251, m/z 249, m/z 233, m/z 231, m/z 205, m/z 203, m/z 187, and m/z 185. The fragment ions at m/z 251 and m/z 249 were

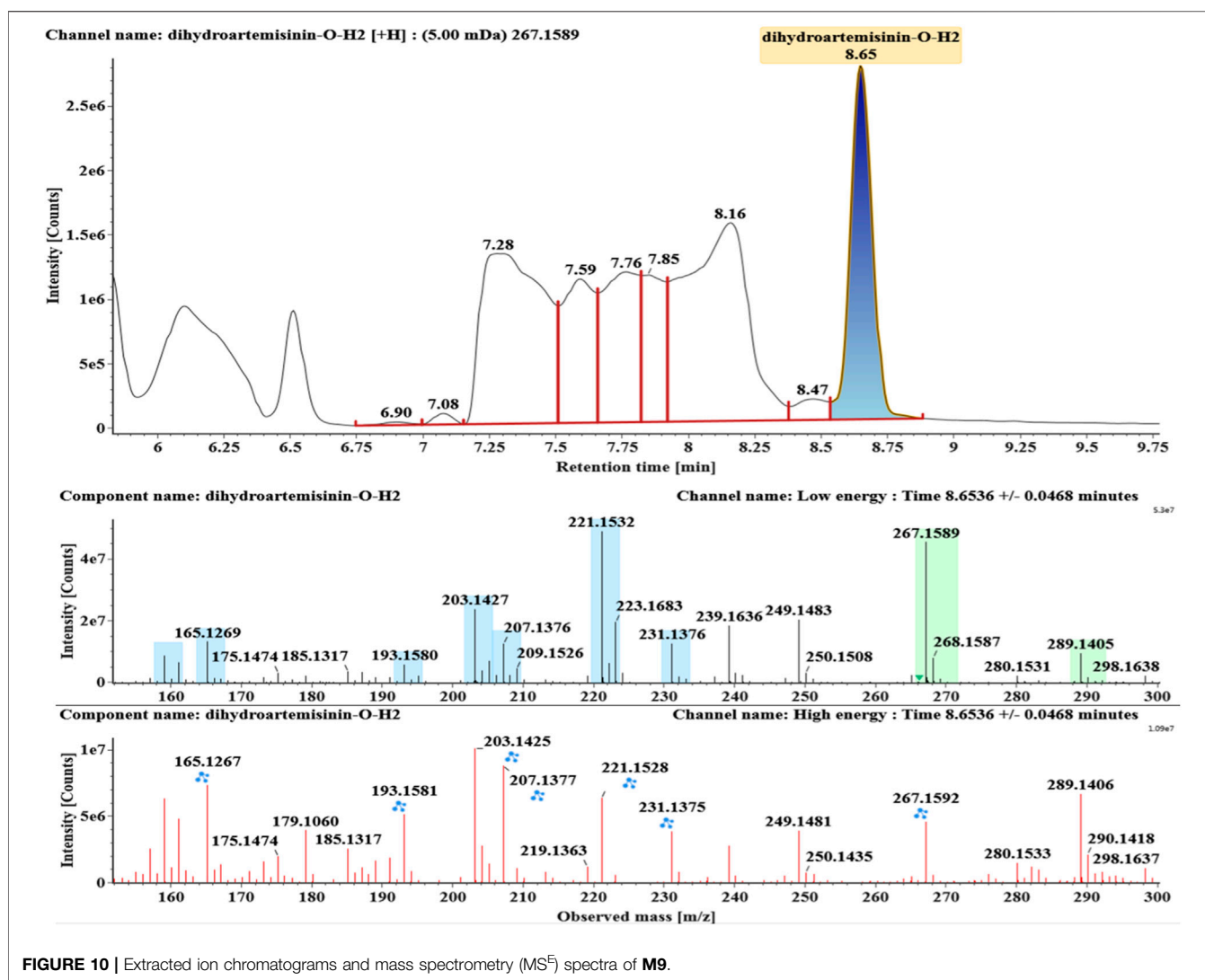


FIGURE 10 | Extracted ion chromatograms and mass spectrometry (MS^E) spectra of **M9**.

generated by the successive loss of water from m/z 291 and m/z 289, respectively. The fragment ions at m/z 205 and m/z 203 represented the loss of CO from m/z 233 and m/z 231, respectively. Their ions exhibited the same mechanism resulting from the loss of CO or H₂O. Extracted ion chromatograms and mass spectrometry (MS^E) spectra of **M8** and **M9** were shown in **Figures 9** and **10**, respectively.

Furthermore, as a semiquantitative comparative chromatography analysis, the relative contents of modified dihydroartemisinins (**M1–M9**) were evaluated by mass spectral response abundance data. As a result, **M1** had the highest content of all compounds, followed by **M8** and **M9**. And the numerical results of response provided the guidance for further isolation. The histogram of the response of all DHA products is shown in **Supplementary Figure S1**.

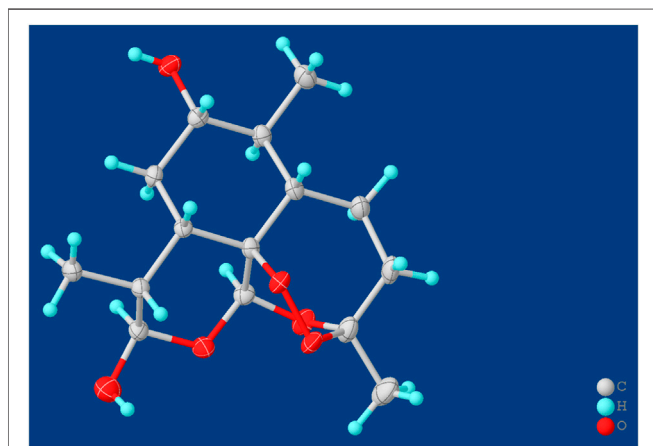
Structural Elucidation of the Compounds Isolated From MT1

Compound **M1** colorless needles (from EtOAc and acetone). ESI-HRMS calcd. for $[M + Na]^+$, $C_{15}H_{24}O_6Na$, 323.1471; found m/z

323.1457. 1H and ^{13}C NMR data are shown in **Table 2**. The HSQC spectrum showed correlations of H-12 (δ 5.39) with C-12 (δ 90.4), C10-OH (δ 4.64) with C-10 (δ 93.7), and H-7 (δ 2.96) with C-7 (δ 72.6), which supported compound **M1** as a hydroxylation product. The HMBC spectrum showed correlations of C10-OH (δ 4.64) with C-8a (δ 43.9), C-7 (δ 72.6) and C-8 (δ 31.2), along with the correlations of C-7 (δ 72.6) with H-14 (δ 0.94) and H-15 (δ 1.28). These spectral dates suggested that the hydroxylation occurred at C-7. Moreover, the absolute configuration of the hydroxylated group in the stereogenic carbon center was determined to be β -OH by single-crystal X-ray diffraction analysis (**Scheme 2**). A single crystal was obtained from EtOAc and acetone by slow evaporation of the solvent at room temperature. A colorless block-shaped crystal with dimensions of $0.20 \times 0.15 \times 0.10$ mm³ was mounted. Data were collected using a Bruker APEX-II CCD diffractometer operating at $T = 150.0$ K and measured and scans using CuK α radiation. The maximum resolution achieved was $= 72.120^\circ$ (0.81 \AA). The final completeness is 98.90% out to 72.120° in. Crystal data: $C_{15}H_{24}O_6$, Mr = 300.34, triclinic, P1, $a = 9.6563$ (6)

TABLE 2 | ^1H NMR (600 MHz) and ^{13}C NMR (150 MHz) data of three compounds (δ : ppm).

Position	Compound M1 (DMSO- d_6)		Compound M8 (CDCl $_3$)		Compound M9 (CDCl $_3$)	
	δ_{H} (J in Hz)	δ_{C}	δ_{H} (J in Hz)	δ_{C}	δ_{H} (J in Hz)	δ_{C}
3		103.67		107.08		108.20
4		36.48	1.56 (m)	33.27	1.72 (t), 1.56 (m)	32.96
5		24.78	1.65 (m)	21.05	1.84 (d)	21.01
5a	1.31-1.35 (dd, 23,13)	49.46		44.65		43.61
6	1.55-1.58 (m)	43.17		34.34		34.34
7	2.96 (s)	72.60	1.14 (m)	33.57	1.72 (t), 1.04 (m)	32.44
8		31.22		21.78	1.84 (d), 0.94 (t)	22.51
8a		43.87		40.34	1.94 (d)	41.41
9		33.97	2.26 (m)	33.00	3.12 (m)	31.75
10	4.64 (s)	93.74		95.99		170.82
12	5.39 (s)	90.41	5.28 (d)	95.13	5.63 (s)	98.62
12a		80.18		81.44		81.38
13	1.28 (s)	26.11	0.94 (d)	23.37	1.46 (s)	22.96
14	0.94 (d)	15.95	0.83 (d)	17.77	0.87 (d)	17.57
15	0.78 (d, 6.3)	13.30	1.47 (s)	13.93	1.13 (d)	11.61
10-OH	6.41 (d, 6.8)		4.71 (t, 6.4)			
7-OH	4.64 (d, J = 4.9 Hz)					

**SCHEME 2** | X-ray crystal structures of compound M1.

\AA , $b = 9.9540$ (6) \AA , $c = 15.6044$ (9) \AA , $\alpha = 93.832$ (3) $^\circ$, $\beta = 90.860$ (3) $^\circ$, $\gamma = 102.948$ (3) $^\circ$, $V = 1,457.78$ (15) \AA^3 , $Z = 4$, $Z' = 4$, $(\text{CuK}\alpha) = 0.875$, 28521 reflections measured, 10327 unique ($R_{\text{int}} = 0.0363$), which were used in all calculations. The final $wR2$ was 0.1013 (all data), and $R1$ was 0.0383 ($I \geq 2$ (I)). Crystallographic data of compound M1 have been deposited to CCDC (<http://www.ccdc.cam.ac.uk>, No. CCDC 2039245). Thus, the structure of compound M1 was elucidated as 7 β -hydroxydihydroartemisinin.

Compound M8 white powder (EtOAc). ESI-HRMS calcd. for $[\text{M} + \text{Na}]^+$, $\text{C}_{15}\text{H}_{24}\text{O}_4\text{Na}$, 291.1572; found m/z 291.1564. ^1H and ^{13}C NMR data are shown in Table 2. The data supported the compound M8 was 1-deoxydihydroartemisinin (Han and Lee, 2017).

Compound M9 white powder (EtOAc). ESI-HRMS calcd. for $[\text{M} + \text{H}]^+$, $\text{C}_{15}\text{H}_{22}\text{O}_4\text{H}$, 267.1596; found m/z 267.1589. HR-ESI-MS: $[\text{M} + \text{H}]^+$ at m/z at 267.1589 (calcd. for $\text{C}_{15}\text{H}_{22}\text{O}_4$). ^1H and

^{13}C NMR data are shown in Table 2. The data supported the compound M9 was 1-deoxyartemisinin (Lee et al., 1989).

Compared the Products M1, M8, and M9 With Metabolites in Erythrocytes

Based on the analysis results of DHA metabolites *in vivo*, the three products from *C. elegans* 40250 were compared with *in vivo* metabolites by UPLC-ESI-Q-TOF-MS^E. The retention time and the mass behavior, such as exact mass, quasi-molecular ions, in-source fragments, and characteristic fragments, are compared to confirm the consistency. The results revealed that M1, M8, and M9 were the common metabolites of DHA in erythrocyte. The extracted ion chromatograms and mass spectrometry (MS^E) spectra of products M1, M8, and M9 and the metabolites of DHA in red blood cells were shown in Figure 11.

Antimalarial Activity *in vitro*

The positive control drug artemisinin exhibited *in vitro* antimalarial activity against *Pf.* 3D7 with an IC_{50} (50% inhibition concentration) value of 11 nM. Compound M1 was indicated to exhibit *in vitro* antimalarial activity against *Pf.* 3D7 with an IC_{50} value of 133 nM. Compound M8 and M9 showed no activity against *Pf.* 3D7.

DISCUSSION

As known, considering the low concentrations and complex detection background, it is a bottleneck for exploring the drug metabolism in erythrocytes. Drugs accumulated in cells are difficult to meet the demand for analysis and isolation. Compared with the traditional metabolism research model *in vitro*, microbial transformation can mimic mammal metabolic action according to the similar CYP 450s in

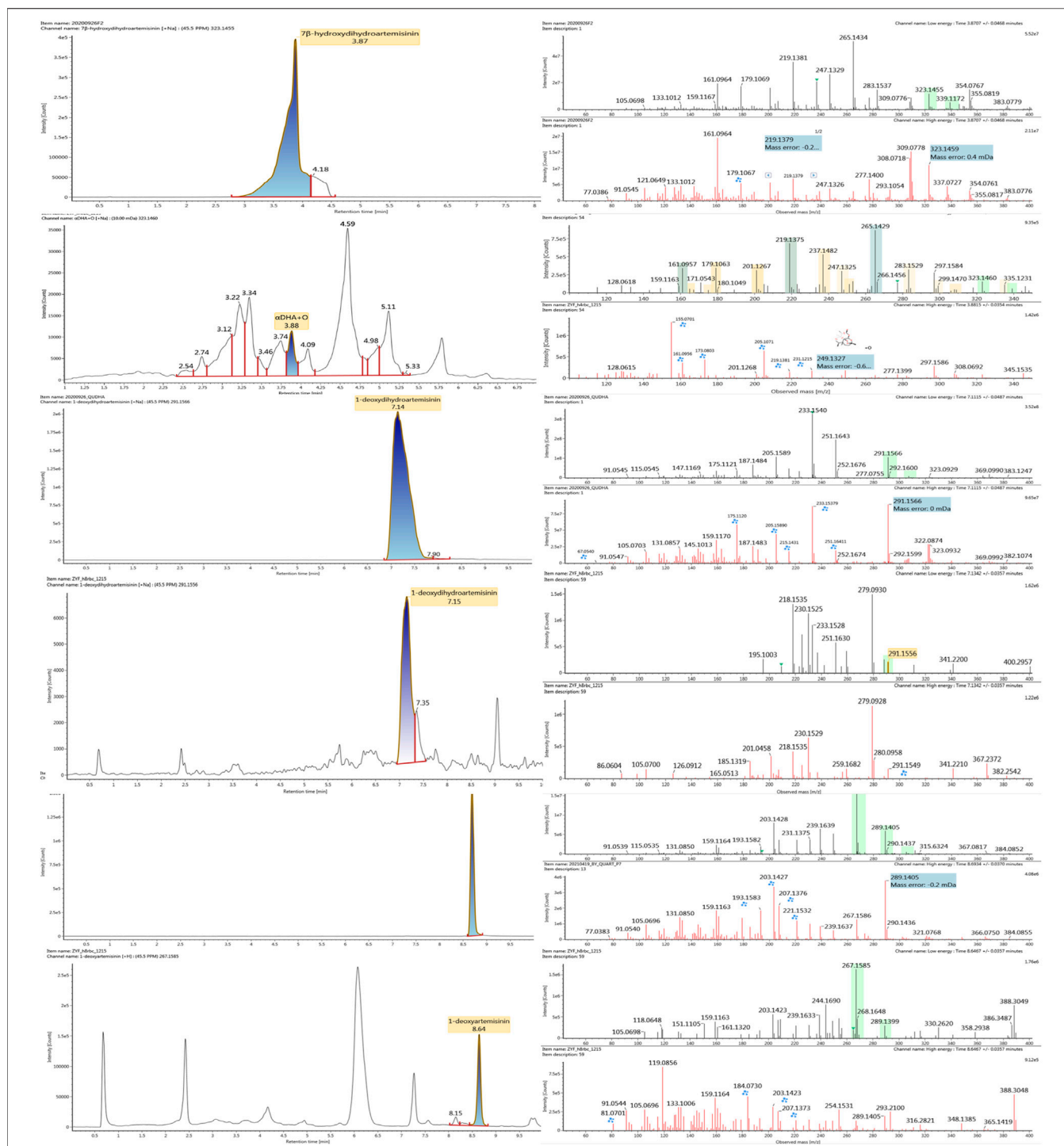


FIGURE 11 | Extracted ion chromatograms and mass spectrometry (MS²) spectra of products **M1**, **M8**, and **M9** and the metabolites of DHA in red blood cells.

microorganisms with the advantage of metabolites accumulation eco-friendly and affordably. Herein, the *C. elegans* was chosen as an applicable model *in vitro* for studying DHA metabolism in red blood cells based on the previous research foundation (the experimental data were unpublished). Artemisinin and its derivatives are the first-line antimalarial agents for saving

millions of people's life. There are four drugs derived from artemisinin, including DHA, artemether, arteether, and artesunate. Given the IC₅₀ value of antimalarial activity against *Pf. 3D7* *in vitro*, the derivatives showed better antimalarial activity than artemisinin, at 4–6 nM approximately, while the value of artemisinin is at 12 nM (Kreidenweiss et al., 2008; Reiter et al.,

2015). In this work, the antimalarial metabolite **M1** exhibited less active against *Pf. 3D7* *in vitro*, for about a 10th of the activity of artemisinin and a 20th of DHA. However, the antimalarial mechanism of artemisinin and its derivatives are not definitely clear. The metabolite **M1** was the first active metabolite discovered in red blood cells, where is the actual site the parasites live and the drug works. Therefore, it is significant for developing novel active metabolite agents and helpful for further antimalarial mechanism research. In particular, the microbial transformation provided a green and powerful approach for preparing the active metabolites.

Liquid chromatography mass spectrometry (LC-MS) is a powerful method for the analysis of compounds, and is increasingly used as a sensitive and efficient tool for metabolite profiling in natural plants or bodies. The numerical results of response, closely related to the conversion rate of the transformation products, were meaningful to guide for isolation work. Herein, UPLC-Q-TOF-MS^E was employed for predicting and identifying biotransformation products of DHA. Although there were nine compounds discovered and analyzed by MS^E, only compounds **M1**, **M8**, and **M9**, the top three high response values, were gained by isolation. Therefore, how to increase the conversion rate from substrates to hydroxylation products is one of the significant for further research. Additionally, to satisfy the need of microbial transformation, the purity of DHA was detected, and the HPLC profile of DHA has been shown in **Supplementary Figure S2**. The two isoforms, α -DHA and β -DHA, are the two peaks in the graph, respectively.

Artemisinin and its derivatives are excellent antimalarial agents due to the unique peroxide bridge. The mechanism of antimalarial action research indicated that the hallmark of artemisinin activation is the generation of highly reactive carbon-centered radicals via endoperoxide cleavage (O'Neill et al., 2010). And 1-deoxidation products were found to be inactive against *P. falciparum* 3D7 strain due to the cleavage of peroxy linkage (Tu, 2011; Kumari et al., 2018; Yang et al., 2020). Furthermore, the *in vitro* experiments verify the above conclusion.

CONCLUSION

Microorganisms can mimic mammal metabolism to synthesize metabolites in an environmentally friendly manner. Herein, microbial transformation by *C. elegans*.40250 was first employed as a biotransformation tool to gain metabolites that were discovered in erythrocyte. Finally, nine products were detected from microbial system by UPLC-ESI-Q-TOF-MS^E, and three intracellular metabolic products were isolated and identified for the first time. Moreover, compound **M1** was a novel antimalarial component, with an antimalarial activity IC₅₀ value of 133 nM. In conclusion, the biotransformation of DHA by *Cunninghamella* proved to be an effective procedure for the

investigation of metabolism, especially with the advantage of accumulating metabolites, and one intracellular metabolite of DHA with antimalarial activity was the first time to discover.

DATA AVAILABILITY STATEMENT

The original contributions presented in the study are included in the article/**Supplementary Material**, further inquiries can be directed to the corresponding authors.

ETHICS STATEMENT

The animal study was reviewed and approved by the Institute of Chinese Materia Medica, Academy of Chinese Medical Sciences. Written informed consent was obtained from the owners for the participation of their animals in this study.

AUTHOR CONTRIBUTIONS

Conceptualization, YM; methodology, investigation and original draft preparation, YB and YZ; activity evaluation, XG; data analysis, DZ; writing—review and editing, PS; funding acquisition, YM and LY; All authors have read and agreed to the published version of the manuscript.

FUNDING

This research was funded by the Beijing Natural Science Foundation (grant number 7214292), the National Natural Science Foundation of China (grant number 82104516 and 82141004), the Fundamental Research Funds for the Central Public Welfare Research Institutes (grant number ZZ14-YQ-054 and ZZ13-YQ-098), and the Scientific and Technological Innovation Project of China Academy of Chinese Medical Sciences (CI2021A05053).

ACKNOWLEDGMENTS

Thanks to Professor Huimin Gao from the Institute of Chinese Materia Medica, China Academy of Chinese Medical Sciences, for critical review of this manuscript.

SUPPLEMENTARY MATERIAL

The Supplementary Material for this article can be found online at: <https://www.frontiersin.org/articles/10.3389/fchem.2022.850133/full#supplementary-material>

REFERENCES

- Asha, S., and Vidyavathi, M. (2009). Cunninghamella - A Microbial Model for Drug Metabolism Studies - A Review. *Biotechnol. Adv.* 27, 16–29. doi:10.1016/j.biotechadv.2008.07.005
- Bai, Y., Zhang, D., Sun, P., Zhao, Y., Chang, X., Ma, Y., et al. (2019). Evaluation of Microbial Transformation of 10-deoxoartemisinin by UPLC-ESI-Q-TOF-MSE. *Molecules* 24, 3874. doi:10.3390/molecules24213874
- Han, F., and Lee, I.-S. (2016). Microbial Transformation of the Antimalarial Sesquiterpene Endoperoxide Dihydroartemisinin. *Nat. Product. Res.* 31, 883–889. doi:10.1080/14786419.2016.1250092
- Han, F., and Lee, I. S. (2017). Microbial Transformation of the Antimalarial Sesquiterpene Endoperoxide Dihydroartemisinin. *Nat. Product. Res.* 31 (8), 883–889. doi:10.1080/14786419.2016.1250092
- Hu, Y., Highet, R. J., Marion, D., and Ziffer, H. (1991). Microbial Hydroxylation of a Dihydroartemisinin Derivative. *J. Chem. Soc. Chem. Commun.* 17, 1176–1177. doi:10.1039/C39910001176
- Kreidenweiss, A., Kremsner, P. G., and Mordmüller, B. (2008). Comprehensive Study of Proteasome Inhibitors against Plasmodium Falciparum Laboratory Strains and Field Isolates from Gabon. *Malar. J.* 7, 187. doi:10.1186/1475-2875-7-187
- Kumari, A., Karnatak, M., Singh, D., Shankar, R., Jat, J. L., Sharma, S., et al. (2018). Current Scenario of Artemisinin and its Analogues for Antimalarial Activity. *Eur. J. Med. Chem.* 163, 804–829. doi:10.1016/j.ejmech.2018.12.007
- Lee, I.-S., Elsohly, H. N., Croom, E. M., and Hufford, C. D. (1989). Microbial Metabolism Studies of the Antimalarial Sesquiterpene Artemisinin. *J. Nat. Prod.* 52 (2), 337–341. doi:10.1021/np50062a020
- Li, Y.-N., Fan, M.-L., Liu, H.-Q., Ma, B., Dai, W.-L., Yu, B.-Y., et al. (2019). Dihydroartemisinin Derivative DC32 Inhibits Inflammatory Response in Osteoarthritic Synovium through Regulating Nrf2/NF-Kb Pathway. *Int. Immunopharmacology* 74, 105701. doi:10.1016/j.intimp.2019.105701
- Ma, Y., Sun, P., Zhao, Y., Wang, K., Chang, X., Bai, Y., et al. (2019a). A Microbial Transformation Model for Simulating Mammal Metabolism of Artemisinin. *Molecules* 24, 315. doi:10.3390/molecules24020315
- Ma, Y., Zhu, Y., Zhang, D., Meng, Y., Tang, T., Wang, K., et al. (2019b). Eco-friendly Decarboxylative Cyclization in Water: Practical Access to the Antimalarial 4-quinolones. *Green. Chem.* 21, 478–482. doi:10.1039/C8GC03570A
- O'Neill, P. M., Barton, V. E., and Ward, S. A. (2010). The Molecular Mechanism of Action of Artemisinin-The Debate Continues. *Molecules* 15 (3), 1705–1721. doi:10.3390/molecules15031705
- Parshikov, I. A., Muraleedharan, K. M., Avery, M. A., and Williamson, J. S. (2004). Transformation of Artemisinin by *Cunninghamella Elegans*. *Appl. Microbiol. Biotechnol.* 64 (6), 782–786. doi:10.1007/s00253-003-1524-z
- Reiter, C., Fröhlich, T., Gruber, L., Hutterer, C., Marschall, M., Voigtländer, C., et al. (2015). Highly Potent Artemisinin-Derived Dimers and Trimers: Synthesis and Evaluation of Their Antimalarial, Antileukemia and Antiviral Activities. *Bioorg. Med. Chem.* 23 (17), 5452–5458. doi:10.1016/j.bmc.2015.07.048
- Tu, Y. (2016). Artemisinin-A Gift from Traditional Chinese Medicine to the World (Nobel Lecture). *Angew. Chem. Int. Ed.* 55, 10210–10226. doi:10.1002/anie.201601967
- Tu, Y. (2011). The Discovery of Artemisinin (Qinghaosu) and Gifts from Chinese Medicine. *Nat. Med.* 17, 1217–1220. doi:10.1038/nm.2471
- Tu, Y. Y. (2009). “Dihydroartemisinin,” in *Artemisinin and Artemisinin Drugs* (Beijing, China: Beijing Chemical Industry Press), 187–191.
- Wang, D., Zhong, B., Li, Y., and Liu, X. (2018). Dihydroartemisinin Increases Apoptosis of colon Cancer Cells through Targeting Janus Kinase 2/signal Transducer and Activator of Transcription 3 Signaling. *Oncol. Lett.* 15, 1949–1954. doi:10.3892/ol.2017.7502
- Wang, X., Xu, C. C., and Liu, J. H. (2013). Optimization of the Biotransformation Medium of Dihydroartemisinin. *Nat. Prod. Res. Dev.* 25, 1690–1695. doi:10.14233/ajchem.2013.oh20
- World Health Organization (2020). World Malaria Report. Available at: <https://apps.who.int/iris/handle/10665/330011>.
- Yang, J., He, Y., Li, Y., Zhang, X., Wong, Y.-K., Shen, S., et al. (2020). Advances in the Research on the Targets of Anti-malaria Actions of Artemisinin. *Pharmacol. Ther.* 216, 107697. doi:10.1016/j.pharmthera.2020.107697
- Yang, L., and Zhang, D. (2017). Summary of Dihydroartemisinin and its Application for the Treatment of Lupus Erythematosus. *Chin. Sci. Bull.* 62, 2007–2012. doi:10.1360/N972017-00172
- Zhan, Y., Wu, Y., Xu, F., Bai, Y., Guan, Y., Williamson, J. S., et al. (2017). A Novel Dihydroxylated Derivative of Artemisinin from Microbial Transformation. *Fitoterapia* 120, 93–97. doi:10.1016/j.fitote.2017.05.015
- Zhang, T., Zhang, Y., Jiang, N., Zhao, X., Sang, X., Yang, N., et al. (2020). Dihydroartemisinin Regulates the Immune System by Promotion of CD8+ T Lymphocytes and Suppression of B Cell Responses. *Sci. China Life Sci.* 63, 737–749. doi:10.1007/s11427-019-9550-4
- Zhao, Y., Sun, P., Ma, Y., Chang, X., Chen, X., Ji, X., et al. (2021). Metabolite Profiling of Dihydroartemisinin in Blood of Plasmodium-Infected and Healthy Mice Using UPLC-Q-TOF-MSE. *Front. Pharmacol.* 11, 614159. doi:10.3389/fphar.2020.614159

Conflict of Interest: The authors declare that the research was conducted in the absence of any commercial or financial relationships that could be construed as a potential conflict of interest.

Publisher's Note: All claims expressed in this article are solely those of the authors and do not necessarily represent those of their affiliated organizations, or those of the publisher, the editors, and the reviewers. Any product that may be evaluated in this article, or claim that may be made by its manufacturer, is not guaranteed or endorsed by the publisher.

Copyright © 2022 Bai, Zhao, Gao, Zhang, Ma, Yang and Sun. This is an open-access article distributed under the terms of the Creative Commons Attribution License (CC BY). The use, distribution or reproduction in other forums is permitted, provided the original author(s) and the copyright owner(s) are credited and that the original publication in this journal is cited, in accordance with accepted academic practice. No use, distribution or reproduction is permitted which does not comply with these terms.



Copper-Promoted Hiyama Cross-Coupling of Arylsilanes With Thiuram Reagents: A Facile Synthesis of Aryl Dithiocarbamates

Yiying Wang¹, Hongtao Shen², Jianhua Qiu², Mengqi Chen^{2*}, Weimin Song^{2*}, Mingqin Zhao¹, Longfei Wang¹, Feng Bai², Hongxia Wang² and Zhiyong Wu^{1*}

¹Flavors and Fragrance Engineering and Technology Research Center of Henan Province, College of Tobacco Science, Henan Agricultural University, Zhengzhou, China, ²Technology Center, China Tobacco Henan Industrial Co., Ltd., Zhengzhou, China

OPEN ACCESS

Edited by:

Simone Brogi,
University of Pisa, Italy

Reviewed by:

David Morales-Morales,
Instituto de Química, Universidad
Nacional Autónoma de México,
Mexico
Kevin Alan Lobb,
Rhodes University, South Africa
Michal Szostak,
Rutgers University, United States

*Correspondence:

Mengqi Chen
479820476@qq.com
Weimin Song
gongyishi@126.com
Zhiyong Wu
zhiyongwu@henau.edu.cn

Specialty section:

This article was submitted to
Organic Chemistry,
a section of the journal
Frontiers in Chemistry

Received: 01 February 2022

Accepted: 09 March 2022

Published: 26 April 2022

Citation:

Wang Y, Shen H, Qiu J, Chen M,
Song W, Zhao M, Wang L, Bai F,
Wang H and Wu Z (2022) Copper-
Promoted Hiyama Cross-Coupling of
Arylsilanes With Thiuram Reagents: A
Facile Synthesis of
Aryl Dithiocarbamates.
Front. Chem. 10:867806.
doi: 10.3389/fchem.2022.867806

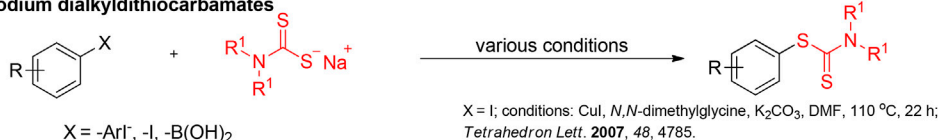
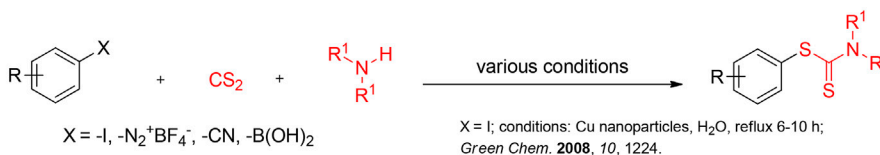
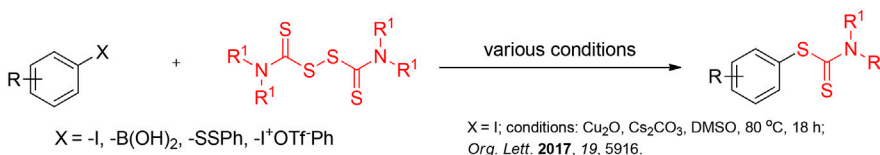
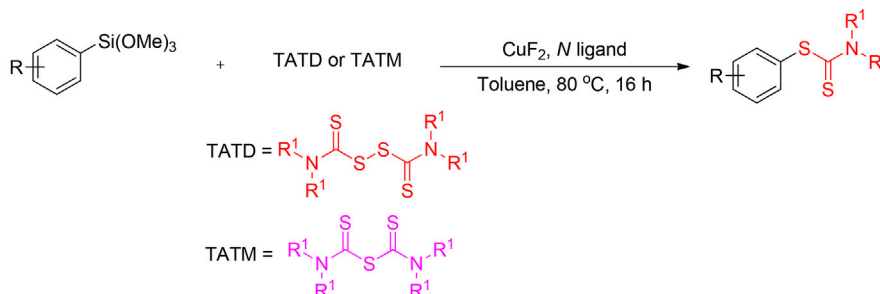
We report herein a facile Hiyama cross-coupling reaction of arylsilanes with thiuram reagents (tetraalkylthiuram disulfides or tetraalkylthiuram monosulfide) enabled by copper fluoride. Compared to our previous work, this protocol is an alternative protocol for the generation of S-aryl dithiocarbamates. It features low toxic and readily available substrates, cost-effective promoter, easy performance, and provides good yields.

Keywords: Hiyama cross-coupling, arylsilanes, thiuram reagents, C-S bond formation, aryl dithiocarbamates

INTRODUCTION

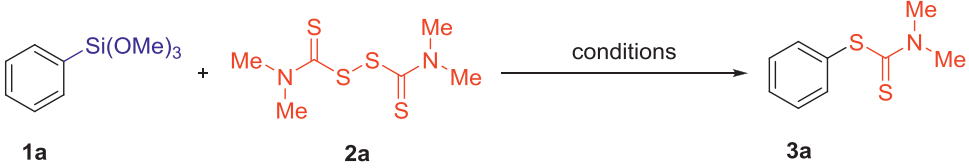
Transition-metal-catalyzed cross-coupling reactions have been found broad applications for the construction of carbon-carbon and carbon-heteroatom bonds enable the facile preparation of more complex molecules (Miyaura, 2002; Magano and Dunetz, 2011; Negishi, 2011; Suzuki, 2011; Guo and Rueping, 2018; Zhang et al., 2020). In 1972, Kumada and Tamao (Tamao et al., 1972) reported the cross-coupling reaction of Grignard reagents (RMgX) with organic halides (R'X) catalyzed by nickel/phosphine system. From then on, a wide range of organometallic reagents such as lithium (Yamamura et al., 1975; Murahashi et al., 1979), aluminum (Negishi et al., 1978), zinc (Sekiya and Ishikawa, 1976; King et al., 1977; Negishi and Van Horn, 1977; Negishi, 2011), zirconium (Negishi et al., 1977; Okukado et al., 1978) and tin (Milstein and Stille, 1979a; Milstein et al., 1979b) have emerged and exerted a ubiquitous influence on the synthesis community. However, their instability, air and moisture sensitivity and the production of corrosive halogen wastes are disadvantageous from both synthetic and environmental points of view. In addition to these well-established organometallic reagents, the silicon reagent which was developed by Hiyama and co-workers, is an alternative and attractive coupling partner for cross-coupling reactions (the so-called Hiyama cross-coupling) (Nakao and Hiyama, 2011; Sore et al., 2012; Denmark and Ambrosi, 2015; Komiyama et al., 2016). Generally, organosilicon reagents exhibit some remarkable advantages such as non-toxicity, high stability, good tolerance toward various functional groups and natural abundance of silicon. In the overpast several decades, significant advances on transition-metal-catalyzed Hiyama cross-coupling have been achieved (Nareddy et al., 2017; Nareddy et al., 2018; González et al., 2019; Han et al., 2019; Zhang et al., 2019; Idris and Lee, 2020; Lu et al., 2020; Wu et al., 2021), nevertheless, the diverse applications of this methodology are still less explored and worthy of in-depth exploration under the concept of green chemistry.

Thiuram reagents (tetraalkylthiuram disulfides TMTD, or tetraalkylthiuram monosulfide TMTM) are cheap and stable organosulfur compounds which can be widely used in biologically

A The reactions of organometallic reagents with tetraalkylthiuram disulfides**B The reactions of arylation reagents with sodium dialkylthiocarbamates****C One pot three component reaction****D The reactions of tetraalkylthiuram disulfides with new coupling partners****E This work****SCHEME 1** | Different methodologies for the synthesis of aryl dithiocarbamates.

active compounds, agricultural pesticides and vulcanization accelerators (Enders et al., 2010), and also act as readily available sulfur reagents in organic synthesis. (Zeng et al., 2017a; Zeng et al., 2017b; Wu and Yan, 2019). Among them, organic dithiocarbamates have been extensively investigated for their outstanding biological activities (Hou et al., 2006; Zou et al., 2014; Liénard et al., 2008; Horita et al., 2011) and synthetic value (Boas et al., 2004; Derouet et al., 2009; Wulfs and Greene, 2007; Zhang et al., 2005). Hence, much attention has been paid to the development of highly efficient and convenient methods for the construction of such scaffolds. Traditionally, the portion of S-aryl dithiocarbamates was prepared through the reactions of classical organometallic reagents with tetramethylthiuram disulfide (Jen and Cava, 1982; Knochel et al., 2006) (**Scheme 1A**). The reactions of sodium dialkylthiocarbamates with diaryliodonium salts (Chen et al., 1987), aryl halide (Liu and Bao, 2007) or aryl boronic acid

(Gao et al., 2018) were also proved to be an effective strategy (**Scheme 1B**). Recently, the three-component reactions of amines, carbon disulfide, and diverse electrophiles including alkyl halides (Azizi et al., 2006), aryl halides (Bhadra et al., 2008), aryldiazonium fluoroborates (Chatterjee et al., 2011), pentafluorobenzonitrile (Yin et al., 2015), and phenylboronic acid (Qi et al., 2016) (**Scheme 1C**) have been achieved by some research groups. Moreover, the cross-coupling reactions of tetraalkylthiuram disulfide with aryl iodide (Dong et al., 2017; Cao et al., 2018; Wu and Yan, 2019), phenylboronic acid (Xu et al., 2018), diaryl disulfides (Peng et al., 2019), or diaryliodonium salts (Zeng et al., 2017b) were also successively established by some chemists (**Scheme 1D**). However, these methods always suffer from one or more disadvantages such as toxic reagents, multiple reaction steps or flammable and explosive substrates, which limit their applications. To our

TABLE 1 | Optimization of reaction conditions ^a.


Entry	Promoter	Ligand (Equiv.)	Solvent	T (°C)	Yields of 3a (%) ^b
1 ^c	CuF2	-	Toluene	120	22
2	-	-	Toluene	120	0
3	CuF2	-	Toluene	120	23
4	CoCl2	-	Toluene	120	0
5	CuF2	bipyridine (2)	Toluene	120	61
6	CuF2	1,10-phenanthroline (2)	Toluene	120	82
7	CuF2	pyridine (2)	Toluene	120	78
8	CuF2	N,N,N',N'-tetramethylethylenediamine (2)	Toluene	120	0
9	CuF2	2,2':6',2''-terpyridine (2)	Toluene	120	43
10	CuF2	(R,R)-2,2'-(2,6-pyridinediyl)bis (4-isopropyl-2-oxazoline) (2)	Toluene	120	39
11	CuF2	8-benzoylaminoquinoline (2)	Toluene	120	76
12	CuF2	1,2-bis(diphenylphosphino)ethane (2)	Toluene	120	<5
13	CuF2	2,2'-bis(diphenylphosphino)-1,1'-biphenyl (2)	Toluene	120	<5
14	CuF2	1,1'-bis(diphenylphosphino)ferrocene (2)	Toluene	120	<5
15	CuF2	(R)-(+)-2,2'-bis(diphenylphosphino)-1,1'-binaphthyl (2)	Toluene	120	11
16	AgF	1,10-phenanthroline (2)	Toluene	120	0
17	CsF	1,10-phenanthroline (2)	Toluene	120	0
18	CuF2	1,10-phenanthroline (2)	Xylene	120	38
19	CuF2	1,10-phenanthroline (2)	Msitylene	120	43
20	CuF2	1,10-phenanthroline (2)	1,4-Dioxane	120	20
21	CuF2	1,10-phenanthroline (2)	Acetonitrile	120	42
22	CuF2	1,10-phenanthroline (2)	DMF	120	0
23	CuF2	1,10-phenanthroline (2)	DMSO	120	0
24	CuF2	1,10-phenanthroline (3)	Toluene	120	58
25	CuF2	1,10-phenanthroline (0.5)	Toluene	120	74
26	CuF2	1,10-phenanthroline (2)	Toluene	120	37
27 ^d	CuF2	1,10-phenanthroline (2)	Toluene	120	55
28 ^e	CuF2	1,10-phenanthroline (2)	Toluene	120	26
29	CuF2	1,10-phenanthroline (2)	Toluene	100	85
30	CuF2	1,10-phenanthroline (2)	Toluene	80	88
31	CuF2	1,10-phenanthroline (2)	Toluene	60	59
32 ^f	CuF2	1,10-phenanthroline (2)	Toluene	120	84
33 ^g	CuF2	1,10-phenanthroline (2)	Toluene	120	54

^aTrimethoxy (phenyl)silane 1a (0.10 mmol), Tetramethylthiuram disulfide 2a (0.20 mmol), promoter (3.0 equiv.), and Toluene (1 ml) for 16 h, under air.

^bIsolated yields.

^c20 mol% of CoCl2 was added.

^dPromoter (4.0 equiv.).

^ePromoter (2.0 equiv.).

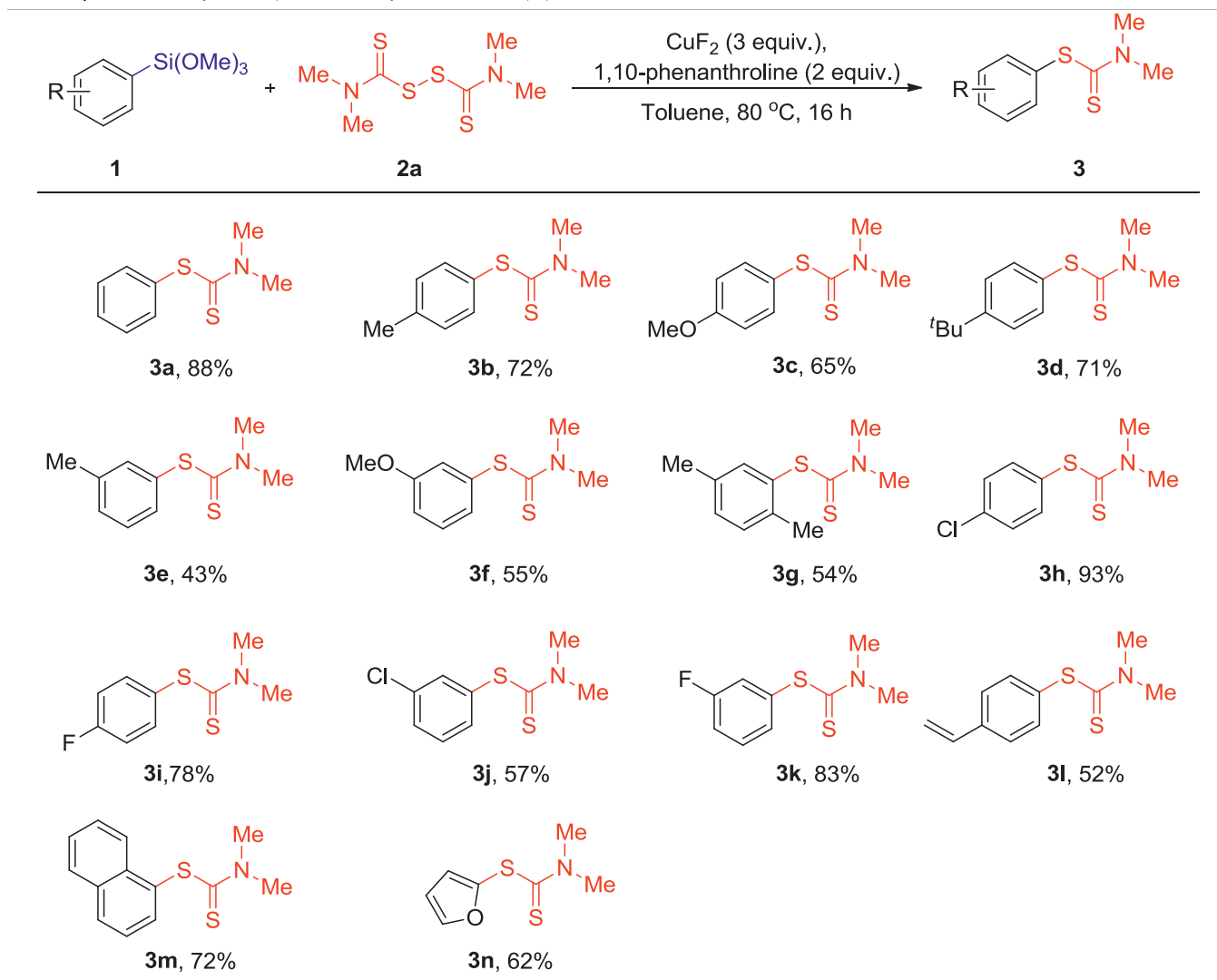
^f24 h.

^g48 h.

knowledge, the synthesis of S-aryl dithiocarbamates using thiuram reagents (tetraalkylthiuram disulfides (TATD), or tetraalkylthiuram monosulfide (TATM)) and arylsilanes as the coupling partners has not been documented so far. As a continuation of our interest in the cross-coupling of tetraalkylthiuram disulfide (Wu et al., 2018; Lai et al., 2019a; Cheng et al., 2019; Hu et al., 2020), herein we wish to report the first example of copper-mediated C-S bond construction by cross-coupling of arylsilanes with thiuram reagents (TATD or TMTM) in the presence of CuF2 and N ligand (**Scheme 1E**), which would be an alternative way for the synthesis of S-aryl dithiocarbamates.

RESULT AND DISCUSSION

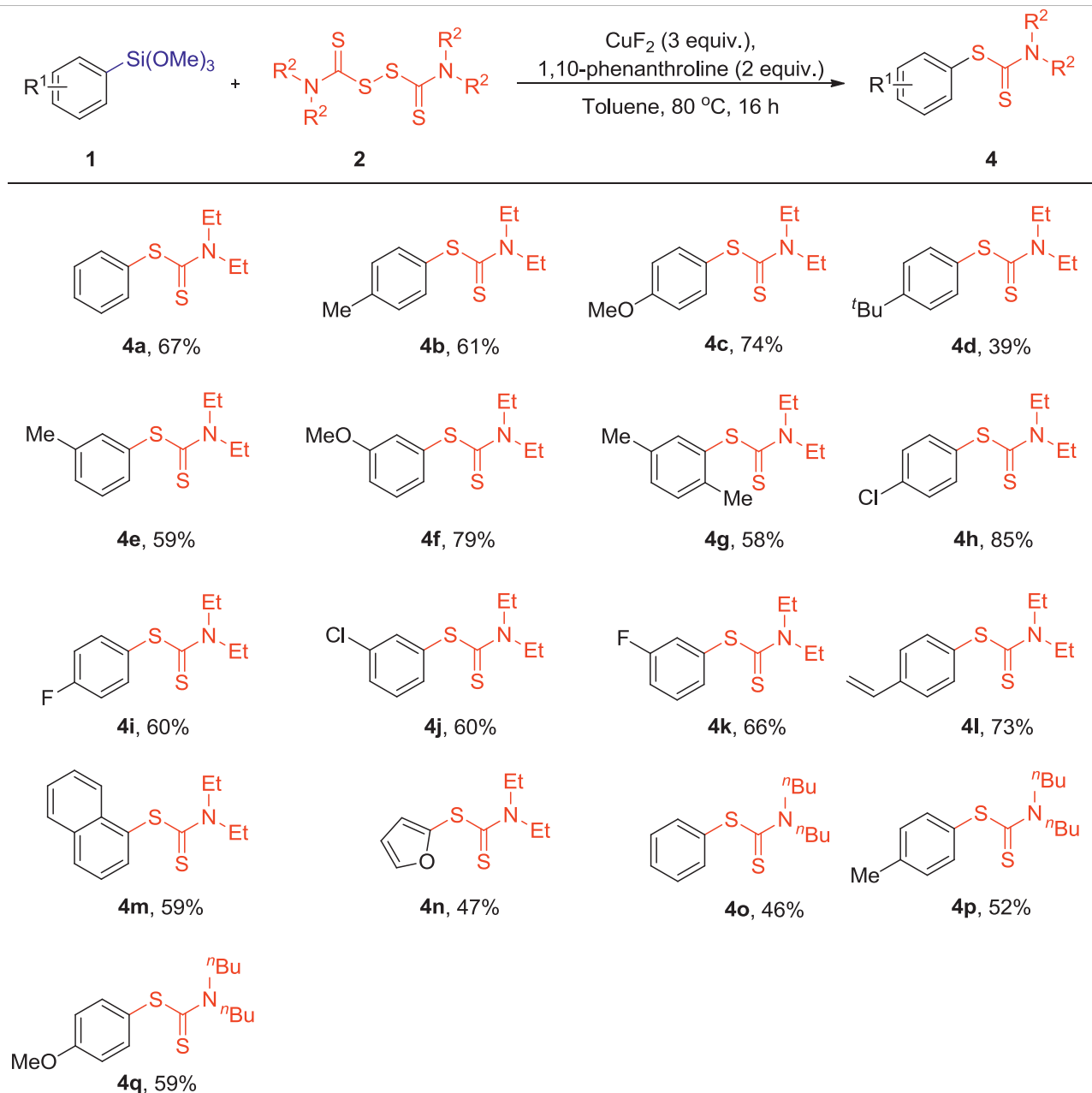
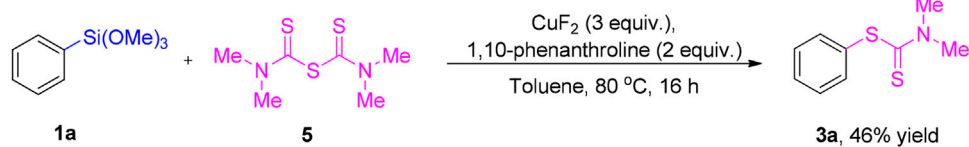
Initially, the reaction parameters were optimized using trimethoxy (phenyl)silane (1a) and tetramethylthiuram disulfide (TMTD, 2a), and the results were summarized in **Table 1**. Firstly, the reaction of 1a (0.1 mmol) and 2a (0.2 mmol) was performed in the presence of CuF2 (3 equiv.) together with 20 mol% of CoCl2 in Toluene at 120°C. To our delight, the initial reaction conditions provided the desired product 3a (phenyl dimethylcarbomodithioate) in 22% yield (**Table 1**, entry 1). The exact structure of 3a was confirmed by NMR and HRMS spectra. When the reaction was carried out in

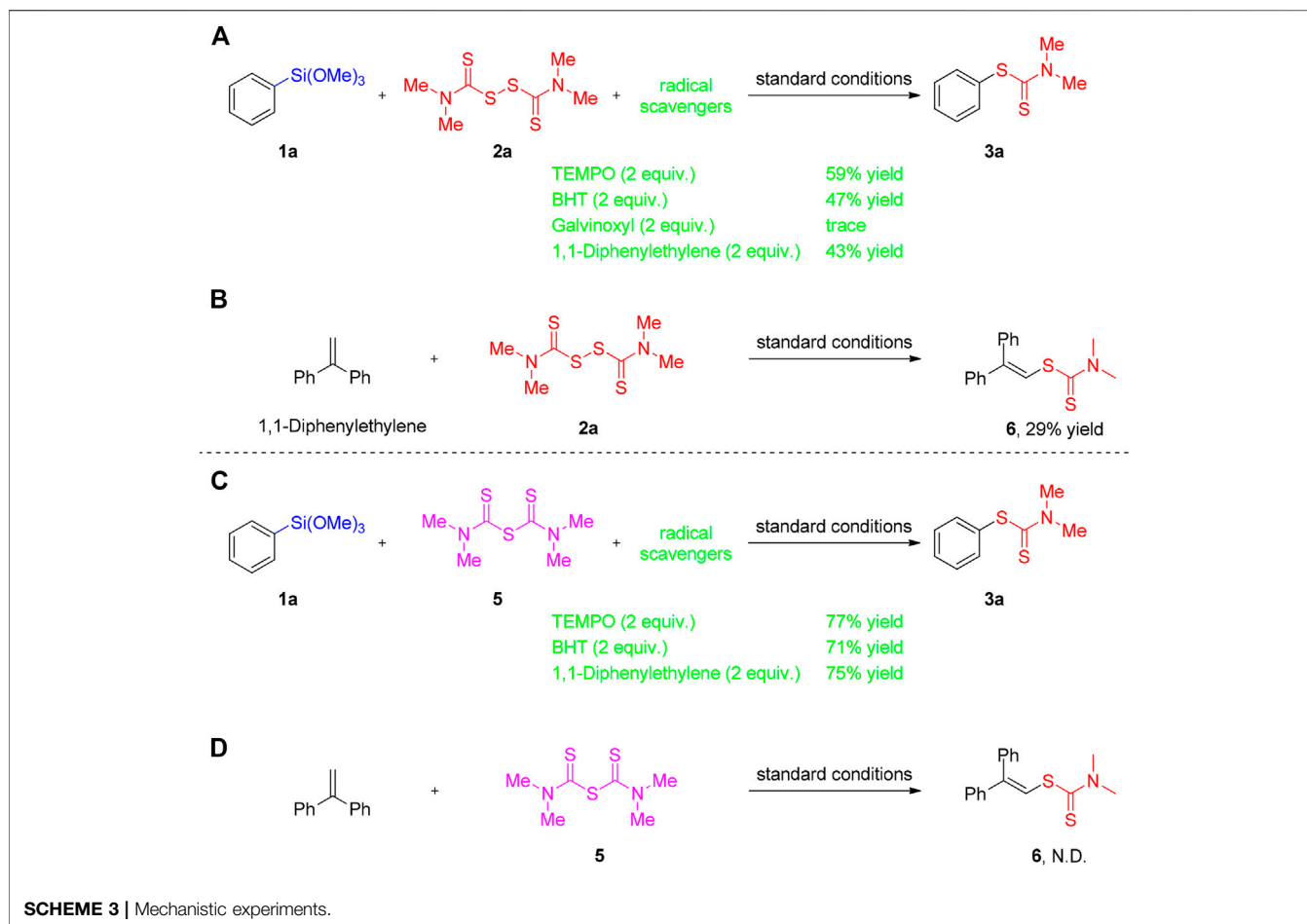
TABLE 2 | Reactions of arylsilanes **1** with tetramethylthiuram disulfide (**2a**)^{a,b}.^a **1** (0.1 mmol), **2a** (0.2 mmol), CuF₂ (3 equiv.), 1,10-phenanthroline (2 equiv.), Toluene (1 ml), 80°C, 16 h, under air.^b Isolated yields.

the absence of CuF₂, it didn't produce any products (**Table 1**, entries 2 and 4). However, the reaction gave 23% yield of product **3a** when CoCl₂ was removed from the reaction system (**Table 1**, entry 3). The control experiment clearly indicated that CuF₂ was indispensable for this reaction. Inspired by the reported literature (Clarke, 2005; McManus et al., 2006; Fihri et al., 2007; Hachiya et al., 2010; Wu et al., 2016; Sahani et al., 2018; Luo et al., 2020), some nitrogen and phosphorus ligands were screened (**Table 1**, entries 5–15, 0–78%), and 1, 10-phenanthroline was proved to be the optimized N ligand, affording the product **3a** in 82% yield (**Table 1**, entry 6). Subsequently, other fluoride activators for the C-Si bond cleavage were evaluated in this reaction (**Table 1**, entries 16–17), but all of them turned out to be invalid. The effect of solvents such as Xylene, Mesitylene, 1,4-Dioxane, Acetonitrile, DMF and DMSO were also examined, and the experimental results showed that Toluene was the most suitable candidate with remarkably higher yields (**Table 1**, entry 6 vs entries 18–23, 82% vs 0–43%). Furthermore, the effect of CuF₂ and N ligand loading

was investigated (**Table 1**, entries 24–28, 26–74%). The obtained results revealed that a relatively lower reaction efficiency was detected in these reactions. Further optimization indicated that the temperature also played an important role in this transformation, and 80°C was identified as the ideal reaction temperature (**Table 1**, entry 6 and entries 29–31, 88% vs 59–85%). Meanwhile, the reaction time was also examined (**Table 1**, entries 32–33, 54–84%), and 16 h was found to be the best choice. Thus, the reaction efficiently proceeded when 3 equiv. of CuF₂ was used in combination with 1,10-phenanthroline (2 equiv.) in Toluene at 80°C for 16 h. Noteworthily, the combination CuF₂/phenanthroline acted as the activator of C-Si bond, and also acted as the promoter on the formation of C-S bond.

Having the optimized conditions in hand, we then proceeded to explore the scope of the reaction with respect to both the organosilane reagents and the thiuram disulfides (**Table 2** and **Table 3**). Generally, phenylsilanes bearing diverse substituents such as methyl, methoxyl, tert-butyl, chloro and fluoro groups

TABLE 3 | Reactions of arylsilanes 1) with tetraalkylthiuram disulfides (2) ^{a,b}.^a 1 (0.10 mmol), 2 (0.20 mmol), CuF₂ (3 equiv.), 1,10-phenanthroline (2 equiv.), Toluene (1 ml), 80°C, 16 h.^b Isolated yields.**SCHEME 2** | Initial cross-coupling reaction of trimethoxy (phenyl)silane and TMTM ^{a,b}. a Reaction conditions: 1 (0.10 mmol), 5 (0.20 mmol), CuF₂ (3 equiv.), 1,10-phenanthroline (2 equiv.), Toluene (1 ml), 80°C, 16 h b Isolated yields.



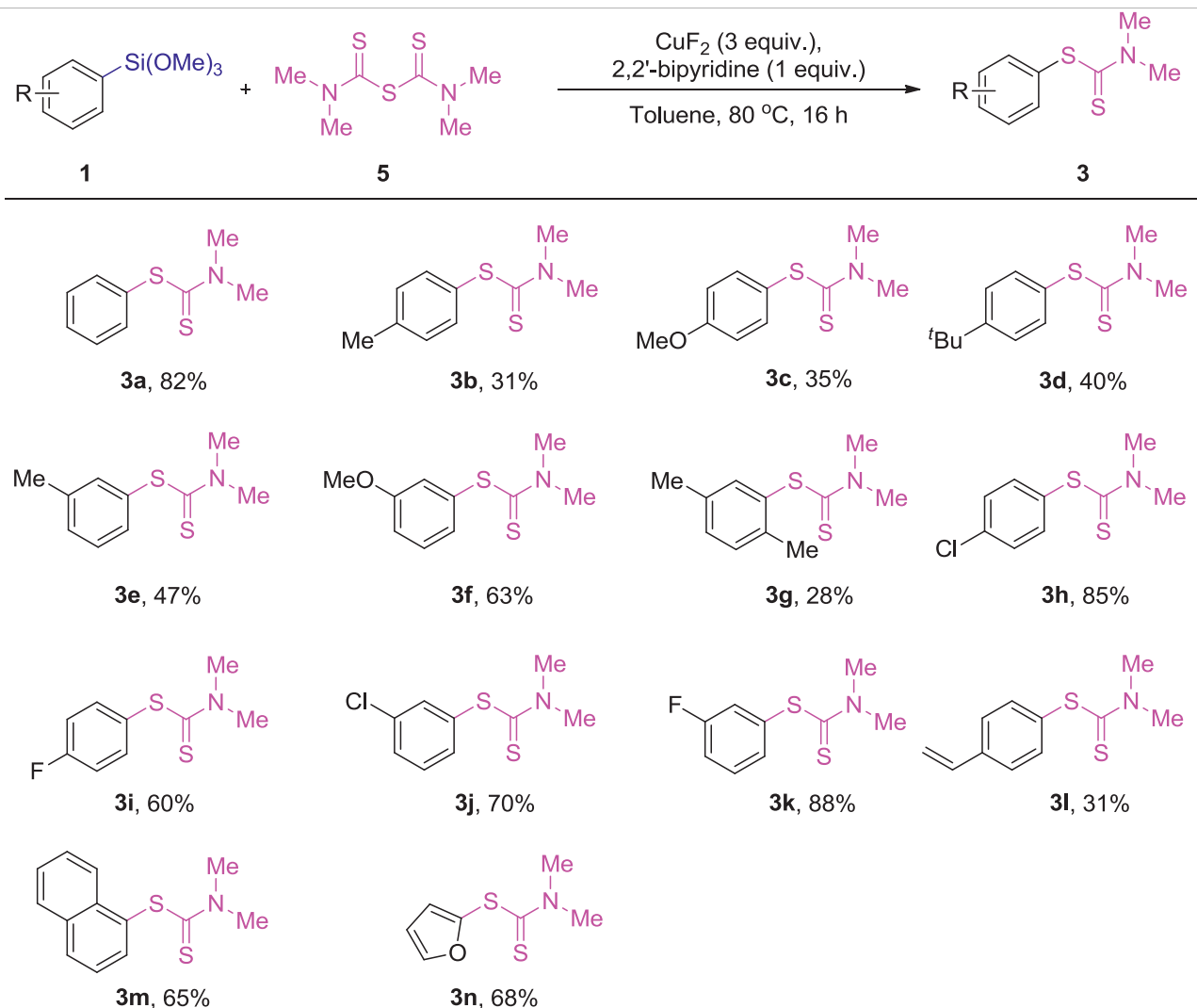
offered the desired products in moderate to good yields. Notably, this reaction tolerated the electron-rich arylsilanes (**Table 2**, **3b-g**), as (4-methylphenyl) trimethoxysilane, (4-methoxyphenyl) trimethoxysilane and (4-(tert-butyl)phenyl) trimethoxysilane coupled efficiently with tetramethylthiuram disulfide **2a** to give **3b-d** in 65–72% yields. When methyl, methoxyl, were introduced into the meta position of phenylsiloxanes, slight lower yields were obtained (**3e-g**, 43–55%), which may be caused by steric hindrance effect. Excellent yields were got for electron-deficient arylsilanes such as (4-chlorophenyl)trimethoxysilane and (4-fluorophenyl) trimethoxysilane. Compared with electron-rich substituents, arylsilanes with electron-withdrawing groups on the aromatic ring presented relatively higher reactivity (**3b-c** vs **3h-i**, 65–72% vs 78–93%). This result makes the said cross-coupling reaction particularly attractive for further transformation by transition-metal-catalyzed coupling reactions. Pleasingly, these reaction conditions were also compatible with trimethoxy (4-vinylphenyl)silane, 1-(trimethoxysilyl)naphthalene and 2-furan-trimethoxysilane, which provided the corresponding products **3l-n** in 52–72 yields.

This cross-coupling reaction also demonstrated a good tolerance toward other N,N,N',N'-tetraalkylthiuram disulfides as shown in **Table 2**. The N,N,N',N'-tetraethylthiuram disulfide (TETD, **2b**) showed a good reactivity and furnished

the corresponding S-aryl dithiocarbamates products in moderate to good yields (**4a-n**, 39–85%). Comparatively, the reaction of N,N,N',N'-tetrabutylthiuram (TBTD, **2c**) and arylsilanes showed relatively lower reactivity, and afforded lower yields of the corresponding products (**4o-q**, 46–59%). It is worth noting that the yields of the resulting products were modulated by the presence of different alkyl substituents on the tetraalkylthiuram disulfides. Slightly lower yields were obtained when longer chain-substituted tetraalkylthiuram disulfides were used in these reactions (**3a** vs **4a** and **4'**).

To further evaluate the applicability of this reaction, the reactivity of trimethoxy (phenyl)silane (**1a**) was investigated using tetramethylthiuram monosulfide (TMTM, **5**) as the coupling partner (Wu et al., 2020). As expected, the cross-coupling reaction occurred smoothly, and the phenyl dimethylcarbamodithioate **3a** was formed in 46% yield (**Scheme 2**).

In order to find the appropriate conditions to achieve an ideal yield, we spent a bit more time on the optimization of reaction conditions. Some bidentate, tridentate N ligands as well as diphosphines ligands and their loading to this reaction were tested, and a summative result of the optimization was presented in **Supplementary Table S1**. After the simple optimization, we found that 1 equiv. of 2, 2'-bipyridine

TABLE 4 | Reactions of arylsilanes 1) with tetramethylthiuram monosulfide (5) ^{a,b}.

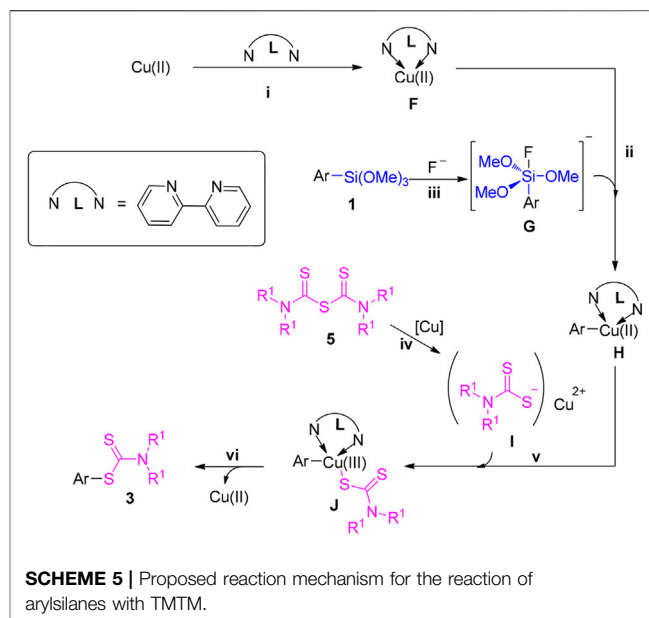
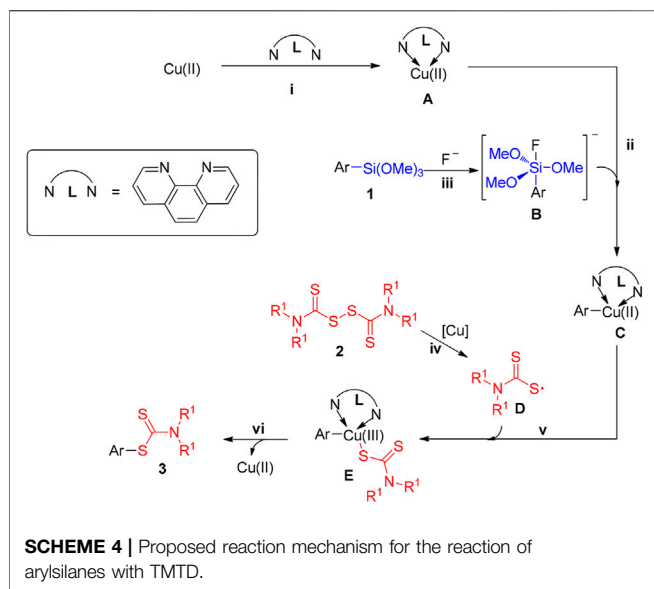
^a1 (0.10 mmol), 5 (0.20 mmol), CuF₂ (3 equiv.), 2, 2'-bipyridine (1 equiv.), Toluene (1 ml), 80°C, 16 h.

^bIsolated yields.

increased the yield to 68% (**Supplementary Table S1**, entry 3), N,N,N',N'-tetramethylethylenediamine, 2,2':6',2''-terpyridine; (R,R)-2,2'-(2,6-pyridinediyl)bis (4-isopropyl-2-oxazoline, 8-benzoylaminoquinoline, 1,2-bis(diphenylphosphino)ethane, 2,2'-bis(diphenylphosphino)-1,1'-biphenyl, 1,1'-bis(diphenylphosphino)ferrocene and (R)-(+)-2,2'-bis(diphenylphosphino)-1,1'-binaphthyl resulted in a relatively lower yields (**Supplementary Table S1**, entries 4-11). It probably because of the coordination of 2, 2'-bipyridine with copper, which provided a more stable and active copper intermediate for the said cross-coupling reaction. After the simple optimization, we found that 1 equiv. of 2, 2'-bipyridine acted as the suitable N ligand. With the new optimized reaction conditions in hand, some more substituted arylsilanes were subjected to this reaction and the results were summarized in **Table 4**.

In general, the results obtained from the cross-coupling reaction of arylsilanes 1) with tetramethylthiuram monosulfide (TMTM, 5) are different from the reaction with tetramethylthiuram disulfide (TMTD, 2a), in which the electron-rich arylsilanes are less active (3b-g, 28–63%). With regard to the electron-deficient arylsilanes, they showed a similar efficiency as the reaction with tetramethylthiuram disulfide (TMTD, 2a), and the products (3h-k) were provided in 60–88% yields. The 1-(trimethoxysilyl)naphthalene and 2-furan-trimethoxysilane also participated in this reaction to give the corresponding products (3m-n) in 65–68% yields, which are nearly the same results compared with the reaction with TMTD (2a). In contrast, the trimethoxy (4-vinylphenyl)silane exhibited a less activity in this reaction and displayed lower yield (3l, 31%).

In order to ascertain the mechanism, some control experiments were conducted and the results were exhibited



in **Scheme 3**. When 2 equiv. of radical scavenger 2,2,6,6-tetramethyl-1-piperidinyloxy (TEMPO), butylated hydroxyl toluene (BHT), galvinoxyl free radical or 1,1-diphenylethylene were added to the reaction of 1a and 2a under the standard conditions, a substantial decrease of the reaction efficiency was observed (**Scheme 3A**). Subsequently, the radical quencher 1,1-diphenylethylene was added to the tetraalkylthiuram disulfides participated reaction system, the thiuram radical was captured to give the corresponding product six in 29% yield (**Scheme 3B**). The above mentioned results illustrating that a radical process may be exist in the reaction of 1a and 2a. In sharp contrast, when the reactions were occurred between 1a and 5 in the presence of radical inhibitors (2.0 equiv of TEMPO, BHT) or 1,1-diphenylethylene, which gave the desired product 3a in 77, 71, and 75% yields, respectively (**Scheme 3C**). Furthermore, no desired product six was observed when 1,1-diphenylethylene react with 5 (TMTM) under the standard conditions (**Scheme 3D**). These results suggesting that the reaction of 1a and 5 is more likely to be an ionic-type pathway.

Considering the experimental evidence as well the previous reports (Lu et al., 2020; Dong et al., 2017; Luo et al., 2020; Hao et al., 2020; Lai et al., 2019b), a plausible reaction mechanism was tentatively proposed and described in **Scheme 4**. Firstly, the coordination of 1, 10-phenanthroline with copper salts to produce the copper complex A. Simultaneously, the C-Si cleavage process occurred lead to the intermediate B, which activated by fluoride ion (Sugiyama et al., 2008). In step ii, the reaction of intermediate B with copper complex A generates the Cu(II) complex C. Subsequently, thiuram radical D may be formed through the homolysis of tetramethylthiuram disulfide at 80°C probably assisted by Cu(II). Then, the interreaction of Cu(II) complex C with thiuram radical D to provide the intermediate E, which undergoes reductive elimination to

yield the desired product three along with the release of Cu(II) species.

With regard to the reaction pathway between 1a and 5 (TMTM), a plausible ionic-type reaction mechanism was tentatively proposed according to the obtained results as well as the reported literatures (Dong et al., 2017; Luo et al., 2020; Wu et al., 2020) and described in **Scheme 5**. Analogously, the initial coordination of bipyridine with copper salts to produce the copper complex F. Concurrently, the intermediate G is generated by the C-Si cleavage manner, which activated by fluoride ion (Sugiyama et al., 2008). Then, the interreaction of intermediate G with copper complex F to generate the Cu(II) complex H. In the meantime, nucleophile F probably produces by the interreaction of copper ion with 5 at 80°C. Subsequently, the interreaction of Cu(II) complex H with nucleophile I to provide the intermediate J, which undergoes reductive elimination lead to the desired product three along with the release of Cu(II) species.

CONCLUSION

In summary, we have developed an interesting methodology on the copper-promoted cross-coupling of arylsilanes and thiuram reagents (TATD or TMTM), affording the valuable S-aryl dithiocarbamates in moderate to good yields. This facile strategy allows practical and friendly reaction conditions, which significantly broadens the substrate scope, improves the functional group compatibility, and emphasizes the synthetic application in complex molecules. It offers not only a protocol for the streamlined synthesis of S-aryl dithiocarbamates from cheap and stable substrates, but also a new example for the application of Hiyama cross-coupling in biological interesting molecules' construction.

DATA AVAILABILITY STATEMENT

The original contributions presented in the study are included in the article/**Supplementary Material**, further inquiries can be directed to the corresponding authors.

AUTHOR CONTRIBUTIONS

MC, WS and ZW contributed to the conception and design of the study. The synthetic work and data collection were carried out by YW, HS, JQ and LW. FB, MZ and HW contributed to the article revision. All authors read and approved the submitted version.

REFERENCES

- Azizi, N., Aryanassab, F., and Saidi, M. R. (2006). Straightforward and Highly Efficient Catalyst-free One-Pot Synthesis of Dithiocarbamates under Solvent-free Conditions. *Org. Lett.* 8, 5275–5277. doi:10.1021/ol0620141
- Bhadra, S., Saha, A., and Ranu, B. C. (2008). One-pot Copper Nanoparticle-Catalyzed Synthesis of S-Aryl- and S-Vinyl Dithiocarbamates in Water: High Diastereoselectivity Achieved for Vinyl Dithiocarbamates. *Green. Chem.* 10, 1224–1230. doi:10.1039/b809200a
- Boas, U., Gertz, H., Christensen, J. B., and Heegaard, P. M. H. (2004). Facile Synthesis of Aliphatic Isothiocyanates and Thioureas on Solid Phase Using Peptide Coupling Reagents. *Tetrahedron Lett.* 45, 269–272. doi:10.1016/j.tetlet.2003.10.182
- Chatterjee, T., Bhadra, S., and Ranu, B. C. (2011). Transition Metal-free Procedure for the Synthesis of S-Aryl Dithiocarbamates Using Aryl Diazonium Fluoroborate in Water at Room Temperature. *Green. Chem.* 13, 1837–1842. doi:10.1039/c1gc00001b
- Chen, Z., Jin, Y., and Stang, P. J. (1987). Polyvalent Iodine in Synthesis. 2. A New Method for the Preparation of Aryl Esters of Dithiocarbamic Acids. *J. Org. Chem.* 52, 4117–4118. doi:10.1021/jo00227a032
- Cheng, C., Zhao, M., Lai, M., Zhai, K., Shi, B., Wang, S., et al. (2019). Synthesis of Aza-Heteroaromatic Dithiocarbamates via Cross-Coupling Reactions of Aza-Heteroaromatic Bromides with Tetraalkylthiuram Disulfides. *Eur. J. Org. Chem.* 2019, 2941–2949. doi:10.1002/ejoc.201900475
- Clarke, M. L. (2005). First Microwave-Accelerated Hiyama Coupling of Aryl- and Vinylsiloxane Derivatives: Clean Cross-Coupling of Aryl Chlorides within Minutes. *Adv. Synth. Catal.* 347, 303–307. doi:10.1002/adsc.200404196
- Denmark, S. E., and Ambrosi, A. (2015). Why You Really Should Consider Using Palladium-Catalyzed Cross-Coupling of Silanols and Silanolates. *Org. Process. Res. Dev.* 19, 982–994. doi:10.1021/acs.oprd.5b00201
- Derouet, D., Tran, Q. N., and Thuc, H. H. (2009). Synthesis of Polymer-Grafted Natural Rubbers by Radical Photopolymerization of Vinyl Monomers Initiated from the Rubber Chains. *J. Appl. Polym. Sci.* 114, 2149–2160. doi:10.1002/app.30266
- Dong, Z.-B., Cao, Q., Peng, H.-Y., and Cheng, Y. (2018). A Highly Efficient CuCl₂-Catalyzed C-S Coupling of Aryl Iodides with Tetraalkylthiuram Disulfides: Synthesis of Aryl Dithiocarbamates. *Synthesis* 50, 1527–1534. doi:10.1055/s-0036-1589166
- Dong, Z.-B., Liu, X., and Bolm, C. (2017). Copper-Catalyzed C(sp²)-S Coupling Reactions for the Synthesis of Aryl Dithiocarbamates with Thiuram Disulfide Reagents. *Org. Lett.* 19, 5916–5919. doi:10.1021/acs.orglett.7b02911
- Dong, Z.-B., Wu, Y.-X., Peng, K., and Li, J.-H. (2020). An Efficient Copper-Catalyzed C(sp²)-S Formation Starting from Aryl Iodides and Tetramethylthiuram Monosulfide (TMTM). *Synthesis* 52, 3001–3006. doi:10.1055/s-0040-1707899
- Enders, D., Rembiak, A., and Liebich, J. (2010). Direct Organocatalytic α -Sulfenylation of Aldehydes and Ketones with Tetramethylthiuram Disulfide. *Synthesis* 2011, 281–286. doi:10.1055/s-0030-1258359
- Fihri, A., Meunier, P., and Hierso, J.-C. (2007). Performances of Symmetrical Achiral Ferrocenylphosphine Ligands in Palladium-Catalyzed Cross-Coupling Reactions: A Review of Syntheses, Catalytic Applications and Structural Properties. *Coord. Chem. Rev.* 251, 2017–2055. doi:10.1016/j.ccr.2007.03.020
- Gao, M.-Y., Xu, W., Zhang, S.-B., Li, Y.-S., and Dong, Z.-B. (2018). Synthesis of Phenyl Dithiocarbamates Starting from Sodium Dithiodylthiocarbamates and Aryl Boronic Acids: a Copper Catalyzed S-Arylation. *Eur. J. Org. Chem.* 2018, 6693–6698. doi:10.1002/ejoc.201801271
- González, J., Schäfer, P., and Fletcher, S. P. (2019). Highly Enantioselective Hiyama Cross-Coupling via Rh-Catalyzed Allylic Arylation of Racemic Allyl Chlorides. *Organometallics* 38, 3991–3995. doi:10.1021/acs.organomet.9b00197
- Guo, L., and Rueping, M. (2018). Transition-Metal-Catalyzed Decarbonylative Coupling Reactions: Concepts, Classifications, and Applications. *Chem. Eur. J.* 24, 7794–7809. doi:10.1002/chem.201704670
- Hachiya, H., Hirano, K., Satoh, T., and Miura, M. (2010). Nickel-Catalyzed Direct CH Arylation and Alkenylation of Heteroarenes with Organosilicon Reagents. *Angew. Chem.* 122, 2248–2251. doi:10.1002/ange.200906996
- Han, C., Zhang, Z., Xu, S., Wang, K., Chen, K., and Zhao, J. (2019). Palladium-Catalyzed Hiyama Coupling of Benzylic Ammonium Salts via C-N Bond Cleavage. *J. Org. Chem.* 84, 16308–16313. doi:10.1021/acs.joc.9b02554
- Hao, S., Ye, X., Zhao, M., Hu, J., Wang, N., Li, J., et al. (2020). Synthesis of 2-Aryl-2-hydroxyethyl Dithiocarbamates via Regioselective Addition of Tetraalkylthiuram Disulfides to Styrenes under Transition-Metal-Free Conditions. *Adv. Synth. Catal.* 362, 5014–5019. doi:10.1002/adsc.202000729
- Horita, Y., Takii, T., Kuroishi, R., Chiba, T., Ogawa, K., Kremer, L., et al. (2011). Synthesis and Evaluation of Anti-tubercular Activity of New Dithiocarbamate Sugar Derivatives. *Bioorg. Med. Chem. Lett.* 21, 899–903. doi:10.1016/j.bmcl.2010.12.084
- Hou, X., Ge, Z., Wang, T., Guo, W., Cui, J., Cheng, T., et al. (2006). Dithiocarbamic Acid Esters as Anticancer Agent. Part 1: 4-Substituted-Piperazine-1-Carbodithioic Acid 3-Cyano-3,3-Diphenyl-Propyl Esters. *Bioorg. Med. Chem. Lett.* 16, 4214–4219. doi:10.1016/j.bmcl.2006.05.085
- Hu, J., Ye, X., Hao, S., Zhao, Q., Zhao, M., Wei, Y., et al. (2020). Amidation Reaction of Quinoline-3-carboxylic Acids with Tetraalkylthiuram Disulfides under Simple Conditions: A Facile Synthesis of Quinoline-3-carboxamides. *Asian J. Org. Chem.* 9, 2191–2195. doi:10.1002/ajoc.202000462
- Idris, M. A., and Lee, S. (2020). Palladium-Catalyzed Amide N-C Hiyama Cross-Coupling: Synthesis of Ketones. *Org. Lett.* 22, 9190–9195. doi:10.1021/acs.orglett.0c03260
- Jen, K.-Y., and Cava, M. P. (1982). A New Synthesis of Aromatic Thiols. *Tetrahedron Lett.* 23, 2001–2004. doi:10.1016/s0040-4039(00)87244-5
- King, A. O., Okukado, N., and Negishi, E.-i. (1977). Highly General Stereo-, Regio-, and Chemo-Selective Synthesis of Terminal and Internal Conjugated Enynes by the Pd-Catalyzed Reaction of Alkynylzinc Reagents with Alkenyl Halides. *J. Chem. Soc. Chem. Commun.*, 683–684. doi:10.1039/c39770000683
- Knochel, P., Krasovskiy, A., and Gavryushin, A. (2006). Highly Stereoselective Access to Sulfur Derivatives Starting from Zinc-Organometallics. *Synlett*, 0792–0794. doi:10.1055/s-2006-933117
- Komiyama, T., Minami, Y., and Hiyama, T. (2016). Recent Advances in Transition-Metal-Catalyzed Synthetic Transformations of Organosilicon Reagents. *ACS Catal.* 7, 631–651. doi:10.1021/acscatal.6b02374

FUNDING

The authors greatly acknowledge the financial support by Natural Science Foundation of Henan Province (212300410163), the Education Department of Henan Province (20A210023), Henan Agricultural University (30500567) and China Tobacco Henan Industrial Co., Ltd. (2021410001300070, 2021410001300071, YN201805).

SUPPLEMENTARY MATERIAL

The Supplementary Material for this article can be found online at: <https://www.frontiersin.org/articles/10.3389/fchem.2022.867806/full#supplementary-material>

- Lai, M., Wu, Z., Li, S.-J., Wei, D., and Zhao, M. (2019b). Regioselective Synthesis of Sulfonyl-Containing Benzyl Dithiocarbamates through Copper-Catalyzed Thiosulfonylation of Styrenes. *J. Org. Chem.* 84, 11135–11149. doi:10.1021/acs.joc.9b01829
- Lai, M., Wu, Z., Wang, Y., Zheng, Y., and Zhao, M. (2019a). Selective Synthesis of Aryl Thioamides and Aryl- α -Ketoamides from α -oxocarboxylic Acids and Tetraalkylthiuram Disulfides: an Unexpected Chemoselectivity from Aryl Sulfonyl Chlorides. *Org. Chem. Front.* 6, 506–511. doi:10.1039/c8qo01127c
- Liénard, B. M. R., Garau, G., Horsfall, L., Karsisiotis, A. I., Damblon, C., Lassaux, P., et al. (2008). Structural Basis for the Broad-Spectrum Inhibition of Metallo- β -Lactamases by Thiols. *Org. Biomol. Chem.* 6, 2282–2294. doi:10.1039/b802311e
- Liu, Y., and Bao, W. (2007). A New Method for the Synthesis of Dithiocarbamates by CuI-Catalyzed Coupling Reaction. *Tetrahedron Lett.* 48, 4785–4788. doi:10.1016/j.tetlet.2007.03.168
- Lu, M.-Z., Ding, X., Shao, C., Hu, Z., Luo, H., Zhi, S., et al. (2020). Direct Hiyama Cross-Coupling of (Hetero)arylsilanes with C(sp²)-H Bonds Enabled by Cobalt Catalysis. *Org. Lett.* 22, 2663–2668. doi:10.1021/acs.orglett.0c00631
- Luo, H., Sun, K., Xie, Q., Li, X., Zhang, X., and Luo, X. (2020). Copper-Mediated Phosphorylation of Arylsilanes with H-Phosphonate Diesters. *Asian J. Org. Chem.* 9, 2083–2086. doi:10.1002/ajoc.202000529
- Magano, J., and Dunetz, J. R. (2011). Large-Scale Applications of Transition Metal-Catalyzed Couplings for the Synthesis of Pharmaceuticals. *Chem. Rev.* 111, 2177–2250. doi:10.1021/cr100346g
- McManus, H. A., Cozzi, P. G., and Guiry, P. J. (2006). Application of Tridentate Bis(oxazoline) Ligands in Catalytic Asymmetric Nozaki-Hiyama Allylation and Crotylation: An Example of High Enantioselection with a Non-symmetric Bis(oxazoline) Ligand. *Adv. Synth. Catal.* 348, 551–558. doi:10.1002/adsc.200505332
- Milstein, D., and Stille, J. K. (1979a). Mechanism of Reductive Elimination. Reaction of Alkylpalladium(II) Complexes with Tetraorganotin, Organolithium, and Grignard Reagents. Evidence for Palladium(IV) Intermediacy. *J. Am. Chem. Soc.* 101, 4981–4991. doi:10.1021/ja00511a031
- Milstein, D., and Stille, J. K. (1979b). Palladium-catalyzed Coupling of Tetraorganotin Compounds with Aryl and Benzyl Halides. Synthetic Utility and Mechanism. *J. Am. Chem. Soc.* 101, 4992–4998. doi:10.1021/ja00511a032
- Murahashi, S., Yamamura, M., Yanagisawa, K., Mita, N., and Kondo, K. (1979). Stereoselective Synthesis of Alkenes and Alkenyl Sulfides from Alkenyl Halides Using Palladium and Ruthenium Catalysts. *J. Org. Chem.* 44, 2408–2417. doi:10.1021/jo01328a016
- N. Miyaura (Editor) (2002). “Cross-coupling Reactions: a Practical Guide,” In *Series Top. Curr. Chem. Vol. 219* (Berlin: Springer). doi:10.1007/3-540-45313-x
- Nakao, Y., and Hiyama, T. (2011). Silicon-based Cross-Coupling Reaction: an Environmentally Benign Version. *Chem. Soc. Rev.* 40, 4893–4901. doi:10.1039/c1cs15122c
- Nareddy, P., Jordan, F., and Szostak, M. (2017). Highly Chemoselective Ruthenium(ii)-Catalyzed Direct Arylation of Cyclic and N,N-dialkyl Benzamides with Aryl Silanes. *Chem. Sci.* 8, 3204–3210. doi:10.1039/c7sc00156h
- Nareddy, P., Jordan, F., and Szostak, M. (2018). Ruthenium(II)-Catalyzed Direct C-H Arylation of Indoles with Arylsilanes in Water. *Org. Lett.* 20, 341–344. doi:10.1021/acs.orglett.7b03567
- Negishi, E.-i. (2011). Magical Power of Transition Metals: Past, Present, and Future (Nobel Lecture). *Angew. Chem. Int. Ed.* 50, 6738–6764. doi:10.1002/anie.201101380
- Negishi, E., King, A. O., and Okukado, N. (1977). Selective Carbon-Carbon Bond Formation via Transition Metal Catalysis. 3. A Highly Selective Synthesis of Unsymmetrical Biaryls and Diarylmethanes by the Nickel- or Palladium-Catalyzed Reaction of Aryl- and Benzylzinc Derivatives with Aryl Halides. *J. Org. Chem.* 42, 1821–1823. doi:10.1021/jo00430a041
- Negishi, E., Okukado, N., King, A. O., Van Horn, D. E., and Spiegel, B. I. (1978). Selective Carbon-Carbon Bond Formation via Transition Metal Catalysts. 9. Double Metal Catalysis in the Cross-Coupling Reaction and its Application to the Stereo- and Regioselective Synthesis of Trisubstituted Olefins. *J. Am. Chem. Soc.* 100, 2254–2256. doi:10.1021/ja00475a059
- Negishi, E., and Van Horn, D. E. (1977). Selective Carbon-Carbon Bond Formation via Transition Metal Catalysis. 4. A Novel Approach to Cross-Coupling Exemplified by the Nickel-Catalyzed Reaction of Alkenylzirconium Derivatives with Aryl Halides. *J. Am. Chem. Soc.* 99, 3168–3170. doi:10.1021/ja00451a0550
- Okukado, N., Van Horn, D. E., Klima, W. L., and Negishi, E. (1978). A Highly Stereo-, Regio-, and Chemoselective Synthesis of Conjugated Dienes by the Palladium-Catalyzed Reaction of (E)-1-alkenylzirconium Derivatives with Alkenyl Halides. *Tetrahedron Lett.* 1027–1030. doi:10.1016/s0040-4039(01)85443-5
- Peng, K., Zhu, H., Liu, X., Peng, H.-Y., Chen, J.-Q., and Dong, Z.-B. (2019). Chemoselective C-S/S-S Formation between Diaryl Disulfides and Tetraalkylthiuram Disulfides. *Eur. J. Org. Chem.* 2019, 7629–7634. doi:10.1002/ejoc.201901401
- Qi, C., Guo, T., and Xiong, W. (2016). Copper-Mediated Coupling of Boronic Acids, Amines, and Carbon Disulfide: An Approach to Organic Dithiocarbamates. *Synlett* 27, 2626–2630. doi:10.1055/s-0035-1560561
- Sahani, A. J., Burange, A. S., Narasimhan, S., and Jayaram, R. V. (2018). Cross-Coupling Reactions of Aryltriethoxysilanes and Diaryldiselenides - A New Route for the Synthesis of Diarylselenides. *ChemistrySelect* 3, 12291–12296. doi:10.1002/slct.201802442
- Sekiya, A., and Ishikawa, N. (1976). The Cross-Coupling of Aryl Halides with Grignard Reagents Catalyzed by iodo(phenyl)bis(triphenylphosphine)Palladium(II). *J. Organomet. Chem.* 118, 349–354. doi:10.1016/s0022-328x(00)93215-7
- Sore, H. F., Galloway, W. R. J. D., and Spring, D. R. (2012). Palladium-catalysed Cross-Coupling of Organosilicon Reagents. *Chem. Soc. Rev.* 41, 1845–1866. doi:10.1039/c1cs15181a
- Sugiyama, A., Ohnishi, Y.-y., Nakaoka, M., Nakao, Y., Sato, H., Sakaki, S., et al. (2008). Why Does Fluoride Anion Accelerate Transmetalation between Vinylsilane and Palladium(II)-Vinyl Complex? Theoretical Study. *J. Am. Chem. Soc.* 130, 12975–12985. doi:10.1021/ja801362e
- Suzuki, A. (2011). Cross-Coupling Reactions of Organoboranes: An Easy Way to Construct CC Bonds (Nobel Lecture). *Angew. Chem. Int. Ed.* 50, 6722–6737. doi:10.1002/anie.201101379
- Tamao, K., Sumitani, K., and Kumada, M. (1972). Selective Carbon-Carbon Bond Formation by Cross-Coupling of Grignard Reagents with Organic Halides. Catalysis by Nickel-Phosphine Complexes. *J. Am. Chem. Soc.* 94, 4374–4376. doi:10.1021/ja00767a075
- Wu, X.-m., and Yan, G.-b. (2019). Copper-Catalyzed Synthesis of S-Aryl Dithiocarbamates from Tetraalkylthiuram Disulfides and Aryl Iodides in Water. *Synlett* 30, 610–614. doi:10.1055/s-0037-1612086
- Wu, X.-X., Ye, H., Jiang, G., and Hu, L. (2021). Domino Heck/Hiyama Cross-Coupling: Trapping of the σ -alkylpalladium Intermediate with Arylsilanes. *Org. Biomol. Chem.* 19, 4254–4257. doi:10.1039/d1ob00595b
- Wu, Y., Zhang, H.-R., Cao, Y.-X., Lan, Q., and Wang, X.-S. (2016). Nickel-Catalyzed Monofluoroalkylation of Arylsilanes via Hiyama Cross-Coupling. *Org. Lett.* 18, 5564–5567. doi:10.1021/acs.orglett.6b02803
- Wu, Z., Lai, M., Zhang, S., Zhong, X., Song, H., and Zhao, M. (2018). An Efficient Synthesis of Benzyl Dithiocarbamates by Base-Promoted Cross-Coupling Reactions of Benzyl Chlorides with Tetraalkylthiuram Disulfides at Room Temperature. *Eur. J. Org. Chem.* 2018, 7033–7036. doi:10.1002/ejoc.201801449
- Wuts, P. G. M., and Greene, T. W. (2006). *Greene's Protective Groups in Organic Synthesis*. John Wiley & Sons. doi:10.1002/0470053488
- Xu, W., Gao, F., and Dong, Z.-B. (2018). Copper-Catalyzed S-Arylation Starting from Arylboronic Acids and Tetraalkylthiuram Disulfide. *Eur. J. Org. Chem.* 2018, 821–828. doi:10.1002/ejoc.201701757
- Yamamura, M., Moritani, I., and Murahashi, S.-I. (1975). The Reaction of σ -vinylpalladium Complexes with Alkylolithiums. Stereospecific Syntheses of Olefins from Vinyl Halides and Alkylolithiums. *J. Organomet. Chem.* 91, 39–42. doi:10.1016/s0022-328x(00)89636-9
- Yin, X., Guo, Y., Liu, C., Wang, Z., and Zhang, B. (2015). One-pot Two-step Facile Synthesis of 2,3,5,6-Tetrafluorobenzonitrile-Containing Dithiocarbamic Acid Esters. *Tetrahedron Lett.* 56, 5135–5139. doi:10.1016/j.tetlet.2015.07.009
- Zeng, M.-T., Xu, W., Liu, M., Liu, X., Chang, C.-Z., Zhu, H., et al. (2017a). Copper-catalyzed Amidation of Benzoic Acids Using Tetraalkylthiuram Disulfides as Amine Sources. *Synth. Commun.* 47, 1434–1440. doi:10.1080/00397911.2017.1330960
- Zeng, M.-T., Xu, W., Liu, X., Chang, C.-Z., Zhu, H., and Dong, Z.-B. (2017b). Copper-Catalyzed S-Arylation of Tetraalkylthiuram Disulfides by Using Diaryliodonium Salts. *Eur. J. Org. Chem.* 2017, 6060–6066. doi:10.1002/ejoc.201701056
- Zhang, D., Chen, J., Liang, Y., and Zhou, H. (2005). Facile Synthesis of Novel Ionic Liquids Containing Dithiocarbamate. *Synth. Commun.* 35, 521–526. doi:10.1081/scc-200049773

- Zhang, J., Hou, Y., Ma, Y., and Szostak, M. (2019). Synthesis of Amides by Mild Palladium-Catalyzed Aminocarbonylation of Arylsilanes with Amines Enabled by Copper(II) Fluoride. *J. Org. Chem.* 84, 338–345. doi:10.1021/acs.joc.8b02874
- Zhang, J., Wang, S., Zhang, Y., and Feng, Z. (2020). Iron-Catalyzed Cross-Coupling Reactions for the Construction of Carbon-Heteroatom Bonds. *Asian J. Org. Chem.* 9, 1519–1531. doi:10.1002/ajoc.202000334
- Zou, Y., Yu, S., Li, R., Zhao, Q., Li, X., Wu, M., et al. (2014). Synthesis, Antifungal Activities and Molecular Docking Studies of Novel 2-(2,4-Difluorophenyl)-2-Hydroxy-3-(1*H*-1,2,4-Triazol-1-yl)propyl Dithiocarbamates. *Eur. J. Med. Chem.* 74, 366–374. doi:10.1016/j.ejmech.2014.01.009

Conflict of Interest: Authors HS, JQ, MC, WS, FB and HW are employed by China Tobacco Henan Industrial Co. Ltd.

The remaining authors declare that the research was conducted in the absence of any commercial or financial relationships that could be construed as a potential conflict of interest.

The authors declare that this study received funding from China Tobacco Henan Industrial Co., Ltd. The funder had the following involvement in the study: study design, data collection and decision to publish.

Publisher's Note: All claims expressed in this article are solely those of the authors and do not necessarily represent those of their affiliated organizations, or those of the publisher, the editors and the reviewers. Any product that may be evaluated in this article, or claim that may be made by its manufacturer, is not guaranteed or endorsed by the publisher.

Copyright © 2022 Wang, Shen, Qiu, Chen, Song, Zhao, Wang, Bai, Wang and Wu. This is an open-access article distributed under the terms of the Creative Commons Attribution License (CC BY). The use, distribution or reproduction in other forums is permitted, provided the original author(s) and the copyright owner(s) are credited and that the original publication in this journal is cited, in accordance with accepted academic practice. No use, distribution or reproduction is permitted which does not comply with these terms.



Pyrene Functionalized Highly Reduced Graphene Oxide-palladium Nanocomposite: A Novel Catalyst for the Mizoroki-Heck Reaction in Water

Mujeeb Khan^{1*}, Muhammad Ashraf², Mohammed Rafi Shaik¹, Syed Farooq Adil¹, Mohammad Shahidul Islam^{1*}, Mufsir Kuniyil¹, Merajuddin Khan¹, Mohammad Rafe Hatshan¹, Riyadh H. Alshammari¹, Mohammed Rafiq H. Siddiqui¹ and Muhammad Nawaz Tahir^{2,3}

¹Department of Chemistry, College of Science, King Saud University, Riyadh, Saudi Arabia, ²Chemistry Department, King Fahd University of Petroleum and Minerals, Dhahran, Saudi Arabia, ³Interdisciplinary Research Center for Hydrogen and Energy Storage (IRC-HES), King Fahd University of Petroleum and Minerals, Dhahran, Saudi Arabia

OPEN ACCESS

Edited by:

Guillermo Raul Castro,
Consejo Nacional de Investigaciones
Científicas y Técnicas (CONICET),
Argentina

Reviewed by:

Mahmoud Nasrollahzadeh,
University of Qom, Iran
Yanliang Yang,
Luoyang Normal University, China

*Correspondence:

Mujeeb Khan
kmujeeb@ksu.edu.sa
Mohammad Shahidul Islam
mislam@ksu.edu.sa

Specialty section:

This article was submitted to
Green and Sustainable Chemistry,
a section of the journal
Frontiers in Chemistry

Received: 09 February 2022

Accepted: 28 March 2022

Published: 29 April 2022

Citation:

Khan M, Ashraf M, Shaik MR, Adil SF,
Islam MS, Kuniyil M, Khan M,
Hatshan MR, Alshammari RH,
Siddiqui MRH and Tahir MN (2022)
Pyrene Functionalized Highly Reduced
Graphene Oxide-palladium
Nanocomposite: A Novel Catalyst for
the Mizoroki-Heck Reaction in Water.
Front. Chem. 10:872366.
doi: 10.3389/fchem.2022.872366

The formation of a C-C bond through Mizoroki-Heck cross-coupling reactions in water with efficient heterogeneous catalysts is a challenging task. In this current study, a highly reduced graphene oxide (HRG) immobilized palladium (Pd) nanoparticle based catalyst (HRG-Py-Pd) is used to catalyze Mizoroki-Heck cross-coupling reactions in water. During the preparation of the catalyst, amino pyrene is used as a smart functionalizing ligand, which offered chemically specific binding sites for the effective and homogeneous nucleation of Pd NPs on the surface of HRG, which significantly enhanced the physical stability and dispersibility of the resulting catalyst in an aqueous medium. Microscopic analysis of the catalyst revealed a uniform distribution of ultrafine Pd NPs on a solid support. The catalytic properties of HRG-Py-Pd are tested towards the Mizoroki-Heck cross-coupling reactions of various aryl halides with acrylic acid in an aqueous medium. Furthermore, the catalytic efficacy of HRG-Py-Pd is also compared with its non-functionalized counterparts such as HRG-Pd and pristine Pd NPs (Pd-NPs). Using the HRG-Py-Pd nanocatalyst, the highest conversion of 99% is achieved in the coupling reaction of 4-bromoanisole and acrylic acid in an aqueous solution in a relatively short period of time (3 h), with less quantity of catalyst (3 mg). Comparatively, pristine Pd NPs delivered lower conversion (~92%) for the same reaction required a long reaction time and a large amount of catalyst (5.3 mg). Indeed, the conversion of the reaction further decreased to just 40% when 3 mg of Pd-NPs was used which was sufficient to produce 99% conversion in the case of HRG-Py-Pd. On the other hand, HRG-Pd did not deliver any conversion and was ineffective even after using a high amount of catalyst and a longer reaction time. The inability of the HRG-Pd to promote coupling reactions can be attributed to the agglomeration of Pd NPs which reduced the dispersion quality of the catalyst in water. Therefore, the high aqueous stability of HRG-Py-Pd due to smart functionalization can be utilized to perform other organic transformations in water which was otherwise not possible.

Keywords: highly reduced graphene, palladium, catalyst, mizoroki-heck, aqueous synthesis

INTRODUCTION

Traditionally, organic reactions are performed in hazardous organic solvents due to the higher solubility of most of the reactants in these mediums (Kitanosono et al., 2018). Since solvents are used in large quantities comparatively to reactants, currently they are considered the greater threat to the environment (Cseri et al., 2018). Therefore, in current circumstances, chemists are facing the challenging task of developing green technologies for important organic transformations (Soh and Eckelman, 2016). The “green processes” should be capable of performing organic reactions utilizing eco-friendly, sustainable, and economically beneficial conditions (Sheldon, 2018). In this regard, the application of water as a reaction medium greatly reduces the environmental impact of organic synthesis (Simon and Li, 2012). Due to its extraordinary characteristics such as biocompatibility, non-flammability and high vapor pressure, etc., water is considered “nature’s choice of solvent” (Gawande et al., 2013). In addition to the environmental and economic benefits, water allows mild reaction conditions, simplifies chemical processes, and also offers unique reactivity and selectivity (Butler and Coyne, 2010). Nowadays, water is largely explored as a safe and suitable alternative to the hazardous organic solvents for the preparation of various industrially important fine chemicals and pharmaceuticals compounds (Nebra and García-Álvarez, 2020).

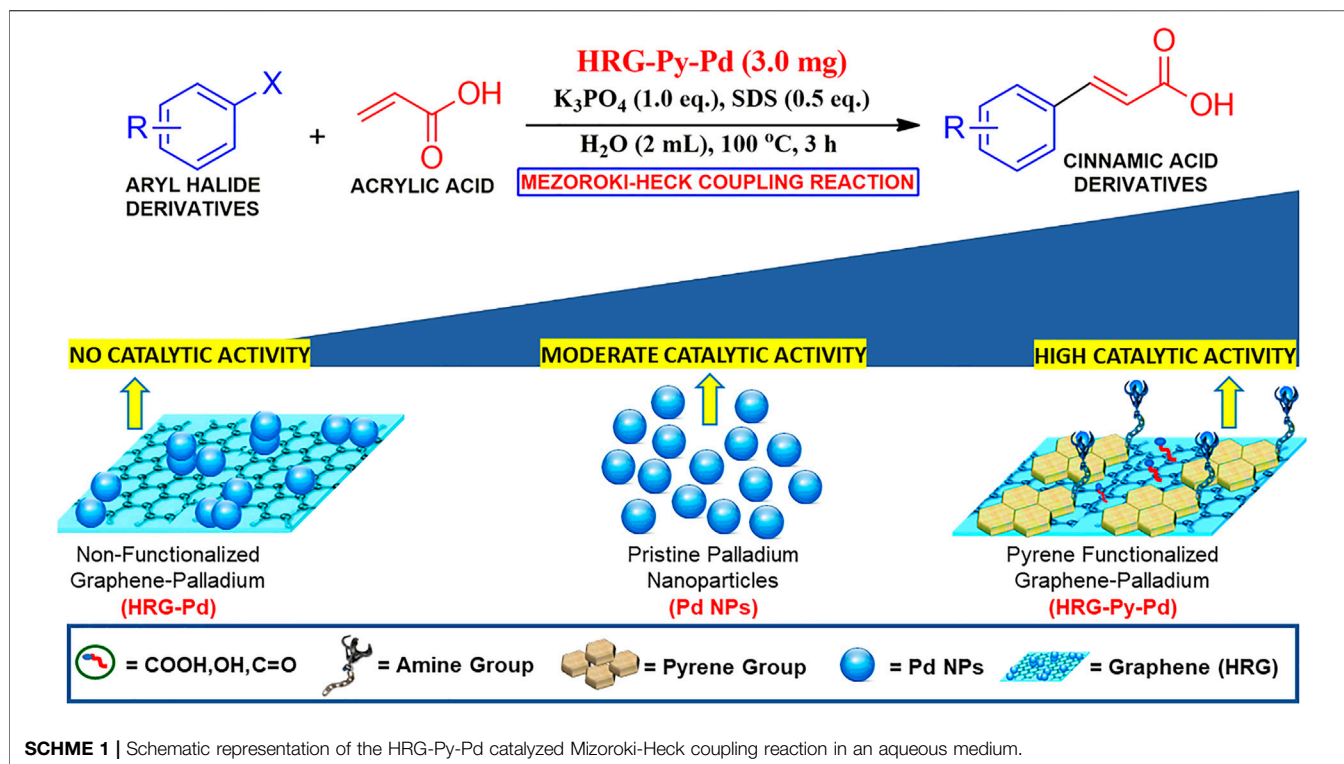
Among these, biphenyl derivatives and acrylates are an important class of compounds that are extensively used as starting materials during the synthesis of several applied chemicals in the pharmaceutical and agrochemical fields. (Kambe et al., 2011). Generally, methods used for the synthesis of these compounds include Suzuki–Miyaura and Mizoroki–Heck cross-coupling reactions (Frisch and Beller, 2005; Khazaei et al., 2017; Baran and Nasrollahzadeh, 2020; Easson et al., 2020). The latter is the coupling of aryl halides with alkenes using palladium-based catalysts in the presence of a base (Amatore and Jutand, 2000; Khan et al., 2017). These types of coupling reactions are typically applied for the preparation of stilbenes and cinnamic acid types of useful natural products, pharmaceuticals, and other compounds with specific properties including the presence of trans double bond (De Filippis et al., 2017; Gao et al., 2019). Mostly, coupling reactions including the Suzuki–Miyaura coupling have a few downsides, like difficulty in the recovery of precious metals-based catalysts, application of costly ligands, and environmental hazards due to the use of organic solvents (Nasrollahzadeh et al., 2015; Guo et al., 2017). Therefore, the use of water as a reaction medium for Mizoroki–Heck reactions would greatly enhance the development of chemical industrial processes and also minimize the environmental impact (De Meijere and Meyer, 1995).

However, in most cases, water is not considered as an appropriate solvent for the Mizoroki–Heck reactions. These are usually carried out in organic solvents due to the relatively higher solubility of reactants involved in the reactions (Phan et al., 2006). Depending on the solubility of reaction components, effortshave been carried out to develop

palladium-catalyzed coupling reactions including Mizoroki–Heck cross-coupling using water as solvent (Nasrollahzadeh et al., 2014b; Jagtap, 2017; Christoffel and Ward, 2018). For this purpose, inorganic salt promoters, the addition of phase-transfer agents, and the use of alternative energy sources like microwave or ultrasound are used to overcome the solubility challenge (Christoffel and Ward, 2018). Nevertheless, continued research in the field of aqueous chemistry of the Mizoroki–Heck reactions would be strongly beneficial to the environment (Jadhav and Rode, 2017).

Typically, coupling reactions are performed using palladium salts or complexes as homogeneous catalysts. However, homogeneous reactions usually suffer from the loss or contamination of residual catalysts and often require tedious workup procedures (Beletskaya and Cheprakov, 2000). To avoid this, Pd NPs are commonly used as catalysts because nanoparticles offer the benefits of both homogeneous (solubility) and heterogeneously (easy recovery and improved cyclability). Particularly, when synthesized using green protocols which are independent of hazardous ligands (Mpungose et al., 2018). The stability, separation, cyclability, and reactivity of Pd NPs can be further enhanced by immobilizing them on suitable solid supports (support materials in the nanosize regime) such as graphene or mesoporous silica nanoparticles (Kuniyil et al., 2019; Hong et al., 2020). Furthermore, these supports compensate for the high cost of palladium because the amount of used palladium in the main catalyst is diluted (Felpin et al., 2006). Therefore, the use of effective supports is highly appreciable (Alonso et al., 2018). Among various supports graphene offers a flat 2D surface with high surface area for better adsorption of reactants, greatest intrinsic carrier mobility, perfect atomic lattice, excellent mechanical strength, and promising chemical and thermal stability (Julkapli and Bagheri, 2015; Naghdi et al., 2016c; Nasrollahzadeh et al., 2018; Qian et al., 2020). In addition, graphene supports can be converted to both hydrophobic and hydrophilic substances with easy customization, which can be very useful in heterogeneous catalysis (Nasrollahzadeh et al., 2014a; Fakhri et al., 2015; Naghdi et al., 2016a; Naghdi et al., 2016b). Hence, the development of a graphene supported Pd based water dispersible catalyst which can be easily separated from the product is highly desirable.

Considering the importance of water in Pd catalyzed reactions, herein we report the synthesis of a water-dispersible, heterogeneous catalyst for the Mizoroki–Heck coupling of aryl halides and acrylic acid in an aqueous medium (cf. **Scheme 1**). The heterogeneous catalyst was prepared by immobilizing smaller size Pd NPs on pyrene functionalized highly reduced graphene oxide according to our previously reported method (Khan et al., 2020). The as-prepared catalyst is highly dispersible in water, stable over weeks, and can be easily separated from the reaction medium by simple filtration or centrifugation. Furthermore, to evaluate the importance of functionalization, the catalytic activity of pyrene functionalized highly reduced graphene oxide-palladium nanocomposite (HRG-Py-Pd) is compared with its non-functionalized counterpart (HRG-Pd) and pristine Pd nanoparticles.



EXPERIMENTAL

Materials and Methods

All reactants and solvents were purchased from commercial suppliers (Sigma-Aldrich) and used without any further purification (extra purified chemicals are specifically indicated in the main text). Graphite powder (99.999%, -200 mesh) was purchased from Alfa Aesar. Other materials used are 1-aminopyrene (1-AP, 97%), sodium tetrachloropalladate (II) (99.9%), concentrated sulfuric acid (H_2SO_4 , 98%), potassium permanganate (KMnO_4 , 99%), sodium nitrate (NaNO_3 , 99%), hydrogen peroxide (H_2O_2 , 30 wt%), Acrylic acid, n-butylacrylate, 4-bromoanisole, sodium dodecyl sulfate (SDS, 98%), K_3PO_4 etc. FT-IR spectra were measured on Perkin Elmer 1,000 FT-IR spectrometer from 400 to $4,000\text{ cm}^{-1}$ by using KBr pellets. ^1H and ^{13}C spectra were obtained on a JEOL JNM-ECP 400 NMR spectrometer. Powder XRD patterns were recorded on D2 Phaser X-ray diffractometer (Bruker, Germany), Cu $\text{K}\alpha$ radiation ($k = 1.5418\text{ \AA}$). High-resolution transmission electron microscopy (HRTEM) images and EDX were measured on JEM 2100F (JEOL, Tokyo, Japan). HPLC analysis on a Shimadzu LC-20A Prominence instrument (Shi-madzu, Kuoto, Japan). Column used: Daicel Chiralcel OD-H columns (Chiral Technologies Europe, Illkirch Graffenstaden, France) (80–95% n-hexane/iso-propanol).

Synthesis and Functionalization of HRG

Highly reduced graphene oxide was prepared according to our previously reported method (Khan et al., 2020). For the preparation of HRG graphene oxide was used as a precursor which was synthesized by the oxidation of graphite powder using

a modified Hummers method (Hummers and Offeman, 1958; Cote et al., 2009). For the functionalization of HRG, freshly prepared HRG is functionalized by using 1-aminopyrene (1-AP) as a ligand. Briefly, a 10 ml dispersion of methanol was prepared using sonication (30 min) by adding 25 mg of HRG. Separately, 25 mg of 1-AP was dissolved in methanol (10 ml) using stirring at room temperature. Both mixtures were combined and stirred together for 48 h at room temperature. Thereafter, the resultant mixture was sonicated at 20°C for 6 h. Finally, the sample was centrifuged for 15 min to get rid of residual 1-AP and the functionalized HRG is isolated. The sample was further purified by re-dispersing in fresh methanol (5 ml). The resulting dispersion was sonicated at 20°C (30 min), centrifuged for 1 hour and the product was isolated by simply decanting the resulting mixture. This process was repeated several times (3–4 times) to achieve maximum purity of the sample which is dried overnight under vacuum.

Synthesis of HRG-Py-Pd, HRG-Pd, and Pristine Pd NPs

To prepare HRG-Py-Pd equivalent weight (1:1) of freshly prepared functionalized HRG and palladium precursor (Na_2PdCl_4) is used. For this purpose, 5 mg of 1-AP functionalized HRG was dispersed in 5 ml of ethanol which was added to a separately prepared 5 ml ethanol solution of Pd precursor (Na_2PdCl_4 , 5 mg, 0.0169 mmol). The mixture was sonicated for 1 h which resulted in the formation of the functionalized nanocomposite. Finally, the product was separated by centrifugation (9,000 rpm), which was re-

dispersed in water (10 ml) for later use. The non-functionalized counterpart of HRG-Py-Pd was also prepared in a similar fashion, however in this case freshly prepared pristine HRG was used to obtain HRG-Pd. Pd NPs were also obtained using sonication in a similar procedure as described above. In a typical procedure, 10 mg of Na_2PdCl_4 (0.0338 mmol) was dissolved in 10 ml of ethanol through stirring at room temperature. The solution was then sonicated for 1 h, subsequently, the product is isolated by centrifugation and redispersed in 10 ml ethanol and sonicated for further purification. The final product was separated by centrifugation.

General Procedure For The Mizoroki-Heck Coupling Reaction in an Aqueous Medium

In an airtight screw-capped vial (5 ml) catalyst (HRG-Py-Pd, 3 mg) or (Pd-NPs, 5.3 mg), K_3PO_4 (106 mg, 0.5 mmol), SDS (72 mg, 0.5 eq., 0.25 mmol) and water (2 ml) were charged with a small magnetic stir bar. Then aryl halide **1** (0.5 mmol) was added to it followed by acrylic acid **2** (36 mg, 0.5 mmol). The reaction was left stirring at 100°C for 3 h. The reaction was monitored by HPLC (30% Hex/*i*PrOH, 0.5 ml/min). Then the vial was cooled to room temperature and the product was extracted in ethyl acetate (3 × 3 ml). The ethyl acetate layer was basified with aqueous 4M K_2CO_3 (5 ml) and separated from the organic layer then the aqueous layer was again acidified with 4N HCl (PH 1-2). Finally, the pure product was then extracted in ethyl acetate (3 × 5 ml) and the combined organics were dried over anhydrous MgSO_4 . The organic layer was then concentrated under reduced pressure to afford pure compounds MH product **3a-f**. All the products were characterized by ^1H -NMR and ^{13}C -NMR spectra.

Large Scale Mizoroki-Heck Reaction

For this, 4-bromoanisole **1** (1.86 g, 10 mmol) and acrylic acid **2** (720 mg, 10 mmol) in the presence of a catalyst (HRG-Py-Pd, 30.0 mg) and (Pd-NPs, 53.0 mg) were reacted according to the general procedure described above (scale 20 times, but the time was doubled to 6 h) to afford pure **3a**. Catalyst HRG-Py-Pd yielded 1.73 g (97%) and Catalyst Pd-NPs yielded 1.58 g (89%) respectively.

(E)-3-(4-methoxyphenyl)acrylic acid (3a): m.p 171–173°C (lit.168–170°C)¹; ^1H -NMR (400 MHz, $\text{DMSO}-d_6$) δ 12.23 (s, 1H, COOH), 7.64 (d, J = 8.8 Hz, 2H, Ar-H), 7.54 (d, J = 16.0 Hz, 1H, CH = CH), 6.97 (d, J = 8.2 Hz, 2H, Ar-H), 6.38 (d, J = 15.8 Hz, 1H, CH = CH), 3.79 (s, 3H, OCH_3); ^{13}C -NMR (101 MHz, $\text{DMSO}-d_6$) δ 168.41, 161.52, 144.33, 130.52, 127.40, 117.07, 114.93, 55.88, 40.29, 40.08.

RESULTS AND DISCUSSION

Graphene-supported metal NPs based nanocatalysts offer several advantages due to the combined effects of the inherent properties of the components involved. For instance, in the case of HRG-Pd nanocatalysts, the novel catalytic activity of Pd and the large surface area of graphene provide sufficient active sites on the

surface of the catalyst leading to the enhancement of the catalytic activity of the resultant composite. However, in many cases, the aggregation of NPs on the surface of the support often diminishes the performance of the material. Besides, the uncontrolled and sporadic growth of NPs on the surface of the support also adversely affects the catalytic potential of supported Pd-based catalysts. To overcome this, herein we have applied non-destructive, π - π interactions-based non-covalent functionalization technique. This was achieved by using 1-amino pyrene as stabilizing ligand, which is a polycyclic aromatic hydrocarbon (PAHs). The PAHs have a strong ability to interact with the 2D flat surface of graphene via π - π interactions due to their unique structures based on fused aromatic rings. The 1-AP functionalized (HRG-Py-Pd) and non-functionalized (HRG-Pd) graphene-palladium nanocomposites and Pd NPs were prepared under facile sonochemical conditions (Khan et al., 2020). Sonochemical preparation is based on high-intensity ultrasound waves which cause acoustic cavitation i.e., the formation, growth, and implosive collapse of bubbles (Xu et al., 2013). The acoustic cavitation generates extreme transient conditions which facilitate the formation of a variety of novel materials, including metallic NPs, under ambient conditions (Prekob et al., 2020). Particularly, high-quality noble metal NPs can be prepared by dissolving nonvolatile precursors in a volatile solvent (usually water or alcohol) (Calcio Gaudino et al., 2018). Such as the *in-situ* deposition of Pd NPs on the surface of HRG, which is performed in this study by using sodium tetrachloropalladate (II) as a nonvolatile precursor and ethanol as a volatile solvent. In this case, ethanol vapors generated by the sonolysis which is caused by high intensity ultrasound waves, act as strong reducing agent, which facilitates the reduction of metal precursor to produce ultrafine Pd NPs. While the ultrasonication produced Pd NPs, the functionalized HRG with 1-AP potentially inhibited the aggregation of NPs and facilitated the homogeneous distribution of Pd NPs on the surface of HRG. In this case, the basal plane of the pyrene ring helps to interact with the surface of HRG through π - π interactions, while, the amine group (NH_2) of 1-AP promote the nucleation and homogeneous growth of Pd NPs leading to the formation of highly dispersed HRG-Py-Pd nanocatalyst. The as-prepared samples including pristine Pd, HRG-Pd, and HRG-Py-Pd nanocatalysts were applied as a catalyst for the Mizoroki-Heck reaction in the aqueous phase.

XRD Analysis

Initially, the phase and crystallinity of Pd, HRG-Pd, and HRG-Py-Pd were confirmed by XRD analysis. The XRD diffractograms of these samples are shown in **Figure 1**. The diffractogram of pristine Pd NPs demonstrates several distinct reflections at 40.02° (111), 46.49° (200), 68.05° (220), 81.74° (311), and 86.24° (222) which are indexed to the face-centered cubic (fcc) structure of Pd (ICDD card number PDF#46-1043 (JCPDS: 87-0641), space group: Fm3m (225)) (Khan et al., 2014). On the other hand, the diffractograms of both HRG-Pd and HRG-Py-Pd consist of a broad reflection at 2θ = 22.4° corresponding to the HRG in addition to the reflections belonging to the face-centered cubic (fcc) structure of Pd NPs (Khan et al., 2014; Kadam et al., 2020).

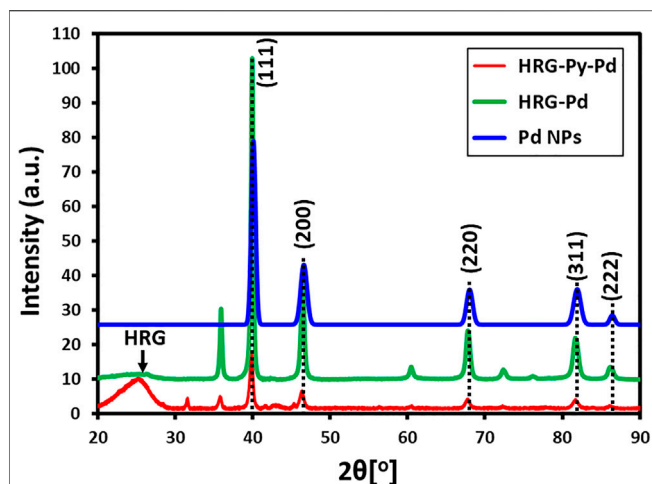


FIGURE 1 | XRD analysis of Pd NPs, HRG-Pd, and HRG-Py-Pd.

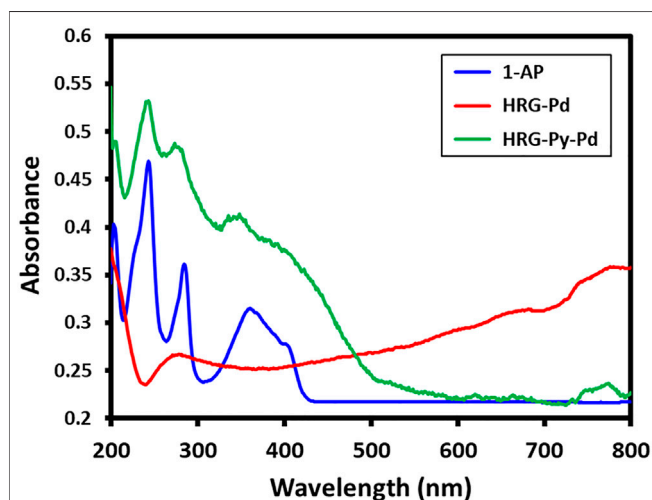


FIGURE 2 | UV-Vis spectrum of pure 1-amino pyrene, HRG-Pd, and HRG-Py-Pd.

This indicates the formation of HRG and Pd-based nanocomposites to produce HRG-Pd and HRG-Py-Pd nanocatalysts.

UV-Visible and FT-IR Analysis

The successful functionalization of HRG with 1-AP in HRG-Py-Pd is confirmed by both UV-Vis and FT-IR analyses. For this purpose, the UV spectra of 1-AP, HRG-Pd, and HRG-Py-Pd are compared as shown in **Figure 2**. The UV spectrum of 1-AP exhibits three characteristic bands at ~242, ~285, and 360 nm (**Figure 2**) which are also present in the UV spectrum of HRG-Py-Pd (**Figure 2**). Apart from these (1-AP) bands, the HRG-Py-Pd also consists of a characteristic absorption band of HRG, which typically appears at ~270 nm, however, in this case, it is not clearly visible due to the coexistence of the 1-AP absorption band in a similar region (~285 nm). Notably, the UV spectrum of

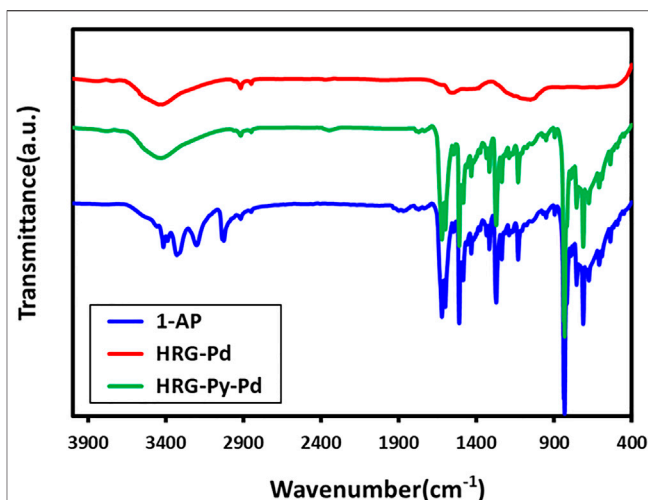


FIGURE 3 | FT-IR spectrum of pure 1-amino pyrene, HRG-Pd, and HRG-Py-Pd.

HRG-Pd only exhibits an absorption band at ~270 nm belonging to HRG, thus the absence of the absorption bands of 1-AP in the UV spectrum of HRG-Pd is also an indication of the successful functionalization of the surface of HRG with 1-AP in HRG-Py-Pd. Similarly, FT-IR analyses of these samples also confirmed the non-covalent functionalization of HRG by 1-AP in HRG-Py-Pd, as revealed by the comparison of the IR spectra of 1-AP, HRG-Pd, HRG-Py-Pd (cf. **Figure 3**). The IR spectrum of 1-AP exhibits several characteristic peaks, and most of these peaks also appeared in the IR spectrum of HRG-Py-Pd. This clearly indicated the presence of 1-AP on the surface of HRG in HRG-Py-Pd. For example, the IR peaks of the fingerprint region of 1-AP between 800 and 1,700 cm^{-1} are also present in the IR spectrum of HRG-Py-Pd, whereas, these characteristic peaks are absent in the IR spectrum of HRG-Pd which points towards the absence of 1-AP in this sample.

Transmission Electron Microscopy and EDX Analysis

Morphology and size of the as-prepared Pd NPs, HRG-Pd, and HRG-Py-Pd were determined using transmission electron microscopy (TEM) (**Figure 4**). The overview image in **Figure 4A** exhibits the formation of spherically shaped, almost homogeneous size Pd NPs with a size distribution of ~20–25 nm. The elemental composition of the as-prepared NPs as determined by using EDX confirmed the presence of only Pd. The morphology and the structure of Pd NPs on the surface of HRG in HRG-Pd is shown in the overview image in **Figure 4B** which indicates the existence of small and spherical shape Pd NPs on the surface of HRG. Whereas, the results of the elemental composition of the as-prepared HRG-Pd nanocatalyst determined by EDX (**Figure 4E**), revealed the presence of both carbon and Pd NPs. Besides, the size and morphology of Pd NPs on the surface of HRG in HRG-Py-Pd were also determined using transmission electron microscopy (TEM). The TEM micrograph

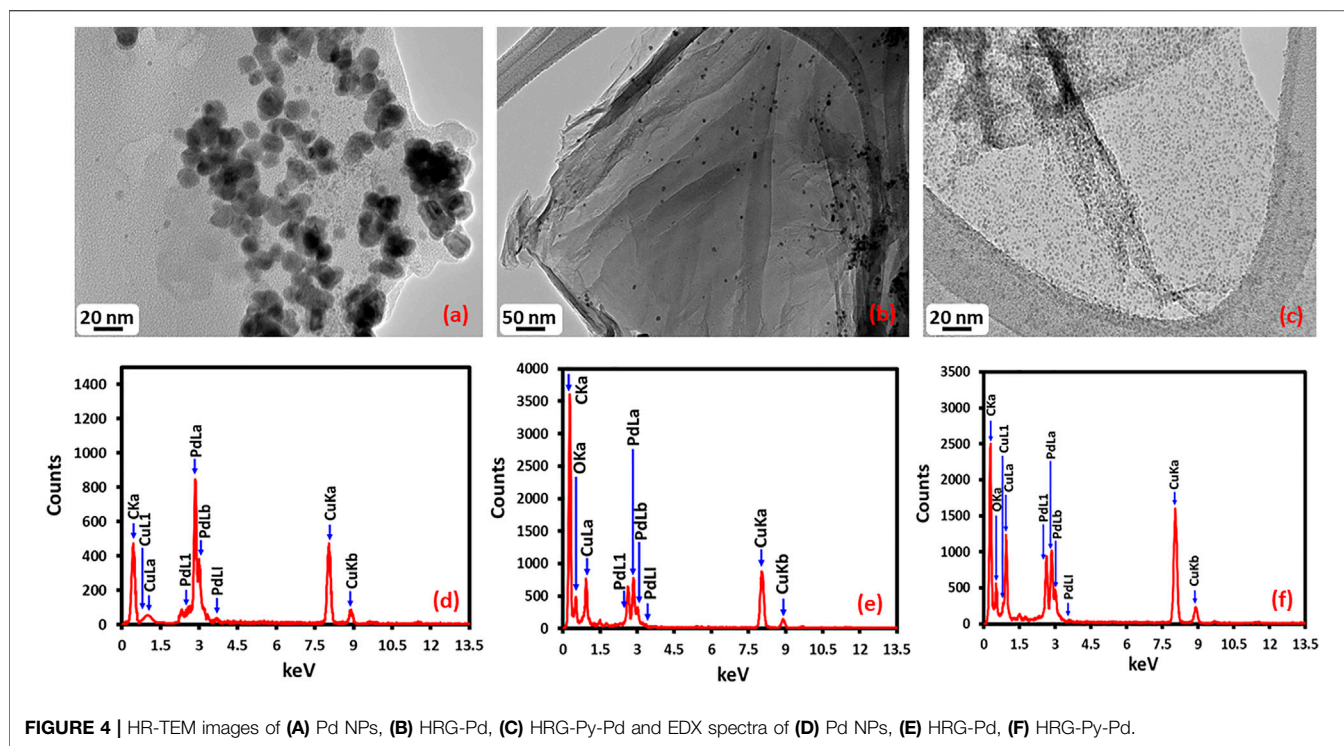


FIGURE 4 | HR-TEM images of (A) Pd NPs, (B) HRG-Pd, (C) HRG-Py-Pd and EDX spectra of (D) Pd NPs, (E) HRG-Pd, (F) HRG-Py-Pd.

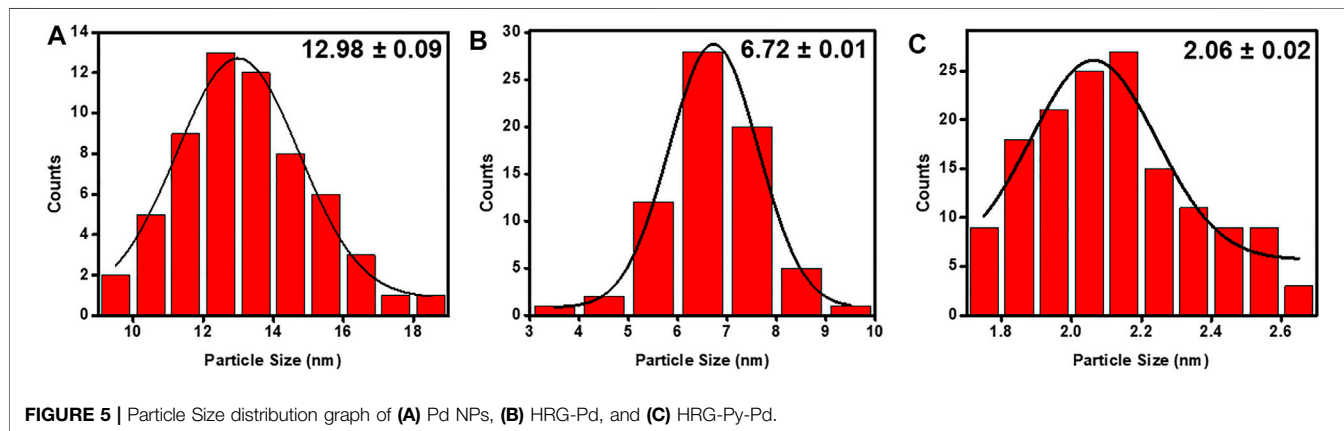


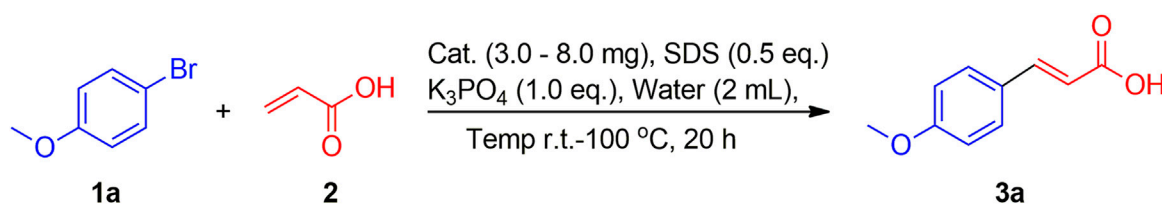
FIGURE 5 | Particle Size distribution graph of (A) Pd NPs, (B) HRG-Pd, and (C) HRG-Py-Pd.

of HRG-Py-Pd is presented in **Figure 4C**. It shows the presence of homogeneously dispersed ultrafine small size Pd NPs on the surface of HRG. Unlike in HRG-Pd which exhibited relatively larger size (10–20 nm), highly aggregated Pd NPs, the HRG-Py-Pd demonstrate the presence of densely distributed, spherical-shaped, smaller size (~2–4 nm) Pd NPs due to the presence of 1-AP. The presence of Pd NPs onto HRG-Py-Pd is also confirmed in the EDX spectrum of the functionalized nanocatalyst in **Figure 4F**. Notably, the Pd to C ratio is relatively higher in HRG-Py-Pd when compare with the Pd:C in HRG-Pd nanocatalyst (**Figure 4**). Additionally, the particle size distribution graph was assessed by using ImageJ software (**Figures 4A–C**), the particle size distribution graph of the Pd NPs (**Figure 5A**) displays the average particle size 12.98 ± 0.09

nm, the particle size distribution graph of the HRG-Pd (**Figure 5B**) displays the average particle size 6.72 ± 0.01 nm and the particle size distribution graph of the HRG-Py-Pd (**Figure 5C**) displays the average particle size 2.06 ± 0.02 nm. This indicates that 1-AP effectively promotes the nucleation and uniform growth of Pd NPs and also inhibits the aggregation of HRG nanosheets may enhance the surface area of the material, while the apparent dense distribution of Pd on the surface of HRG offers increased catalytic active sites.

Catalytic Application

Water dispersible Pd-based heterogeneous catalysts are highly required for various catalytic transformations including the Mizoroki-Heck reaction in the aqueous phase. Particularly, Pd



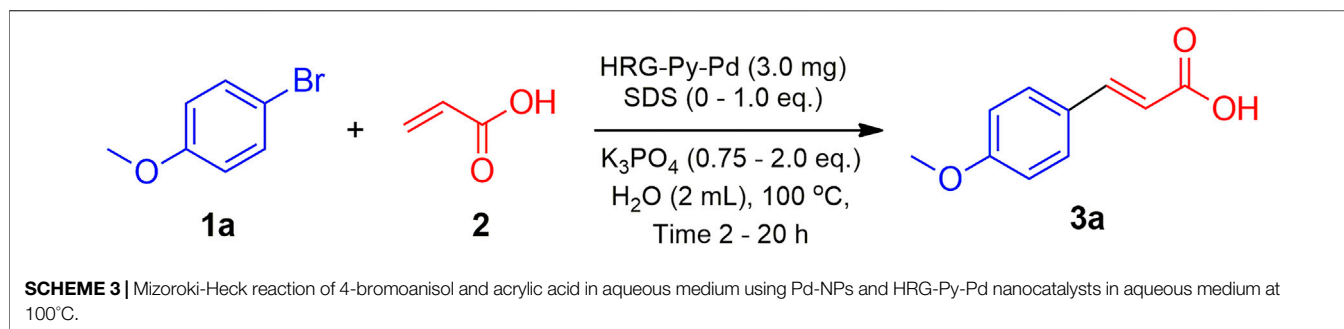
SCHEME 2 | Mizoroki-Heck reaction (MH) of 4-bromoanisole and acrylic acid in aqueous solution using newly prepared nanocatalysts (Pd-NPs, HRG-Pd, and HRG-Py-Pd).

NPs immobilized on various solid supports including carbonaceous materials, silica, and metal oxide NPs have demonstrated excellent catalytic activity for these types of coupling reactions. Therefore, heterogeneous catalysts based on Pd have attracted significant attention for the Mizoroki-Heck reactions under aqueous conditions. However, in many cases, the catalytic efficiency of Pd-based nanocatalysts is seriously hindered due to the aggregation of nanoparticles on the surface of the support. This is typically avoided through the functionalization of nanocatalyst with effective ligands. For instance, in our previous study, we have demonstrated the enhancement of the catalytic activity of HRG-Py-Pd nanocatalyst in the Suzuki-Miyaura coupling reactions. Stabilization of the surface of HRG with 1-AP has enhanced the dispersibility and uniformity of nanocatalyst on the support surface and solubility in water. This improved the efficiency of the catalyst compared to its non-functionalized counterpart (HRG-Pd). 1-AP with its active amine group offered efficient binding sites for the growth of well-separated, densely distributed Pd NPs on the surface of HRG, which increased the surface area of the resulting nanocatalyst. In this study, we investigated the catalytic activity of both functionalized (HRG-Py-Pd) and non-functionalized HRG-Pd for the Mizoroki-Heck reactions under aqueous conditions. Besides, the catalytic activity of these nanocatalysts is also compared with the pristine Pd NPs which were prepared using the ultrasonication method. In order to examine the catalytic efficiency of our freshly prepared nanocatalysts (Pd NPs, HRG-Pd, and HRG-Py-Pd) for the Mizoroki-Heck cross-coupling reaction, 4-Bromoanisole (**1a**) and acrylic acid (**2**) have been chosen as model substrate and the reaction was performed in aqueous medium as shown in **Scheme 2**.

The Mizoroki-Heck cross-coupling reaction of 4-bromoanisole **1a** (0.5 mmol) and acrylic acid **2** (0.5 mmol) as model substrate was carried out using freshly prepared catalyst Pd-NPs, HRG-Pd, and HRG-Py-Pd (3.0–8.0 mg) in the presence of K_3PO_4 (1.0 mmol) and SDS (0.25 mmol) in water (2 ml) at different temperatures such as room temperature (r.t.), 90°C, and 100 °C for 20 h (cf. **Scheme 3**). The results are summarized in **Table 1**. Initially, catalyst Pd-NPs, HRG-Pd, and HRG-Py-Pd (5.3 mg) were used in order to carry out the MH-reactions using K_3PO_4 (1.0 mmol) and SDS (0.25 mmol) at r.t. as well as at 90°C for 20 h, but unfortunately, no MH product formation was observed (**Table 1**, entries 1, 2, 6, 7, 11, 12). The reaction temperature was then elevated to 100°C, keeping other parameters unchanged,

catalysts Pd-NPs and HRG-Py-Pd performed extremely well, producing MH coupling products 4-Methoxycinnamic acid (**3a**) with 92 and 84% conversion respectively (**Table 1**, entries 4, 14) while catalyst HRG-Pd remained inactive (**Table 1**, entry 8). To optimize catalyst loading, the MH reactions were further performed using 3.0–8.0 mg of each catalyst (Pd-NPs, HRG-Pd, and HRG-Py-Pd). It is observed that, the catalyst Pd-NPs produced 40% (3 mg) and 74% (8 mg) conversion (**Table 1**, entries 3 and 5) whereas catalyst HRG-Py-Pd furnished 93% (3 mg) and 71% (8 mg) conversion (**Table 1**, entries 13 and 15) respectively. Catalyst HRG-Pd was again found to be inactive even at higher temperatures and high catalyst loading (**Table 1**, entries 8 and 10). Interestingly catalyst HRG-Py-Pd (3.0 mg) performed excellently as compared to Pd-NPs (3 mg) at expense of lower catalyst usage (**Table 1**, entries 13, 3). Upon increasing the catalyst loading to 8 mg, yields were not improved for both the catalyst Pd-NPs and HRG-Py-Pd, in fact, conversion significantly dropped to 74 and 71% (**Table 1** entries 5 and 15) which could be because of the aggregation of particles (particle-particle interactions) which tend to decrease the exposed surface area of the catalyst active sites. Therefore, our preliminary investigation revealed that 5.3 mg of catalyst Pd-NPs and 3.0 mg of catalyst HRG-Py-Pd are the best choice for catalyzing MH reaction of 4-bromoanisole and acrylic acid in water as a green medium at 100°C. Notably, non-functionalized HRG-Pd proved to be an inactive catalyst that did not produce any conversion even after a long reaction time, higher temperature, and using a high amount of catalyst. Although pristine Pd-NPs were active for the coupling reaction of 4-bromoanisole and acrylic acid in an aqueous medium, the inactivity of HRG-Pd under similar reaction conditions can be attributed to the severe aggregation of Pd-NPs on the surface of HRG which is also established by the HRTEM results. Aggregated NPs not only decreased the number of active sites but also affected the dispersibility of nanocatalysts in the aqueous medium, which led to the inactivity of the HRG-Pd.

After examining the efficiency of all the as-prepared nanocatalysts at different catalyst loading, the effect of reagents (SDS, K_3PO_4), solvent, and reaction time were evaluated on the same model MH reaction, using the best performing catalyst mass loading condition i.e. Pd-NPs (5.3 mg) and HRG-Py-Pd (3.0 mg), respectively, as both the catalyst demonstrated best results with small amount of catalyst loading and the outputs are shown in **Table 2**. When reactions were performed in the absence of SDS using both the

**TABLE 1** | Mizoroki-Heck reaction (MH), 4-bromoanisole and acrylic acid as a model substrate. Catalyst screening.

Sl. No	Catalyst	Cat. Wt. (mg)	K ₃ PO ₄ (eq.)	SDS (Eq.)	Temp (°C)	HPLC Conversion
1	Pd-NPs	5.3	2	0.5	R.T.	—
2		5.3	2	0.5	90°C	traces
3		3.0	2	0.5	100°C	40%
4		5.3	2	0.5	100°C	92%
5		8.0	2	0.5	100°C	74%
6	HRG-Pd	5.3	2	0.5	R.T.	—
7		5.3	2	0.5	90°C	—
8		3.0	2	0.5	100°C	—
9		5.3	2	0.5	100°C	—
10		8.0	2	0.5	100°C	—
11	HRG-Py-Pd	5.3	2	0.5	R.T.	—
12		5.3	2	0.5	90°C	traces
13		3.0	2	0.5	100°C	93%
14		5.3	2	0.5	100°C	84%
15		8.0	2	0.5	100°C	71%

Reaction condition: 4-bromoanisole (0.5 mmol) and acrylic acid (0.5 mmol), catalyst (3.0–8.0 mg), K₃PO₄ (1.0 mmol), SDS (0.25 mmol) and water (2 ml) at R.T.—100°C, time 20 h.

catalysts Pd-NPs (5.3 mg) and HRG-Py-Pd (3.0 mg), no conversion was observed (**Table 2**, entries 1 and 5). The MH reaction was further carried out by using 0.25 eq., 0.5 eq., and 1.0 eq. of SDS without changing other parameters, and 0.5 eq. of SDS was found to be the best choice for this catalytic reaction as it produced 92 and 93% conversion respectively (**Table 2**, entries 3 and 7). This is in accordance with the literature, where the role of SDS as a stabilizing agent in Pd catalyzed coupling reactions is well established. For example, in the absence of SDS either the reaction does not occur or the yield of the reaction is sharply decreased (Sherwood, James, et al., 2019). After optimizing the amount of SDS (0.5 eq.), we focused on the effects of K₃PO₄ under the optimized parameters (catalyst 5.3 mg of Pd-NPs and 3.0 mg HRG-Py-Pd mg, 0.5 eq. of SDS in water 2 ml at 100°C for 20 h). Therefore, MH reactions were carried out using 0.75 eq. as well as 1.0 eq. of K₃PO₄ without altering the other optimized parameters, and the conversions sharply increased from 68 to 98% (**Table 2**, entries 12 and 13) in the case of catalyst HRG-Py-Pd, while significant improvement in conversion was achieved 20–37% (**Table 2**, entries 9 and 10) in case of catalyst Pd-NPs at a much slower pace as compared to catalyst HRG-Py-Pd. Further, we increased the amount of K₃PO₄ to 1.5 eq. in order to achieve further improvement in the reaction using both the catalysts under the identical conditions, and this time yields of the reaction

doubled from 37 to 78% (**Table 2**, entries 10 and 11) while using Pd-NPs; however, in case of HRG-Py-Pd, virtually no effect on the conversion (97%) were observed it almost remained same (**Table 2**, entries 14). Finally, reaction time optimization has been done using both the catalyst under the individual optimized reaction parameters. The MH reaction was performed using Pd-NPs (5.3 mg) as the catalyst and other optimized parameters such as K₃PO₄ (2.0 eq), SDS (0.5 eq.) in water (2.0 ml) at 100°C for 2, 3, and 8 h and the respective yields (20, 36, and 62%) were observed (**Table 2**, entries 15–17). These findings tell us that the yield of the product is continuously increasing with time at a slower pace while using Pd-NPs as the catalyst. As we know from the previous observation catalyst Pd-NPs took a longer time (20 h) to obtain 92% conversion (**Table 1**, entry 4). On the contrary, using HRG-Py-Pd as a catalyst under the optimized condition [K₃PO₄ (1.0 eq.), SDS (0.5 eq.) in water (2.0 ml) at 100°C], MH reactions were carried out for 2, 3, and 8 h. The results were surprising and fascinating as 99% conversion was achieved just within 3 h (**Table 2**, entry 19). However, very good conversion (90%) was noticed just in 2 h while 98% were observed after 8 h (**Table 2**, entries 18 and 20). From **Table 2** findings, the time of reaction has a diverse effect on the conversion of the reaction when different catalysts were used. For example, in the case of

TABLE 2 | Mizoroki-Heck reaction of 4-bromoanisole (1a) and acrylic acid (2) in aqueous solution using best catalyst HRG-Py-Pd; Optimization for K₃PO₄, SDS, and reaction time.

Sl. No	Catalyst	Cat. Wt. (mg)	K3PO4 (Eq.)	SDS (Eq.)	Time (h)	HPLC Conversion
SDS optimization						
1	Pd-NPs	5.3	2	—	20	—
2		5.3	2	0.25	20	19%
3		5.3	2	0.5	20	92%
4		5.3	2	1.0	20	88%
5	HRG-Py-Pd	3.0	2	—	20	—
6		3.0	2	0.25	20	24%
7		3.0	2	0.5	20	93%
8		3.0	2	1.0	20	92%
K3PO4 Optimization						
9	Pd-NPs	5.3	0.75	0.5	20	20%
10		5.3	1.0	0.5	20	37%
11		5.3	1.5	0.5	20	78%
12	HRG-Py-Pd	3.0	0.75	0.5	20	68%
13		3.0	1.0	0.5	20	98%
14		3.0	1.5	0.5	20	97%
Reaction Time Optimization						
15	Pd-NPs	5.3	2.0	0.5	2	20%
16		5.3	2.0	0.5	3	36%
17		5.3	2.0	0.5	8	62%
18	HRG-Py-Pd	3.0	1.0	0.5	2	90%
19		3.0	1.0	0.5	3	99%
20		3.0	1.0	0.5	8	98%
Different Solvent System (DMF)						
21	Pd-NPs	5.3	2.0	0.5	20	-
22	HRG-Py-Pd	3.0	1.0	0.5	20	-

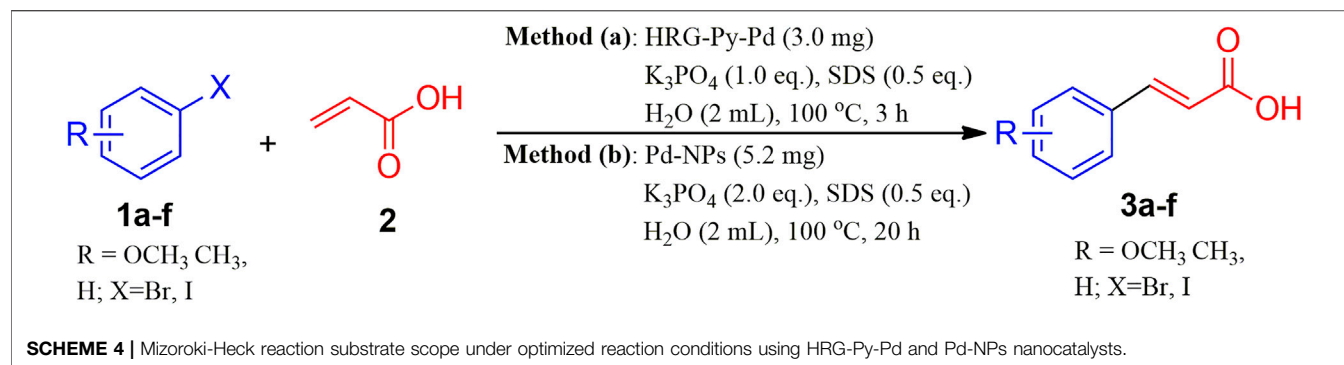
Reaction condition: 4-bromoanisole 1a (0.5 mmol) and acrylic acid 2 (0.5 mmol), catalyst used Pd-NPs, 5.3 mg and HRG-Py-Pd 3.0, water (2 ml) at 100°C, time 2–20 h.

catalyst Pd-NPs, a longer reaction time was required as the conversion of product increases slowly with time, whereas, functionalized catalyst HRG-Py-Pd completed the conversion in a very short time compared to Pd-NPs. Notably, in just 3 hours with 3.0 mg of catalyst HRG-Py-Pd, almost complete conversion (99%, **Table 2**, entry 19). Additionally, the effect of solvent was evaluated using DMF as a solvent instead of water. It is noteworthy to mention that the reaction did not occur at all when water is replaced with DMF (**Table 2**, entry 21 and 22), in the case of both the catalysts. This can be attributed to the low dispersibility of catalysts in solvents other than water.

To further explore the scope of functionalized nanocatalysts HRG-Py-Pd and non-functionalized Pd-NPs on different substrates in cross-coupling reaction, a series of aryl halides with diverse organic functional groups were applied as substrates in the same model reaction under the above-optimized reaction condition. For instance, in the case of Pd-NPs, 5.3 mg of catalyst, 2.0 Eq. of K₃PO₄, 0.5 Eq. of SDS, 2 ml of H₂O, and 20 h of reaction time were applied, whereas, for HRG-Py-Pd, the amount of catalyst and the reaction time was reduced to 3 mg and 3 h respectively (cf. **Scheme 4**). The results of these reactions are summarized in **Table 3**, which indicate that the as-

prepared nanocatalysts have efficiently facilitated the coupling reactions of diverse aryl halides including phenyl iodide, phenyl bromide, etc., with acrylic acid under optimized conditions. These diverse aryl halides with substituents at different positions have resulted in the formation of corresponding cinnamic acid derivatives in very good yield ranging from 83 to 92% in the case of Pd-NPs (5.3 mg) with 20 h reaction time, whereas, HRG-Py-Pd (3.0 mg) has delivered excellent yield between 87 and 99% for the same reactions (**Table 3**, entries 1–6). Notably, in both cases, the substrates with functional groups at ortho positions have yielded a lower amount of product as compared to meta and para substitution (**Table 3**, entry 3), which can be attributed to the higher steric hindrance caused by the substituents at ortho position positions. However, iodo-benzene and iodo-toluene furnished maximum yields in the case of both the catalysts (**Table 3**, entries 4 and 5). Both the catalysts were unable to produce MH products when 2-bromopyridin was used as substrate (**Table 3**, entry 7).

Additionally, the efficacy of the HRG-Py-Pd was determined by comparing the data published in the literature with the results of Mizoroki-Heck coupling reaction of 4-bromoanisole and acrylic acid under similar reaction conditions obtained with a variety of

**TABLE 3** | Mizoroki-Heck reaction catalyzed by HRG-Py-Pd and Pd-NPs nanocatalysts, Substrate scope.

Sl. No	Aryl Halides	1a-g	3a-f	Yield ^{a,c} HRG-Py-Pd	Yield ^{b,c} Pd-NPs
1	4-bromoanisole	1a	3a	98% (99%) ^d	91% (93%) ^d
2	3-bromoanisole	1b	3b	94%	88%
3	2-bromoanisole	1c	3c	87%	83%
4	4-iodotoluene	1d	3d	98%	92%
5	4-iodobenzene	1e	3e	98%	90%
6	4-bromobenzene	1f	3f	96%	87%
7	2-bromopyridine	1g	3f	—	—

Aryl halides (0.5 mmol), Acrylic acid (0.5 mmol); a Catalyst HRG-Py-Pd (3.0 mg), K_3PO_4 (1.0 eq.), SDS (0.5 eq.) in H_2O (2 mL), 100°C, 2 h; b Catalyst Pd-NPs (5.3 mg), K_3PO_4 (2.0 eq.), SDS (0.5 eq.) in H_2O (2 mL), 100°C, 20 h; c Isolated yields; d HPLC, conversion.

TABLE 4 | Comparison of the results obtained with the HRG-Py-Pd nanocatalyst for the Mizoroki-Heck reaction of 4-bromoanisole and acrylic acid in an aqueous solution with previously reported results in the literature.

S. No	Catalyst System	Base	Solvent System	Temp. (°C)	Conversion (%)	References
1	HRG-Py-Pd	K_3PO_4	H_2O	100	99	This study
2	Pd@SP-CMP	K_2CO_3	DMF	80	95	Ju et al. (2019)
3	MPCS-Ti/Pd	Et ₃ N	DMF/ H_2O	110	91	Rezaei 2015
4	$Fe_3O_4@PCA/Pd$ (0)-b-PEG	K_2CO_3	H_2O	90	91	Tabatabaee Rezaei et al. (2017)
5	PANI-Pd	K_2CO_3	DMA	120	85	Patel et al. (2015)
6	Pd-CS@SiO ₂	K_2CO_3	DMF	110	85	Jadhav et al. (2015)
7	Pd(OAc) ₂	Et ₃ N	H_2O	100	79	Patil et al. (2020)

TABLE 5 | Comparison of the reaction yield of Mizoroki-Heck reaction catalyzed by pristine Pd-NPs, HRG-Pd, and functionalized HRG-Py-Pd nanocatalysts using the same amount of catalysts under similar reaction conditions.

Sl. No	Catalyst	Cat. Wt. (mg)	K_3PO_4 (eq.)	SDS (Eq.)	Time (h)	Temp (°C)	HPLC Conversion
1	Pd-NPs	3.0	2	0.5	20	100	40%
2	HRG-Pd	3.0	2	0.5	20	100	—
3	HRG-Py-Pd	3.0	2	0.5	3	100	99%

supported Pd NPs based heterogeneous catalysts. Conversion values obtained from the literature are listed in **Table 4**, which indicate that the functionalized HRG-Py-Pd nanocatalyst evaluated in this study has delivered a much higher catalytic activity and is relatively superior to other catalyst systems used for this reaction. Therefore, the non-covalent pyrene functionalized HRG-Py-Pd nanocatalyst applied in this study is an effective approach in terms of the use of efficient support (HRG, consisting

of high surface area and enormous active sites), smart design, ease of deployment of catalyst, high dispersibility in water, versatility, i.e., compatibility with a wide range of systems, and high conversion.

To test the stability and reusability of HRG-Py-Pd, the coupling of 4-bromoanisole **1a** (3 mmol) and acrylic acid **2** (3 mmol) was used as a model reaction which generated the highest yield (99%). The reaction was performed for 3 h using

18 mg of HRG-Py-Pd, water (12 ml) at 100°C. The stability of the catalyst was tested up to five reactions (5 cycles) (**Supplementary Figure 37A,B**). After every reaction, the catalyst was recovered via centrifugation, washed three times with DI water, dried in an oven, and reused. Fresh catalyst in the first reaction yielded 99% conversion, while in the successive reactions, the catalyst activity reduced negligibly up to ~6–8% as shown in **Supplementary Figure 37B** in the supplementary information. Even after five cycles, the structure of HRG-Py-Pd catalyst almost remained intact which is confirmed by XRD analysis **Supplementary Figure 37A**.

CONCLUSION

Herein, a non-covalently functionalized HRG, decorated with Pd nanoparticles (HRG-Py-Pd) based nanocomposite is prepared, characterized, and applied as a nanocatalyst for the Mizoroki-Heck reaction in an aqueous medium. Initially, the catalytic efficacy of HRG-Py-Pd is tested for the conversion of 4-bromoanisole and acrylic acid in water. The activity of HRG-Py-Pd is also compared with non-functionalized HRG-Pd and pristine Pd NPs based nanocatalysts. Among all the catalysts, the HRG-Py-Pd has delivered the best results and yielded an almost complete conversion of 4-bromoanisole and acrylic acid to corresponding cinnamic acid (99%) in water. The reaction occurred in a short time (3 h) and just required a relatively small amount of catalyst (3 mg). On the other hand, with the same amount of catalysts (3 mg), the pristine Pd NPs just yielded a meager 40% conversion even after 20 h, while the non-functionalized HRG-Pd did not deliver any results and proved to be ineffective for the same reaction (cf. **Table 5**). The superior catalytic activity of HRG-Py-Pd is ascribed to the smart design of nanocatalyst consisting of pyrene as the functionalizing ligand because; 1) it significantly increased the physical stability and dispersibility of the catalyst in water, and 2) it provides nucleation sites for the homogenous and uniform growth of Pd

nanoparticles. Besides, a variety of aryl halides are also investigated for the Suzuki-Miyaura C-C bond formation reaction and the use of HRG-Py-Pd also resulted in high conversion. Therefore, the HRG-Py-Pd due to its high dispersibility delivered excellent catalytic activity for the coupling reactions in water, and thus offers a new route for the development of similar catalysts with other metal nanoparticles for a range of other catalytic transformations.

DATA AVAILABILITY STATEMENT

The raw data supporting the conclusions of this article will be made available by the authors, without undue reservation. Additional information on HPLC chromatograms and NMR spectra is provided in the supplementary material (**Supplementary Figures S1–S36**).

AUTHOR CONTRIBUTIONS

All authors listed have made a substantial, direct, and intellectual contribution to the work and approved it for publication.

ACKNOWLEDGMENTS

The authors extend their appreciation to the Deanship of Scientific Research at King Saud University for funding this work through Research Group No. RG-1436-032.

SUPPLEMENTARY MATERIAL

The Supplementary Material for this article can be found online at: <https://www.frontiersin.org/articles/10.3389/fchem.2022.872366/full#supplementary-material>

REFERENCES

- Alonso, D., Baeza, A., Chinchilla, R., Gómez, C., Guillena, G., Pastor, I., et al. (2018). Solid-Supported Palladium Catalysts in Sonogashira Reactions: Recent Developments. *Catalysts* 8, 202. doi:10.3390/catal8050202
- Amatore, C., and Jutand, A. (2000). Anionic Pd(0) and Pd(II) Intermediates in Palladium-Catalyzed Heck and Cross-Coupling Reactions. *Acc. Chem. Res.* 33, 314–321. doi:10.1021/ar980063a
- Baran, T., and Nasrollahzadeh, M. (2020). Cyanation of Aryl Halides and Suzuki-Miyaura Coupling Reaction Using Palladium Nanoparticles Anchored on Developed Biodegradable Microbeads. *Int. J. Biol. Macromolecules* 148, 565–573. doi:10.1016/j.ijbiomac.2020.01.157
- Beletskaya, I. P., and Cheprakov, A. V. (2000). The Heck Reaction as a Sharpening Stone of Palladium Catalysis. *Chem. Rev.* 100, 3009–3066. doi:10.1021/cr9903048
- Butler, R. N., and Coyne, A. G. (2010). Water: Nature's Reaction Enforcer—Comparative Effects for Organic Synthesis "In-Water" and "On-Water". *Chem. Rev.* 110, 6302–6337. doi:10.1021/cr100162c
- Calcio Gaudino, E., Manzoli, M., Carnaroglio, D., Wu, Z., Grillo, G., Rotolo, L., et al. (2018). Sonochemical Preparation of Alumina-Spheres Loaded with Pd Nanoparticles for 2-Butyne-1,4-Diol Semi-hydrogenation in a Continuous Flow Microwave Reactor. *RSC Adv.* 8, 7029–7039. doi:10.1039/c8ra00331a
- Christoffel, F., and Ward, T. R. (2018). Palladium-catalyzed Heck Cross-Coupling Reactions in Water: A Comprehensive Review. *Catal. Lett.* 148, 489–511. doi:10.1007/s10562-017-2285-0
- Cote, L. J., Kim, F., and Huang, J. (2009). Langmuir–Blodgett Assembly of Graphite Oxide Single Layers. *J. Am. Chem. Soc.* 131, 1043–1049. doi:10.1021/ja806262m
- Cseri, L., Razali, M., Pogany, P., and Szekely, G. (2018). Organic Solvents in Sustainable Synthesis and Engineering. *Green. Chem.*, 513–553. doi:10.1016/b978-0-12-809270-5.00020-0
- De Filippis, B., Ammazalorso, A., Fantacuzzi, M., Giampietro, L., Maccallini, C., and Amoroso, R. (2017). Anticancer Activity of Stilbene-Based Derivatives. *ChemMedChem* 12, 558–570. doi:10.1002/cmdc.201700045
- De Meijere, A., and Meyer, F. E. (1995). Fine Feathers Make fine Birds: The Heck Reaction in Modern Garb. *Angew. Chem. Int. Ed. Engl.* 33, 2379–2411. doi:10.1002/anie.199423791
- Easson, M. W., Jordan, J. H., Bland, J. M., Hinchliffe, D. J., and Condon, B. D. (2020). Application of Brown Cotton-Supported Palladium Nanoparticles in Suzuki-Miyaura Cross-Coupling Reactions. *ACS Appl. Nano Mater.* 3, 6304–6309. doi:10.1021/acsanm.0c01303

- Fakhri, P., Vaziri, M. R. R., Jaleh, B., and Shabestari, N. P. (2015). Nonlocal Nonlinear Optical Response of Graphene Oxide-Au Nanoparticles Dispersed in Different Solvents. *J. Opt.* 18, 015502. doi:10.1088/2040-8978/18/1/015502
- Felpin, F. X., Ayad, T., and Mitra, S. (2006). Pd/C: An Old Catalyst for New Applications - its Use for the Suzuki-Miyaura Reaction. *Eur. J. Org. Chem.* 2006, 2679–2690. doi:10.1002/ejoc.200501004
- Frisch, A. C., and Beller, M. (2005). Catalysts for Cross-Coupling Reactions with Non-activated Alkyl Halides. *Angew. Chem. Int. Ed.* 44, 674–688. doi:10.1002/anie.200461432
- Gao, Y., Ou, Y., and Gooßen, L. J. (2019). Pd-Catalyzed Synthesis of Vinyl Arenes from Aryl Halides and Acrylic Acid. *Chemistry* 25, 8709–8712. doi:10.1002/chem.201902022
- Gawande, M. B., Bonifácio, V. D. B., Luque, R., Branco, P. S., and Varma, R. S. (2013). Benign by Design: Catalyst-free In-Water, On-Water green Chemical Methodologies in Organic Synthesis. *Chem. Soc. Rev.* 42, 5522–5551. doi:10.1039/c3cs60025d
- Guo, Y., Li, J., Shi, X., Liu, Y., Xie, K., Liu, Y., et al. (2017). Cyclodextrin-supported Palladium Complex: A Highly Active and Recoverable Catalyst for Suzuki-Miyaura Cross-Coupling Reaction in Aqueous Medium. *Appl. Organometal. Chem.* 31, e3592. doi:10.1002/aoc.3592
- Hong, K., Sajjadi, M., Suh, J. M., Zhang, K., Nasrollahzadeh, M., Jang, H. W., et al. (2020). Palladium Nanoparticles on Assorted Nanostructured Supports: Applications for Suzuki, Heck, and Sonogashira Cross-Coupling Reactions. *ACS Appl. Nano Mater.* 3, 2070–2103. doi:10.1021/acsnan.9b02017
- Hummers, W. S., Jr, and Offeman, R. E. (1958). Preparation of Graphitic Oxide. *J. Am. Chem. Soc.* 80, 1339. doi:10.1021/ja01539a017
- Jadhav, S., Kumbhar, A., and Salunkhe, R. (2015). Palladium Supported on Silica-Chitosan Hybrid Material (Pd-CS@SiO₂) for Suzuki-Miyaura and Mizoroki-Heck Cross-Coupling Reactions. *Appl. Organometal. Chem.* 29, 339–345. doi:10.1002/aoc.3290
- Jadhav, S. N., and Rode, C. V. (2017). An Efficient Palladium Catalyzed Mizoroki-Heck Cross-Coupling in Water. *Green. Chem.* 19, 5958–5970. doi:10.1039/c7gc02869e
- Jagtap, S. (2017). Heck Reaction-State of the Art. *Catalysts* 7, 267. doi:10.3390/catal7090267
- Ju, P., Wu, S., Su, Q., Li, X., Liu, Z., Li, G., et al. (2019). Salen-porphyrin-based Conjugated Microporous Polymer Supported Pd Nanoparticles: Highly Efficient Heterogeneous Catalysts for Aqueous C-C Coupling Reactions. *J. Mater. Chem. A* 7, 2660–2666. doi:10.1039/c8ta11330k
- Julkapli, N. M., and Bagheri, S. (2015). Graphene Supported Heterogeneous Catalysts: An Overview. *Int. J. Hydrogen Energ.* 40, 948–979. doi:10.1016/j.ijhydene.2014.10.129
- Kadam, J., Madiwale, S., Bashte, B., Dindorkar, S., Dhawal, P., and More, P. (2020). Green Mediated Synthesis of Palladium Nanoparticles Using Aqueous Leaf Extract of *Gymnema Sylvestre* for Catalytic Reduction of Cr (VI). *SN Appl. Sci.* 2, 1854. doi:10.1007/s42452-020-03663-5
- Kambe, N., Iwasaki, T., and Terao, J. (2011). Pd-catalyzed Cross-Coupling Reactions of Alkyl Halides. *Chem. Soc. Rev.* 40, 4937–4947. doi:10.1039/c1cs15129k
- Khan, M., Shaik, M. R., Adil, S. F., Kuniyil, M., Ashraf, M., Frerichs, H., et al. (2020). Facile Synthesis of Pd@graphene Nanocomposites with Enhanced Catalytic Activity towards Suzuki Coupling Reaction. *Sci. Rep.* 10, 11728–11814. doi:10.1038/s41598-020-68124-w
- Khan, M., Khan, M., Kuniyil, M., Adil, S. F., Al-Warthan, A., Alkhathlan, H. Z., et al. (2014). Biogenic Synthesis of Palladium Nanoparticles Using *Pulicaria Glutinosa* Extract and Their Catalytic Activity towards the Suzuki Coupling Reaction. *Dalton Trans.* 43, 9026–9031. doi:10.1039/c3dt53554a
- Khan, M., Kuniyil, M., Shaik, M., Khan, M., Adil, S., Al-Warthan, A., et al. (2017). Plant Extract Mediated Eco-Friendly Synthesis of Pd@Graphene Nanocatalyst: An Efficient and Reusable Catalyst for the Suzuki-Miyaura Coupling. *Catalysts* 7, 20. doi:10.3390/catal7010020
- Khazaei, A., Khazaei, M., and Nasrollahzadeh, M. (2017). Nano-Fe₃O₄@SiO₂ Supported Pd(0) as a Magnetically Recoverable Nanocatalyst for Suzuki Coupling Reaction in the Presence of Waste Eggshell as Low-Cost Natural Base. *Tetrahedron* 73, 5624–5633. doi:10.1016/j.tet.2017.05.054
- Kitanosono, T., Masuda, K., Xu, P., and Kobayashi, S. (2018). Catalytic Organic Reactions in Water toward Sustainable Society. *Chem. Rev.* 118, 679–746. doi:10.1021/acs.chemrev.7b00417
- Kuniyil, M., Kumar, J. V. S., Adil, S. F., Shaik, M. R., Khan, M., Assal, M. E., et al. (2019). One-Pot Synthesized Pd@N-Doped Graphene: An Efficient Catalyst for Suzuki-Miyaura Couplings. *Catalysts* 9, 469. doi:10.3390/catal9050469
- Mpungose, P., Vundla, Z., Maguire, G., and Friedrich, H. (2018). The Current Status of Heterogeneous Palladium Catalysed Heck and Suzuki Cross-Coupling Reactions. *Molecules* 23, 1676. doi:10.3390/molecules23071676
- Naghdi, S., Jaleh, B., and Shahbazi, N. (2016a). Reversible Wettability Conversion of Electrodeposited Graphene Oxide/titania Nanocomposite Coating: Investigation of Surface Structures. *Appl. Surf. Sci.* 368, 409–416. doi:10.1016/j.apsusc.2016.01.193
- Naghdi, S., Rhee, K. Y., Jaleh, B., and Park, S. J. (2016b). Altering the Structure and Properties of Iron Oxide Nanoparticles and Graphene Oxide/iron Oxide Composites by Urea. *Appl. Surf. Sci.* 364, 686–693. doi:10.1016/j.apsusc.2015.12.225
- Naghdi, S., Rhee, K. Y., Kim, M. T., Jaleh, B., and Park, S. J. (2016c). Atmospheric Chemical Vapor Deposition of Graphene on Molybdenum Foil at Different Growth Temperatures. *Carbon Lett.* 18, 37–42. doi:10.5714/cl.2016.18.037
- Nasrollahzadeh, M., Issaabadi, Z., Tohidi, M. M., and Mohammad Sajadi, S. (2018). Recent Progress in Application of Graphene Supported Metal Nanoparticles in C–C and C–X Coupling Reactions. *Chem. Rec.* 18, 165–229. doi:10.1002/tcr.201700022
- Nasrollahzadeh, M., Jaleh, B., and Jabbari, A. (2014a). Synthesis, Characterization and Catalytic Activity of Graphene oxide/ZnO Nanocomposites. *RSC Adv.* 4, 36713–36720. doi:10.1039/c4ra05833j
- Nasrollahzadeh, M., Maham, M., and Tohidi, M. M. (2014b). Green Synthesis of Water-Dispersable Palladium Nanoparticles and Their Catalytic Application in the Ligand- and Copper-free Sonogashira Coupling Reaction under Aerobic Conditions. *J. Mol. Catal. A: Chem.* 391, 83–87. doi:10.1016/j.molcata.2014.04.004
- Nasrollahzadeh, M., Sajadi, S. M., Honarmand, E., and Maham, M. (2015). Preparation of Palladium Nanoparticles Using *Euphorbia Thymifolia* L. Leaf Extract and Evaluation of Catalytic Activity in the Ligand-free Stille and Hiyama Cross-Coupling Reactions in Water. *New J. Chem.* 39, 4745–4752. doi:10.1039/c5nj00244c
- Nebra, N., and García-Álvarez, J. (2020). Recent Progress of Cu-Catalyzed Azide-Alkyne Cycloaddition Reactions (CuAAC) in Sustainable Solvents: Glycerol, Deep Eutectic Solvents, and Aqueous Media. *Molecules* 25, 2015. doi:10.3390/molecules25092015
- Patel, H. A., Patel, A. L., and Bedekar, A. V. (2015). Polyaniline-anchored Palladium Catalyst-Mediated Mizoroki-Heck and Suzuki-Miyaura Reactions and One-Pot Wittig-Heck and Wittig-Suzuki Reactions. *Appl. Organometal. Chem.* 29, 1–6. doi:10.1002/aoc.3234
- Patil, S. P., Jadhav, S. N., Rode, C. V., Shejwal, R. V., and Kumbhar, A. S. (2020). Bio-surfactant: a green and Environmentally Benign Reaction Medium for Ligand-free Pd-Catalyzed Mizoroki-Heck Cross-Coupling Reaction in Water. *Transit. Met. Chem.* 45, 403–411. doi:10.1007/s11243-020-00392-x
- Phan, N. T. S., Van Der Sluys, M., and Jones, C. W. (2006). On the Nature of the Active Species in Palladium Catalyzed Mizoroki-Heck and Suzuki-Miyaura Couplings - Homogeneous or Heterogeneous Catalysis, A Critical Review. *Adv. Synth. Catal.* 348, 609–679. doi:10.1002/adsc.200505473
- Prekob, Á., Muránszky, G., Kocserha, I., Fiser, B., Kristály, F., Halasi, G., et al. (2020). Sonochemical Deposition of Palladium Nanoparticles onto the Surface of N-Doped Carbon Nanotubes: A Simplified One-step Catalyst Production Method. *Catal. Lett.* 150, 505–513. doi:10.1007/s10562-019-03074-1
- Qian, H., Wang, J., and Yan, L. (2020). Synthesis of Lignin-poly(N-Methylaniline)-Reduced Graphene Oxide Hydrogel for Organic Dye and lead Ions Removal. *J. Bioresources Bioproducts* 5, 204–210. doi:10.1016/j.jobab.2020.07.006
- Sheldon, R. A. (2018). Metrics of green Chemistry and Sustainability: Past, Present, and Future. *ACS Sustain. Chem. Eng.* 6, 32–48. doi:10.1021/acssuschemeng.7b03505
- Simon, M.-O., and Li, C.-J. (2012). Green Chemistry Oriented Organic Synthesis in Water. *Chem. Soc. Rev.* 41, 1415–1427. doi:10.1039/c1cs15222j

- Soh, L., and Eckelman, M. J. (2016). Green Solvents in Biomass Processing. *ACS Sustain. Chem. Eng.* 4, 5821–5837. doi:10.1021/acssuschemeng.6b01635
- Tabatabaei Rezaei, S. J., Shamseddin, A., Ramazani, A., Mashhadi Malekzadeh, A., and Azimzadeh Asiabi, P. (2017). Palladium Nanoparticles Immobilized on Amphiphilic and Hyperbranched Polymer-Functionalized Magnetic Nanoparticles: An Efficient Semi-heterogeneous Catalyst for Heck Reaction. *Appl. Organometal Chem.* 31, e3707. doi:10.1002/aoc.3707
- Xu, H., Zeiger, B. W., and Suslick, K. S. (2013). Sonochemical Synthesis of Nanomaterials. *Chem. Soc. Rev.* 42, 2555–2567. doi:10.1039/c2cs35282f

Conflict of Interest: The authors declare that the research was conducted in the absence of any commercial or financial relationships that could be construed as a potential conflict of interest.

Publisher's Note: All claims expressed in this article are solely those of the authors and do not necessarily represent those of their affiliated organizations, or those of the publisher, the editors and the reviewers. Any product that may be evaluated in this article, or claim that may be made by its manufacturer, is not guaranteed or endorsed by the publisher.

Copyright © 2022 Khan, Ashraf, Shaik, Adil, Islam, Kuniyil, Khan, Hatshan, Alshammari, Siddiqui and Tahir. This is an open-access article distributed under the terms of the Creative Commons Attribution License (CC BY). The use, distribution or reproduction in other forums is permitted, provided the original author(s) and the copyright owner(s) are credited and that the original publication in this journal is cited, in accordance with accepted academic practice. No use, distribution or reproduction is permitted which does not comply with these terms.



Levoglucosenone: Bio-Based Platform for Drug Discovery

Jason E. Camp^{1*} and Ben W. Greatrex²

¹Circa Sustainable Chemicals, York, United Kingdom, ²School of Science and Technology, University of New England, Armidale, NSW, Australia

Levoglucosone (LGO) is a bio-privileged molecule that can be produced on scale from waste biomass. This chiral building block has been converted via well-established chemical processes into previously difficult-to-synthesize building blocks such as enantiopure butenolides, dihydropyrans, substituted cyclopropanes, deoxy-sugars and ribonolactones. LGO is an excellent starting material for the synthesis of biologically active compounds, including those which have anti-cancer, anti-microbial or anti-inflammatory activity. This review will cover the conversion of LGO to biologically active compounds as well as provide future research directions related to this platform molecule.

Keywords: levoglucosenone, bio-mass, platform chemical, chiral building block, drug discovery

OPEN ACCESS

Edited by:

Florent Allais,
AgroParisTech Institut des Sciences et
Industries du Vivant et de
L'environnement, France

Reviewed by:

Donald Mencer,
Wilkes University, United States
Rolando A. Spanevello,
Universidad Nacional de Rosario,
Argentina

*Correspondence:

Jason E. Camp
jason.camp@circa-group.com

Specialty section:

This article was submitted to
Green and Sustainable Chemistry,
a section of the journal
Frontiers in Chemistry

Received: 22 March 2022

Accepted: 21 April 2022

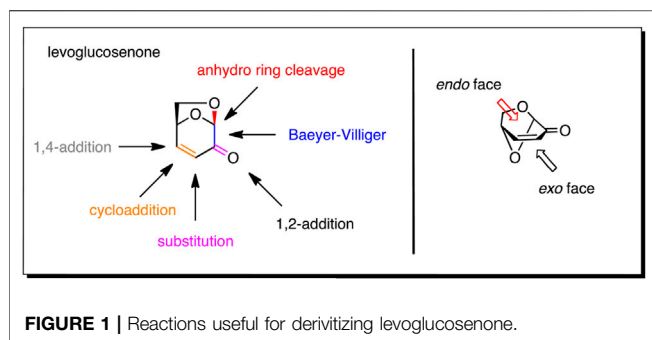
Published: 31 May 2022

Citation:

Camp JE and Greatrex BW (2022)
Levoglucosenone: Bio-Based Platform
for Drug Discovery.
Front. Chem. 10:902239.
doi: 10.3389/fchem.2022.902239

INTRODUCTION

Levoglucosenone (LGO, 1) is a chiral building block that is readily available from the pyrolysis of materials containing cellulose, including biomass waste such as wood chips and bagasse. Over the past 50 years, research into the chemistry of LGO has established the high degree of orthogonality in the reactive functional groups, and demonstrated the excellent stereochemical control offered by the bicyclic ring-system (Witczak and Tatsuta, 2002; Witczak, 2007; Sarotti et al., 2012a; Comba et al., 2018; Kühlborn et al., 2020). The chirality at C1 and C5 in LGO gives it advantages in stereoselective synthesis compared to achiral biomass derivatives such as furfural, while the reduced number of chiral centers simplifies its use compared to monosaccharides. Enantio-, stereo-, regio- and chemoselective reactions have been executed around the core ring-system. These include, 1,6-anhydro ring opening (Shafizadeh et al., 1979; Tagirov et al., 2015; Comba et al., 2016; Pedersen and Pedersen, 2021), Baeyer-Villiger oxidation (Koseki et al., 1990; Koseki et al., 1991; Teixeira et al., 2016; Bonneau et al., 2018; Diot-Neant et al., 2018), 1,2-addition (Shafizadeh and Chin, 1977; Tsypysheva et al., 2000; Giordano et al., 2012; Debsharma et al., 2019; Sharipov et al., 2019), α -substitution (Ward and Shafizadeh, 1981; Ledingham E. et al., 2017; Ledingham E. T. et al., 2017; Giri et al., 2017; Hughes et al., 2018; Liu et al., 2020), cycloaddition/cyclization (Yatsynich et al., 2003; Novikov et al., 2009; Faizullina et al., 2011; Samet et al., 2011; Sarotti et al., 2012b; Banwell et al., 2020; Fadlallah et al., 2020; Liu et al., 2020), and conjugate addition reactions (Shafizadeh et al., 1982; Essig, 1986; Samet et al., 1996; Trahanovsky et al., 2003) (**Figure 1**). These reactions have led to the controlled synthesis of a multitude of important biologically active motifs, including enantiopure butenolides, dihydropyrans, substituted cyclopropanes, deoxy-sugars and ribonolactones. The reactivity of the ketone and enone functionalities is influenced by the 1,6-anhydro bridge, which strongly biases reaction to occur from the less hindered *exo*-face of the molecule. Whilst the reactivity and potential of this molecule is well understood, it is only recently that it has been produced on industrial scale allowing its use as a chiral feedstock (Lawrence et al., 2012). This review will focus on the use of LGO as a starting material used for the synthesis of biologically active materials, specifically: known bioactive compounds, analogues of bioactives



where the intact LGO ring-system has been incorporated into the final structure as a bioisostere, and novel materials. In addition, this review will briefly highlight how LGO derivatives can intercept routes to drugs currently in production.

Synthesis of Known Biologically Active Molecules

Enantiopure cyclopropanes are found in a variety of existing biologically active molecules, and are favoured for their rigidity and relative stability under biological conditions. There are a number of approaches for the preparation of cyclopropanes from LGO including the direct cyclopropanation of the alkene of either LGO or one of its derivatives (Samet et al., 2007; Ledingham E. et al., 2017), reactions of malonates with the 3-iododerivative of LGO (Valeev et al., 1999), or by transformation of LGO into a suitably reactive species for cyclization. Using this last approach, Stockton and Greatrex (2016) converted LGO into substituted butyrolactones via either 1) reductive cross-coupling and Baeyer-Villiger oxidation, or 2) reduction then Baeyer-Villiger oxidation (**Figure 2**). Lactone **2** and **6** were then converted to epoxides **3** and **7** using standard protocols. Finally, treatment of the epoxysters **3** or **7** with lithium hexamethyldisilazide (LHMDS) in tetrahydrofuran (THF) gave cyclopropanes **4** and **8**, which following elaboration of functional groups led to

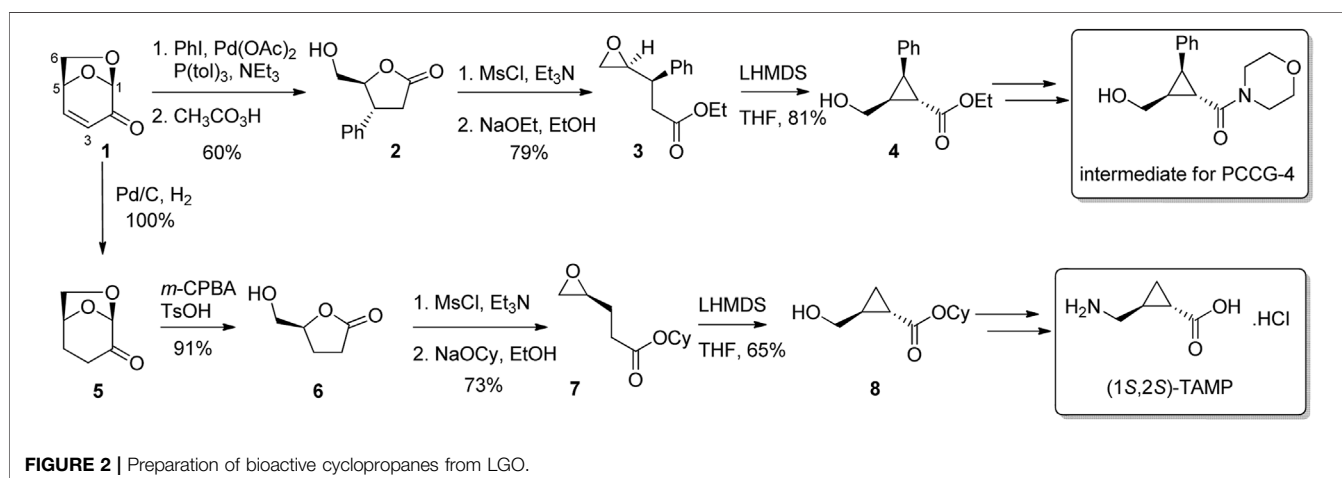
an intermediate used for the synthesis of the selective glutamate receptor antagonist PCCG-4 and GABA_c receptor agonist (1*S*, 2*S*)-TAMP, respectively.

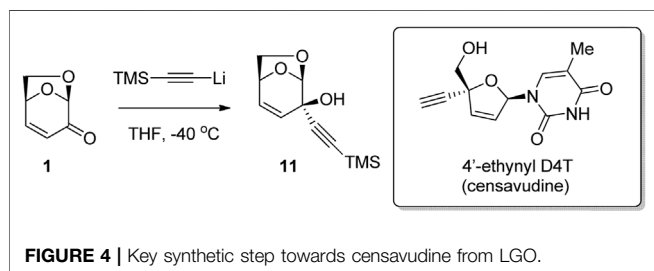
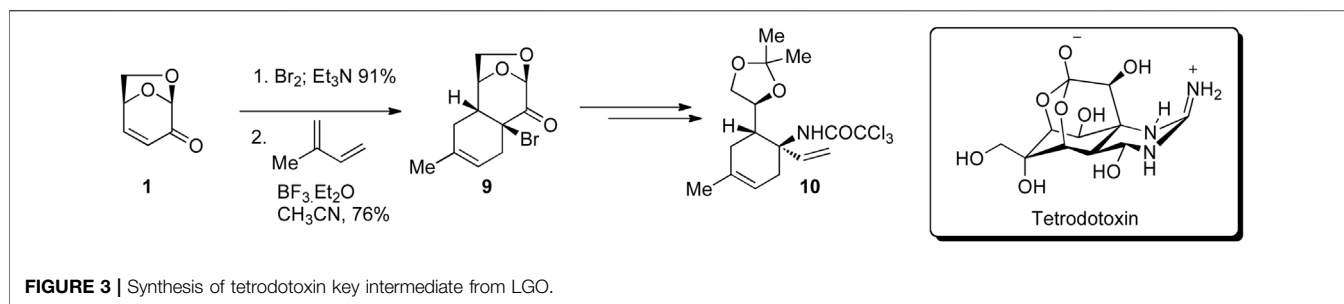
Tetrodotoxin is the principal toxin of the pufferfish that acts through specific inhibition of sodium ion influx through excitable membranes. In a series of publications, Isobe and co-workers reported the first enantioselective total synthesis of this potent biologically active compound using LGO as a key building block (**Figure 3**) (Bamba et al., 1996; Urabe et al., 2006; Nishikawa and Isobe, 2013). This example demonstrates the utility and reaction control possible using LGO, whereby a one-pot two step C3 bromination of LGO followed by Diels-Alder cycloaddition afforded tricycle **9** as a single regio- and diastereomeric isomer. This transformation set key stereocenters that were then relayed into the final natural product tetrodotoxin via key intermediate **10**.

Oncolys Bipharma used the reaction of LGO with TMS-acetylide to give alkyne-alcohol **11** as a result of selective 1,2-addition of the nucleophile to the ketone (**Figure 4**) (Nagai et al., 2015). The bicyclic alcohol **11** was then converted to 4'-ethynyl D4T (censavudine), which is a stavudine analogue with decreased cytotoxicity. This route via LGO allowed for the synthesis of the active substance in a simpler way, at lower cost and in larger quantities than previous routes. Censavudine has been investigated as a novel drug therapy for human immunodeficiency (HIV), with greater activity against the less common HIV-2 variant (Smith et al., 2015).

Levoglucosenone in Analogue Synthesis or as a Bioisostere

In addition to the synthesis of known biologically active compounds, LGO has been used extensively in the synthesis of analogues of bioactives. For example, many substituted naphthoquinone compounds are known to have antibiotic activity, such as the natural product eleutherin isolated from *Eleutherine bulbosa* (Bianchi and Ceriotti, 1975). LGO has been used for the synthesis of a series of quinone derivatives, with the core of the LGO converted into a tetrahydropyran or





dihydropyranone ring. Freskos and Swenton (1985) performed a cycloaddition reaction between LGO and benzofuranone 12 to afford tetracycle 13 in moderate yield (**Figure 5**). Opening of the acetal ring and deoxygenation afforded naphthohydroquinone derivative 14 as a single enantiomer, while a later report from the same group gave the natural product hongkonin (Swenton et al., 1996). Chew et al. (1988) subjected LGO and dibromoxylene 15 to sonication to afford tetracycle 16 as a single enantiomer (**Figure 5**). Functional group modification gave pyranonaphthoquinone derivative 17.

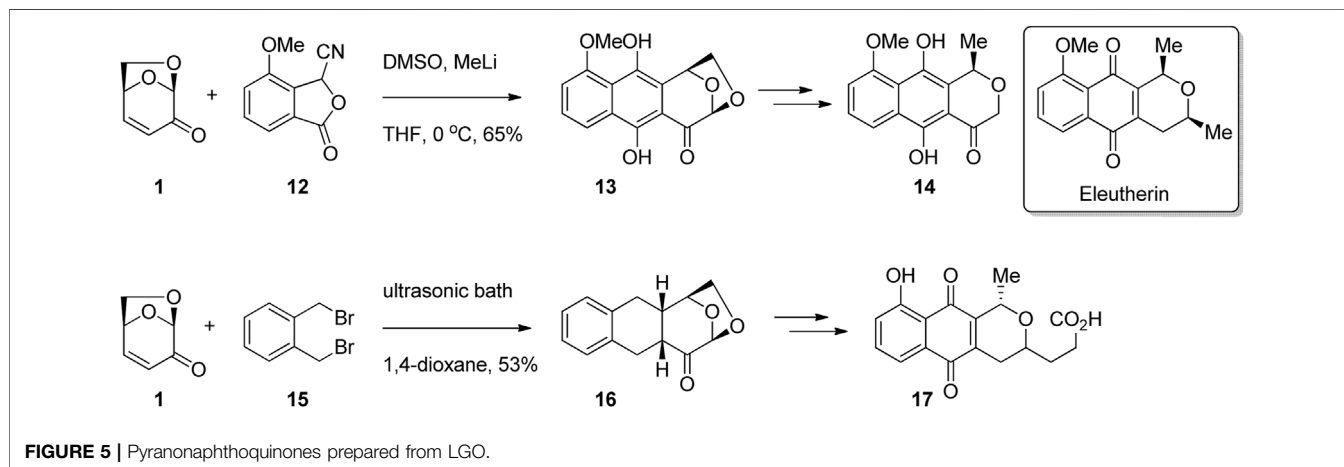
Conjugate addition to the enone functionality of LGO has also been used to synthesize biologically active derivatives of known compounds. Thromboxanes play a major role in blood clot formation (thrombosis) and are formed via the oxidation of arachidonic acid *in vivo*. Tolstikov and Tolstikov (2007) employed the LGO ring-system as a bioisostere for the cyclic ether motif found in thromboxane A2. The authors used the

regio- and stereoselective addition of a mixed cuprate 18 to LGO to give the alkene addition product 19 as a key step in their synthesis of the thromboxane analogue (**Figure 6**). Alkylation of tin enolate 19 followed by deprotection afford the desired thromboxane analogue 20.

The use of the 6,8-dioxabicyclo [3.2.1]octane as a bioisostere for the cyclohexyl group was examined by Eiden et al. (1994) in their study of materials that bind to the *N*-methyl-D-aspartate receptor NMDA receptor complex (**Figure 7**). Starting with LGO, reduction and then Strecker reaction afforded the aminonitrile 21. Reactions of the aminonitrile 21 with aryl Grignard reagents gave a series of CNS-active arylamines including 22, which was shown to possess low micromolar activity at the NMDA receptor.

Synthesis of Novel Bioactive Materials

Due to the highly functionalized and rigid nature of LGO, as well as its well understood reactivity, it has been used extensively as a building block for the synthesis of novel biologically active compounds. 1,2-Addition to the carbonyl of LGO was used by Czubatka-Bienkowska et al. (2017) for the preparation of *S*-glycosylated thiosemicarbazone derivatives, a class of molecules that have shown potential medical applications as antiviral, antibacterial and anticancer drugs. Thus, condensation of the thiosemicarbazide with LGO in acetic acid in ethanol afforded the desired adduct 23 in good yield (**Figure 8**). Subsequent conjugate addition of the 1-thioglucose derivative to thiosemicarbazone 23 gave *S*-glycosylated thiosemicarbazone 24. Testing of the compound library for *in vitro* anticancer activity



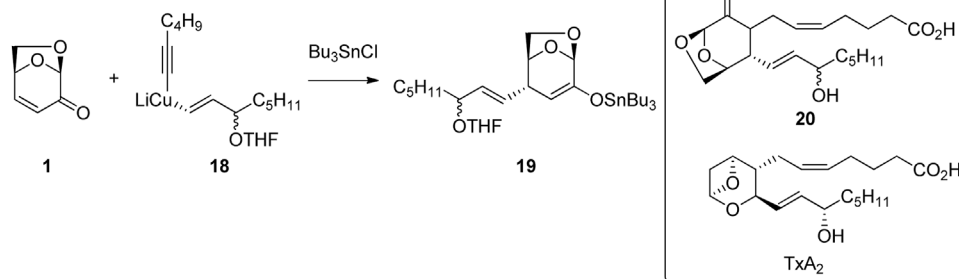


FIGURE 6 | 1,4-Additions of vinyl cuprates to LGO for the preparation of thromboxane analogues.

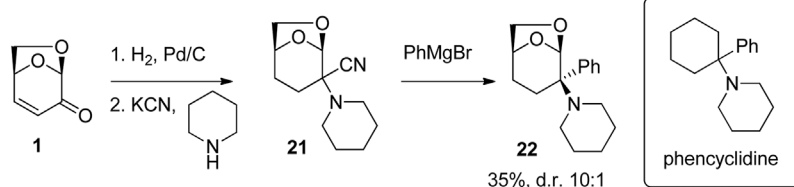


FIGURE 7 | Preparation of phencyclidine analogues using LGO.

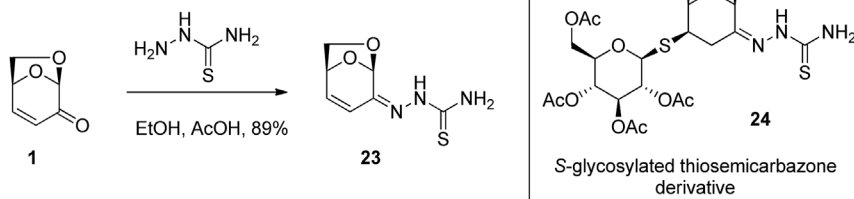


FIGURE 8 | Anticancer thioglycosides prepared from LGO.

showed significant activity against A2780 cancer cell line via induction of DNA damage, though this effect is not associated with apoptosis or oxidative stress induction.

The 1,4-addition of thiols to LGO has been used extensively for the synthesis of biologically active levoglucosenone derivatives. Giri *et al.* (2016) used the reaction of 1-hexanethiol with LGO in the presence of a base to afford adduct 25 in good yield (Figure 9). The series of thio-derivatives synthesized in this way showed activity against hepatocarcinoma cell lines and also illuminated the key role of the carbonyl functionality to exert biological activity. Similarly, Witczak *et al.* (2014) demonstrated that substituted thiophenols could be efficiently added to LGO in the presence of triethylamine to give thio-acid 26 (Figure 9). In the same report, 1-thiosugars were shown to be competent nucleophiles for conjugate addition into LGO. For example, addition of protected 1-thioglucose 27 to LGO in the presence of triethylamine afford the desired adduct 28

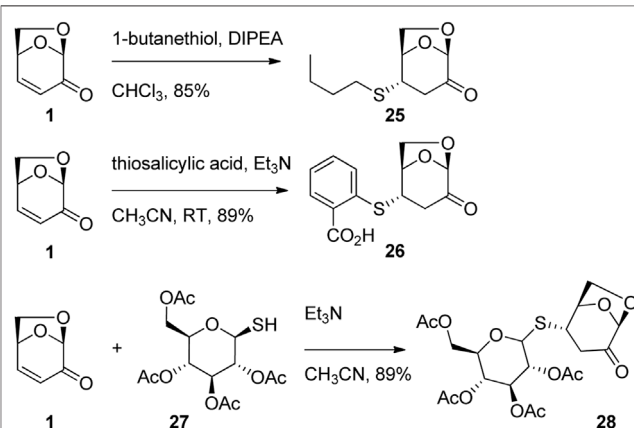
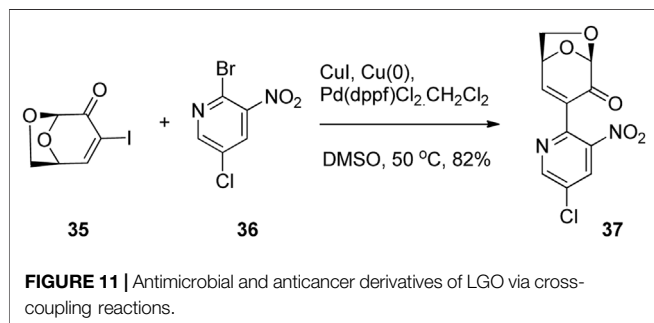
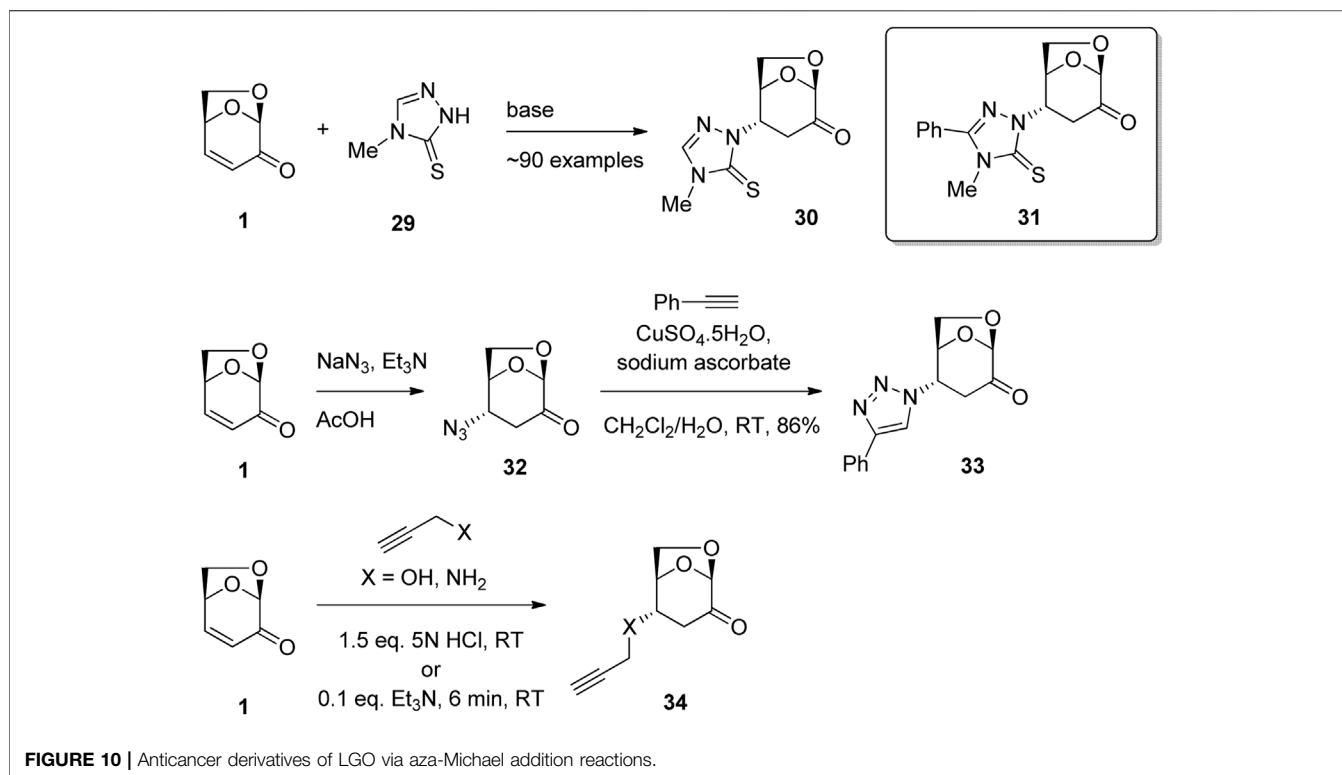


FIGURE 9 | Anticancer compounds through conjugate addition of thiols to LGO.



in good yield (**Figure 9**). Importantly, this series of functional CARB-pharmacophores demonstrated cytotoxicity and apoptosis against human cancer cell lines (A549, LoVo, MCF-7 and HeLa). The thio-sugar motif was shown to be a promising construct for the development of novel antineoplastic drugs.

Nitrogen and oxygen nucleophiles have also been shown to undergo conjugate addition to LGO and a number of biologically active derivatives have been formed using this chemistry. For example, Westman et al. (2007) have patented the synthesis of LGO derivatives for the treatment of disorders such as cancer, autoimmune diseases and heart diseases (**Figure 10**). The reaction of LGO with triazole derivative 29 in the presence of base afford the desired 1,4-addition adduct 30 as a single enantiomer. The approximately 90 derivatives were tested in a range of assays, including in human H1299 lung carcinoma cells lacking p53 expression and in H1299 His175 cells that carry tetracycline-regulated mutant p53 constructs. From these studies,

a group of LGO derivatives were identified including 31 that showed promise in the treatment of disorders in which a malfunctioning p53 pathway could be involved. In a similar synthetic approach, Sarotti and co-workers used the reaction of sodium azide in acetic acid with LGO in the presence of triethylamine to give β -azidoketone 32 (**Figure 10**) (Tsai et al., 2018). A subsequent click reaction with phenyl acetylene performed without isolation of the β -azidoketone 32 afforded triazole 33. Application of the methodology to a diverse series of acetylenes gave triazole products, which showed satisfactory antitumor activity when evaluated against TNBC cancer cell lines. Primary amines have also been shown to be good nucleophiles for addition to the enone functionality of LGO. For example, further work by Sarotti and co-workers showed that the reaction of propargyl amine to LGO in the presence of base gave addition adduct 34 (**Figure 10**) (Tsai et al., 2020). Testing of this chain extended series on MDA-MB-231 cells, specifically endogenous mutant p53 knock down (R280K), and by reintroducing p53 R280K in cells lacking p53 expression, anti-proliferative activities against lung and colon cancer cell lines were demonstrated. Further examples of LGO derivatives with anticancer activity have been reported by the same group (Delbart et al., 2022).

Carbon-Carbon bond formation via metal-mediated cross-couplings has also been used for the production of novel biologically active molecules based on LGO. Banwell and co-workers employed a palladium-catalyzed Ullmann cross-coupling between the C3 iodo derivative of LGO 35 and a variety of bromonitropyridines such as 36 affording a range of LGO derivatives (**Figure 11**) (Liu et al., 2020). It was found that the α -

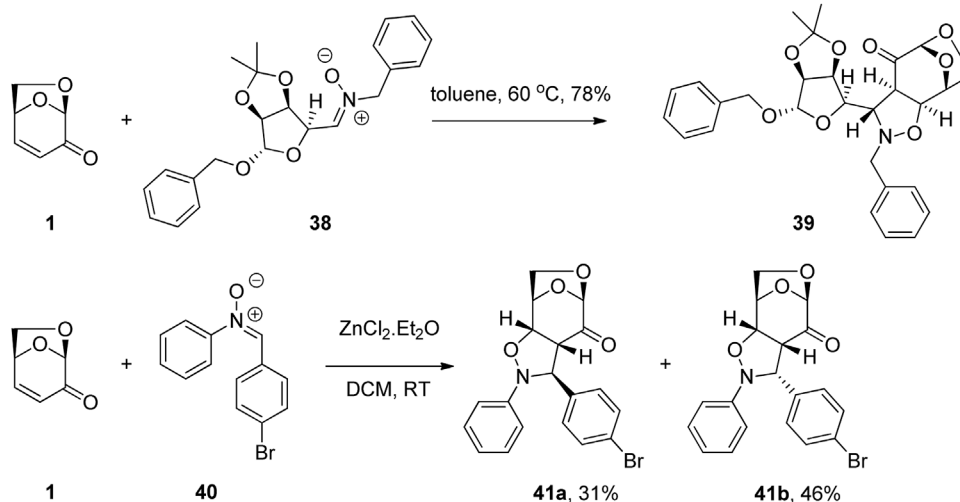


FIGURE 12 | Cycloaddition reactions of LGO for the preparation of carbonic anhydrase and RAS activation inhibitors.

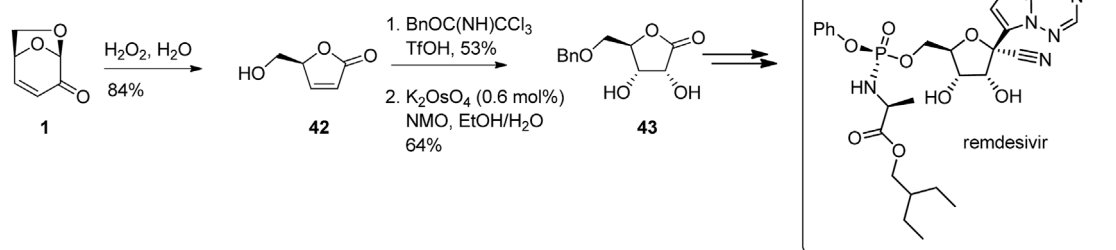


FIGURE 13 | Conversion of LGO into protected ribonolactone derivatives used to synthesise antiviral compounds.

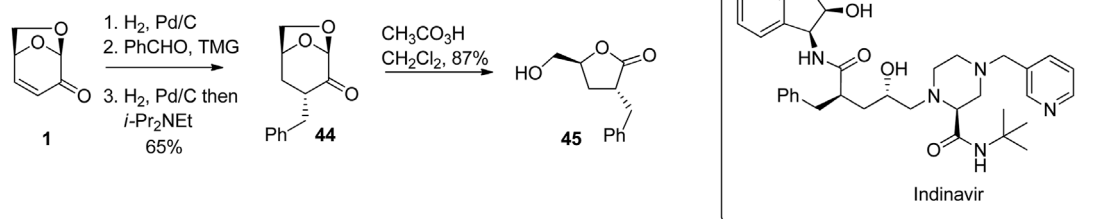


FIGURE 14 | Preparation of a key intermediate that can be used in the preparation of indinavir.

pyridinylated derivatives of type 37 had potent and selective antimicrobial and/or cytotoxic properties, whereas the azaindole derivatives were essentially inactive in all of the tests conducted.

1,3-Dipolar cycloadditions of nitrones with LGO have also been used for the synthesis of biologically active derivatives. The

selectivity of the process was controlled by the 1,6-anhydro bridge and the polarization of the conjugated alkene. Pratesi *et al.* (2020) exploited the reactivity of the enone functionality of LGO in a dipolar cycloaddition reaction to give derivative 39 via reaction of LGO with nitrone 38 (Figure 12). One of the glycomimetics

showed strong inhibition of the central nervous system expressed hCA VIII as well as selectivity towards a specific isoform, while inhibitory activity against tumor associated hCA IX ($K_i = 35.9$ nM) was shown by another of the LGO derivatives. A similar strategy was employed by Peri and co-workers for the construction of Ras activation inhibitors (Müller et al., 2009). Thus, the reaction of LGO with a series of aromatic nitrones 40 in the presence of zinc(II) chloride afforded the desired levoglucosenone fused isoxazolidines 41a and 41b as a mixture of diastereomers (Figure 12). These scaffolds were then further manipulated to give a total of nine functionalized derivatives and their biological activity examined. These molecules were shown to be a novel set of Ras inhibitors with interesting biological activity both *in vitro* and towards cells against a representative set of human cancer cell lines.

Using LGO to Intercept Existing Routes to Pharmaceuticals

LGO and its derivatives are attractive building block for the synthesis of key intermediates used in the production of pharmaceuticals, largely due to its well-understood chemistry and availability on scale. As an example, Allais and his team at AgroParisTech have developed straight forward protocols for the facile conversion of LGO to 5-*O*-benzyl-D-(+)-ribo-1,4-lactone 43, which is a key building block for the synthesis of the COVID-19 anti-infective drug remdesivir (Figure 13) (Flourat et al., 2015; Moreaux et al., 2019). In this work, Baeyer-Villiger oxidation of LGO to the butenolide 42 followed by alcohol protection and *syn*-dihydroxylation gave the protected ribonolactone 43 in good yield and selectivity.

The ready transformation of LGO or its derivatives to 5-hydroxymethylbutyrolactones via the Baeyer-Villiger reaction can be used to access a variety of pharmaceuticals. For example, a hydrogenation-aldol condensation-hydrogenation sequence starting with LGO afforded ketone 44, which was then hydrogenated and oxidized using peracetic acid to give the benzylated butyrolactone 45 (Figure 14) (Ledingham E. T. et al., 2017). The configuration of the benzyl group in the intermediate ketone 44 was controlled by steric interactions with the oxymethylene bridge, resulting in the requisite *anti*-configuration of substituents in the final butyrolactone. The original route to 45, which was used to construct the core section of

the HIV protease inhibitor indinavir reported by Dorsey et al. (1994) was prepared in 5-steps from glutamic acid. This synthesis involved protection/deprotections steps, and strong base, while the more atom-economic synthesis of 45 starting with LGO proceeds in four-high yielding steps in 57% overall yield. This same benzylated butyrolactone has been used for the preparation of vasoactive intestinal peptide inhibitors, and drugs for Alzheimer's disease.

CONCLUSION

This brief outline has identified a diverse set of bioactive materials that can be prepared from LGO, and include materials that retain the chiral bicyclic structure, or transfer the chirality to new motifs. The orthogonal reactive groups, and the diastereoselectivity imparted by the bicyclic ring-system gives unique opportunities to prepare bioactive compounds. The trend towards using single enantiomer drugs in place of racemates places LGO in a unique position among renewable chemicals. LGO is one of the few chiral pyrolysis products obtained from cellulose, and is the principle product in bio oils formed from the acid-catalysed pyrolysis of cellulose. This sets it apart from other platform chemicals such as furfural, itaconic acid, and chloromethyl furfural which have lost the chirality present in the carbohydrate precursor, and require asymmetric strategies for their use in chiral bioactive synthesis. The development of reactions for the LGO ring-system coupled with its availability on large scale will provide additional opportunities to access known and new bioactive chemicals.

AUTHOR CONTRIBUTIONS

JC and BG both contributed to the writing of this review.

SUPPLEMENTARY MATERIAL

The Supplementary Material for this article can be found online at: <https://www.frontiersin.org/articles/10.3389/fchem.2022.902239/full#supplementary-material>

REFERENCES

- Bamba, M., Nishikawa, T., and Isobe, M. (1996). Tin-assisted Cyclization for Chiral Cyclohexane Synthesis, an Alternative Route to (–)-tetrodotoxin Skeleton. *Tetrahedron Lett.* 37 (45), 8199–8202. doi:10.1016/0040-4039(96)01860-6
- Banwell, M. G., Liu, X., Connal, L. A., and Gardiner, M. G. (2020). Synthesis of Functionally and Stereochemically Diverse Polymers via Ring-Opening Metathesis Polymerization of Derivatives of the Biomass-Derived Platform Molecule Levoglucosenone Produced at Industrial Scale. *Macromolecules* 53 (13), 5308–5314. doi:10.1021/acs.macromol.0c01305
- Bianchi, C., and Ceriotti, G. (1975). Chemical and Pharmacological Investigations of Constituents of Eleutherine Bulbosa (Miller) Urb. (Iridaceae). *J. Pharm. Sci.* 64 (8), 1305–1308. doi:10.1002/jps.2600640809
- Bonneau, G., Peru, A. A. M., Flourat, A. L., and Allais, F. (2018). Organic Solvent- and Catalyst-free Baeyer-Villiger Oxidation of Levoglucosenone and Dihydrolevoglucosenone (Cyrene): a Sustainable Route to (S)- γ -hydroxymethyl- α,β -butenolide and (S)- γ -hydroxymethyl- γ -butyrolactone. *Green Chem.* 20 (11), 2455–2458. doi:10.1039/c8gc00553b
- Chew, S., Ferrier, R. J., and Sinnwell, V. (1988). An Approach to the Pyranonaphthoquinones. *Carbohydr. Res.* 174, 161–168. doi:10.1016/0008-6215(88)85089-4
- Comba, M. B., Suárez, A. G., Sarotti, A. M., Mangione, M. I., Spanevello, R. A., and Giordano, E. D. V. (2016). Synthesis of a 3-Thiomannoside. *Org. Lett.* 18 (8), 1748–1751. doi:10.1021/acs.orglett.6b00428
- Comba, M. B., Tsai, Y.-h., Sarotti, A. M., Mangione, M. I., Suárez, A. G., and Spanevello, R. A. (2018). Levoglucosenone and its New Applications: Valorization of Cellulose Residues. *Eur. J. Org. Chem.* 2018 (5), 590–604. doi:10.1002/ejoc.201701227
- Czubatka-Bieńkowska, A., Sarnik, J., Macieja, A., Galita, G., Witczak, Z. J., and Poplawski, T. (2017). Thio-functionalized Carbohydrate Thiosemicarbazones and Evaluation of Their Anticancer Activity. *Bioorg. Med. Chem. Lett.* 27 (12), 2713–2720. doi:10.1016/j.bmcl.2017.04.051

- Debsharma, T., Behrendt, F. N., Laschewsky, A., and Schlaad, H. (2019). Ring-Opening Metathesis Polymerization of Biomass-Derived Levoglucosenol. *Angew. Chem. Int. Ed.* 58 (20), 6718–6721. doi:10.1002/anie.201814501
- Delbart, D. I., Giri, G. F., Cammarata, A., Pan, M. D., Bareño, L. A., Amigo, N. L., et al. (2022). Antineoplastic Activity of Products Derived from Cellulose-Containing Materials: Levoglucosenone and Structurally-Related Derivatives as New Alternatives for Breast Cancer Treatment. *Invest. New Drugs* 40, 30–41. doi:10.1007/s10637-021-01167-6
- Diot-Néant, F., Rastoder, E., Miller, S. A., and Allais, F. (2018). Chemo-enzymatic Synthesis and Free Radical Polymerization of Renewable Acrylate Monomers from Cellulose-Based Lactones. *ACS Sustain. Chem. Eng.* 6 (12), 17284–17293. doi:10.1021/acssuschemeng.8b04707
- Dorsey, B. D., Levin, R. B., McDaniel, S. L., Vacca, J. P., Guare, J. P., Darke, P. L., et al. (1994). L-735,524: the Design of a Potent and Orally Bioavailable HIV Protease Inhibitor. *J. Med. Chem.* 37 (21), 3443–3451. doi:10.1021/jm00047a001
- Eiden, F., Denk, F., and Höfner, G. (1994). ZNS-wirksame Pyrane: Amin- und arylsubstituierte Dioxabicyclooctane. *Arch. Pharm. Pharm. Med. Chem.* 327 (7), 405–412. doi:10.1002/ardp.19943270702
- Essig, M. G. (1986). Michael Additions of Thiols to Levoglucosenone. *Carbohydr. Res.* 156, 225–231. doi:10.1016/s0008-6215(00)90115-0
- Fadlallah, S., Peru, A. A. M., Flourat, A. L., and Allais, F. (2020). A Straightforward Access to Functionalizable Polymers through Ring-Opening Metathesis Polymerization of Levoglucosenone-Derived Monomers. *Eur. Polym. J.* 138, 109980. doi:10.1016/j.eurpolymj.2020.109980
- Faizullina, L. K., Safarov, M. G., Spirikhin, L. V., Kolosnitsyn, V. S., Kondrova, Y. A., and Valeev, F. A. (2011). Reaction of Nitroalkanes with Levoglucosenone and its α -bromo and α -iodo Derivatives. Cyclopentaannulation of α -halocyclonones. *Russ. J. Org. Chem.* 47 (6), 914–919. doi:10.1134/s1070428011060145
- Flourat, A. L., Peru, A. A. M., Teixeira, A. R. S., Brunissen, F., and Allais, F. (2015). Chemo-enzymatic Synthesis of Key Intermediates (S)- γ -hydroxymethyl- α , β -butenolide and (S)- γ -hydroxymethyl- γ -butyrolactone via Lipase-Mediated Baeyer-Villiger Oxidation of Levoglucosenone. *Green Chem.* 17 (1), 404–412. doi:10.1039/c4gc01231c
- Freskos, J. N., and Swenton, J. S. (1985). Annulation Reaction of Levoglucosenone. Chiral Intermediates for the Synthesis of naphtho[2,3-C]pyran-5,10-Quinone Antibiotics. *J. Chem. Soc. Chem. Commun.* 10, 658–659. doi:10.1039/c39850000658
- Giordano, E. D. V., Frinchaboy, A., Suárez, A. G., and Spanevello, R. A. (2012). Synthesis of Tri-O-acetyl-d-allal from Levoglucosenone. *Org. Lett.* 14 (17), 4602–4605. doi:10.1021/ol302061a
- Giri, G. F., Danielli, M., Marinelli, R. A., and Spanevello, R. A. (2016). Cytotoxic Effect of Levoglucosenone and Related Derivatives against Human Hepatocarcinoma Cell Lines. *Bioorg. Med. Chem. Lett.* 26 (16), 3955–3957. doi:10.1016/j.bmcl.2016.07.007
- Giri, G. F., Viarengo, G., Furlán, R. L. E., Suárez, A. G., García Vescovi, E., and Spanevello, R. A. (2017). Soybean Hulls, an Alternative Source of Bioactive Compounds: Combining Pyrolysis with Bioguided Fractionation. *Industrial Crops Prod.* 105, 113–123. doi:10.1016/j.indcrop.2017.05.005
- Hughes, L., McElroy, C. R., Whitwood, A. C., and Hunt, A. J. (2018). Development of Pharmaceutically Relevant Bio-Based Intermediates Through Aldol Condensation and Claisen-Schmidt Reactions of Dihydrolevoglucosenone (Cyrene). *Green Chem.* 20 (19), 4423–4427. doi:10.1039/c8gc01227j
- Jæger Pedersen, M., and Pedersen, C. M. (2021). Reactivity, Selectivity, and Synthesis of 4- C -Silylated Glycosyl Donors and 4-Deoxy Analogues. *Angew. Chem.* 133 (5), 2721–2725. doi:10.1002/ange.202009209
- Koseki, K., Ebata, T., Kawakami, H., Matsushita, H., Itoh, K., and Naoi, Y. (1991). Method of Preparing (S)- γ -Hydroxymethyl- α , β -butenolide. *European Patent No EP0411403A1*. Munich, Germany: European Patent Office.
- Koseki, K., Ebata, T., Kawakami, H., Matsushita, H., Naoi, Y., and Itoh, K. (1990). A Method for Easy Preparation of Optically Pure (S)-5-Hydroxy-2-penten-4-olide and (S)-5-Hydroxypenten-4-olide. *Heterocycles* 31 (40), 423–426. doi:10.3987/com-89-5300
- Kühlborn, J., Groß, J., and Opatz, T. (2020). Making Natural Products from Renewable Feedstocks: Back to the Roots? *Nat. Prod. Rep.* 37 (3), 380–424. doi:10.1039/c9np00040b
- Lawrence, C. H., Raverty, W. D., and Duncan, A. J. (2012). *Method for Converting Lignocellulosic Materials into Useful Chemicals*. Washington, DC: U.S. Patent and Trademark Office. U.S. Patent Application US2012011714A1.
- Ledingham, E., Merritt, C., Sumby, C., Taylor, M., and Greatrex, B. (2017a). Stereoselective Cyclopropanation of (-)-Levoglucosenone Derivatives Using Sulfonium and Sulfoxonium Ylides. *Synthesis* 49 (12), 2652–2662. doi:10.1055/s-0036-1588971
- Ledingham, E. T., Stockton, K. P., and Greatrex, B. W. (2017b). Efficient Synthesis of an Indinavir Precursor from Biomass-Derived (-)-Levoglucosenone. *Aust. J. Chem.* 70 (10), 1146–1150. doi:10.1071/ch17227
- Liu, X., Carr, P., Gardiner, M. G., Banwell, M. G., Elbanna, A. H., Khalil, Z. G., et al. (2020). Levoglucosenone and its Pseudoenantiomer Iso-Levoglucosenone as Scaffolds for Drug Discovery and Development. *ACS Omega* 5 (23), 13926–13939. doi:10.1021/acsomega.0c01331
- Moreaux, M., Bonneau, G., Peru, A., Brunissen, F., Janvier, M., Haudrechy, A., et al. (2019). High-Yielding Diastereoselective Syn -Dihydroxylation of Protected HBO: An Access to D-(+)-Ribono-1,4-lactone and 5-O -Protected Analogues. *Eur. J. Org. Chem.* 2019 (7), 1600–1604. doi:10.1002/ejoc.201801780
- Sarotti, A. M., Zanardi, M., Spanevello, R. A., and Suarez, A. G. (2012a). Recent Applications of Levoglucosenone as Chiral Synthons. *Cos* 9 (4), 439–459. doi:10.2174/157017912802651401
- Müller, C., Gomez-Zurita Frau, M. A., Ballinari, D., Colombo, S., Bitto, A., Martegani, E., et al. (2009). Design, Synthesis, and Biological Evaluation of Levoglucosenone-Derived Ras Activation Inhibitors. *ChemMedChem* 4 (4), 524–528. doi:10.1002/cmdc.200800416
- Nagai, K., Kiguchi, S., Koyama, H., Hume, W. E., and Tsujimoto, S. (2015). *Method for Producing 4'-ethynyl d4T*. Geneva, Switzerland: WIPO. PCT Application WO/2009/084655.
- Nishikawa, T., and Isobe, M. (2013). Synthesis of Tetrodotoxin, a Classic but Still Fascinating Natural Product. *Chem. Rec.* 13 (3), 286–302. doi:10.1002/tcr.201200025
- Novikov, R. A., Rafikov, R. R., Shulishov, E. V., Konyushkin, L. D., Semenov, V. V., and Tomilov, Y. V. (2009). Reactions of Levoglucosenone and its Derivatives with Diazo Compounds. *Russ. Chem. Bull.* 58 (2), 327–334. doi:10.1007/s11172-010-0011-9
- Pratesi, D., Matassini, C., Goti, A., Angeli, A., Carta, F., Supuran, C. T., et al. (2020). Glycomimetic Based Approach toward Selective Carbonic Anhydrase Inhibitors. *ACS Med. Chem. Lett.* 11 (5), 727–731. doi:10.1021/acsmchemlett.9b00590
- Samet, A. V., Niyazymbetov, M. E., Semenov, V. V., Laikhter, A. L., and Evans, D. H. (1996). Comparative Studies of Cathodically-Promoted and Base-Catalyzed Michael Addition Reactions of Levoglucosenone. *J. Org. Chem.* 61 (25), 8786–8791. doi:10.1021/jo961019g
- Samet, A. V., Shestopalov, A. M., Lutov, D. N., Rodinovskaya, L. A., Shestopalov, A. A., and Semenov, V. V. (2007). Preparation of Chiral Cyclopropanes with a Carbohydrate Fragment from Levoglucosenone. *Tetrahedron Asymmetry* 18 (16), 1986–1989. doi:10.1016/j.tetasy.2007.08.013
- Samet, A. V., Lutov, D. N., Firgang, S. I., Lyssenko, K. A., and Semenov, V. V. (2011). A Concise Approach to Chiral Chromenes Based on Levoglucosenone. *Tetrahedron Lett.* 52 (23), 3026–3028. doi:10.1016/j.tetlet.2011.04.004
- Sarotti, A. M., Spanevello, R. A., Suárez, A. G., Echeverría, G. A., and Piro, O. E. (2012b). 1,3-Dipolar Cycloaddition Reactions of Azomethine Ylides with a Cellulose-Derived Chiral Enone. A Novel Route for Organocatalysts Development. *Org. Lett.* 14 (10), 2556–2559. doi:10.1021/ol3008588
- Shafizadeh, F., and Chin, P. P. S. (1977). Preparation of 1,6-Anhydro-3,4-Dideoxy- β -D-Glycero-Hex-3-Enopyranos-2-Ulose (Levoglucosenone) and Some Derivatives Thereof. *Carbohydr. Res.* 58 (1), 79–87. doi:10.1016/s0008-6215(00)83406-0
- Shafizadeh, F., Furneaux, R. H., and Stevenson, T. T. (1979). Some Reactions of Levoglucosenone. *Carbohydr. Res.* 71 (1), 169–191. doi:10.1016/s0008-6215(00)86069-3
- Shafizadeh, F., Ward, D. D., and Pang, D. (1982). Michael-addition Reactions of Levoglucosenone. *Carbohydr. Res.* 102 (1), 217–230. doi:10.1016/s0008-6215(00)88064-7
- Sharipov, B. T., Davidova, A. N., Ryabova, A. S., Galimzyanova, N. F., and Valeev, F. A. (2019). Synthesis and Fungicidal Activity of Methylsulfanylmethyl Ether

- Derivatives of Levoglucosenone. *Chem. Heterocycl. Comp.* 55 (1), 31–37. doi:10.1007/s10593-019-02415-7
- Smith, R. A., Raugi, D. N., Wu, V. H., Leong, S. S., Parker, K. M., Oakes, M. K., et al. (2015). The Nucleoside Analog BMS-986001 Shows Greater *In Vitro* Activity against HIV-2 Than against HIV-1. *Antimicrob. Agents Chemother.* 59 (12), 7437–7446. doi:10.1128/aac.01326-15
- Stockton, K. P., and Greatrex, B. W. (2016). Synthesis of Enantiopure Cyclopropyl Esters from (–)-levoglucosenone. *Org. Biomol. Chem.* 14 (31), 7520–7528. doi:10.1039/c6ob00933f
- Swenton, J. S., Freskos, J. N., Dalidowicz, P., and Kerns, M. L. (1996). A Facile Entry into Naphthopyran Quinones via an Annulation Reaction of Levoglucosenone. The Total Synthesis of (–)-Hongconin I. *J. Org. Chem.* 61 (2), 459–464. doi:10.1021/jo951607e
- Tagirov, A. R., Biktairov, I. M., Galimova, Y. S., Faizullina, L. K., Salikhov, S. M., and Valeev, F. A. (2015). Opening of the 1,6-anhydro Bridge with Selective Reduction of the Acetal Moiety in Levoglucosenone and its Derivatives. *Russ. J. Org. Chem.* 51 (4), 569–575. doi:10.1134/s1070428015040181
- Teixeira, A. R. S., Flourat, A. L., Peru, A. A. M., Brunissen, F., and Allais, F. (2016). Lipase-Catalyzed Baeyer-Villiger Oxidation of Cellulose-Derived Levoglucosenone into (S)- γ -Hydroxymethyl- α,β -Butenolide: Optimization by Response Surface Methodology. *Front. Chem.* 4, 16. doi:10.3389/fchem.2016.00016
- Tolstikov, G. A., and Tolstikov, G. A. (2007). Unsaturated Sugars in Enantiospecific Synthesis of Natural Low-Molecular Bioregulators and Their Structural Analogues. *Russ. J. Bioorg. Chem.* 33 (1), 3–23. doi:10.1134/s1068162007010025
- Trahanovsky, W. S., Ochaoda, J. M., Wang, C., Revell, K. D., Arvidson, K. B., Wang, Y., et al. (2003). “A Convenient Procedure for the Preparation of Levoglucosenone and its Conversion to Novel Chiral Derivatives,” in *Carbohydrate Synthons in Natural Products Chemistry: Synthesis, Functionalization, and Applications*. Editors Z. J. Witzczak and K. Tatsuta (Washington, DC: American Chemical Society).
- Tsai, Y.-h., Borini Etichetti, C. M., Cicetti, S., Girardini, J. E., Spanevello, R. A., Suárez, A. G., et al. (2020). Design, Synthesis and Evaluation of Novel Levoglucosenone Derivatives as Promising Anticancer Agents. *Bioorg. Med. Chem. Lett.* 30 (14), 127247. doi:10.1016/j.bmcl.2020.127247
- Tsai, Y.-h., Borini Etichetti, C. M., Di Benedetto, C., Girardini, J. E., Martins, F. T., Spanevello, R. A., et al. (2018). Synthesis of Triazole Derivatives of Levoglucosenone as Promising Anticancer Agents: Effective Exploration of the Chemical Space through Retro-Aza-Michael/aza-Michael Isomerizations. *J. Org. Chem.* 83 (7), 3516–3528. doi:10.1021/acs.joc.7b03141
- Tsypysheva, I. P., Valeev, F. A., Vasil'eva, E. V., Spirikhin, L. V., and Tolstikov, G. A. (2000). Stereochemical Differentiation in the Reactions of Organometallic Reagents with Levoglucosenone and Some of its Dihydro Derivatives. *Russ. Chem. Bull.* 49 (7), 1237–1240. doi:10.1007/bf02495766
- Urabe, D., Nishikawa, T., and Isobe, M. (2006). An Efficient Total Synthesis of Optically Active Tetrodotoxin from Levoglucosenone. *Chem. Asian J.* 1 (1–2), 125–135. doi:10.1002/asia.200600038
- Valeev, F. A., Gorobets, E. V., and Miftakhov, M. S. (1999). Reactions of 3-iodolevoglucosenone with Sodium Derivatives of Some CH Acids. Chiral Cyclopropanes and Stable Oxetenes. *Russ. Chem. Bull.* 48 (1), 152–156. doi:10.1007/bf02494418
- Ward, D. D., and Shafizadeh, F. (1981). Bromination of Levoglucosenone. *Carbohydr. Res.* 93 (2), 284–287. doi:10.1016/s0008-6215(00)80858-7
- Westman, J., Wiman, K., and Mohell, N. (2007). *Levoglucosenone Derivatives for the Treatment of Disorders Such as Cancer, Autoimmune Diseases and Heart Diseases*. Geneva, Switzerland: WIPO. PCT Application WO/2007/139497.
- Witzczak, Z. J. (2007). “New Stereoselective Functionalization of Cellulose-Derived Pyrolysis Derivatives: Levoglucosenone and its Dimer,” in *Materials, Chemicals, and Energy from Forest Biomass*. Editor D. S. Argyropoulos (American Chemical Society), 332–349. doi:10.1021/bk-2007-0954.ch021
- Witzczak, Z. J., Sarnik, J., Czubatka, A., Forma, E., and Poplawski, T. (2014). Thio-sugar Motif of Functional CARB-Pharmacophore for Antineoplastic Activity. Part 2. *Bioorg. Med. Chem. Lett.* 24 (24), 5606–5611. doi:10.1016/j.bmcl.2014.10.095
- Witzczak, Z. J., and Tatsuta, K. (2002). *Carbohydrate Synthons in Natural Products Chemistry: Synthesis, Functionalization, and Applications*. Washington, DC: American Chemical Society.
- Yatsynich, E. A., Petrov, D. V., Valeev, F. A., and Dokichev, V. A. (2003). Synthesis of Pyrazolines Based on Levoglucosenone. *Chem. Nat. Compd.* 39 (4), 337–339. doi:10.1023/b:conc.0000003411.19962.39

Conflict of Interest: JEC is the CTO of Circa Group who have patents for the production of levoglucosenone, the precursor to Cyrene™, from waste biomass (Lawrence et al., 2012).

The remaining author declares that the work was conducted in the absence of any commercial or financial relationships that could be construed as a potential conflict of interest.

Publisher's Note: All claims expressed in this article are solely those of the authors and do not necessarily represent those of their affiliated organizations, or those of the publisher, the editors and the reviewers. Any product that may be evaluated in this article, or claim that may be made by its manufacturer, is not guaranteed or endorsed by the publisher.

Copyright © 2022 Camp and Greatrex. This is an open-access article distributed under the terms of the Creative Commons Attribution License (CC BY). The use, distribution or reproduction in other forums is permitted, provided the original author(s) and the copyright owner(s) are credited and that the original publication in this journal is cited, in accordance with accepted academic practice. No use, distribution or reproduction is permitted which does not comply with these terms.



Enzymatic Active Release of Violacein Present in Nanostructured Lipid Carrier by Lipase Encapsulated in 3D-Bioprinted Chitosan-Hydroxypropyl Methylcellulose Matrix With Anticancer Activity

Ignacio Rivero Berti¹, Boris E. Rodenak-Kladniew², Sergio F. Katz¹, Eva Carolina Arrua^{3,4}, Vera A. Alvarez⁵, Nelson Duran^{6,7} and Guillermo R. Castro^{3,7*}

OPEN ACCESS

Edited by:

Rosaria Ciriminna,
National Research Council (CNR), Italy

Reviewed by:

Deniz Yildirim,
Çukurova University, Turkey
Amiya Kumar Panda,
Vidyasagar University, India

*Correspondence:

Guillermo R. Castro
grcastro@gmail.com

Specialty section:

This article was submitted to
Green and Sustainable Chemistry,
a section of the journal
Frontiers in Chemistry

Received: 06 April 2022

Accepted: 07 June 2022

Published: 07 July 2022

Citation:

Rivero Berti I, Rodenak-Kladniew BE, Katz SF, Arrua EC, Alvarez VA, Duran N and Castro GR (2022) Enzymatic Active Release of Violacein Present in Nanostructured Lipid Carrier by Lipase Encapsulated in 3D-Bioprinted Chitosan-Hydroxypropyl Methylcellulose Matrix With Anticancer Activity. *Front. Chem.* 10:914126. doi: 10.3389/fchem.2022.914126

¹Laboratorio de Nanobiomaterials, CINDEFI, Departamento de Química, Facultad de Ciencias Exactas, CONICET (CCT La Plata), Universidad Nacional de La Plata (UNLP), La Plata, Argentina, ²Instituto de Investigaciones Bioquímicas de La Plata (INIBIOLP), CONICET-UNLP, CCT-La Plata, Facultad de Ciencias Médicas, La Plata, Argentina, ³Max Planck Laboratory for Structural Biology, Chemistry and Molecular Biophysics of Rosario (MPLbioR, UNR-MPLbpC), Partner Laboratory of the Max Planck Institute for Biophysical Chemistry (MPLbpC, MPG), Centro de Estudios Interdisciplinarios (CEI), Universidad Nacional de Rosario, Rosario, Argentina, ⁴Centro de Investigación y Desarrollo en Materiales Avanzados y Almacenamiento de Energía de Jujuy-Univ. Nac., de Jujuy, Argentina, ⁵Grupo de Materiales Compuestos Termoplásticos (CoMP), Instituto de Investigaciones en Ciencia y Tecnología de Materiales (INTEMA), Facultad de Ingeniería, Universidad Nacional de Mar del Plata (UNMDP), CONICET, Mar del Plata, Argentina, ⁶Laboratory of Urogenital Carcinogenesis and Immunotherapy, Department of Structural and Functional Biology, Universidade Estadual de Campinas (UNICAMP), Campinas, Brazil, ⁷Nanomedicine Research Unit (Nanomed), Center for Natural and Human Sciences (CCNH), Universidade Federal do ABC (UFABC), Santo André, Brazil

Violacein (Viol) is a bacterial purple water-insoluble pigment synthesized by *Chromobacterium violaceum* and other microorganisms that display many beneficial therapeutic properties including anticancer activity. Viol was produced, purified in our laboratory, and encapsulated in a nanostructured lipid carrier (NLC). The NLC is composed of the solid lipid myristyl myristate, an oily lipid mixture composed of capric and caprylic acids, and the surfactant poloxamer P188. Dormant lipase from *Rhizomucor miehei* was incorporated into the NLC-Viol to develop an active release system. The NLC particle size determined by dynamic light scattering brings around 150 nm particle size and $\zeta \approx -9.0$ mV with or without lipase, but the incorporation of lipase increase the Pdl from 0.241 to 0.319 ($\approx 32\%$). For scaffold development, a 2.5 hydroxypropyl methylcellulose/chitosan ratio was obtained after optimization of a composite for extrusion in a 3D-bioprinter developed and constructed in our laboratory. Final Viol encapsulation efficiency in the printings was over 90%. Kinetic release of the biodye at pH = 7.4 from the mesh containing NLC-lipase showed roughly 20% Viol fast release than without the enzyme. However, both Viol kinetic releases displayed similar profiles at pH = 5.0, where the lipase is inactive. The kinetic release of Viol from the NLC-matrices was modeled and the best correlation was found with the Korsmeyer-Peppas model ($R^2 = 0.95$) with $n < 0.5$ suggesting a Fickian release of Viol from the matrices. Scanning Electron Microscope (SEM) images of the NLC-meshes showed significant differences before and

after Viol's release. Also, the presence of lipase dramatically increased the gaps in the interchain mesh. XRD and Fourier Transform Infrared (FTIR) analyses of the NLC-meshes showed a decrease in the crystalline structure of the composites with the incorporation of the NLC, and the decrease of myristyl myristate in the mesh can be attributed to the lipase activity. TGA profiles of the NLC-meshes showed high thermal stability than the individual components. Cytotoxic studies in A549 and HCT-116 cancer cell lines revealed high anticancer activity of the matrix mediated by mucoadhesive chitosan, plus the biological synergistic activities of violacein and lipase.

Keywords: Violacein, nanostructured lipid carriers, Lipase, chitosan, 3D-bioprinter, controlled release, Violacein active release

1 INTRODUCTION

Bacterial metabolites make up a great pool of molecules that, in addition to having a wide range of biological activities, are relatively simple and inexpensive to produce in a sustainable way (Venil et al., 2020). In 2020, the GLOBALCAN reported more than 19 million new cases and 10 million deaths. Additionally, 80% of new cases occur in individuals over 50 years of age, so as the world population ages, the prevalence of these diseases grows accordingly (Ferlay et al., 2020). Violacein (Viol) is a violet-purple pigment synthesized by numerous Gram-negative bacterial strains that have demonstrated beneficial antibacterial, antifungal, trypanocide, antiviral, and antitumoral activities, among others (Durán et al., 2021). Particularly, Viol inhibits the expression of some cell markers associated with proliferation (e.g., cyclin-dependent, mitogen-activated kinases, etc.), inhibit metalloproteinases, enzymes essential to metastatic processes, and induces tumoral cell death by different mechanisms mentioned recently (Durán et al., 2016).

Viol is practically insoluble in aqueous media and its high hydrophobicity correlated well with the parameter XLogP3-aa = 2.7. XLogP3-aa is a statistical parameter used to estimate the hydrophobicity/hydrophilicity of a molecule considering the contribution of each atom, hydrogen bridges, and the terminal groups (Cheng et al., 2007). The Viol insolubility in aqueous media is a serious limitation for its prospective application as a therapeutic agent because of low bioavailability. Besides, it is estimated that between 50% and 90% of the new drugs in development and 40% of the drugs currently available in the market present the same drawback (Liu, 2018). Thus, Viol could be a promising new drug but also an excellent therapeutic agent if a suitable drug delivery system is developed. Since Viol is a hydrophobic molecule, lipid systems can be considered as a potential best drug carrier (Rivero Berti et al., 2020). Among them, liposomes, and lipid nanoparticles are probably the most popular structures employed for the development of drug delivery systems because of their simple preparation, non-toxic, easy scale-up, and reproducibility. However, liposomes are thermodynamically unstable, with high structural dependence on environmental conditions, unknown cargo concentration, and unpredictable kinetic release. Meanwhile, solid lipid nanoparticles display several advantages, such as

improving the solubility of poorly soluble drugs, and also increasing circulation time, thus avoiding possible resistance mechanisms displayed by tumor cells, such as efflux pumps (Creixell and Peppas, 2012). Solid lipid delivery systems propose platforms that are relatively simple to prepare, extremely stable, have high loading efficiency for hydrophobic drugs and have high biocompatibility (Scioli Montoto et al., 2020). Although SLNs have a high encapsulation efficiency, in some cases when the nanoparticles mature, the lipids of the matrix crystallize, and the drug is expelled during the process with the consequent loss of loaded drug. In nanostructured lipid carriers (NLC) systems an oily lipid is added to the solid lipid core to introduce entropy and prevent and/or reduce lipid crystallization (Gordillo-Galeano and Mora-Huertas, 2018). In the present work, myristyl myristate (MM) was selected as the main lipid component for the NLC, since MM has shown advantages in NLC preparation such as emulsification enhancer, effective thickener, low acute toxicity in oral or dermal tests, and its extensively used in personal care and cosmetic products (Islan et al., 2016; Shilling, 1990; Berti, et al., 2019). Also, a commercial mixture of caprylic and capric acids was employed in the NLC preparation because it is an oily liquid lipid at RT and used as a thickener to improve the texture and stability of emulsions, it is biodegradable and commonly used in pharmaceutical and cosmetic formulations (Islan et al., 2016).

However, one of the main problems in cancer therapies for the delivery of nanoparticles containing hydrophobic and/or environmentally sensitive drugs is the low attachment of nanoparticles to the cancer cell surfaces, insufficient drug penetration, and inadequate drug release kinetics (Wang et al., 2018). The consequent drug release failure can result in molecular degradation under physiological conditions (i.e., lytic enzymes), fast clearance, and/or formation of insoluble complexes (i.e., π -stacking) that result in low drug bioavailability and could produce also undesirable side effects. A potential solution could be the development of a stimuli-responsive controlled release system (SRCRS), which will be particularly useful for the treatment of solid tumors. Among the main advantages of SRCRS is the circumvention of premature drug clearance, high accumulation on targeted cells or tissues, and proper stimuli-responsive drug release with controlled kinetics (Rahim et al., 2021). Importantly, SRCRS reduces the drug amount to be administered and gets the

same therapeutic results, which is a substantial advantage for improving the individuals' quality of life, and principally for oncological patients. The use of enzymes for the development of SRCRS to release the cargo in place and with appropriate kinetics was described. Enzymes such as proteases, glycosidases, and lipases were tested for the release of growth factors (i.e., hepatocyte growth factors and VEGF), insulin, doxorubicin, nitric oxide, etc. from nanoparticle and hydrogel devices (Chandrawati, 2016; Wang et al., 2018; Shahriari et al., 2019).

Specifically, Viol release from the NLC during nanoparticle disintegration can be affected because the hydrophobic character of the biodye could be stuck to the lipids, and consequently Viol bioavailability will be reduced. In this sense, the inclusion of an inactive but dormant "alive" lipase in the NLC can improve Viol release from the lipids by hydrolyzing the ester linkages of the lipids in the presence of a physiological environment. Lipase from *R. miehei* showed optimum activity at temperatures between 37°C and 40°C, in the presence of surfactants, but the optimal pH is strain-dependent and goes from the alkaline range (i.e., pH between 8.0 and 8.8) to the acid one (i.e., pH = 5.0–5.4) (Takó et al., 2017). Both simultaneous conditions are relevant for cancer treatment since solid tumors show high temperatures compared to the nearby normal tissue because of high metabolic rates, and also an acid surrounding environment due to the exacerbated production of lactic and acetic acids (Rahim et al., 2021). In addition, lipase released from the NLC can act on the membrane surface of cancer cells, not only disturbing its structure and function but also hydrolyzing lipids that could facilitate the diffusion of Viol into the cells. Moreover, the presence of lipase released from the NLC could catalyze the hydrolysis of triglycerides present in the serum, reducing the formation of precancerous lesions as well as colon, pancreatic, and prostate cancers (Chandra et al., 2020).

On the other hand, medical implants provide a novel platform from which the drug can be released over time. Medical implants show at least two obvious advantages: first, the release is site-specific (or locoregional), reducing the adverse side effects resulting from the systemic drug circulation and allowing a better quality of life for the patient since no other tissues and organs will be in contact with the drug. Second, they guarantee the patient's adherence to the treatment (Ahmed et al., 2019). In the specific case of solid tumors, whenever possible, resection surgery is the first treatment option, but combined therapies are key in cancer treatment, and surgery is frequently associated with adjuvant chemotherapy treatments (Wolinsky et al., 2012).

Three-dimensional bioprinters can be used for the development of organoids, tissue engineering, scaffolds for drug delivery, tissue printing, and novel hybrid devices (Stanisz et al., 2020). Particularly, a 3D bioprinter was designed and constructed in our laboratory to develop different matrix structures for drug delivery used as patches or implants for the treatment of different pathologies (Katz and Castro, 2019). The treatment of solid tumors with 3D-bioprinted matrices has the advantages of personalized medicine because it is possible to adjust the implant to the characteristics, size, and location of the tumor. In addition, 3D implants can be placed as

close as possible to the tumor surfaces adjusted to the tumor microenvironment or also in the cavity left by the resected tumor after a surgery that reduces the drug circulation in the body and consequently, the administered drug amount and its adverse effects.

Two biopolymers were selected for the development of a 3D-bioprinted matrix: chitosan (Chi) and hydroxypropyl methylcellulose (HPMC) because of their advantages. Chi is composed of β -linked N-acetyl-D-glucosamine and D-glucosamine randomly distributed. Chi possesses a residual positive charge making the biopolymer mucoadhesive and cell-adhesive, very relevant properties to enhance the attachment of the biopolymer gels to the cell surfaces, which increases tissue permeability and drug residence time. In addition, Chi displays antimicrobial and antioxidant activities. Chi is nontoxic, biocompatible, and biodegradable by mammalian enzymes, making the biopolymer an excellent candidate for biomedical applications in the form of gels, nanoparticles, fibers, and films (Shariatnia and Jalali, 2018).

Cellulose is the most abundant biopolymer found in nature and is composed of linear β -D-glucose units of different lengths, but its limited solubility reduces applications. HPMC is a derivate of methylcellulose containing propylene glycol ether. Also, HPMC is a nontoxic polymer, considered generally recognized as safe (GRAS) by the FDA, and approved as a food additive by the EU (Siepmann and Peppas, 2012).

In the present work, a platform of stimuli-responsive controlled release system (SRCRS) based on NLC containing lipase as a trigger agent and covered with Chi was integrated into a polymeric matrix composed of Chi and HPMC. The composite polymeric matrix was optimized for stability and to be extruded by a 3D bioprinter developed and constructed in our laboratory. The purpose of the 3D-printed matrix was to be used as an implant. Violacein was selected as a hydrophobic drug model entrapped in NLC for the potential treatment of solid tumors. The matrix system was characterized using biophysical techniques, TEM, FTIR, TGA, and dispersive light. The release of Viol from the matrices was studied by structured kinetic models. Cytotoxicity *in vitro* was studied in A549 and HCT116 cancer cell lines.

2 MATERIALS AND METHODS

2.1 Materials

Violacein [3-(1,2-dihydro-5-(5-hydroxy-1H-indol-3-yl)-2-oxo-3H-pyrrol-3-ylidene)-1,3-dihydro-2H-indole-2-one] was synthesized by *Chromobacterium violaceum* CCT 3496 and used following earlier techniques reported elsewhere. Briefly, an isolated colony of *C. violaceum* from an agar plate was inoculated in 250 ml Erlenmeyer containing 100 ml of a medium composed of 5 g l⁻¹ D-glucose, 5 g l⁻¹ peptone, and 2 g l⁻¹ yeast extract dissolved in MiliQ water. The vessel was incubated at 150 rpm on a rotatory at 30°C for about 36 h. Later the bacterial culture was centrifuged at 10,000 × g for 15 min at 5°C, and the supernatant was discarded. Violacein was purified from the cells using a Soxhlet extractor. The Viol purity was 98%

purity determined spectroscopically (data not shown) (Mendes et al., 2001; Berti, et al., 2019).

Lipase, from *R. miehei* lyophilized powder (Lip), 4-nitrophenyl palmitate (pNPP), Poloxamer 188 (Kolliphor® P188), chitosan (Chi, poly (D-glucosamine) deacetylated chitin, MW \approx 161 kDa), and (hydroxypropyl)methylcellulose (HPMC, MW \approx 26 kDa) were bought from Sigma-Aldrich (Buenos Aires, Argentina). Myristyl myristate a solid lipid at RT (MM, Crodamol® MM, MP = 36–40°C), and cetyl palmitate an oily triglyceride with saturated fatty acids (Crodamol® GTCC-LQ, MP = –4°C) were a generous donation of CRODA® (Argentina). All other chemicals, solvents, and reagents employed in the present work were of analytical grade.

2.2 Lipase Activity and Stability Measurements

Lipase activity was measured by the release of the colored compound 4-nitrophenol from 4-nitrophenyl palmitate (pNPP) as previously reported (Romero et al., 2012). Briefly, pNPP was pre-dissolved in 1:4 acetonitrile-isopropanol supplemented with 0.1% (w/v) Triton X-100. The pNPP solution was dispersed in a 10 mM buffer supplemented with 0.2% (w/v) Arabic gum to reach a final concentration of 500 μ M. One ml of pNPP was placed in a 48-well plate to run the enzymatic reaction. A lipase sample was added, and the solution's absorbance was measured at 405 nm at 37°C every minute for 20 min to determine 4-nitrophenol concentrations. Lipase activity was displayed as μ mol of 4-nitrophenol released per second.

The stability of lipase was determined at different pH values by incubating the enzyme in different buffers at room temperature, and then its activity was evaluated using buffer phosphate (pH = 7.4) and 37°C for 1 h.

2.3 Nanostructured Lipid Carrier and Nanostructured Lipid Carrier With Lipase Preparation

NLCs were synthesized by ultrasonication (Rodenak-Kladniew et al., 2017). Concisely, a lipid phase containing 400 mg of the solid lipid myristyl myristate (MM), 100 μ l of a commercial mixture of caprylic and capric acids (Crodamol® GTCC), and 20 μ mol Viol was melted in a 70°C bath. Later, 20 ml of 4.0% (w/v) poloxamer 188 adjusted to pH = 5.0 with acetic acid/sodium acetate buffer was mixed with the lipid phase and sonicated in an ultrasonic processor (130 W, Cole-Parmer, United States) at 70% amplitude for 15 min.

The Viol remaining in the NLC was assayed in a 500 μ l sample of the NLC-Viol formulations taken and filtered in 100 kDa cut-off filters (Amicon® Ultra- 0.5 ml, Merck Millipore, Ireland). The absorbance of the filtered solution was measured at 580 nm.

For formulations containing lipase (Lip), 5.0 ml of NLC dispersion was incubated with enough lipase to produce an activity of 2.0 μ mol of 4-nitrophenol/s at 5°C overnight with an agitation of 150 rpm with a magnetic stirrer.

2.4 Nanoparticle Measurements

The average hydrodynamic diameter (D_H), polydispersity index (Pdl), and Z-potential (ζ) were determined for NLC-Viol and NLC-Viol-Lip samples diluted 1/100 [2.0% (w/v) initial concentration and 0.02% (w/v) final concentration of MM] in ultrapure water using a Zetasizer Nano ZS series (Malvern Instruments, United Kingdom). The determinations were performed at a 633 nm (He-Ne) laser at a 173° measurement angle at 25°C by triplicate.

Transmission electron microscopy (TEM) images of the nanoparticles were acquired in a Jeol-1200 EX II-TEM microscope (Jeol, Columbia, MD, United States). NLC suspensions were diluted 1/100 [2% (w/v) and 0.02% (w/v) initial and the final concentration of MM, respectively] in ultrapure water or 10 mM phosphate buffer (pH = 7.4) followed by spreading a 10 μ l sample on a 400 mesh Cu grid. The excess sample was removed with filter paper. A phosphotungstic acid drop was added to the samples for contrast enhancement.

2.5 Biopolymer Ink Preparation and Extrusion

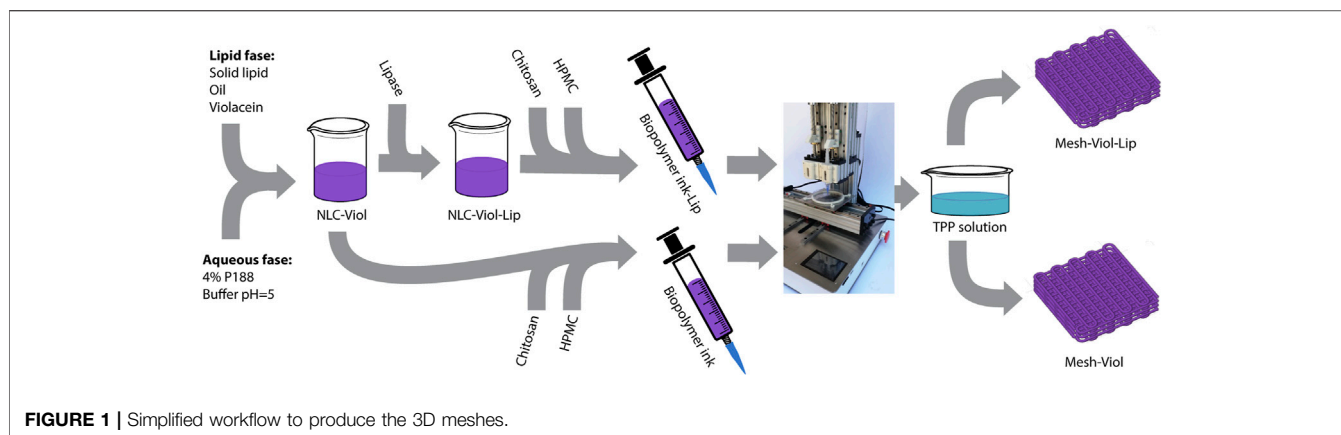
A weighted amount of 200 mg chitosan was hydrated in 1.0 ml of 10% acetic acid to form a homogenous paste. Later, 1.5 ml of NLC formulation with or without Lip was added and mixed, and then, 500 mg of HPMC was added, and the ink was thoroughly mixed and charged in a sterilized 5 ml syringe with Luer lock (TERUMO®, Philippines). The loaded syringe was later centrifuged at 7,000 \times g for 20 min to eliminate any air bubbles from the 3D ink. A conic plastic tip or nozzle (Fish Dispensing, China) with a 0.41 mm exit orifice was attached to the syringe before extrusion.

The 3D meshes were produced by extrusion in a 3D printer designed in our laboratory. Briefly, the 3D printer consists of an extruder that precisely pushes ink out of the syringe, a positioning system for the movements on three axes, and a controller. The extruder is composed of a socket for the syringe and a bipolar Nema 17 stepper motor with a high precision planetary system; the movement on the three axes is provided by two bipolar Nema 17 stepper motors coupled with 8 mm THSL screws and anti-backlash nuts. The open-source electronics used contain a 16 MHz ATmega 2560 processor that is commanded with Marlin firmware.

The 3D meshes produced by 3D bioprinting were submerged for 10 min in a 3.0% tripolyphosphate (TPP) solution, washed with ultrapure water, and saved in the fridge for biophysical characterization. Samples of TPP solution and ultrapure water used for washing were taken to determine Viol concentration. **Figure 1** shows a simplified workflow of NLC and 3D-mesh production.

2.6 Entrapment Efficiency of the Meshes

Entrapment efficiency was measured for both matrices prepared with NLC-Viol (Mesh-Viol) and meshes prepared with NLC-Viol-Lip (Mesh-Viol-Lip). This was conducted by two methods. The indirect method was carried out by



measuring Viol in the TPP solution and in the water used to wash the 3D meshes, and then subtracting the violacein amount in those solutions from the initial amount of drug, using the following equation: **Eq. 1**

$$EE_{indirect} (\%) = \frac{mViol_i - (cViol_{TPP_{sol}} \times V_{TPP_{sol}}) - (cViol_{ww} \times V_{ww})}{mViol_i} \times 100\% \quad (1)$$

where $mViol_i$ is the initial amount of Viol present in the preparation, $cViol_{TPP_{sol}}$ is the concentration of violacein in the TPP solution, $cViol_{ww}$ is the concentration of Viol in the ultrapure water after washing, and $V_{TPP_{sol}}$ and V_{ww} are the volumes of those solutions.

On the other hand, the direct method consisted in adding 3.0 ml of ethanol to a weighted amount of Mesh-Viol or Mesh-Viol-Lip followed by sonication in an ultrasonic cleaning bath for 30 min. The procedure was performed twice with ethanol replacement. The efficiency was then calculated by the following equation: **Eq. 2**

$$EE_{direct} (\%) = \frac{cViol_1 \times V_1 + cViol_2 \times V_2}{mViol_i} \times 100\% \quad (2)$$

where $mViol_i$ is the initial amount of Viol added to the preparation, $cViol_1$ and $cViol_2$ are the concentration of Viol in the first and second ethanol extraction, and V_1 and V_2 are the volumes of those solutions.

2.7 Violacein Release From the 3D-Printed Meshes

Four meshes were weighed and placed in 30 ml of 10 mM phosphate buffer at pH = 7.4 and 37°C, in duplicate. Every hour a 1.0 ml sample of the media was taken and replaced with an equal volume of fresh buffer. The samples were later filtered in 100 kDa cut-off filters (Amicon® Ultra- 0.5 ml, Merck Millipore, Ireland). Filtered solution absorbance was determined at 580 nm to evaluate Viol's release. The results were expressed as a fraction of a total load of Viol released versus time. The Viol release profiles were analyzed by structured kinetic release models (**Supplementary Table S1**).

2.8 Physicochemical Characterization of the 3D Meshes

2.8.1 Fourier Transform Infrared Spectroscopy

FTIR spectra were performed in freeze-dried in a Nicolet 6700 model (Thermo Scientific CT, United States) spectrometer coupled with an attenuated total reflectance (ATR) accessory. Scans were performed 32 times for each sample in the range from 600 to 4,000 cm^{-1} with a 4 cm^{-1} resolution.

2.8.2 X-Ray Diffraction

Diffraction patterns of the freeze-dried samples were obtained in an Analytical Expert instrument using Cu-K radiation ($\theta = 1.54 \text{ \AA}$) from $2\theta = 10^\circ$ to 70° in continuous mode with 0.07° step size.

2.8.3 Thermal Analysis

Thermogravimetric analysis (TGA) was performed in a Shimadzu TGA-50 instrument. All assays were carried out in the range of 20°C–900°C at a heating rate of 10°C/min under an N_2 atmosphere.

Differential scanning calorimetry (DSC) was carried out on a Perkin Elmer Inc., Model Pyris 1 (Waltham, MA, United States) instrument under an N_2 atmosphere. The heating rate of 10°C/min was used in the range of 0–250°C. All samples were previously frozen-dried.

2.9 Scanning Electron Microscope Image Acquisition

SEM analysis of 3D-printed meshes was run with freeze-dried samples that were then covered with a gold layer thickness of 15–20 nm using a Balzers SCD 030 metallizer. Images were obtained in a Philips SEM 505 scanning electron microscope and processed in an image digitizer program (Soft Imaging System ADDA II, SIS). Later, the images were analyzed with ImageJ® software (NIH, United States), and the surface roughness was estimated by the standard deviation of grey values in the image histogram (Wang et al., 2005).

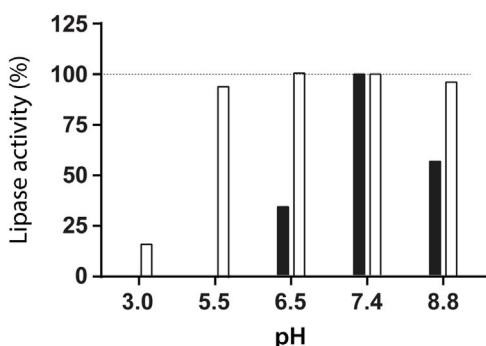


FIGURE 2 | Lipase activity measured at pH = 7.4 and 37°C after incubation for 6 h at room temperature at the indicated pH (white, □) and lipase activity assayed at the indicated pH and 37°C (black, ■).

2.10 Cytotoxic Studies

Human colorectal carcinoma HCT-116 and lung adenocarcinoma epithelial A549 cells were cultured in Minimal Essential Medium (MEM, HyClone, CA, United States) supplemented with 10% fetal bovine serum (Interneccios S.A., Argentina) and 1.0% penicillin/streptomycin (Gibco Invitrogen Corporation, United States) in 5.0% CO₂ at 37°C. The viability of the cells was assayed using MTT [3-(4,5-dimethylthiazol-2-yl)-2,5-diphenyltetrazolium bromide] assay (Mosmann, 1983). HCT-116 and A549 cells (4.0×10^3 cells/ml) were seeded in 96-well plates and incubated under standard conditions for 24 h. Then, the cells were exposed to 0.5, 2, or 4.0 μ M of free Viol (prepared in DMSO lower than 0.05% (v/v) final concentration), or equivalent amounts (μ M of Viol or mg/ml of MM) of NLC and NLC-Lip with and without Viol for 24 h. The medium was discarded and incubated in the presence of 100 μ l of 500 μ g/ml MTT solution prepared in MEM with 3 h incubation. Formazan was dissolved in 100 μ l DMSO. The microplates were stirred for 5 min and readings of absorbance at $\lambda = 560$ nm were determined in a microplate reader (Beckman Coulter DTX 880 Multimode Detector, United States). A reduction in cell viability by more than 30% was considered a cytotoxic effect (Doktorovova et al., 2014). A conditioned medium was used to assay Mesh-Viol and Mesh-Viol-Lip. That is, meshes with and without viol, and with and without Lip were incubated in MEM supplemented as before for 48 h. Then, the media was used to incubate A549 and HCT116 cells for 24 h. Later, MTT colorimetric assays were performed as previously described.

3 RESULTS AND DISCUSSION

3.1 Lipase Activity and Nanostructured Lipid Carrier Preparation

The lipase activity was evaluated at different pH values at room temperature. The high activity of lipase from *R. miehei* was detected at pH = 7.4, but no enzyme activity was observed at pH = 5.5 (Figure 2). However, 95% of enzyme activity was

recovered at pH = 7.4 after lipase incubation at pH = 5.5 for 6 h, indicating a reversible enzyme inhibition. Based on this result, the synthesis of NLC containing lipase was performed at pH = 5.5.

Encapsulation efficiency of Viol in the NLC-Viol without and with lipase was near 100% since Viol concentration in the filtered solution was below the limit of detection (Supplementary Material Table S3).

3.2 Nanostructured Lipid Carrier Size and Z-Pot

The average hydrodynamic diameter (D_H), PdI, and Z-Pot (ζ) are shown in Supplementary Table S2. The addition of lipase does not significantly alter the mean particle size (154.3 nm for NLC-Viol and 151.5 nm for NLC-Viol-Lip; $p > 0.05$), but it does significantly alter the PdI (0.241 for NLC-Viol and 0.319 for NLC-Viol-Lip; $p < 0.05$). The ζ value is close to zero, as might be expected from the fact that the surfactant used to stabilize NLC, P188, is neutral in charge. The ζ change between formulations with and without lipase is significant ($p < 0.05$) but still very small. Results are summarized in Supplementary Table S2.

TEM images for NLC-Viol-Lip before and after incubation in a 10 mM phosphate buffer (pH = 7.4) for 6 h are shown in Figure 3. Before incubation NLC-Viol-Lip showed an average diameter of 93.6 nm based on 36 measurements from micrographs (Figure 3A). After incubation aggregates were observed (Figure 3B, arrows). These aggregates can be explained since lipase activity probably weakens the structure of the nanoparticle by catalyzing lipid hydrolysis, and therefore remnant NLC produces aggregate structures.

3.3 Biopolymer Ink Preparation and Extrusion

Different proportions of Chi and HPMC were tested to create an appropriate polymer mixture to be extruded by the 3D bioprinter. The final polymer concentrations for the bioink were 6.6% (w/w) Chi and 16.6% (w/w) HPMC, equivalent to HPMC/Chi: 2.5 ratio. Lower HPMC content resulted in an unstable printed bioink, while higher HPMC concentrations drastically reduced the cross-linking with TPP.

Maximum printing speed that did not produced errors in ink continuity found was 400 mm/min. For the nozzle diameter used (0.41 mm) a layer height of 0.33 mm was found optimal, since layer heights less than that, caused the nozzle to damage the lower layer and larger layer sizes prevented the correct adhesion of the developing layer on the lower layer. A video illustrating the printing process can be found in Supplementary Material.

The two methods used to estimate EE (%) gave differences lower than 10% among them (Supplementary Table S3). However, the average EE (%) of Mesh-Viol and Mesh-Viol-Lip was 93.8% and 92.3%, respectively. These values are very close considering the several experimental steps for the production of the drug delivery devices (i.e., sonication, mixing, cross-linking, and washing).

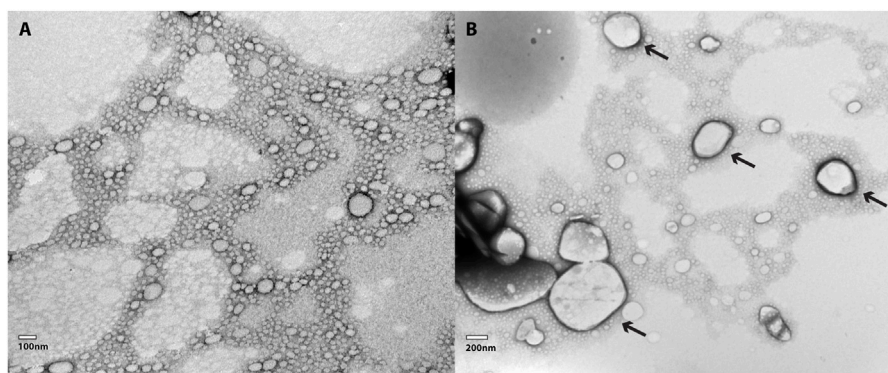


FIGURE 3 | (A) TEM micrography of a 1:100 dilution of NLC-Viol-Lip, and **(B)** TEM micrography of a 1:100 dilution of NLC-Viol-Lip after it was incubated at a pH = 7.4 for 6 h. Arrows in **(B)** point aggregates.

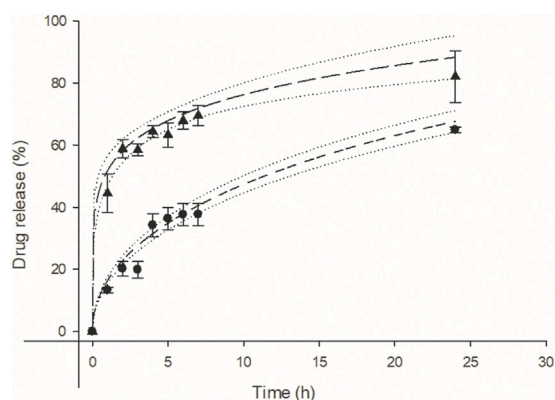


FIGURE 4 | Violacein kinetic release from mesh (●), and mesh containing lipase (▲) at pH = 7.4 respectively. Baker and Lonsdale model fit for mesh (—, $R^2 = 0.95$) and Korsmeyer-Peppas model fit (---, $R^2 = 0.95$) for mesh containing lipase. Upper and lower 95% confidence interval for each fit (.....).

3.4 Violacein Release From the Meshes

The difference between the two Viol release profiles of matrices with or without lipase is obvious (**Figure 4**). Lipase strongly stimulates the release of Viol from the polymeric matrix, reaching 60% release at pH 7.4 after 2 h incubation. While only 20% of Viol was released from the matrix without lipase under the same experimental conditions. The kinetic release of Viol from Mesh-Viol and Mesh-Viol-Lip was analyzed with typical structured kinetic models (**Supplementary Table S1**). The best correlations of Viol release were found with Higuchi ($R^2 = 0.94$), Korsmeyer-Peppas ($R^2 = 0.95$) and Baker-Lonsdale ($R^2 = 0.95$) tested models for the matrix without lipase. While the best correlation of Viol release from the matrix containing lipase was observed in the Korsmeyer-Peppas model ($R^2 = 0.95$) (**Supplementary Table S5**). The kinetic of Viol release from the matrices and Baker-Lonsdale fit for Mesh-viol and Korsmeyer-Peppas for Mesh-Viol-Lip are displayed in **Figure 4**. The “n” parameter in the Korsmeyer-

Peppas model can be used to predict the potential mechanism involved in the drug release (**Supplementary Table S1**). In this case, Mesh-Viol fitted an $n = 0.17$ and Mesh-Viol-Lip an $n = 0.46$; both cases fall below $n < 0.5$ condition. Considering these experimental values, the Korsmeyer-Peppas model predicts a Viol release based mostly on Fick’s law, i.e., only based on the diffusional mechanism (Ritger and Peppas, 1987).

Additionally, Viol releases from the Mesh-Viol and Mesh-Viol-Lip matrices were performed at pH = 5.0. No significant differences were found between the Viol release in both matrices (**Supplementary Figure S1**). These results are indicative of the relevant lipase role in Viol release. However, the Viol release was faster than in pH = 7.4 buffer, with around 65% of the drug released in the first 2 h, which can be expected since Chi solubility is greatly enhanced at lower pH (Kou et al., 2017).

3.5 Mesh Physicochemical Characterization

3.5.1 Scanning Electron Microscope Micrograph Results

The SEM images display the matrix structure after exposing the 3D prints to 10 mM phosphate buffer (pH = 7.4) for 24 h (**Figure 5**). The SEM images showed a relaxed matrix structure with mesh gaps expanded, determined by the ImageJ software (**Supplementary Table S4**). Meshes before drug release did not exhibit any significant difference ($p > 0.05$) and are presented as one single group. However, changes in the structure of the meshes with and without Lip after Viol release were significant ($p < 0.05$). The Mesh-Viol-Lip displayed a big variation in the matrix structure that can be attributed to the presence of lipase in the matrix. This loosening in polymeric structure can also be observed in the microstructure at higher magnifications ($\times 1,000$) (**Figure 5**). Mesh-Viol-Lip shows a larger number of cavities between polymer areas. Also, the roughness of Mesh-Viol-Lip estimated by the grey histogram confirmed this result (**Supplementary Table S4**). A comparative analysis of the standard deviations of the matrices showed that Mesh-Viol and Mesh-Viol-Lip before drug release possess smoother surfaces (SD = 35.5) than Mesh-Viol or Mesh-Viol-Lip after the release (SD = 40.1 and 48.3 respectively).

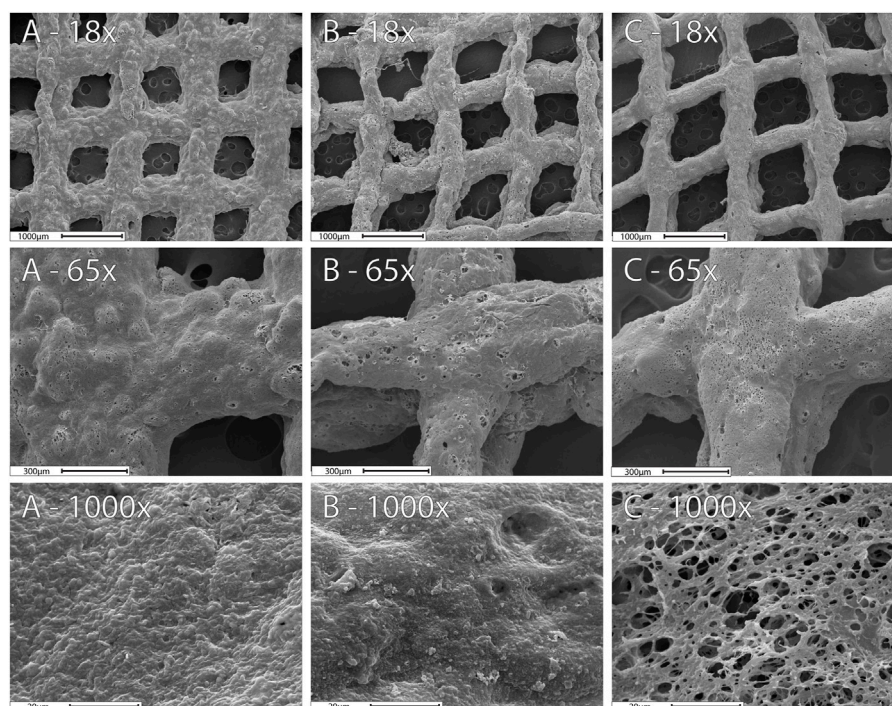


FIGURE 5 | SEM images for the 3D-Mesh previous release (A), Mesh-Viol and Mesh-Viol-Lip released in phosphate buffer (pH = 7.4) after 24 h incubation (B) and (C) respectively.

3.5.2 X-Ray Diffraction Analysis

Figure 6 shows XRD patterns for both 3D meshes after 24 h incubation in release buffer (pH = 7.4) as well as their pure components. P188 showed a high degree of crystallinity when pure, with two intense and characteristic peaks at 19.1° and 23.3° , and a dimmer broader peak between 25.5° and 27.0° (He et al., 2011). Chi showed a small peak at 19.7° and a dim broad peak at 9° , while HPMC exhibited a wide peak between 15° and 25° . However, none of these peaks appear in the mixtures, indicating a loss of the crystalline structure of the polymers in the composite. Mesh-Viol and Mesh-Viol-Lip show a small compound peak at 21.6° and 23.7° (**Figure 6** inset); these peaks also appear and are characteristic of the MM diffraction pattern, although in much higher intensity, which indicates that a few amounts of MM remain in crystals after NLC preparation.

3.5.3 Fourier Transform Infrared Analysis

FTIR spectra for both 3D meshes as well as their major constituents incubated in phosphate buffer (pH = 7.4) for 24 h are displayed in **Figure 7**. P188 showed an intense peak at $2,877.32\text{ cm}^{-1}$ attributed to C-H aliphatic stretching, a smaller peak at $1,342.23\text{ cm}^{-1}$ attributed to in-plane O-H bending, and a sharp peak at $1,099.24\text{ cm}^{-1}$, and a smaller peak at 960.39 cm^{-1} corresponding to ether C-O symmetric and asymmetric stretching vibrations (Lal and Datta, 2014). HPMC spectrum shows a broad peak between $3,100$ and $3,600\text{ cm}^{-1}$ corresponding to O-H stretching vibrations, $2,894.67$, and $1,049.10\text{ cm}^{-1}$ in agreement with C-H and

C-O stretching respectively (Furqan et al., 2017). Chi also showed a broad O-H stretching vibration band between $3,100$ and $3,600\text{ cm}^{-1}$, but partially overlapped with broadband due to asymmetric/symmetric N-H bonds. The band at $2,871.53\text{ cm}^{-1}$ was assigned to C-H axial stretching, while the $1,641\text{ cm}^{-1}$ band was attributed to -C=O stretching in the acetamide groups, and the $1,556\text{ cm}^{-1}$ to the trans-secondary amides (Acosta-Ferreira et al., 2020; Peng et al., 2020); additionally, the $1,019\text{ cm}^{-1}$ band was attributed to C-N primary amine stretch (Peng et al., 2020). MM showed three sharp peaks at $2,848.39$, $2,915.88$, and $2,954.45\text{ cm}^{-1}$, attributed to asymmetric, symmetric stretching of C-H bonds on -CH_2 and C-H bond asymmetric stretching on -CH_3 groups respectively. Another relevant sharp peak was found at $1,731.8\text{ cm}^{-1}$, corresponding to ester carbonyl stretching vibrations (Castro et al., 2021). Finally, both 3D meshes showed a complex broad peak between $1,150$ and 900 cm^{-1} , from overlapping P188, HPMC, and Chi peaks in that band of the spectrum, and broadband between $3,000$ and $3,500\text{ cm}^{-1}$ from O-H and N-H vibrations in HPMC and Chi. However, the 3D meshes containing Lip (Mesh-Viol-Lip) exhibited weaker peaks at $2,848.39$ and $2,915.88\text{ cm}^{-1}$, the bands presented by MM. Furthermore, Mesh-Viol-Lip did not show the characteristic peak at $1,731.8\text{ cm}^{-1}$ attributed to -C=O stretching of the ester group, while it appeared in the 3D mesh without Lip (Mesh-Viol). All these points could reflect a loss in MM content in Mesh-Viol-Lip due to lipase activity in the 3D mesh.

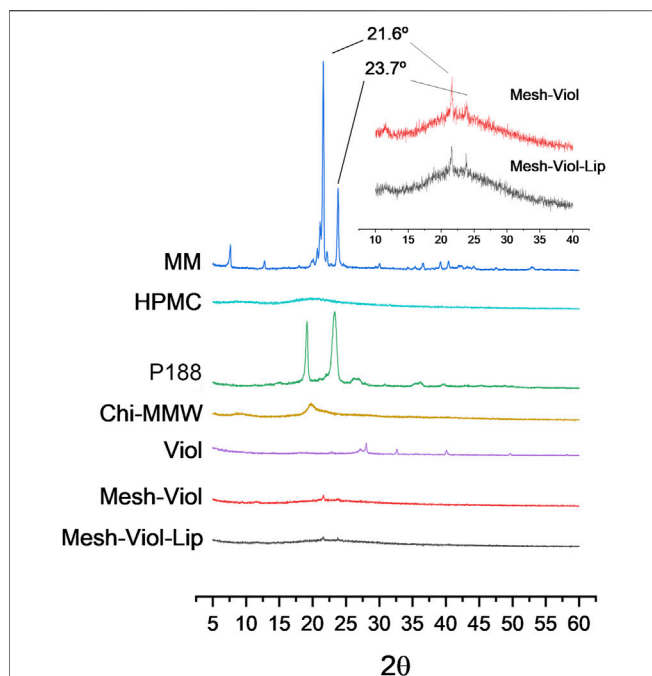


FIGURE 6 | Diffractograms for Mesh-Viol-Lip, Mesh-Viol, MM (myristyl myristate), Chi-MMW (medium molecular weight chitosan), HPMC (hydroxypropyl methylcellulose), and P188 (Poloxamer P188). Mesh-Viol and Mesh-Viol-Lip were incubated for Viol release in phosphate buffer (pH = 7.4) for 24 h before performing the analysis. Inset is a detail for Mesh-Viol-Lip and Mesh-Viol between 10° and 40°.

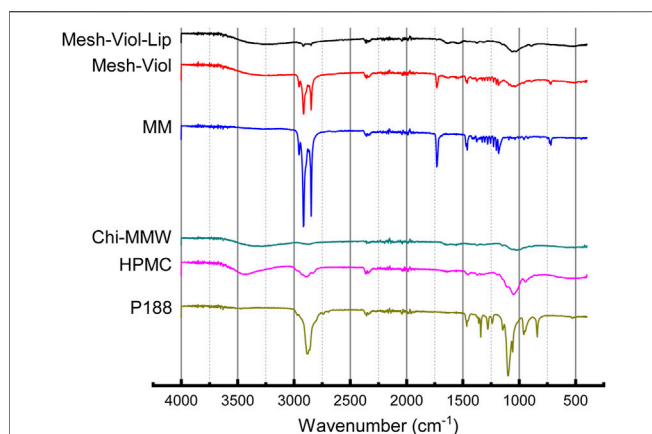


FIGURE 7 | FTIR spectra for Mesh-Viol-Lip, Mesh-Viol, MM (myristyl myristate), Chi-MMW (medium molecular weight chitosan), HPMC (hydroxypropyl methylcellulose), and P188 (Poloxamer P188). Mesh-Viol and Mesh-Viol-Lip were incubated in release buffer (pH = 7.4) for 24 h before performing the analysis.

3.5.4 Thermogravimetric Analysis

The thermal stability of the 3D meshes after release was studied. **Figure 8** shows the percentage mass loss versus temperature.

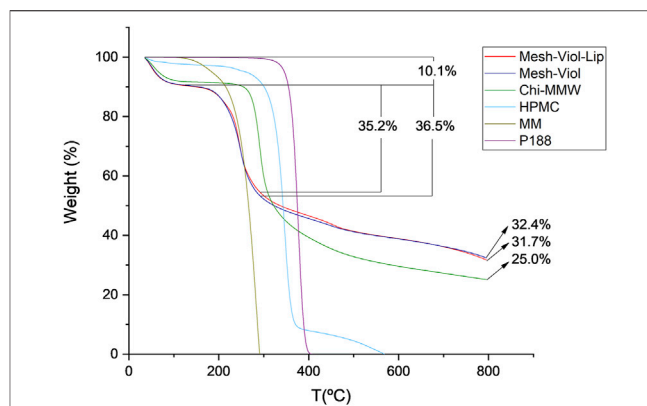


FIGURE 8 | Thermogravimetric analysis for Mesh-Viol-Lip, Mesh-Viol, MM (myristyl myristate), Chi-MMW (medium molecular weight chitosan), HPMC (hydroxypropyl methylcellulose), and P188 (Poloxamer P188). Mesh-Viol and Mesh-Viol-Lip were incubated in phosphate buffer (pH = 7.4) for 24 h before performing the analysis.

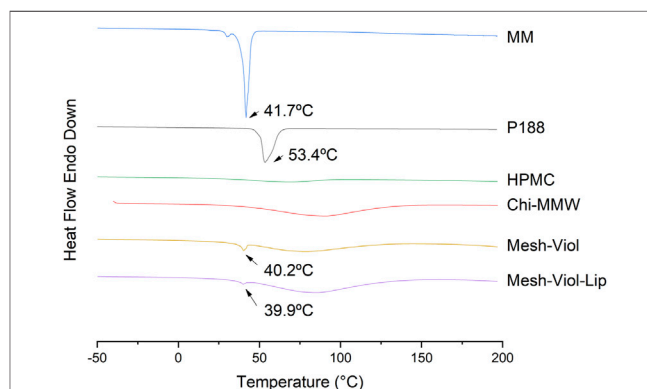


FIGURE 9 | DSC thermograms for Mesh-Viol-Lip, Mesh-Viol, MM (myristyl myristate), Chi-MMW (medium molecular weight chitosan), HPMC (hydroxypropyl methylcellulose), and P188 (Poloxamer P188). Mesh-Viol and Mesh-Viol-Lip were incubated in phosphate buffer (pH = 7.4) for 24 h before performing the analysis. Y-axis represents heat flow (exothermic is up).

Both 3D meshes lose 10% of their weight between 0°C and 125°C, which is due to remnant water in the samples; similarly, Chi and HPMC lose 9% and 3% of their weight respectively.

The maximal HPMC weight loss was at 346°C, and before 400°C more than 90% of its mass was lost. This process is normally attributed to the decomposition of cellulose esters, and volatilization of these degraded residues (Hasanin et al., 2022). On the other hand, Chi-MMW, weight loss after 250°C is due to further dehydration, deacetylation, and depolymerization (de Britto and Campana-Filho, 2007). MM maximum weight loss was found at 283°C; this step is normally attributed to volatilization rather than thermal degradation (Xu et al., 2022).

Between 125°C and 290°C Mesh-Viol and Mesh-Viol-Lip lose 36.5% and 35.2% of their mass respectively, which coincides with the acute mass loss of MM. Moreover, after finishing the essay,

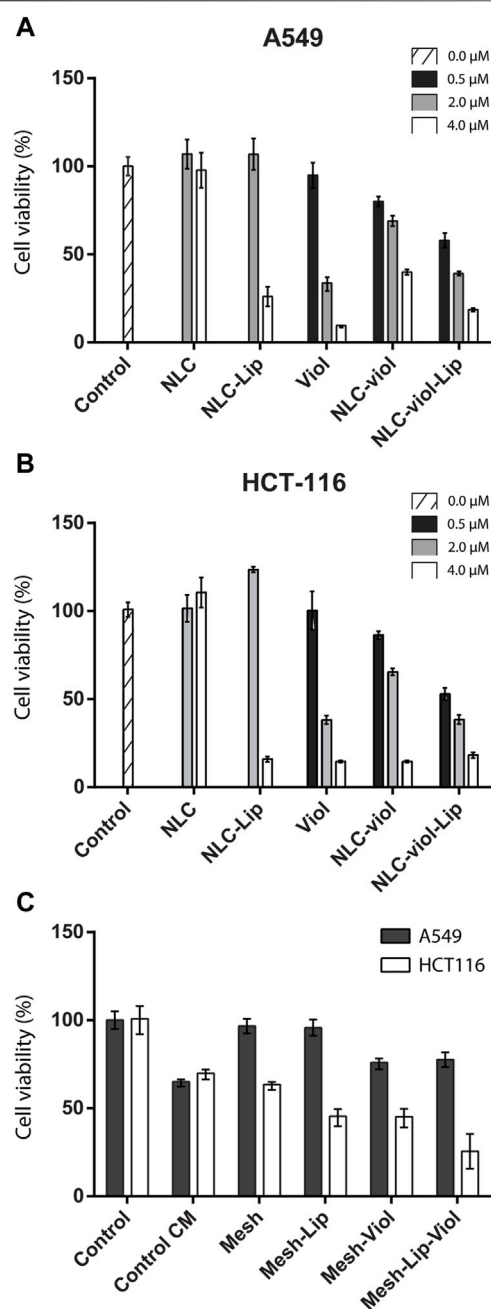


FIGURE 10 | Cell viability For NLC formulations and free Viol in A549 (A) and HCT-116 (B) cell lines, respectively. Cell viability on conditioned medium (C).

the Mesh-Viol has a remnant of 32.4% of its weight, 31.7% of Mesh-Viol-Lip, and 25.0% of Chi. Since none of the other constituents remain at this temperature, the meshes exhibit greater thermal stability than pure materials, suggesting a chemical interaction between the biopolymers. In the **Supplementary Material**, a figure showing weight derivative (%) versus temperature is provided (**Supplementary Figure S2**).

3.5.5 Differential Scanning Calorimetry Analysis

The heat flow from the 3D mesh samples and their main constituents versus temperature, “up” curves in the Y-axis representing the exothermic process, and “down” curves showing the endothermic process, are displayed in **Figure 9**. MM shows a sharp intense peak at 41.7°C, corresponding to its melting temperature (T_m), with an area under peak, that is, a melting enthalpy (ΔH_m) of -205 J/g, both results are consistent with the bibliography (Aydn and Okutan, 2011), a small shoulder can be attributed to a pleiomorphism transition. Similarly, T_m for P188 is 53.4°C (He et al., 2011), and a ΔH_m of -145 J/g. The broad endothermic peak between 50°C and 100°C in HPMC and Chi-MMW can be attributed to a loss of water (El Maghraby and Alomrani, 2009). DSC analysis for mixtures, Mesh-Viol and Mesh-Viol-Lip showed a sharp and small peak near MM T_m , at 40.2°C and 39.9°C respectively. This T_m depression can be explained by the Gibbs-Thomson equation (**Supplementary Equation S1**) and (**Supplementary Material**) (Han et al., 2008). Based on the Gibbs-Thomson equation, as the radius of the nanoparticle decreases, so does its melting point. Also, a bigger and wider peak appears before 100°C. Mesh-Viol-Lip small peak was smaller, while the big broad peak was bigger, which may indicate a change in Mesh lipid and water content after drug release.

3.6 Cytotoxicity Assays

Figure 10 A and B show cytotoxicity for different NLC formulations and free Viol. At 0.5 μM (filled in black) NLC-Viol showed a greater effect than free Viol. On the contrary, the cytotoxic effect was greater in 2.0 μM free Viol (filled in grey). This was observed for both cell lines tested. This phenomenon was already reported in previous works where Viol was nanovehiculized (Berti, et al., 2019; Berti et al., 2022).

Additionally, in both cell lines tested NLC-Viol-Lip showed more cytotoxicity at 2.0 μM (filled in grey) than NLC-Viol ($p < 0.05$), even though at this concentration lipase and empty NLC showed no toxic effects. This result revealed that a more efficient biocide effect between NLC, Lip, and Viol could be attributed to the increase of free biocide due to nanoparticle degradation by lipase activity. However, other effects could contribute to this result. Recently, Viol was described as a membrane disruptor in an attempt to explain its various biological effects (Gupta et al., 2021). Considering this hypothesis, the activity of lipase and the activity of violacein could produce a positive effect at their site of action. Additionally, the incorporation of Lip into the formulation can impact positively on the treatment of solid tumors since it was found that lipase activity is suppressed or absent in some breast, colorectal, and lung tumors; therefore, lipase activity may have a tumor-suppressive effect (Sun et al., 2013).

Figure 10C shows the cytotoxicity assay for A549 and HCT116 cell lines when they were incubated in a medium that was in contact with 3D-printed meshes. CM-control represents a medium without treatment, that is, without 3D-printed mesh, which was incubated for the same period as the treated media. This experimental procedure was considered the “aging” of the medium alone, which presents a reduction in viability in the HCT116 cell line ($p < 0.005$). However, the

biopolymeric matrix alone without violacein or lipase (Mesh) did not further reduce viability when compared with CM-control ($p > 0.5$). Besides, both the lipase effect (Mesh-Lip) and violacein effect (Mesh-Viol) significantly decreased the cell viability ($p < 0.005$). Additionally, the major cytotoxic effect on the HCT116 cell line was observed with Mesh-Lip-Viol, being greater than that of Mesh-Lip or Mesh-Viol ($p < 0.05$ in both cases).

4 CONCLUSION

Recent strategies for the treatment of several diseases could involve the use of enzymes, with more than 100 potential candidates. However, marketed enzymes applied in biomedicine are still scarce (Bosio et al., 2016). The emergence of nanotechnology opened a new landscape for the development of efficient devices used in the treatment and diagnosis of diverse pathologies, particularly cancer. In this regard, diverse approaches of nanoparticles containing enzymes to target tumors were recently reviewed (Li et al., 2020; Kapalatiya et al., 2022). Smart nanoparticles containing enzymes were developed using different strategies such as decorating nanoparticle surface with specific enzymes acting over the tumor surface or a ligand of nanoparticle surface for releasing covalently linked molecules, nanoparticles loaded with prodrugs enzyme-activable, and nanoparticles with enzyme-degradable core for drug controlled release. In all cases, the effect of the environmental conditions to trigger the drug is crucial, particularly with enzymes located on the surface of the nanoparticle which could be exposed to extreme conditions such as high shear rate and acid pHs produced by the high metabolism of tumor cells (i.e., lactic, and acetic acids) that can inactivate and/or denature the biocatalyst. In the present work, NLC contains a hydrophobic potential drug, Viol, and a latent lipase that can be activated under physiological conditions by hydrolyzing the lipid structure of the nanoparticle with consequent release of the biodye with controlled kinetic. Also, active lipase could act over cancer cells' membrane facilitating the contact of Viol within the cells and the entrance into the cytoplasm. Particularly, the amount of enzyme can be optimized to control the lipid hydrolysis and consequently change the amount of Viol release. Additionally, the NLC coated with Chi could guarantee the attachment of the NLC to the surface of the tumor cells (Ahmad et al., 2017).

The progress of 3D scaffolds made of biopolymer is a new trend for personalized medicine not only for the study of the development of cancer tumors but also to find novel strategies for cancer therapy, particularly after tumor resection and/or intensive treatments when surgeries are not advised (Augustine et al., 2021). In previous work, bacterial cellulose scaffolds containing SLN loaded with doxorubicin were successfully applied *in-vivo* to treat an orthotopic breast cancer mouse model. The results indicate a substantial decrease in tumor growth and metastasis, as well as drug amount by the treatment with a doxorubicin-NLC-loaded scaffold (Cacicedo et al., 2018).

The novel trends in biomedicine are involving the development of more complex structures for tissue engineering and repair, drug delivery, and organ fabrications. Among them, the 3D bioprinter allowed for the printing of hydrogels for the construction of 3D matrices (i.e., scaffolds) with defined and unique properties. Considering a personalized tumor therapy, the use of a 3D-bioprinter allows tailoring scaffolds with defined chemical composition and dimensions (i.e., size and thickness). In addition, the inclusion of the NLC into the 3D Chi-HPMC printed matrix will help to reduce the dispersion of the nanoparticles in the body. Also, the contact of the 3D scaffold containing the NLC-Viol with the solid tumor can be associated with a decrease in the administered drug amount which reduces the undesirable side effects of cancer drugs and increases patient comfort.

Finally, a novel Stimuli-Responsive Controlled Release System platform based on a 3D bioprinter and NLC containing a hydrophobic molecule actively released by an enzyme was developed. The main advantages of the platform are the versatility of the system based on: 1) the development of the composition of an appropriate nanostructured lipid carrier according to the physicochemical properties of the drug; 2) the incorporation of lipase in the NLC-drug that can control the kinetics of the drug release and the amount of the drug; 3) the inclusion of the NLC-drug-enzyme in a biodegradable 3D matrix that can be tailored based on the tumor characteristics; 4) the 3D matrix containing the drug could be placed on the tumor site avoiding drug dispersion in the body and/or inactivation and/or undesirable side effects; 5) the 3D matrix containing chitosan, a mucoadhesive and cell-adhesive polymer, can increase the contact with the tumor cells; 6) the presence of lipase and chitosan in the formulation could produce a positive effect, facilitating the entrance of the drug into the cells since both components could act over cell membranes just hydrolyzing lipids and interfering with the transport cell mechanisms.

DATA AVAILABILITY STATEMENT

The original contributions presented in the study are included in the article/**Supplementary Material**, further inquiries can be directed to the corresponding author.

AUTHOR CONTRIBUTIONS

IR, main experimental work, design, and data analyses and curation, writing, and drawing. BR-K, cellular assay experiments, and data analysis, writing. SK, 3D bioprinter experiments. EA, characterization of nanoparticles and discussion. VA, experimental determination of biophysical properties of materials. ND, critical review, and text edition and discussion. GC, supervision, experimental design, writing, review and editing, funding acquisition.

FUNDING

Financial support by UNLP (X815), CONICET (PIP 0034), and ANPCyT (PICT 2016-4597; PICT 2017-0359) is gratefully acknowledged.

ACKNOWLEDGMENTS

Financial support by UNLP (X815), CONICET (PIP 0034), and ANPCyT (PICT 2016-4597; PICT 2017-0359) is gratefully

acknowledged. We would also like to thank Lucia S. Carnaghi for her help along with the development of the experimental work.

SUPPLEMENTARY MATERIAL

The Supplementary Material for this article can be found online at: <https://www.frontiersin.org/articles/10.3389/fchem.2022.914126/full#supplementary-material>

REFERENCES

- Acosta-Ferreira, S., Castillo, O. S., Madera-Santana, J. T., Mendoza-García, D. A., Núñez-Colín, C. A., Grijalva-Verdugo, C., et al. (2020). Production and Physicochemical Characterization of Chitosan for the Harvesting of Wild Microalgae Consortia. *Biotechnol. Rep.* 28, e00554. doi:10.1016/j.btre.2020.e00554
- Ahmad, M., Manzoor, K., Singh, S., and Ikram, S. (2017). Chitosan Centered Bionanocomposites for Medical Specialty and Curative Applications: A Review. *Int. J. Pharm.* 529 (1-2), 200–217. doi:10.1016/j.jpharm.2017.06.079
- Ahmed, K. K., Tamer, M. A., Ghareeb, M. M., and Salem, A. K. (2019). Recent Advances in Polymeric Implants. *AAPS PharmSciTech* 20, 1–10. doi:10.1208/s12249-019-1510-0
- Augustine, R., Kalva, S. N., Ahmad, R., Zahid, A. A., Hasan, S., Nayeem, A., et al. (2021). 3D Bioprinted Cancer Models: Revolutionizing Personalized Cancer Therapy. *Transl. Oncol.* 14 (4), 101015. doi:10.1016/j.tranon.2021.101015
- Aydın, A. A., and Okutan, H. (2011). High-chain Fatty Acid Esters of Myristyl Alcohol with Even Carbon Number: Novel Organic Phase Change Materials for Thermal Energy Storage-1. *Sol. Energy Mater. Sol. Cells* 95, 2752–2762. doi:10.1016/j.solmat.2011.04.015
- Berti, I. R., Rodenak-Kladniew, B., Perez, A. A., Santiago, L., Duran, N., and Castro, G. R. (2019). Development of Biocarrier for Violaecine Controlled Release in the Treatment of Cancer. *React. Funct. Polym.* 136, 122–130. doi:10.1016/j.reactfunctpolym.2019.01.001
- Berti, I. R., Singh, T., Boztepe, T., Leon, I. E., Nadda, A. K., and Castro, G. R. (2022). "CHAPTER 17. Design of Nanostructured Lipid Carriers and Hybrid Lipid Nanoparticles," in *Concepts and Design of Materials Nanoarchitectonics RSC Nanoscience and Nanotechnology*. Editors O. Azzaroni and K. Ariga (London, UK: Royal Society of Chemistry), 381–416. ISBN-13: 978-1788018029. doi:10.1039/9781788019613-00381
- Bosio, V. E., Islan, G. A., Martínez, Y. N., Durán, N., and Castro, G. R. (2016). Nanodevices for the Immobilization of Therapeutic Enzymes. *Crit. Rev. Biotechnol.* 36 (3), 1–18. doi:10.3109/07388551.2014.990414
- Cacicedo, M. L., Islan, G. A., León, I. E., Álvarez, V. A., Chourpa, I., Allard-Vannier, E., et al. (2018). Bacterial Cellulose Hydrogel Loaded with Lipid Nanoparticles for Localized Cancer Treatment. *Colloids Surfaces B Biointerfaces* 170, 596–608. doi:10.1016/j.colsurfb.2018.06.056
- Castro, S. R., Ribeiro, L. N. M., Breitzkreitz, M. C., Guilherme, V. A., Rodrigues da Silva, G. H., Mitsutake, H., et al. (2021). A Pre-formulation Study of Tetracaine Loaded in Optimized Nanostructured Lipid Carriers. *Sci. Rep.* 11, 1–15. doi:10.1038/s41598-021-99743-6
- Chandra, P., EnespaSingh, R., Singh, R., and Arora, P. K. (2020). Microbial Lipases and Their Industrial Applications: A Comprehensive Review. *Microb. Cell. Fact.* 19, 1–42. doi:10.1186/s12934-020-01428-8
- Chandrawati, R. (2016). Enzyme-responsive Polymer Hydrogels for Therapeutic Delivery. *Exp. Biol. Med. (Maywood)* 241, 972–979. doi:10.1177/1535370216647186
- Cheng, T., Zhao, Y., Li, X., Lin, F., Xu, Y., Zhang, X., et al. (2007). Computation of Octanol–Water Partition Coefficients by Guiding an Additive Model with Knowledge. *J. Chem. Inf. Model.* 47, 2140–2148. doi:10.1021/ci700257y
- Creixell, M., and Peppas, N. A. (2012). Co-delivery of siRNA and Therapeutic Agents Using Nanocarriers to Overcome Cancer Resistance. *Nano Today* 7, 367–379. doi:10.1016/j.nantod.2012.06.013
- de Britto, D., and Campana-Filho, S. P. (2007). Kinetics of the Thermal Degradation of Chitosan. *Thermochim. Acta* 465, 73–82. doi:10.1016/j.tca.2007.09.008
- Doktorovova, S., Souto, E. B., and Silva, A. M. (2014). Nanotoxicology Applied to Solid Lipid Nanoparticles and Nanostructured Lipid Carriers - A Systematic Review of *In Vitro* Data. *Eur. J. Pharm. Biopharm.* 87, 1–18. doi:10.1016/j.ejpb.2014.02.005
- Durán, N., Justo, G. Z., Durán, M., Brocchi, M., Cordi, L., Tasic, L., et al. (2016). Advances in *Chromobacterium Violaecum* and Properties of Violaecine-Its Main Secondary Metabolite: A Review. *Biotechnol. Adv.* 34 (5), 1030–1045. doi:10.1016/j.biotechadv.2016.06.003
- Durán, N., Nakazato, G., Durán, M., Berti, I. R., Castro, G. R., Stanisic, D., et al. (2021). Multi-target Drug with Potential Applications: Violaecine in the Spotlight. *World J. Microbiol. Biotechnol.* 37, 1–20. doi:10.1007/s11274-021-03120-4
- El Maghraby, G. M., and Alomrani, A. H. (2009). Synergistic Enhancement of Itraconazole Dissolution by Ternary System Formation with Pluronic F68 and Hydroxypropylmethylcellulose. *Sci. Pharm.* 77, 401–417. doi:10.3797/scipharm.0901-08
- Ferlay, J., Ervik, M., Lam, F., Colombet, M., Mery, L., Piñeros, M., et al. (2020). Global Cancer Observatory: Cancer Today, Int. Agency Res. Cancer. Available at: <https://gco.iarc.fr/today> (Accessed November 14, 2021).
- Furqan, M., Iqbal, F., and Tulain, R. (2017). Microwave Radiation Induced Synthesis of Hydroxypropyl Methylcellulose-Graft-(polyvinyl Alcohol-Co-Acrylic Acid) Polymeric Network and its *In Vitro* Evaluation. *Acta Pol. Pharm. - Drug Res.* 74, 527–541.
- Gordillo-Galeano, A., and Mora-Huertas, C. E. (2018). Solid Lipid Nanoparticles and Nanostructured Lipid Carriers: A Review Emphasizing on Particle Structure and Drug Release. *Eur. J. Pharm. Biopharm.* 133, 285–308. doi:10.1016/j.ejpb.2018.10.017
- Gupta, R., Mitra, S., Chowdhury, S., Das, G., Priyadarshini, R., Mukhopadhyay, M. K., et al. (2021). Discerning Perturbed Assembly of Lipids in a Model Membrane in Presence of Violaecine. *Biochimica Biophysica Acta (BBA) - Biomembr.* 1863, 183647. doi:10.1016/j.bbamem.2021.183647
- Han, F., Li, S., Yin, R., Liu, H., and Xu, L. (2008). Effect of Surfactants on the Formation and Characterization of a New Type of Colloidal Drug Delivery System: Nanostructured Lipid Carriers. *Colloids Surfaces A Physicochem. Eng. Aspects* 315, 210–216. doi:10.1016/j.colsurfa.2007.08.005
- Hasanin, M. S., El-Sakhawy, M., Ahmed, H. Y., and Kamel, S. (2022). Hydroxypropyl Methylcellulose/graphene Oxide Composite as Drug Carrier System for 5-fluorouracil. *Biotechnol. J.* 17, 2100183. doi:10.1002/biot.202100183
- He, X., Pei, L., Tong, H. H. Y., and Zheng, Y. (2011). Comparison of Spray Freeze Drying and the Solvent Evaporation Method for Preparing Solid Dispersions of Baicalein with Pluronic F68 to Improve Dissolution and Oral Bioavailability. *AAPS PharmSciTech* 12, 104–113. doi:10.1208/s12249-010-9560-3
- Islan, G. A., Tornello, P. C., Abraham, G. A., Duran, N., and Castro, G. R. (2016). Smart Lipid Nanoparticles Containing Levofloxacin and DNase for Lung Delivery. Design and Characterization. *Colloids Surfaces B Biointerfaces* 143, 168–176. doi:10.1016/j.colsurfb.2016.03.040

- Kapalatiya, H., Madav, Y., Tambe, V. S., and Wairkar, S. (2022). Enzyme-responsive Smart Nanocarriers for Targeted Chemotherapy: an Overview. *Drug Deliv. Transl. Res.* 12 (6), 1293–1305. doi:10.1007/s13346-021-01020-6
- Katz, S., and Castro, G. R. (2019). *Bioimpresoras* (In Spanish). *Asoc. Civ. Cienc. Hoy* 1, 4–5.
- Kou, C. H., Han, J., Han, X. L., Zhuang, H. J., and Zhao, Z. M. (2017). Preparation and Characterization of the Adriamycin-loaded A-mphiphilic C-chitosan N-anoparticles and T-heir A-pplcation in the T-reatment of L-iver C-ancer. *Oncol. Lett.* 14, 7833–7841. doi:10.3892/ol.2017.7210
- Lal, S., and Datta, M. (2014). Organoclay Pluronic F68 – Montmorillonite, as a Sustained Release Drug Delivery Vehicle for Propanolol Hydrochloride. *Eur. Chem. Bull.* 3, 593–604.
- Li, M., Zhao, G., Su, W.-K., and Shuai, Q. (2020). Enzyme-responsive Nanoparticles for Anti-tumor Drug Delivery. *Front. Chem.* 8, 647. doi:10.3389/fchem.2020.00647
- Mendes, A. S., de Carvalho, J. E., Duarte, M. C. T., Durán, N., and Bruns, R. E. (2001). Factorial Design and Response Surface Optimization of Crude Violacein for *Chromobacterium Violaceum* Production. *Biotechnol. Lett.* 23, 1963–1969. doi:10.1023/a:1013734315525
- Mosmann, T. (1983). Rapid Colorimetric Assay for Cellular Growth and Survival: Application to Proliferation and Cytotoxicity Assays. *J. Immunol. Methods* 65, 55–63. doi:10.1016/0022-1759(83)90303-4
- Peng, J., Wang, X., and Lou, T. (2020). Preparation of Chitosan/gelatin Composite Foam with Ternary Solvents of Dioxane/acetic Acid/water and its Water Absorption Capacity. *Polym. Bull.* 77, 5227–5244. doi:10.1007/s00289-019-03016-2
- R. Liu (Editor) (2018). *Water-Insoluble Drug Formulation*. Third Edition 3rd ed. (Florida, United States: CRC Press). doi:10.1201/9781315120492
- Rahim, M. A., Jan, N., Khan, S., Shah, H., Madni, A., Khan, A., et al. (2021). Recent Advancements in Stimuli Responsive Drug Delivery Platforms for Active and Passive Cancer Targeting. *Cancers* 13, 670–752. doi:10.3390/cancers13040670
- Ritger, P. L., and Peppas, N. A. (1987). A Simple Equation for Description of Solute Release II. Fickian and Anomalous Release from Swellable Devices. *J. Control. Release* 5, 37–42. doi:10.1016/0168-3659(87)90035-6
- Rivero Berti, I., Rodenak-Kladniew, B., Onaandia, C., Adam, C. G., Islan, G. A., Durán, N., et al. (2020). Assessment of *In Vitro* Cytotoxicity of Imidazole Ionic Liquids and Inclusion in Targeted Drug Carriers Containing Violacein. *RSC Adv.* 10, 29336–29346. doi:10.1039/d0ra05101b
- Rodenak-Kladniew, B., Islan, G. A., de Bravo, M. G., Durán, N., and Castro, G. R. (2017). Design, Characterization and *In Vitro* Evaluation of Linalool-Loaded Solid Lipid Nanoparticles as Potent Tool in Cancer Therapy. *Colloids Surfaces B Biointerfaces* 154, 123–132. doi:10.1016/j.colsurfb.2017.03.021
- Romero, C. M., Pera, L. M., Loto, F., Vallejos, C., Castro, G., and Baigori, M. D. (2012). Purification of an Organic Solvent-Tolerant Lipase from *Aspergillus niger* MYA 135 and its Application in Ester Synthesis. *Biocatal. Agric. Biotechnol.* 1 (1), 25–31. doi:10.1016/j.bcab.2011.08.013
- Scioli Montoto, S., Muraca, G., and Ruiz, M. E. (2020). Solid Lipid Nanoparticles for Drug Delivery: Pharmacological and Biopharmaceutical Aspects. *Front. Mol. Biosci.* 7, 319. doi:10.3389/fmolb.2020.587997
- Shahriari, M., Zahiri, M., Abnous, K., Taghdisi, S. M., Ramezani, M., and Alibolandi, M. (2019). Enzyme Responsive Drug Delivery Systems in Cancer Treatment. *J. Control. Release* 308, 172–189. doi:10.1016/j.jconrel.2019.07.004
- Shariatnia, Z., and Jalali, A. M. (2018). Chitosan-based Hydrogels: Preparation, Properties and Applications. *Int. J. Biol. Macromol.* 115, 194–220. doi:10.1016/j.ijbiomac.2018.04.034
- Shilling, J. L. (1990). Final Report on the Safety Assessment of Butyl Myristate. *J. Am. Coll. Toxicol.* 9, 247–258.
- Siepmann, J., and Peppas, N. A. (2012). Modeling of Drug Release from Delivery Systems Based on Hydroxypropyl Methylcellulose (HPMC). *Adv. Drug Deliv. Rev.* 64, 163–174. doi:10.1016/j.addr.2012.09.028
- Stanisz, M., Klapiszewski, L., and Jesionowski, T. (2020). Recent Advances in the Fabrication and Application of Biopolymer-Based Micro- and Nanostructures: A Comprehensive Review. *Chem. Eng. J.* 397, 125409. doi:10.1016/j.cej.2020.125409
- Sun, H., Jiang, L., Luo, X., Jin, W., He, Q., An, J., et al. (2013). Potential Tumor-Suppressive Role of Monoglyceride Lipase in Human Colorectal Cancer. *Oncogene* 32, 234–241. doi:10.1038/onc.2012.34
- Tako, M., Kotogan, A., Papp, T., Kadaikunnan, S., Alharbi, N. S., and Vagvolgyi, C. (2017). Purification and Properties of Extracellular Lipases with Transesterification Activity and 1,3-regioselectivity from *Rhizomucor Miehei* and *Rhizopus Oryzae*. *J. Microbiol. Biotechnol.* 27, 277–288. doi:10.4014/jmb.1608.08005
- Venil, C. K., Dufossé, L., and Renuka Devi, P. (2020). Bacterial Pigments: Sustainable Compounds with Market Potential for Pharma and Food Industry. *Front. Sustain. Food Syst.* 4, 100. doi:10.3389/fsufs.2020.00100
- Wang, C., Chen, S., Wang, Y., Liu, X., Hu, F., Sun, J., et al. (2018). Lipase-Triggered Water-Responsive "Pandora's Box" for Cancer Therapy: Toward Induced Neighboring Effect and Enhanced Drug Penetration. *Adv. Mat.* 30, 1706407. doi:10.1002/adma.201706407
- Wang, Y.-W., Wu, Q., and Chen, G.-Q. (2005). Gelatin Blending Improves the Performance of Poly(3-Hydroxybutyrate-Co-3-Hydroxyhexanoate) Films for Biomedical Application. *Biomacromolecules* 6, 566–571. doi:10.1021/bm049342d
- Wolinsky, J. B., Colson, Y. L., and Grinstaff, M. W. (2012). Local Drug Delivery Strategies for Cancer Treatment: Gels, Nanoparticles, Polymeric Films, Rods, and Wafers. *J. Control. Release* 159, 14–26. doi:10.1016/j.jconrel.2011.11.031
- Xu, S., Du, M., Zhang, Z., Shao, M., Zhang, G., and Zhou, L. (2022). Synthesis, Properties and Thermokinetics of a Kind of Diesters as Phase Change Materials. *Sol. Energy* 235, 180–186. doi:10.1016/j.solener.2022.02.043

Conflict of Interest: The authors declare that the research was conducted in the absence of any commercial or financial relationships that could be construed as a potential conflict of interest.

Publisher's Note: All claims expressed in this article are solely those of the authors and do not necessarily represent those of their affiliated organizations, or those of the publisher, the editors and the reviewers. Any product that may be evaluated in this article, or claim that may be made by its manufacturer, is not guaranteed or endorsed by the publisher.

Copyright © 2022 Rivero Berti, Rodenak-Kladniew, Katz, Arrua, Alvarez, Duran and Castro. This is an open-access article distributed under the terms of the Creative Commons Attribution License (CC BY). The use, distribution or reproduction in other forums is permitted, provided the original author(s) and the copyright owner(s) are credited and that the original publication in this journal is cited, in accordance with accepted academic practice. No use, distribution or reproduction is permitted which does not comply with these terms.



OPEN ACCESS

EDITED BY

Simone Brogi,
University of Pisa, Italy

REVIEWED BY

Premalata Kumari,
Sardar Vallabhbhai National Institute of
Technology Surat, India
Andrew David Westwell,
Cardiff University, United Kingdom

*CORRESPONDENCE

Hong Chen,
chenwepo@sina.com
Jianliang Shen,
shenjl@wiucas.ac.cn
Jingguo Li,
lijingguo@zzu.edu.cn

SPECIALTY SECTION

This article was submitted to Organic
Chemistry,
a section of the journal
Frontiers in Chemistry

RECEIVED 18 May 2022

ACCEPTED 14 July 2022

PUBLISHED 15 August 2022

CITATION

Qi Y, Chen H, Chen S, Shen J and Li J
(2022), Synthesis, bioactivity, and
molecular docking of novel
arylpiperazine derivatives as potential
AR antagonists.
Front. Chem. 10:947065.
doi: 10.3389/fchem.2022.947065

COPYRIGHT

© 2022 Qi, Chen, Chen, Shen and Li.
This is an open-access article
distributed under the terms of the
Creative Commons Attribution License
(CC BY). The use, distribution or
reproduction in other forums is
permitted, provided the original
author(s) and the copyright owner(s) are
credited and that the original
publication in this journal is cited, in
accordance with accepted academic
practice. No use, distribution or
reproduction is permitted which does
not comply with these terms.

Synthesis, bioactivity, and molecular docking of novel arylpiperazine derivatives as potential AR antagonists

Yueheng Qi^{1,2}, Hong Chen^{2*}, Shijin Chen², Jianliang Shen^{3*} and Jingguo Li^{1*}

¹Henan Provincial People's Hospital, People's Hospital of Zhengzhou University, Zhengzhou, Henan, China, ²Luoyang Key Laboratory of Organic Functional Molecules, College of Food and Drug, Luoyang Normal University, Luoyang, Henan, China, ³School of Ophthalmology & Optometry, School of Biomedical Engineering, Wenzhou Medical University, Wenzhou, Zhejiang, China

Prostate cancer is one of the malignant tumors and the second most common malignant tumor in men. Clinically used androgen receptor (AR)-targeted drugs can antagonize androgen and inhibit tumor growth, but these drugs can cause serious resistance problems. To develop novel AR antagonists, 22 kinds of arylpiperazine derivatives were designed and synthesized, and the derivatives **5**, **8**, **12**, **19**, **21**, **22**, **25**, and **26** not only showed strong antagonistic potency (>55% inhibition) and binding affinities (IC₅₀ <3 μM) to AR, but also showed stronger inhibitory activity to LNCaP cells *versus* PC-3 cells. Among them, derivative **21** exhibited the highest binding affinity for AR (IC₅₀ = 0.65 μM) and the highest antagonistic potency (76.2% inhibition). Docking studies suggested that the derivative **21** is primarily bound to the AR-LBP site by the hydrophobic interactions. Overall, those results provided experimental methods for developing novel arylpiperazine derivatives as potent AR antagonists.

KEYWORDS

prostate cancer, synthesis, antagonistic activity, binding affinities, molecular docking

Highlights

1. A series of arylpiperazine derivatives were synthesized
2. Antiproliferative (LNCaP cells *versus* PC-3 cells), AR antagonist activity, and AR binding affinity of arylpiperazine derivatives were investigated.
3. Some derivatives exhibited strong cytotoxic activities against LNCaP cells *versus* PC-3 cells and exhibited potent antagonistic potency against AR and AR binding affinities.
4. Molecular docking and SAR of arylpiperazine derivatives were also studied.

Introduction

Prostate cancer (PCa) is one of the malignant tumors and the second most common malignant tumor in men that seriously endanger human health, with nearly 140,000 new cases and 375,304 deaths in the year 2020 (Gandaglia et al., 2021; Sung et al., 2021). Androgen receptors (AR) are steroid receptors in the nuclear receptor superfamily and are highly expressed in prostate cancer cells, which play an important role in prostatic hyperplasia and growth. AR is involved in the progression of PCa, and AR is expressed to a certain extent in each stage of PCa (Bentel and Cardi, 1996; Bosland, 2000; Culig et al., 2002; Gelmann, 2002; Taplin and Balk, 2004; Dehm and Tindall, 2007). AR overexpression is also found in most castration-resistant prostate cancer (CRPC). The AR pathway still plays a key role in the growth and reproduction of CRPC, and the reactivation of the AR signaling pathway is a key driving force for the progression of CRPC. Therefore, AR has become an important target for the treatment of PCa.

At present, the main treatment methods for CRPC include endocrine therapy, chemotherapy, molecular targeted therapy and immunotherapy, and androgen-deprivation therapy is the standard treatment for advanced prostate cancer, but most patients progress to an incurable CRPC stage within 2–3 years. CRPC patients have a poor prognosis, difficult treatment, and are prone to metastasis, with median overall survival <2 years. Once PCa has metastasized, no obvious therapies exist (Zou et al., 2012; Dorff and Glode, 2013; Han et al., 2013; Loblaw et al., 2013). Although chemotherapy is most commonly used to treat advanced diseases (Beedassy and Cardi, 1999), and to inhibit tumor growth and prolong the life of patients, none of the conventional cancer therapy approaches have been shown to be effective against PCa. Thus, it is urgent to find and develop new therapeutic agents with obvious curative effects for the treatment of PCa. AR antagonists inhibit the activity of AR by directly binding and blocking the ligand-binding domain of AR and preventing androgens to exert the corresponding biological activity, thereby inhibiting the development of PCa. Although clinically used AR-targeted antagonists such as flutamide, hydroxyflutamide, bicalutamide, enzalutamide, and ARN-509 (Figure 1) can antagonize the function of androgens at the receptor level to inhibit tumor growth, these drugs produce serious adverse reactions and drug resistance after several years of targeted therapy. Therefore, as the second most frequent malignancy in men worldwide, it is an urgent problem to find and develop effective anti-drug AR-targeted antagonists for treating PCa.

Piperazine is a six-membered heterocyclic compound, which is one of the most popular heterocyclic compounds for new drug candidates under development and existing marketed drugs (Chaudhary et al., 2006). Moreover, piperazine compounds have a broad spectrum of pharmacological activities because

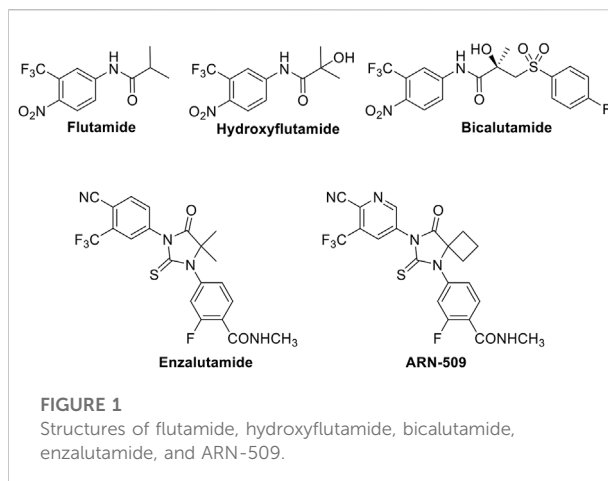


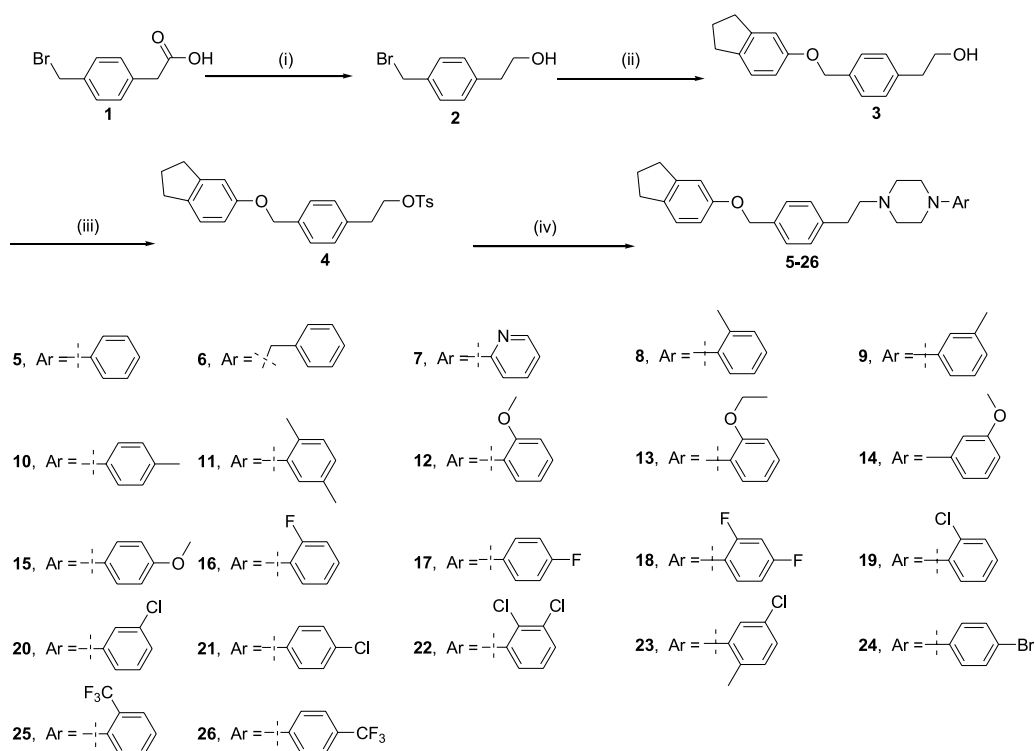
FIGURE 1
Structures of flutamide, hydroxyflutamide, bicalutamide, enzalutamide, and ARN-509.

of their receptor-blocking (Leopoldo et al., 2007; Romeiro et al., 2011; Chen et al., 2012; Ananthan et al., 2014; Baran et al., 2014) and antiproliferative properties (Berardi et al., 2008; Lee et al., 2010; Abate et al., 2011; Cao et al., 2013; Lin et al., 2013; Liu et al., 2013; Arnatt et al., 2014; Guo et al., 2015). Arylpiperazine derivatives also have obvious AR antagonism with an IC_{50} of 0.11 μ M, whereas the IC_{50} of bicalutamide is 50 μ M. Results of animal experiments have shown that the mass of the prostate in rats is significantly reduced, and the concentration of serum testosterone is not significantly changed (Kinoyama et al., 2004; Kinoyama et al., 2005; Gupta et al., 2016). Recently, our group has also reported that some piperazine derivatives exhibit excellent inhibitory activity to AR (Chen et al., 2019a; Chen et al., 2019b). Inspired by these findings, in order to obtain more effective AR antagonists to treat PCa, here, a class of arylpiperazine derivatives (Scheme 1) was synthesized and their biological activity was evaluated. The structure–activity relationship (SAR) was also studied to further design the potent AR antagonists and develop the novel arylpiperazine derivatives. Compared to the reported derivatives, some arylpiperazine derivatives exhibited relatively excellent bioactivity.

Materials and methods

Materials and instruments

Anhydrous tetrahydrofuran was dried using standard experimental procedures. Chemical reagents and other solvents were purchased from Energy Chemical. Melting points of compounds were obtained using an SGW X-4 micromelting point instrument (Uncorrected). NMR spectra were recorded on a Bruker AVANCE-500 MHz instrument in $CDCl_3$. The chemical shifts are given in ppm, and J -values are reported in Hz. High-resolution mass spectra (AB Sciex X500R

**Scheme 1**

Reagents and conditions are as follows: (i) $\text{BH}_3 \cdot \text{S}(\text{CH}_3)_2$, tetrahydrofuran, 11 h; (ii) 2,3-dihydro-1H-inden-5-ol, potassium carbonate, acetonitrile, 85°C, 16 h; (iii) TsCl, Et_3N and 4-dimethylaminopyridine, methylene chloride, 0°C, 16 h; (iv) arylpiperazines, potassium carbonate, acetonitrile, 85°C, 16 h.

QTOF) of the intermediates and the final compounds were obtained equipped with an ESI source.

Synthesis of 2-(4-(bromomethyl)phenyl)ethanol (2)

The intermediate **2** was obtained using previous literature methods (Chen et al., 2018).

2-(4-((2,3-dihydro-1H-inden-5-yloxy)methyl)phenyl)ethanol (3)

The intermediate **3** was obtained using methods outlined in previous literature (Chen et al., 2018). White solid (ethyl acetate). Yield: 60% (from compound **1**); Mp, 45.8–46.5 °C; ^1H NMR (500 MHz, CDCl_3) δ 7.42 (d, $J = 7.9$ Hz, 2H), 7.28 (d, $J = 7.9$ Hz, 2H), 7.16 (d, $J = 8.0$ Hz, 1H), 6.91 (d, $J = 2.0$ Hz, 1H), 6.80 (dd, $J = 8.0, 2.0$ Hz, 1H), 5.05 (s, 2H), 3.89 (t, $J = 6.6$ Hz, 2H), 2.93–2.87 (m, 6H), 2.08–2.14 (m, 2H); HRMS (ESI) m/z $[\text{M}+1]^+$: calcd for $\text{C}_{18}\text{H}_{20}\text{O}_2$, 269.1536, found, 269.1536.

4-((2,3-dihydro-1H-inden-5-yloxy)methyl)phenethyl 4-methylbenzenesulfonate (4)

The intermediate **4** was obtained using previously reported methods (Chen et al., 2018). White solid (ethyl acetate). Yield: 95%. Mp 63.2–64.3 °C; ^1H NMR (500 MHz, CDCl_3) δ 7.70 (d, $J = 8.2$ Hz, 2H), 7.34 (d, $J = 8.0$ Hz, 2H), 7.30 (d, $J = 8.4$ Hz, 2H), 7.14 (d, $J = 8.0$ Hz, 3H), 6.89 (d, $J = 2.0$ Hz, 1H), 6.78 (dd, $J = 8.2, 2.0$ Hz, 1H), 5.02 (s, 2H), 4.23 (t, $J = 7.0$ Hz, 2H), 2.99 (t, $J = 7.0$ Hz, 2H), 2.89–2.83 (m, 4H), 2.45 (s, 3H), 2.07–2.13 (m, 2H); HRMS (ESI) m/z $[\text{M}+1]^+$: calcd for $\text{C}_{25}\text{H}_{26}\text{O}_4\text{S}$, 423.1625, found, 423.1621.

General procedure for the synthesis of arylpiperazine derivative 5–26

To a solution of **4** (100 mg, 0.23 mmol) in acetonitrile (10 ml) was added arylpiperazine (1.2 equiv) and potassium carbonate (6.0 equiv), and the reaction mixture was stirred at 85 °C for 16 h. The inorganic solids were filtered by the Buchner funnel, and the remaining filtrate was evaporated *in vacuo*. Obtained crude

products were purified using column chromatography ($V_{PE}: V_{EA} = 15:1$) to give the respective product (**5–26**).

1-(4-((2,3-dihydro-1H-inden-5-yloxy)methyl)phenethyl)-4-phenylpiperazine (**5**)

White solid (ethyl acetate); Yield: 64%; Mp 82.2–83.5 °C; ^1H NMR (500 MHz, CDCl_3) δ 7.42 (d, $J = 7.9$ Hz, 2H), 7.36–7.28 (m, 4H), 7.17 (d, $J = 8.2$ Hz, 1H), 7.00 (d, $J = 8.2$ Hz, 2H), 6.92 (t, $J = 7.2$ Hz, 2H), 6.82 (dd, $J = 8.2, 2.2$ Hz, 1H), 5.06 (s, 2H), 3.29 (t, $J = 5.0$ Hz, 4H), 2.95–2.85 (m, 6H), 2.80–2.67 (m, 6H), 2.12 (m, 2H); ^{13}C NMR (126 MHz, CDCl_3) δ 157.85, 151.35, 145.76, 139.95, 136.47, 135.23, 129.16, 128.95, 127.74, 124.79, 119.77, 116.11, 112.86, 110.96, 70.12, 60.48, 53.29, 49.20, 33.38, 33.23, 32.04, 25.89; HRMS (ESI) m/z $[M+1]^+$: calcd for $\text{C}_{28}\text{H}_{32}\text{N}_2\text{O}$, 413.2587, found, 413.2584.

1-(4-((2,3-dihydro-1H-inden-5-yloxy)methyl)phenethyl)-4-benzylpiperazine (**6**)

White solid (ethyl acetate); Yield: 60%; Mp 71.1–73.3 °C; ^1H NMR (500 MHz, CDCl_3) δ 7.39–7.28 (m, 7H), 7.21 (d, $J = 8.0$ Hz, 2H), 7.11 (d, $J = 8.1$ Hz, 1H), 6.86 (d, $J = 2.0$ Hz, 1H), 6.75 (dd, $J = 8.2, 2.0$ Hz, 1H), 4.99 (s, 2H), 3.53 (s, 2H), 2.88–2.809 (m, 6H), 2.77–2.31 (m, 10H), 2.11–2.01 (m, 2H); ^{13}C NMR (126 MHz, CDCl_3) δ 157.93, 145.85, 140.08, 138.11, 136.56, 135.27, 129.39, 129.01, 128.36, 127.80, 127.21, 124.86, 112.94, 111.05, 70.22, 63.17, 60.54, 53.25, 53.09, 33.38, 33.31, 32.12, 25.97; HRMS (ESI) m/z $[M+1]^+$: calcd for $\text{C}_{29}\text{H}_{34}\text{N}_2\text{O}$, 427.2744, found, 427.2742.

1-(4-((2,3-dihydro-1H-inden-5-yloxy)methyl)phenethyl)-4-(pyridin-2-yl)piperazine (**7**)

White solid (ethyl acetate); Yield: 90%; Mp 90.1–91.8 °C; ^1H NMR (500 MHz, CDCl_3) δ 8.24 (dd, $J = 5.0, 1.5$ Hz, 1H), 7.56–7.47 (m, 1H), 7.39 (d, $J = 7.9$ Hz, 2H), 7.28 (d, $J = 7.9$ Hz, 2H), 7.15 (d, $J = 8.2$ Hz, 1H), 6.90 (br s, 1H), 6.79 (dd, $J = 8.2, 2.0$ Hz, 1H), 6.74–6.60 (m, 2H), 5.03 (s, 2H), 3.62 (t, $J = 5.0$ Hz, 4H), 2.95–2.81 (m, 6H), 2.71–2.68 (m, 6H), 2.16–2.03 (m, 2H); ^{13}C NMR (126 MHz, CDCl_3) δ 159.55, 157.81, 148.00, 145.75, 139.85, 137.50, 136.45, 135.22, 128.94, 127.73, 124.77, 113.39, 112.82, 110.93, 107.13, 70.09, 60.47, 53.01, 45.19, 33.24, 33.21, 32.02, 29.74, 25.87, 22.73; HRMS (ESI) m/z $[M+1]^+$: calcd for $\text{C}_{27}\text{H}_{31}\text{N}_3\text{O}$, 414.2540, found, 414.2536.

1-(4-((2,3-dihydro-1H-inden-5-yloxy)methyl)phenethyl)-4-o-tolylpiperazine (**8**)

White solid (ethyl acetate); Yield: 85%; Mp 62.3–63.1 °C; ^1H NMR (500 MHz, CDCl_3) δ 7.37 (d, $J = 8.0$ Hz, 2H), 7.25 (d, $J = 8.0$ Hz, 2H), 7.18 ($J = 7.6$ Hz, 2H), 7.12 (d, $J = 8.2$ Hz, 1H), 7.05 (d, $J = 7.5$ Hz, 1H), 6.99 (td, $J = 7.5, 2.0$ Hz, 1H), 6.87 (d, $J = 2.0$ Hz, 1H), 6.77 (dd, $J = 8.2, 2.0$ Hz, 1H), 5.01 (s, 2H), 3.00 (t, $J = 5.0$ Hz, 4H), 2.94–2.78 (m, 6H), 2.71–2.67 (m, 6H), 2.32 (s, 3H), 2.15–1.97 (m, 2H); ^{13}C NMR (126 MHz, CDCl_3) δ 158.06, 151.68, 146.01, 140.19, 136.71, 135.45, 132.87, 131.33, 129.20,

128.00, 126.87, 125.02, 123.45, 119.29, 113.07, 111.17, 70.35, 60.83, 53.98, 51.89, 33.58, 33.46, 32.27, 26.12, 18.17; HRMS (ESI) m/z $[M+1]^+$: calcd for $\text{C}_{29}\text{H}_{34}\text{N}_2\text{O}$, 427.2744, found, 427.2742.

1-(4-((2,3-dihydro-1H-inden-5-yloxy)methyl)phenethyl)-4-m-tolylpiperazine (**9**)

White solid (ethyl acetate); Yield: 65%; Mp 61.2–62.7 °C; ^1H NMR (500 MHz, CDCl_3) δ 7.35 (d, $J = 8.0$ Hz, 2H), 7.23 (d, $J = 8.0$ Hz, 2H), 7.15 (t, $J = 7.8$ Hz, 1H), 7.10 (d, $J = 8.0$ Hz, 1H), 6.86 (d, $J = 2.0$ Hz, 1H), 6.76–6.74 (m, 3H), 6.69 (d, $J = 7.6$ Hz, 1H), 4.99 (s, 2H), 3.22 (t, $J = 5.0$ Hz, 4H), 2.88–2.81 (m, 6H), 2.70–2.63 (m, 6H), 2.32 (s, 3H), 2.09–2.03 (m, 2H); ^{13}C NMR (126 MHz, CDCl_3) δ 157.88, 151.42, 145.81, 139.94, 138.88, 136.51, 135.28, 129.06, 129.00, 127.80, 124.84, 120.77, 117.03, 113.31, 112.89, 110.99, 70.14, 60.50, 53.31, 49.26, 33.34, 33.28, 32.09, 29.81, 25.94, 21.90; HRMS (ESI) m/z $[M+1]^+$: calcd for $\text{C}_{29}\text{H}_{34}\text{N}_2\text{O}$, 427.2744, found, 427.2740.

1-(4-((2,3-dihydro-1H-inden-5-yloxy)methyl)phenethyl)-4-p-tolylpiperazine (**10**)

White solid (ethyl acetate); Yield: 68%; Mp 105.1–106.3 °C; ^1H NMR (500 MHz, CDCl_3) δ 7.40 (d, $J = 8.0$ Hz, 2H), 7.28 (d, $J = 8.0$ Hz, 2H), 7.15 (d, $J = 8.2$ Hz, 1H), 7.12 (d, $J = 8.2$ Hz, 2H), 6.91–6.89 (m, 3H), 6.80 (dd, $J = 8.2, 2.0$ Hz, 1H), 5.04 (s, 2H), 3.24 (t, $J = 5.0$ Hz, 4H), 2.95–2.84 (m, 6H), 2.81–2.68 (m, 6H), 2.31 (s, 3H), 2.15–2.06 (m, 2H); ^{13}C NMR (126 MHz, CDCl_3) δ 157.80, 149.18, 145.75, 139.80, 136.46, 135.24, 129.68, 129.38, 128.94, 127.74, 124.76, 116.50, 112.82, 110.93, 70.09, 60.42, 53.24, 49.67, 33.21, 32.01, 25.86, 20.46; HRMS (ESI) m/z $[M+1]^+$: calcd for $\text{C}_{29}\text{H}_{34}\text{N}_2\text{O}$, 427.2744, 427.2741.

1-(4-((2,3-dihydro-1H-inden-5-yloxy)methyl)phenethyl)-4-(2,5-dimethylphenyl)piperazine (**11**)

White solid (ethyl acetate); Yield: 46%; Mp 70.4–71.5 °C; ^1H NMR (500 MHz, CDCl_3) δ 7.41 (d, $J = 8.0$ Hz, 2H), 7.29 (d, $J = 8.0$ Hz, 2H), 7.16 (d, $J = 8.2$ Hz, 1H), 7.11 (d, $J = 7.8$ Hz, 1H), 6.92 (d, $J = 2.0$ Hz, 1H), 6.90 (br s, 1H), 6.85 (d, $J = 7.6$ Hz, 1H), 6.81 (dd, $J = 8.2, 2.0$ Hz, 1H), 5.05 (s, 2H), 3.02 (t, $J = 5.0$ Hz, 4H), 2.94–2.87 (m, 6H), 2.75–2.71 (m, 6H), 2.36 (s, 3H), 2.31 (s, 3H), 2.15–2.08 (m, 2H); ^{13}C NMR (126 MHz, CDCl_3) δ 157.85, 151.31, 145.75, 140.01, 136.46, 136.14, 135.20, 130.91, 129.30, 128.95, 127.73, 124.77, 123.80, 119.78, 112.86, 110.96, 70.13, 60.53, 53.72, 51.64, 33.29, 33.22, 32.03, 25.87, 21.24, 17.51; HRMS (ESI) m/z $[M+1]^+$: calcd for $\text{C}_{30}\text{H}_{36}\text{N}_2\text{O}$, 441.2900, found, 441.2896.

1-(4-((2,3-dihydro-1H-inden-5-yloxy)methyl)phenethyl)-4-(2-methoxyphenyl)piperazine (**12**)

White solid (ethyl acetate); Yield: 50%; Mp 77.3–78.5; ^1H NMR (500 MHz, CDCl_3) δ 7.40 (d, $J = 7.9$ Hz, 2H), 7.28 (d, $J = 7.9$ Hz, 2H), 7.15 (d, $J = 8.1$ Hz, 1H), 7.07–6.95 (m, 3H),

6.93–6.88 (m, 2H), 6.80 (dd, $J = 8.2, 2.0$ Hz, 1H), 5.04 (s, 2H), 3.90 (s, 3H), 3.19 (br s, 4H), 2.93–2.86 (m, 6H), 2.81–2.72 (m, 6H), 2.13–2.07 (m, 2H); ^{13}C NMR (126 MHz, CDCl_3) δ 157.83, 152.30, 145.73, 141.28, 139.91, 136.45, 135.21, 128.94, 127.72, 124.76, 123.00, 121.04, 118.27, 112.85, 111.22, 110.95, 70.11, 60.49, 55.39, 53.40, 50.56, 33.21, 32.02, 29.73, 25.86; HRMS(ESI) m/z $[\text{M}+1]^+$: calcd for $\text{C}_{29}\text{H}_{34}\text{N}_2\text{O}_2$, 443.2693, found, 443.2691.

1-(4-((2,3-dihydro-1H-inden-5-yloxy)methyl)phenethyl)-4-(2-ethoxyphenyl)piperazine (**13**)

White solid (ethyl acetate); Yield: 54%; Mp 65.2–66.1 °C; ^1H NMR (500 MHz, CDCl_3) δ 7.40 (d, $J = 8.0$ Hz, 2H), 7.29 (d, $J = 8.0$ Hz, 2H), 7.15 (d, $J = 8.2$ Hz, 1H), 7.04–6.94 (m, 3H), 6.93–6.87 (m, 2H), 6.80 (dd, $J = 8.2, 2.0$ Hz, 1H), 5.04 (s, 2H), 4.11 (q, $J = 7.0$ Hz, 2H), 3.22 (br s, 4H), 2.96–2.84 (m, 6H), 2.85–2.69 (m, 6H), 2.16–2.05 (m, 2H), 1.51 (t, $J = 7.0$ Hz, 3H); ^{13}C NMR (126 MHz, CDCl_3) δ 157.84, 151.60, 145.74, 141.33, 139.93, 136.45, 135.21, 128.95, 127.72, 124.76, 122.81, 121.05, 118.22, 112.85, 112.52, 110.96, 77.34, 77.08, 76.83, 70.12, 63.59, 60.50, 53.41, 50.46, 33.21, 32.02, 25.87, 14.99; HRMS (ESI) m/z $[\text{M}+1]^+$: calcd for $\text{C}_{30}\text{H}_{36}\text{N}_2\text{O}_2$, 457.2850, found, 457.2845.

1-(4-((2,3-dihydro-1H-inden-5-yloxy)methyl)phenethyl)-4-(3-methoxyphenyl)piperazine (**14**)

White solid (ethyl acetate); Yield: 68%; Mp 74.2–75.4 °C; ^1H NMR (500 MHz, CDCl_3) δ 7.40 (d, $J = 7.8$ Hz, 2H), 7.28 (d, $J = 7.8$ Hz, 2H), 7.21 (t, $J = 8.2$ Hz, 1H), 7.15 (d, $J = 8.2$ Hz, 1H), 6.90 (br s, 1H), 6.79 (dd, $J = 8.2, 2.0$ Hz, 1H), 6.59 (dd, $J = 8.2, 2.0$ Hz, 1H), 6.52 (br s, 1H), 6.46 (dd, $J = 8.1, 2.0$ Hz, 1H), 5.04 (s, 2H), 3.83 (s, 3H), 3.28 (t, $J = 5.0$ Hz, 4H), 2.99–2.82 (m, 6H), 2.80–2.63 (m, 6H), 2.17–2.03 (m, 2H); ^{13}C NMR (126 MHz, CDCl_3) δ 160.61, 157.81, 152.67, 145.74, 139.81, 136.46, 135.25, 129.81, 128.92, 127.73, 124.76, 112.83, 110.94, 108.91, 104.50, 102.57, 70.10, 60.39, 55.21, 53.16, 49.02, 33.24, 33.20, 32.01, 29.73, 25.86; HRMS (ESI) m/z $[\text{M}+1]^+$: calcd for $\text{C}_{29}\text{H}_{34}\text{N}_2\text{O}_2$, 443.2693, found, 443.2689.

1-(4-((2,3-dihydro-1H-inden-5-yloxy)methyl)phenethyl)-4-(4-methoxyphenyl)piperazine (**15**)

White solid (ethyl acetate); Yield: 45%; Mp 78.1–79.3 °C; ^1H NMR (500 MHz, CDCl_3) δ 7.39 (d, $J = 7.9$ Hz, 2H), 7.28 (d, $J = 7.9$ Hz, 2H), 7.14 (d, $J = 8.2$ Hz, 1H), 6.95 (d, $J = 9.0$ Hz, 2H), 6.89 (br s, 1H), 6.87 (t, $J = 7.9$ Hz, 2H), 6.79 (dd, $J = 8.1, 2.0$ Hz, 1H), 5.03 (s, 2H), 3.80 (s, 3H), 3.23 (t, $J = 5.0$ Hz, 4H), 2.93–2.84 (m, 6H), 2.81–2.67 (m, 6H), 2.13–2.06 (m, 2H); ^{13}C NMR (126 MHz, CDCl_3) δ 157.82, 153.90, 145.74, 145.67, 139.82, 136.46, 135.24, 128.92, 127.72, 124.75, 118.28, 114.47, 112.84, 110.94, 70.10, 60.37, 55.59, 53.30, 50.58, 33.20, 32.01, 29.72, 25.85; HRMS (ESI) m/z $[\text{M}+1]^+$: calcd for $\text{C}_{29}\text{H}_{34}\text{N}_2\text{O}_2$, 443.2693, found, 443.2690.

1-(4-((2,3-dihydro-1H-inden-5-yloxy)methyl)phenethyl)-4-(2-fluorophenyl)piperazine (**16**)

White solid (ethyl acetate); Yield: 90%; Mp 64.2–65.3 °C; ^1H NMR (500 MHz, CDCl_3) δ 7.41 (d, $J = 8.0$ Hz, 2H), 7.28 (d, $J = 8.0$ Hz, 2H), 7.15 (d, $J = 8.1$ Hz, 1H), 7.13–6.94 (m, 4H), 6.91 (d, $J = 2.0$ Hz, 1H), 6.80 (dd, $J = 8.2, 2.0$ Hz, 1H), 5.04 (s, 2H), 3.19 (t, $J = 5.0$ Hz, 4H), 2.96–2.84 (m, 6H), 2.83–2.66 (m, 6H), 2.14–2.08 (m, 2H); ^{13}C NMR (126 MHz, CDCl_3) δ 157.82, 145.76, 139.95, 136.46, 135.19, 128.95, 127.74, 124.77, 124.51, 124.49, 118.96, 118.94, 116.22, 116.05, 112.83, 110.93, 70.09, 60.50, 53.31, 50.59, 50.56, 33.34, 33.22, 32.02, 25.88; HRMS (ESI) m/z $[\text{M}+1]^+$: calcd for $\text{C}_{28}\text{H}_{31}\text{FN}_2\text{O}$, 431.2493, found, 431.2492.

1-(4-((2,3-dihydro-1H-inden-5-yloxy)methyl)phenethyl)-4-(4-fluorophenyl)piperazine (**17**)

White solid (ethyl acetate); Yield: 52%; Mp 79.8–80.5 °C; ^1H NMR (500 MHz, CDCl_3) δ 7.40 (d, $J = 7.9$ Hz, 2H), 7.28 (d, $J = 7.9$ Hz, 2H), 7.15 (d, $J = 8.2$ Hz, 1H), 7.00 (t, $J = 8.5$ Hz, 2H), 6.94–6.92 (m, 2H), 6.90 (br s, 1H), 6.80 (dd, $J = 8.2, 2.0$ Hz, 1H), 5.04 (s, 2H), 3.20 (t, $J = 5.0$ Hz, 4H), 2.97–2.84 (m, 6H), 2.82–2.66 (m, 6H), 2.15–2.06 (m, 2H); ^{13}C NMR (126 MHz, CDCl_3) δ 158.18, 157.82, 156.28, 147.97, 145.75, 139.83, 136.47, 135.25, 128.92, 127.73, 124.77, 117.90, 117.84, 115.63, 115.45, 112.84, 110.94, 70.10, 60.36, 53.23, 50.17, 33.29, 33.21, 32.02, 29.73, 25.86; HRMS (ESI) m/z $[\text{M}+1]^+$: calcd for $\text{C}_{28}\text{H}_{31}\text{FN}_2\text{O}$, 431.2493, found, 431.2487.

1-(4-((2,3-dihydro-1H-inden-5-yloxy)methyl)phenethyl)-4-(2,4-difluorophenyl)piperazine (**18**)

White solid (ethyl acetate); Yield: 43%; Mp 86.1–86.5 °C; ^1H NMR (500 MHz, CDCl_3) δ 7.40 (d, $J = 8.0$ Hz, 2H), 7.28 (d, $J = 8.0$ Hz, 2H), 7.15 (d, $J = 8.2$ Hz, 1H), 6.99–6.92 (m, 1H), 6.90 (d, $J = 5.0$ Hz, 1H), 6.88–6.77 (m, 3H), 5.04 (s, 2H), 3.12 (d, $J = 5.0$ Hz, 4H), 2.93–2.86 (m, 6H), 2.81–2.67 (m, 6H), 2.16–2.05 (m, 2H); ^{13}C NMR (126 MHz, CDCl_3) δ 158.06, 145.99, 140.13, 136.70, 135.46, 129.16, 127.97, 125.00, 119.73, 119.69, 119.65, 119.62, 113.07, 111.17, 111.04, 111.01, 110.87, 110.84, 105.15, 104.95, 104.75, 70.33, 60.65, 53.50, 51.18, 51.16, 33.54, 33.45, 32.25, 26.10; HRMS (ESI) m/z $[\text{M}+1]^+$: calcd for $\text{C}_{28}\text{H}_{30}\text{F}_2\text{N}_2\text{O}$, 449.2399, found, 449.2398.

1-(4-((2,3-dihydro-1H-inden-5-yloxy)methyl)phenethyl)-4-(2-chlorophenyl)piperazine (**19**)

White solid (ethyl acetate); Yield: 43%; Mp 91.4–92.1 °C; ^1H NMR (500 MHz, CDCl_3) δ 7.40 (d, $J = 7.8$ Hz, 3H), 7.28 (d, $J = 7.8$ Hz, 2H), 7.25 (t, $J = 7.6$ Hz, 1H), 7.15 (d, $J = 8.2$ Hz, 1H), 7.10 (d, $J = 7.6$ Hz, 1H), 7.01 (t, $J = 7.6$ Hz, 1H), 6.90 (br s, 1H), 6.80 (dd, $J = 8.2, 2.0$ Hz, 1H), 5.04 (s, 2H), 3.16 (br s, 4H), 2.96–2.86 (m, 6H), 2.84–2.65 (m, 6H), 2.14–2.05 (m, 2H); ^{13}C NMR (126 MHz, CDCl_3) δ 157.83, 149.30, 145.74, 139.97, 136.46, 135.20, 130.67, 128.93, 128.82, 127.72, 127.62, 124.76, 123.71, 120.41, 112.84, 110.95, 70.12, 60.46, 53.38,

51.22, 33.35, 33.21, 32.02, 25.86; HRMS (ESI) m/z $[M+1]^+$: calcd for $C_{28}H_{31}ClN_2O$, 447.2198, found, 447.2195.

1-(4-((2,3-dihydro-1H-inden-5-yloxy)methyl)phenethyl)-4-(3-chlorophenyl)piperazine (**20**)

White solid (ethyl acetate); Yield: 71%; Mp 83.2–84.3 °C; 1H NMR (500 MHz, $CDCl_3$) δ 7.40 (d, J = 7.9 Hz, 2H), 7.28 (d, J = 2.3 Hz, 1H), 7.20 (t, J = 8.1 Hz, 1H), 7.15 (d, J = 8.2 Hz, 1H), 6.92 (t, J = 2.0 Hz, 1H), 6.90 (s, 1H), 6.86–6.79 (m, 3H), 5.04 (s, 2H), 3.35–3.18 (m, 4H), 2.99–2.81 (m, 6H), 2.71 (dd, J = 16.0, 7.0 Hz, 6H), 2.16–2.05 (m, 2H); ^{13}C NMR (126 MHz, $CDCl_3$) δ 157.81, 152.29, 145.75, 139.72, 136.48, 135.29, 134.99, 130.05, 128.92, 127.74, 124.76, 119.36, 115.81, 113.91, 112.84, 110.94, 70.10, 60.30, 53.00, 48.62, 33.21, 32.02, 29.73, 25.86; HRMS (ESI) m/z $[M+1]^+$: calcd for $C_{28}H_{31}ClN_2O$, 447.2198, found, 447.2196.

1-(4-((2,3-dihydro-1H-inden-5-yloxy)methyl)phenethyl)-4-(4-chlorophenyl)piperazine (**21**)

White solid (ethyl acetate); Yield: 57%; Mp 117.2–118.6 °C; 1H NMR (500 MHz, $CDCl_3$) δ 7.40 (d, J = 7.9 Hz, 2H), 7.29–7.23 (m, 4H), 7.14 (d, J = 8.2 Hz, 1H), 6.90 (br s, 1H), 6.88 (d, J = 8.2 Hz, 2H), 6.79 (dd, J = 8.2, 2.0 Hz, 1H), 5.04 (s, 2H), 3.23 (t, J = 5.0, 4H), 2.89 (m, 6H), 2.79–2.65 (m, 6H), 2.15–2.05 (m, 2H); ^{13}C NMR (126 MHz, $CDCl_3$) δ 157.82, 149.93, 145.74, 139.82, 136.47, 135.26, 128.97, 128.91, 127.72, 124.76, 124.57, 117.25, 112.84, 110.94, 70.10, 60.33, 53.07, 49.16, 33.29, 33.20, 32.01, 25.85; HRMS (ESI) m/z $[M+1]^+$: calcd for $C_{28}H_{31}ClN_2O$, 447.2198, found, 447.2194.

1-(4-((2,3-dihydro-1H-inden-5-yloxy)methyl)phenethyl)-4-(2,3-dichlorophenyl)piperazine (**22**)

White solid (ethyl acetate); Yield: 45%; Mp 77.2–78.4 °C; 1H NMR (500 MHz, $CDCl_3$) δ 7.40 (d, J = 7.9 Hz, 2H), 7.29 (d, J = 7.9 Hz, 2H), 7.20–7.14 (m, 3H), 7.01 (dd, J = 7.0, 2.5 Hz, 1H), 6.90 (br s, 1H), 6.80 (dd, J = 8.2, 2.0 Hz, 1H), 5.04 (s, 2H), 3.14 (br s, 4H), 2.93–2.83 (m, 6H), 2.83–2.66 (m, 6H), 2.14–2.06 (m, 2H); ^{13}C NMR (126 MHz, $CDCl_3$) δ 157.82, 151.28, 145.74, 139.92, 136.46, 135.21, 134.06, 128.92, 127.73, 127.48, 124.76, 124.62, 118.64, 112.83, 110.94, 70.11, 60.41, 53.30, 51.34, 33.35, 33.20, 32.01, 29.73, 25.86; HRMS (ESI) m/z $[M+1]^+$: calcd for $C_{28}H_{30}Cl_2N_2O$, 481.1808, found, 481.1796.

1-(4-((2,3-dihydro-1H-inden-5-yloxy)methyl)phenethyl)-4-(5-chloro-2-methylphenyl)piperazine (**23**)

White solid (ethyl acetate); Yield: 72%; Mp 87.4–88.3 °C; 1H NMR (500 MHz, $CDCl_3$) δ 7.42 (d, J = 8.0 Hz, 2H), 7.29 (d, J = 8.0 Hz, 2H), 7.16 (d, J = 8.2 Hz, 1H), 7.13 (d, J = 8.0 Hz, 1H), 7.03 (d, J = 2.0 Hz, 1H), 7.00 (dd, J = 8.0, 2.0 Hz, 1H), 6.92 (br s, 1H), 6.81 (dd, J = 8.0, 2.0 Hz, 1H), 5.05 (s, 2H), 3.00 (t, J = 5.0 Hz, 4H), 2.96–2.85 (m, 6H), 2.74–2.71 (m, 6H), 2.30 (s, 3H), 2.16–2.04 (m, 2H); ^{13}C NMR (126 MHz, $CDCl_3$) δ 157.84, 152.58, 145.75,

139.96, 136.47, 135.22, 131.97, 131.77, 130.82, 128.95, 127.75, 124.78, 122.97, 119.49, 112.85, 110.95, 70.11, 60.49, 53.57, 51.55, 33.36, 33.23, 32.04, 29.75, 25.88, 17.57; HRMS (ESI) m/z $[M+1]^+$: calcd for $C_{29}H_{33}ClN_2O$, 461.2354, found, 461.2350.

1-(4-((2,3-dihydro-1H-inden-5-yloxy)methyl)phenethyl)-4-(4-bromophenyl)piperazine (**24**)

White solid (ethyl acetate); Yield: 70%; Mp 114.1–115.2 °C; 1H NMR (500 MHz, $CDCl_3$) δ 7.40 (d, J = 8.0 Hz, 2H), 7.38 (d, J = 8.2 Hz, 2H), 7.28 (d, J = 8.0 Hz, 2H), 7.15 (d, J = 8.2 Hz, 1H), 6.90 (s, 1H), 6.83 (d, J = 8.5 Hz, 2H), 6.80 (d, J = 8.2 Hz, 1H), 5.04 (s, 2H), 3.24 (t, J = 5.0 Hz, 4H), 2.92–2.85 (m, 6H), 2.79–2.69 (m, 6H), 2.16–2.04 (m, 2H); ^{13}C NMR (126 MHz, $CDCl_3$) δ 157.81, 150.30, 145.75, 139.75, 136.48, 135.27, 131.89, 128.92, 127.74, 124.77, 117.66, 112.83, 111.88, 110.94, 70.09, 60.30, 53.01, 48.94, 33.23, 33.21, 32.02, 29.74, 25.86; HRMS (ESI) m/z $[M+1]^+$: calcd for $C_{28}H_{31}BrN_2O$, 491.1693, found, 491.1689.

1-(4-((2,3-dihydro-1H-inden-5-yloxy)methyl)phenethyl)-4-(2-(trifluoromethyl)phenyl)piperazine (**25**)

White solid (ethyl acetate); Yield: 46%; Mp 53.6–54.8 °C; 1H NMR (500 MHz, $CDCl_3$) δ 7.66 (d, J = 7.7 Hz, 1H), 7.55 (t, J = 7.7 Hz, 1H), 7.44 (d, J = 8.0 Hz, 1H), 7.41 (d, J = 7.9 Hz, 2H), 7.28 (d, J = 7.9 Hz, 2H), 7.26 (t, J = 7.7 Hz, 1H), 7.15 (d, J = 8.0 Hz, 1H), 6.91 (br s, 1H), 6.80 (dd, J = 8.1, 2.0 Hz, 1H), 5.04 (s, 2H), 3.04 (t, J = 5.0 Hz, 4H), 2.96–2.83 (m, 6H), 2.72 (m, 6H), 2.15–2.05 (m, 2H); ^{13}C NMR (126 MHz, $CDCl_3$) δ 157.84, 152.61, 145.74, 140.00, 136.45, 135.19, 132.76, 128.93, 127.73, 127.24, 127.19, 124.76, 124.05, 112.85, 110.95, 70.12, 60.52, 53.57, 53.45, 33.38, 33.21, 32.02, 25.86; HRMS (ESI) m/z $[M+1]^+$: calcd for $C_{29}H_{31}F_3N_2O$, 481.2461, found, 481.2458.

1-(4-((2,3-dihydro-1H-inden-5-yloxy)methyl)phenethyl)-4-(4-(trifluoromethyl)phenyl)piperazine (**26**)

White solid (ethyl acetate); Yield: 42%; Mp 135.3–136.5 °C; 1H NMR (500 MHz, $CDCl_3$) δ 7.52 (d, J = 8.6 Hz, 2H), 7.40 (d, J = 7.9 Hz, 2H), 7.28 (d, J = 7.9 Hz, 2H), 7.14 (d, J = 8.2 Hz, 1H), 6.96 (d, J = 8.6 Hz, 2H), 6.90 (br s, 1H), 6.79 (dd, J = 8.2, 2.0 Hz, 1H), 5.04 (s, 2H), 3.35 (t, J = 5.0 Hz, 4H), 2.93–2.85 (m, 6H), 2.77–2.65 (m, 6H), 2.15–2.05 (m, 2H); ^{13}C NMR (126 MHz, $CDCl_3$) δ 157.81, 153.28, 145.75, 139.72, 136.49, 135.30, 128.90, 127.73, 126.42, 126.39, 124.76, 114.54, 112.83, 110.94, 70.10, 60.28, 52.91, 47.96, 33.25, 33.20, 32.00, 29.71, 25.84; HRMS (ESI) m/z $[M+1]^+$: calcd for $C_{29}H_{31}F_3N_2O$, 481.2461, found, 481.2454.

Biological evaluation

Assay of antiproliferative activity

The antiproliferative activity of compounds **5–26** was assessed using the CCK-8 assay (Chen et al., 2016; Chen

et al., 2017; Chen et al., 2018; Han et al., 2020; Guo et al., 2021; Hu et al., 2022; Zhou et al., 2022). The 96-well plates (1×10^5 cells/mL) were seeded with cells in a medium, the plates were cultured at 37 °C for 24 h, then different concentrations of tested drugs were added, and the plates were cultured for 24 h. After 24 h, 10 μ L of CCK-8 solution (5 mg/mL) was added to the wells, and the cells were cultured for 1 h at 37 °C. Cell growth inhibition was performed by measuring the absorbance at 450 nm using a microplate reader, and the percentage of cell growth inhibition was then calculated for each tested drug.

Antagonistic activity in α_1 -ARs by dual-luciferase reporter gene assay

The AR antagonist effect of tested compounds was evaluated using the luciferase reporter gene assay (Xu et al., 2014; Xu et al., 2015; Zuo et al., 2017; Xu et al., 2018). Briefly, RLUs were used to indicate firefly and Renilla luciferase activity, and the activities were evaluated using dual luciferase assay kits (Promega) in accordance with the manufacturer's instructions. RLUs were measured using a GloMax™ 96-Microplate Luminometer (Promega) and three individual experiments were performed as the mean \pm SEM. For agonists, fold of induction = $LU_{\text{induced}}/LU_{\text{uninduced}}$. For antagonists, % of control = $100 \times RLU(\text{agonist} + \text{antagonist})/RLU(\text{agonist alone})$. All RLUs were normalized according to firefly RLUs/Renilla RLUs. EC_{50}/IC_{50} values were expressed as μ M, and Graph-pad Prism 5 software was used to calculate the IC_{50} of phenylephrine (μ M) by plotting the data using nonlinear regression analysis.

Fluorescence polarization

The binding of the derivatives 5, 8, 12, 14, 15, 19, 21, 22, 25, 26 and enzalutamide to the AR was analyzed by FP technique using the PolarScreen™ AR Competitor Assay according to the manufacturer's instructions (Chen et al., 2019a; Chen et al., 2019b). Briefly, titrations are performed between the tested compounds and the preformed Fluormone™AL Green and the AR-LBD (GST) complex. The tested mixture was allowed to equilibrate at room temperature in 384-well plates for 4 h. Then, the fluorescence polarization values of the tested mixture were performed using a SpectraMax®Paradigm® Multi-Mode Detection Platform at 485 nm (excitation wavelength) and 535 nm (emission wavelength). Data of the ligand binding assays were analyzed using Prism software (GraphPad Software, Inc.).

Molecular docking simulation

The crystal structure file (PDB code: 2OZ7) of the complex was downloaded from the protein crystal structure database

(Protein Data Bank, <http://www.rcsb.org/pdb/>) as the basis for molecular docking. Molecular docking was performed using the Surflex-Dock module in SYBYL-X2.0 and the program package in AutoDock (Chen et al., 2019a; Chen et al., 2019b). The X-ray crystallographic structures of androgen receptors were obtained from the RCSB Protein Data Bank (<http://www.rcsb.org/>). A box of $40 \times 40 \times 30$ Å³ around the binding site was built and grid spacing is 1 Å whose center was considered the geometric center of the ligand. Finally, the representative compounds and the exogenous ligands with 3D structure were docked into the binding cavity of AR to obtain the lowest energy docking method from 10 docking modes given by cluster analysis.

Results and discussions

Chemistry

Arylpiperazine derivatives 5–26 were synthesized using 1 as starting material (Scheme 1). Firstly compound 1 is reduced by borane–methyl sulfide complex (2 M in tetrahydrofuran) to obtain compound 2. The obtained crude products 2 were directly used in the next step without purification. Then, compound 3 was obtained after treatment of compound 2 and 2,3-dihydro-1H-inden-5-ol in the presence of potassium carbonate in acetonitrile. Subsequently, compound 4 was achieved by treatment of compound 3 with 4-toluene-ulfonyl chloride in the presence of triethylamine and 4-dimethylaminopyridine in methylene chloride. Finally, compound 4 was treated with the different arylpiperazines in the presence of potassium carbonate in acetonitrile to obtain arylpiperazine derivatives 5–26 (Yield: 40–90%). All synthesized derivatives were confirmed by ¹H NMR, ¹³C NMR, and HRMS.

SAR analysis for antiproliferative and AR antagonist assay

Antiproliferative activity of the novel arylpiperazine derivatives was firstly evaluated against LNCaP cells using the CCK-8 assay. Then, PC-3 cells were used to determine whether the arylpiperazine derivatives depended on AR to exhibit inhibitory activity and potent cytotoxic activities. Naftopidil and finasteride (Banday et al., 2014) were used as control compounds. RWPE-1 cells were used to compare their toxicity. To clarify whether the antiproliferative activity was related to any interference with AR function, the AR antagonist effect was evaluated using the luciferase reporter gene assay. In order to determine whether anti-proliferation activities of derivatives were related to the interference of AR function, the AR antagonist effect of tested compounds was evaluated using the luciferase reporter gene assay. The AR luciferase assays were conducted under the co-treatment of

TABLE 1 Antiproliferative and AR antagonist activity of derivatives 5–26.

Compound	PC-3 ^a IC ₅₀ (μM) ^b	LNCaP ^a IC ₅₀ (μM) ^b	RWPE-1 ^a IC ₅₀ (μM) ^b	AR antagonistic activity % (10 μM) ^c
5	>50	3.67 ± 0.14	>50	62.5 ± 1.2
6	11.34 ± 0.15	23.45 ± 0.12	11.58 ± 0.21	N.D
7	>50	15.29 ± 0.13	7.68 ± 0.15	N.D
8	>50	7.37 ± 0.15	>50	58.1 ± 0.8
9	>50	42.68 ± 0.14	10.96 ± 0.16	N.D
10	17.23 ± 0.21	20.87 ± 0.22	9.24 ± 0.23	N.D
11	4.31 ± 0.13	>50	>50	35.2 ± 1.1
12	25.62 ± 0.17	8.12 ± 0.11	>50	56.3 ± 1.2
13	>50	>50	>50	N.D
14	0.87 ± 0.12	3.09 ± 0.11	>50	56.2 ± 0.7
15	8.94 ± 0.21	9.72 ± 0.13	21.69 ± 0.23	54.4 ± 0.6
16	>50	18.56 ± 0.17	>50	N.D
17	1.45 ± 0.17	17.92 ± 0.13	>50	43.3 ± 0.7
18	1.92 ± 0.24	10.69 ± 0.14	>50	44.2 ± 0.5
19	>50	6.87 ± 0.06	32.67 ± 0.14	59.2 ± 0.9
20	1.56 ± 0.14	16.98 ± 0.15	>50	45.2 ± 0.3
21	>50	3.74 ± 0.24	>50	76.2 ± 0.4
22	23.48 ± 0.23	6.32 ± 0.14	>50	57.0 ± 1.2
23	0.95 ± 0.14	12.56 ± 0.22	>50	40.1 ± 0.8
24	2.31 ± 0.23	14.73 ± 0.15	>50	42.7 ± 1.1
25	>50	1.24 ± 0.15	>50	68.4 ± 0.5
26	>50	2.57 ± 0.24	>50	65.3 ± 1.2
Naftopidil	42.10 ± 0.79	22.36 ± 0.61	>50	N.D
Finasteride	17.80	13.53	N.D	N.D
R1881	N.D	N.D	N.D	N.E
Enzalutamide	N.D	N.D	N.D	84.7 ± 1.4

N.D, not determined.

N.E, no antagonistic effect.

^aPC-3, and LNCaP, human prostate cancer cell line; RWPE-1, normal non-cancer human prostate epithelial cell line.^bIC₅₀ values were the mean ± standard deviation of the three experiments.^cInhibition rate was shown as a ratio to the R1881 control.

1 nM AR agonist R1881, and the antagonistic activity was measured by inhibiting the R1881-induced luciferase expression.

As shown in Table 1, the derivatives 5, 8, 12, 15, 19, 21, 22, 25, and 26 exhibited strong cytotoxic activities against LNCaP cells (IC₅₀ <10 μM). Compared to arylpiperazine derivatives (Chen et al., 2016; Chen et al., 2017; Chen et al., 2019a), some derivatives exhibited potent cytotoxic activities against LNCaP cells. In addition, the majority of derivatives exhibited higher anticancer activity than reported arylpiperazine derivatives (Chen et al., 2016; Chen et al., 2017; Chen et al., 2018; Chen et al., 2019b) against PC-3 cells. Moreover, those derivatives displayed relatively strong AR-antagonistic potency (>55% inhibition), which exhibited higher antagonistic potency than previously reported derivatives (Chen et al., 2019a; <50% inhibition). Meanwhile, those derivatives displayed comparable antagonistic activity to ABO analogs containing the piperazine moiety (Chen et al., 2019b). But, compared to ABO analogs, the

derivatives 5, 21, 25, and 26 exhibited strong antagonistic potency against AR (>60% inhibition). Especially, derivative 21 demonstrated the highest antagonistic potency (76.2% inhibition). The derivatives 14 and 15 had relatively strong antagonistic potency against AR (>50% inhibition), consistent with the LNCaP cells' antiproliferation activity (IC₅₀ <10 μM). However, they also exhibited toxicity against PC-3 cells. Moreover, 11, 17, 18, 20, 23, and 24 displayed weak cytotoxic activities against LNCaP cells and weak antagonistic potency against AR. However, they displayed strong cytotoxic activities against PC-3 cells and exhibited low cytotoxic character toward RWPE-1 cells.

The SAR of the arylpiperazine derivatives was fully explored and discussed. Taking compound 5 as a lead compound, (1) first, compared with 6 and 7, strong cytotoxic activity was displayed by 5 against LNCaP cells (IC₅₀ = 3.67 μM), and it had potent antagonistic potency against AR (62.5% inhibition). These

TABLE 2 Binding affinity of 5, 8, 12, 14, 15, 19, 21, 22, 25, and 26 to mutant AR.

Compound	IC ₅₀ /μM ^a
5	1.46 ± 0.24
8	2.35 ± 0.09
12	2.53 ± 0.15
14	2.62 ± 0.25
15	2.85 ± 0.65
19	2.06 ± 0.21
21	0.65 ± 0.08
22	2.47 ± 0.11
25	1.22 ± 0.15
26	1.43 ± 0.18
Enzalutamide	1.32 ± 0.78

^aThe data represent the mean ± standard deviation of the three experiments.

results suggested that other aryl groups substituted at the 4-position of the piperazine ring were inauspicious for improved activity. However, estrone derivatives containing the piperazine moiety **6** (IC₅₀ = 1.42 μM) displayed strong cytotoxic activities against LNCaP cells (Chen et al., 2018). (2) The substitute's position and type on the phenyl group also affected the biological activities. Compared with **9** (3-CH₃) and **10** (4-CH₃), **8** (2-CH₃) displayed strong cytotoxic activity against LNCaP cells (IC₅₀ = 7.37 μM) and relatively strong antagonistic potency against AR (58.1% inhibition). Meanwhile, estrone piperazine derivatives (2-CH₃, IC₅₀ = 0.83 μM) displayed strong cytotoxic activity against LNCaP cells (Chen et al., 2018). However, other derivatives with a methyl substituent on the phenyl group exhibited weak cytotoxic activity against the tested cells (Chen et al., 2017; Chen et al., 2018). The activity profiles indicated that the *o*-substituted phenyl group derivative (2-CH₃) was beneficial for cytotoxic activity and antagonistic activity. (3) Compared with compounds **8** and **9**, relatively strong cytotoxic activities were exhibited by **11** (2,5-2CH₃) against PC-3 cells. Meanwhile, estrone piperazine derivative (2,5-2CH₃) also displayed strong cytotoxic activity against PC-3 cells (IC₅₀ = 3.41 μM). These results suggested that the disubstituted methyl derivative was beneficial for cytotoxic activities. (4) Methoxyl-substituted derivatives **12** (2-OCH₃), **14** (3-OCH₃), and **15** (4-OCH₃) had strong cytotoxic activities against LNCaP cells and relatively strong antagonistic potency against AR. But, methoxyl-substituted derivatives exhibited weak or no cytotoxic activity LNCaP cells except the derivative **11** (Chen et al., 2017; Chen et al., 2018). Moreover, the *m*-substituted phenyl group derivative (**14**) and *p*-substituted phenyl group derivative (**15**) also exhibited toxicity against PC-3 cells (Iwasa et al., 2007; Dreaden et al., 2012; George et al., 2018; Saito et al., 2018), and methoxyl-substituted derivatives also exhibited toxicity against PC-3 cells except the derivative **12** (Chen et al., 2017; Chen et al.,

TABLE 3 The binding affinities (kcal/mol) of docking of derivative 21 with three binding sites of AR.

Binding site	Compound 21
LBP (PDB ID: 2OZ7)	-10.8
AF2 (PDB ID: 2YHD)	-5.5
BF3 (PDB ID: 2YLO)	-5.6

2018). (5) Compared with **16**, strong cytotoxic activity was displayed by **17** and **18** against PC-3 cells. However, fluoro-substituted derivatives displayed weak cytotoxic activity against PC-3 cells (Chen et al., 2017; Chen et al., 2018). Moreover, these compounds displayed relatively weak antagonistic potency against AR (<50% inhibition). These findings indicated that fluoro-substituted phenyl group derivatives were inauspicious for improved activity. (6) Strong cytotoxic activities were displayed by **19** (2-Cl) and **21** (4-Cl) against LNCaP cells, and they had relatively strong antagonistic potency against AR and weak cytotoxic activity against PC-3 cells. The derivative **20** (3-Cl) displayed relatively weak antagonistic potency against AR and strong toxicity against PC-3 cells. However, **14** (2-Cl) and **16** (4-Cl) displayed weak cytotoxic activity against PC-3 and LNCaP cells, and **15** (3-Cl) displayed strong cytotoxic activity against PC-3 cells (Chen et al., 2017). In addition, in Chen et al. (2018), fluoro-substituted derivatives displayed strong cytotoxic activities against LNCaP cells except **18** and exhibited weak cytotoxic activity against PC-3 cells. (6) More effective cytotoxic activity was displayed by **23** (2-CH₃, 5-Cl, IC₅₀ = 0.95 μM) than **8** (2-CH₃) and **20** (3-Cl) against PC-3 cells. Activity profiles indicated that the introduction of methyl and chloro into the phenyl group was beneficial for cytotoxic activity. (7) The trifluoromethyl-substituted derivatives **25** and **26** exhibited strong cytotoxic activities against LNCaP cells (IC₅₀ <3 μM) and relatively strong antagonistic potency against AR (>65% inhibition). These derivatives also exhibited weak inhibitory activity toward PC-3 cells and normal human prostate epithelial cells (RWPE-1). However, in Chen et al. (2018) and Chen et al. (2017), the trifluoromethyl-substituted derivatives displayed weak cytotoxic activities against PC-3 and LNCaP cells except **21** against PC-3.

Taken together, compared to the reported derivatives (Chen et al., 2019a; Chen et al., 2019b), the SAR studies indicated that the *o*-substituted phenyl group derivatives displayed moderate to strong cytotoxic activities against LNCaP cells and relatively strong antagonistic potency against AR. These derivatives also exhibited weak inhibitory activity toward PC-3 cells, suggesting that these compounds depended on AR to exert inhibitory activity. The abovementioned results can also lead to a tool that can further design these derivatives as AR antagonists for *in vitro* and *in vivo* studies.

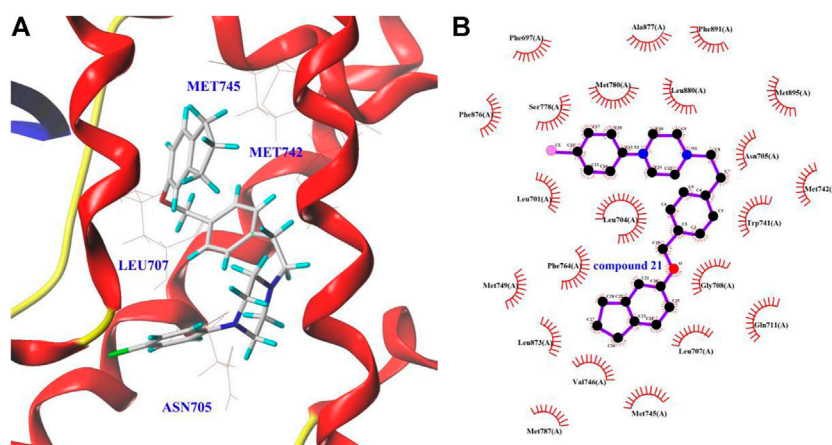


FIGURE 2
The docking view of compound **21**–AR interaction.

Binding affinity assay of arylpiperazine derivatives with potent AR antagonistic potency

To further study the binding affinity of the arylpiperazine derivatives with potent AR antagonistic potency, based on the fluorescent tracer and nonfluorescent antagonist competing for binding to AR, the binding affinity of **5**, **8**, **12**, **14**, **15**, **19**, **21**, **22**, **25**, and **26** to AR was examined using the binding assay by the fluorescence polarization technique. The results are shown in Table 2; the tested arylpiperazine derivatives exhibited strong AR-binding affinities ($IC_{50} < 3 \mu M$), and the majority of derivatives possessed higher binding affinities than some reported derivatives (Chen et al., 2019a; Chen et al., 2019b). Among these derivatives, the derivative **21** ($IC_{50} = 0.65 \mu M$) demonstrated the highest binding affinity to the AR, possessing higher binding affinities than enzalutamide ($IC_{50} = 1.32 \mu M$). Among all tested derivatives, a correlation can be identified between the effect on antagonistic activity and AR-binding affinity. For example, **5**, **21**, **25**, and **26** with higher affinity for AR ($IC_{50} < 2 \mu M$) also showed relatively strong antagonistic activity ($>60\%$ inhibition). These results indicated that the AR-binding affinity may play a key role in promoting the AR antagonistic activity, and these arylpiperazine derivatives may be efficient AR antagonists for PCa treatment. So, derivative **21** was selected to further investigate the binding site to the AR.

Docking study

To further understand the binding sites (ligand binding pocket (LBP), activation function-2 (AF2), and binding function 3 (BF3)) of the derivative **21** and AR, and to explore

their dominant interactions with AR, the docking experiment was carried out using SYBYL and AutoDock software (Axerio-Cilies et al., 2011; Lack et al., 2011). The results were summarized in Table 3.

As shown in Table 3, the binding free energy of derivative **21** with LBP was -10.8 kcal/mol. However, the binding free energy of it with AF2 and BF3 was between -5.5 and -5.6 kcal/mol, respectively. The results suggested that the AR-LBP site was the major binding site for derivative **21**. It can be observed in Figure 2 that the binding of derivative **21** to the AR-LBP site mainly through the hydrophobic interactions with Asn705, Met742, Met745, Leu707, etc. However, in Chen et al. (2019a), a molecular docking study suggested that derivative **16** mainly binds to the AR-LBP site by hydrogen bonding interactions, and in Chen et al. (2019b), ABO piperazine analogs **23** mainly bind to the AR-LBP site through the formation of Van der Waals force with amino acid residues.

Conclusion

In this work, 22 novel arylpiperazine derivatives were designed and synthesized, and their biological evaluation and molecular docking were reported. The derivatives **5**, **8**, **12**, **19**, **21**, **22**, **25**, and **26** exhibited strong cytotoxic activities against LNCaP cells versus PC-3 cells, and those derivatives displayed relatively strong AR antagonistic potency ($>55\%$ inhibition) and excellent AR-binding affinities ($IC_{50} < 3 \mu M$), which exhibited higher bioactivity than previously reported arylpiperazine derivatives. Among them, derivative **21** exhibited the highest binding affinity for AR ($IC_{50} = 0.65 \mu M$) and the highest antagonistic potency (76.2% inhibition). A molecular docking study suggested the binding of derivative **21** to the AR-LBP site

mainly occurred through the hydrophobic interactions with amino acid residues. The SAR studies suggested that the *o*-substituted phenyl group derivatives exhibited relatively improved bioactivity. These results can lead to a tool that can further design these novel derivatives as AR antagonists for *in vitro* and *in vivo* studies.

Data availability statement

The original contributions presented in the study are included in the article/Supplementary Material; further inquiries can be directed to the corresponding authors.

Author contributions

YQ, HC, and SC performed synthesis experiments. YQ, HC, and SC conducted the biological evaluation and molecular docking. YQ, JL, and JS designed experiments. YQ and HC interpreted the data and wrote the paper. All authors contributed to the article and approved the submitted version.

Funding

The work was supported by the Natural Science Foundation of China (No. 52173143), Zhongyuan Thousand Talents Plan

Project, Henan Province Science and Technology Attack Plan Foundation (Nos. 212102110241 and 222102310356), the Key Scientific Research Project of Higher Education of Henan Province (Nos. 21A350006 and 22B350004).

Conflict of interest

The authors declare that the research was conducted in the absence of any commercial or financial relationships that could be construed as a potential conflict of interest.

Publisher's note

All claims expressed in this article are solely those of the authors and do not necessarily represent those of their affiliated organizations, or those of the publisher, the editors, and the reviewers. Any product that may be evaluated in this article, or claim that may be made by its manufacturer, is not guaranteed or endorsed by the publisher.

Supplementary material

The Supplementary Material for this article can be found online at: <https://www.frontiersin.org/articles/10.3389/fchem.2022.947065/full#supplementary-material>

References

- Abate, C., Niso, M., Contino, M., Colabufo, N. A., Ferorelli, S., Perrone, R., et al. (2011). 1-Cyclohexyl-4-(4-aryl cyclohexyl) piperazines: Mixed σ and human $\Delta(8)$ - $\Delta(7)$ sterol isomerase ligands with antiproliferative and P-glycoprotein inhibitory activity. *ChemMedChem* 6, 73–80. doi:10.1002/cmdc.201000371
- Ananthan, S., Saini, S. K., Zhou, G., Hobrath, J. V., Padmalayam, I., Zhai, L., et al. (2014). Design, synthesis, and structure-activity relationship studies of a series of [4-(4-carboxamidobutyl)]-1-arylpiperazines: Insights into structural features contributing to dopamine D3 versus D2 receptor subtype selectivity. *J. Med. Chem.* 57, 7042–7060. doi:10.1021/jm500801r
- Arnatt, C. K., Adams, J. L., Zhang, Z., Haney, K. M., Li, G., Zhang, Y., et al. (2014). Design, syntheses, and characterization of piperazine based chemokine receptor CCR5 antagonists as anti-prostate cancer agents. *Bioorg. Med. Chem. Lett.* 24, 2319–2323. doi:10.1016/j.bmcl.2014.03.073
- Axerio-Cilies, P., Lack, N. A., Nayana, M. R., Chan, K. H., Yeung, A., Leblanc, E., et al. (2011). Inhibitors of androgen receptor activation function-2 (AF2) site identified through virtual screening. *J. Med. Chem.* 54, 6197–6205. doi:10.1021/jm200532b
- Banday, A. H., Giri, A. K., Parveen, R., and Bashir, N. (2014). Design and synthesis of D-ring steroidal isoxazolines and oxazolines as potential antiproliferative agents against LNCaP, PC-3 and DU-145 cells. *Steroids* 87, 93–98. doi:10.1016/j.steroids.2014.05.009
- Baran, M., Kepczynska, E., Zylewski, M., Siwek, A., Bednarski, M., Cegla, M. T., et al. (2014). Studies on novel pyridine and 2-pyridone derivatives of N-arylpiperazine as α -adrenoceptor ligands. *Med. Chem. Los Angeles* 10, 144–153. doi:10.2174/0929867320999131122114922
- Beedassy, A., and Cardi, G. (1999). Chemotherapy in advanced prostate cancer. *Semin. Oncol.* 26, 428–438. <https://pubmed.ncbi.nlm.nih.gov/10482185/>.
- Bentel, J. M., and Tilley, W. D. (1996). Androgen receptors in prostate cancer. *J. Endocrinol.* 151, 1–11. doi:10.1677/joe.0.1510001
- Berardi, F., Abate, C., Ferorelli, S., De Robertis, A. F., Leopoldo, M., Colabufo, N. A., et al. (2008). Novel 4-(4-Aryl)cyclohexyl-1-(2-pyridyl)piperazines as Δ_8 - Δ_7 sterol isomerase (emopamil binding protein) selective ligands with antiproliferative activity. *J. Med. Chem.* 51, 7523–7531. doi:10.1021/jm800965b
- Bosland, M. C. (2000). Chapter 2: The role of steroid hormones in prostate carcinogenesis. *JNCI Monogr.* 27, 39–66. doi:10.1093/oxfordjournals.jncimonographs.a024244
- Cao, S. L., Han, Y., Yuan, C. Z., Wang, Y., Xiahou, Z. K., Liao, J., et al. (2013). Synthesis and antiproliferative activity of 4-substituted-piperazine-1-carbodithioate derivatives of 2, 4-diaminoquinazoline. *Eur. J. Med. Chem.* 64, 401–409. doi:10.1016/j.ejmech.2013.04.017
- Chaudhary, P., Kumar, R., Verma, A. K., Singh, D., Yadav, V., Chhillar, A. K., et al. (2006). Synthesis and antimicrobial activity of N-alkyl and N-aryl piperazine derivatives. *Bioorg. Med. Chem.* 14, 1819–1826. doi:10.1016/j.bmc.2005.10.032
- Chen, H., Liang, X., Sun, T., Qiao, X. G., Zhou, Z., Li, Z. Y., et al. (2018). Synthesis and biological evaluation of estrone 3-O-ether derivatives containing the piperazine moiety. *Steroids* 134, 101–109. doi:10.1016/j.steroids.2018.02.002
- Chen, H., Xu, B. B., Sun, T., Zhou, Z., Ya, H. Y., Yuan, M., et al. (2017). Synthesis and antitumor activity of novel arylpiperazine derivatives containing the saccharin moiety. *Molecules* 22, 1857. doi:10.3390/molecules22111857
- Chen, H., Xu, F., Xu, B. B., Xu, J. Y., Shao, B. H., Huang, B. Y., et al. (2016). Design, synthesis and biological evaluation of novel arylpiperazine derivatives on human prostate cancer cell lines. *Bioorg. Med. Chem. Lett.* 27, 285–287. doi:10.1016/j.bmcl.2014.11.049
- Chen, H., Yu, Y. Z., Tian, X. M., Wang, C. L., Qian, Y. N., Deng, Z. A., et al. (2019a). Synthesis and biological evaluation of arylpiperazine derivatives as potential anti-prostate cancer agents. *Bioorg. Med. Chem.* 27, 133–143. doi:10.1016/j.bmc.2018.11.029

- Chen, H., Zhang, J. X., Hu, P. X., Qian, Y. N., Li, J., Shen, J. L., et al. (2019b). Synthesis, biological evaluation and molecular docking of 4-Amino-2Hbenzo[h]chromen-2-one (ABO) analogs containing the piperazine moiety. *Bioorg. Med. Chem.* 27, 115081. doi:10.1016/j.bmc.2019.115081
- Chen, X., Sassano, M. F., Zheng, L. Y., Setola, V., Chen, M., Bai, X., et al. (2012). Structure-Functional selectivity relationship studies of β -arrestin-biased dopamine D₂Receptor agonists. *J. Med. Chem.* 55, 7141–7153. doi:10.1021/jm300603y
- Culig, Z., Klocker, H., Bartsch, G., and Hobisch, A. (2002). Androgen receptors in prostate cancer. *Endocr. Relat. Cancer.* 9, 155–170. doi:10.1677/erc.0.0090155
- Dehm, S. M., and Tindall, D. J. (2007). Androgen receptor structural and functional elements: Role and regulation in prostate cancer. *Mol. Endocrinol.* 21, 2855–2863. doi:10.1210/me.2007-0223
- Dorff, T. B., and Glode, L. M. (2013). Current role of neoadjuvant and adjuvant systemic therapy for high-risk localized prostate cancer. *Curr. Opin. Urol.* 23, 366–371. doi:10.1097/MOU.0b013e328361d467
- Dreaden, E. C., Gryder, B. E., Austin, L. A., Tene Defo, B. A., Hayden, S. C., Pi, M., et al. (2012). Antiandrogen gold nanoparticles dual-target and overcome treatment resistance in hormone-insensitive prostate cancer cells. *Bioconjug. Chem.* 23, 1507–1512. doi:10.1021/bc300158k
- Gandaglia, G., Leni, R., Bray, F., Fleschner, N., Freedland, S. J., Kibel, A., et al. (2021). Epidemiology and prevention of prostate cancer. *Eur. Urol. Oncol.* 4, 877–892. doi:10.1016/j.euo.2021.09.006
- Gelmann, E. P. (2002). Molecular biology of the androgen receptor. *J. Clin. Oncol.* 20, 3001–3015. doi:10.1200/JCO.2002.10.018
- George, A., Raji, I., Cinar, B., Kucuk, O., and Oyelere, A. K. (2018). Design, synthesis, and evaluation of the antiproliferative activity of hydantoin-derived antiandrogen-genistein conjugates. *Bioorg. Med. Chem.* 26, 1481–1487. doi:10.1016/j.bmc.2018.01.009
- Guo, F. J., Sun, J., Gao, L. L., Wang, X. Y., Zhang, Y., Qian, S. S., et al. (2015). Discovery of phenylpiperazine derivatives as IGF-1R inhibitor with potent antiproliferative properties *in vitro*. *Bioorg. Med. Chem. Lett.* 25, 1067–1071. doi:10.1016/j.bmcl.2015.01.011
- Guo, Z. H., Shi, L. Q., Feng, H. Y., Yang, F., Li, Z. R., Zhang, J. J., et al. (2021). Reduction-sensitive nanomicelles: Delivery celastrol for retinoblastoma cells effective apoptosis. *Chin. Chem. Lett.* 32, 1046–1050. doi:10.1016/j.ccl.2020.03.066
- Gupta, S., Pandey, D., Mandalapu, D., Bala, V., Sharma, V., Shukla, M., et al. (2016). Design, synthesis and biological profiling of aryl piperazine based scaffolds for the management of androgen sensitive prostatic disorders. *MedChemComm* 7, 2111–2121. doi:10.1039/C6MD00426A
- Han, F. Q., Lv, S. P., Li, Z. R., Jin, L., Fan, B. B., Zhang, J. J., et al. (2020). Triple-synergistic 2D material-based dual-delivery antibiotic platform. *NPG Asia Mat.* 12, 15. doi:10.1038/s41427-020-0195-x
- Han, J. Y., Zhu, F. Q., Xu, X., Huang, H., Huang, W. Q., Cui, W. H., et al. (2013). Tetramethylpyrazine hydrochloride inhibits proliferation and apoptosis in human prostate cancer PC3 cells through Akt signaling pathway. *J. Third. Mil. Med. Univ.* 35, 105–108. doi:10.16016/j.1000-5404.2013.02.003
- Hu, F. Y., Song, B., Wang, X. H., Bao, S., Shang, S. Y., Lv, S. P., et al. (2022). Green rapid synthesis of Cu₂O/Ag heterojunctions exerting synergistic antibiosis. *Chin. Chem. Lett.* 33, 308–313. doi:10.1016/j.ccl.2021.07.018
- Iwasa, Y., Mizokami, A., Miwa, S., Koshida, K., and Namiki, M. (2007). Establishment and characterization of androgen-independent human prostate cancer cell lines, LN-REC4 and LNCaP-SF, from LNCaP. *Int. J. Urol.* 14, 233–239. doi:10.1111/j.1442-2042.2007.01532.x
- Kinoyama, I., Taniguchi, N., Kawaminami, E., Nozawa, E., Koutoku, H., Furutani, T., et al. (2005). N-aryl piperazine-1-carboxamide derivatives: A novel series of orally active nonsteroidal androgen receptor antagonists. *Chem. Pharm. Bull. (Tokyo)*. 53, 402–409. doi:10.1248/cpb.53.402
- Kinoyama, I., Taniguchi, N., Yoden, T., Koutoku, H., Furutani, T., Kudoh, M., et al. (2004). Synthesis and pharmacological evaluation of novel arylpiperazine derivatives as nonsteroidal androgen receptor antagonists. *Chem. Pharm. Bull. (Tokyo)* 52, 1330–1333. doi:10.1248/cpb.52.1330
- Lack, N. A., Axericiolies, P., Tavassoli, P., Han, F. Q., Chan, K. H., Feau, C., et al. (2011). Targeting the binding function 3 (BF3) site of the human androgen receptor through virtual screening. *J. Med. Chem.* 54, 8563–8573. doi:10.1021/jm201098n
- Lee, Y. B., Gong, Y. D., Yoon, H., Ahn, C. H., Jeon, M. K., Kong, J. Y., et al. (2010). Synthesis and anticancer activity of new 1-[(5 or 6-substituted 2-alkoxyquinoxalin-3-yl)aminocarbonyl]-4-(hetero)aryl piperazine derivatives. *Bioorg. Med. Chem.* 18, 7966–7974. doi:10.1016/j.bmc.2010.09.028
- Leopoldo, M., Lacivita, E., Passafiume, E., Contino, M., Colabufio, N. A., Berardi, F., et al. (2007). 4-[ω-[4-Arylpiperazin-1-yl]alkoxy]phenyl]imidazo[1,2-a]pyridine Derivatives: fluorescent high-affinity dopamine D₃ receptor ligands as potential probes for receptor visualization. *J. Med. Chem.* 50, 5043–5047. doi:10.1021/jm070721+
- Lin, H. H., Wu, W. Y., Cao, S. L., Liao, J., Ma, L., Gao, M., et al. (2013). Synthesis and antiproliferative evaluation of piperazine-1-carbothiohydrazide derivatives of indolin-2-one. *Bioorg. Med. Chem. Lett.* 23, 3304–3307. doi:10.1016/j.bmcl.2013.03.099
- Liu, W. H., Chang, J. X., Liu, Y., Luo, J. W., and Zhang, J. W. (2013). Design, synthesis and activities of novel benzothiazole derivatives containing arylpiperazine. *Acta. Pharm. Sin.* 48, 1259–1265. doi:10.16438/j.0513-4870.2013.08.002
- Loblaw, D. A., Walker-Dilks, C., Winquist, E., and Hotte, S. J. Genitourinary Cancer Disease Site Group of Cancer Care Ontario's Program in Evidence-Based Care (2013). Systemic therapy in men with metastatic castration-resistant prostate cancer: A systematic review. *Clin. Oncol. R. Coll. Radiol.* 25, 406–430. doi:10.1016/j.clon.2013.03.002
- Romeiro, L. A., Da Silva Ferreira, M., Da Silva, L. L., Castro, H. C., Miranda, A. L., Silva, C. L., et al. (2011). Discovery of LASSBio-772, a 1, 3-benzodioxole N-phenylpiperazine derivative with potent α 1A/D-adrenergic receptor blocking properties. *Eur. J. Med. Chem.* 46, 3000–3012. doi:10.1016/j.ejmech.2011.04.032
- Saito, Y., Mizokami, A., Tsurimoto, H., Izumi, K., Goto, M., Nakagawa-Goto, K., et al. (2018). 5'-Chloro-2, 2'-dihydroxychalcone and related flavanoids as treatments for prostate cancer. *Eur. J. Med. Chem.* 157, 1143–1152. doi:10.1016/j.ejmech.2018.08.069
- Sung, H., Ferlay, J., Siegel, R. L., Laversanne, M., Soerjomataram, I., Jemal, A., et al. (2021). Global cancer statistics 2020: GLOBOCAN estimates of incidence and mortality worldwide for 36 cancers in 185 countries. *Ca. A Cancer J. Clin.* 71, 209–249. doi:10.3322/caac.21660
- Taplin, M. E., and Balk, S. P. (2004). Androgen receptor: A key molecule in the progression of prostate cancer to hormone independence. *J. Cell. Biochem.* 91, 483–190. doi:10.1002/jcb.10653
- Xu, F., Chen, H., He, X. L., Xu, J. Y., Xu, B. B., Huang, B. Y., et al. (2014). Identification of two novel α 1-AR agonists using a high-throughput screening model. *Molecules* 19, 12699–12709. doi:10.3390/molecules190812699
- Xu, F., Chen, H., Xu, J. Y., Liang, X., He, X. L., Shao, B. H., et al. (2015). Synthesis, structure-activity relationship and biological evaluation of novel arylpiperazines as α 1A/1D-AR subselective antagonists for BPH. *Bioorg. Med. Chem.* 23, 7735–7742. doi:10.1016/j.bmc.2015.11.020
- Xu, X., Ge, R., Li, L., Wang, J., Lu, X., Xue, S., et al. (2018). Exploring the tetrahydroisoquinoline thiohydantoin scaffold blockade the androgen receptor as potent anti-prostate cancer agents. *Eur. J. Med. Chem.* 143, 1325–1344. doi:10.1016/j.ejmech.2017.10.031
- Zhou, Z., Wang, Y. L., Peng, F., Meng, F. Q., Zha, J. J., Ma, L., et al. (2022). Intercalation-activated layered MoO₃ nanobelts as biodegradable nanozymes for tumor-specific photo-enhanced catalytic therapy. *Angew. Chem. Int. Ed. Engl.* 61, e202115939. doi:10.1002/anie.202115939
- Zou, C., Li, X., and Jiang, R. (2012). The progress of molecular mechanism studies for Chinese traditional medicine on prostate cancer therapy. *Chin. J. Androl.* 26, 66–68. doi:10.3969/j.issn.1008-0848.2012.06.020
- Zuo, M., Xu, X., Xie, Z., Ge, R., Zhang, Z., Li, Z., et al. (2017). Design and synthesis of indoline thiohydantoin derivatives based on enzalutamide as antiproliferative agents against prostate cancer. *Eur. J. Med. Chem.* 125, 1002–1022. doi:10.1016/j.ejmech.2016.10.049



Advances in Research at Synthesis Process Optimization and Quality Standard Improvement of O-desmethylvenlafaxine Succinate

Shiwei Yang^{1*}, Shiyun Chen², Cheng Wang¹, Shibo Zhang¹, Shuaifei Li¹, Xinsong Yuan¹, Fuyun Peng¹ and Yong He^{3*}

¹Department of Chemistry and Chemical Engineering, Hefei Normal University, Hefei, China, ²Department of Chemistry and Chemical Engineering, Hefei University of Technology, Hefei, China, ³Department of Energy Materials and Chemical Engineering, Hefei University, Hefei, China

OPEN ACCESS

Edited by:

Veroniki P. Vidali,
National Centre of Scientific Research
Demokritos, Greece

Reviewed by:

Hamid Hashemi-Moghaddam,
Islamic Azad University Damghan, Iran
Stojan Stavber,
Institut Jožef Stefan (IJS), Slovenia

*Correspondence:

Shiwei Yang
yangsw@hfnu.edu.cn
Yong He
h13956000400@163.com

Specialty section:

This article was submitted to
Organic Chemistry,
a section of the journal
Frontiers in Chemistry

Received: 22 January 2022

Accepted: 10 June 2022

Published: 17 August 2022

Citation:

Yang S, Chen S, Wang C, Zhang S,
Li S, Yuan X, Peng F and He Y (2022)
Advances in Research at Synthesis
Process Optimization and Quality
Standard Improvement of
O-desmethylvenlafaxine Succinate.
Front. Chem. 10:860292.
doi: 10.3389/fchem.2022.860292

We herein describe an optimal approach for the efficient synthesis of O-desmethylvenlafaxine succinate monohydrate (DVS) with high yield and high purity through 5-step reactions, including benzyl protection of the phenolic hydroxyl group, cyclohexanone condensation, deprotection, cyano reduction, dimethylation, and succinic acid salt formation from *p*-hydroxybenzene acetonitrile as a starting material. 4-Benzyloxyphenylacetonitrile (Intermediate I) was prepared by the hydroxyl protection of the bromide benzyl-*p*-hydroxyphenylacetonitrile catalyzed by potassium carbonate with 99.83% purity and 98.92% yields. The 1, 2-nucleophilic addition of intermediate I to cyclohexanone promoted by sodium hydroxide with the homogeneous catalyst (n-Bu)₄N⁺Br⁻ to the preparation of 1-[Cyano(4-benzyloxyphenyl)methyl]cyclohexanol (Intermediate II) was obtained by 99.13% purity and 99.71% yields. Cyclohexanone residues and benzyl bromide residues were trace, and tetrabutylammonium bromide residues were UNDER 0.7 ppm, which further improves the residual standards for genotoxic impurities (GIs). 1-[2-amino-1-(4-hydroxyphenyl)ethyl]cyclohexanol hydrochloride (Intermediate III) was prepared by 10% palladium-carbon under 2.0 MPa up to 98.32% purity and 94.20% yields. O-desmethylvenlafaxine (ODV) was synthesized by dimethylation of intermediate III with 37% formaldehyde solution and 85% formic acid solution. The highest purity was up to 99.20% and the yield was up to 84.77%. O-desmethylvenlafaxine succinate monohydrate (DVS) was formed from succinic acid and O-desmethylvenlafaxine (ODV) and crystallized in a mixed solvent of acetone and water (3:1) to obtain 99.92% purity and 90.27% yields. The 5-step total yields of desvenlafaxine succinate monohydrate is 71.09%, and its crystal form has characteristic peaks at 5, 10, 21, and 26 min by XRD powder diffraction, which is consistent with the crystalline form I. Compared with conventional synthesis strategy, we revealed a novel and green process with a high total yield, high atomic economy, low environmental pollution, high operational safety, and high residual standards for genotoxic impurities (GIs), which improves drug safety.

Keywords: O-desmethylvenlafaxine, genotoxic impurities, XRD powder diffraction, 1, 2-nucleophilic addition, antidepressants

INTRODUCTION

O-desmethylvenlafaxine (Deecher et al., 2006; Sopko et al., 2008; Venu et al., 2008; Liu et al., 2016; Da Silva et al., 2020; Gahr et al., 2020) is the major active metabolite of the third serotonin-norepinephrine reuptake inhibitor (SNRI) venlafaxine approved by the US Food and Drug Administration for major depressive disorder (MDD), used to treat mild or severe depression, anxiety, and other mental disorders with superior clinical advantages (Klamerus et al., 1992; Safer and Zito, 2019; Zhang et al., 2019; Agüera-Ortiz et al., 2020). The efficacy, safety, or tolerability of preparation prescription drugs developed through O-desmethylvenlafaxine succinate (@Pristiq) has been favored by more and more psychiatrists as their first choice for the treatment of depression and anxiety (Khandpekar et al., 2014; Llorca et al., 2019). Therefore, the improvement of the novel synthesis process and quality standards of desvenlafaxine succinate has great practical significance and market value, attracting more and more synthetic scholars to conduct research (Kamath and Handratta, 2008; Duggirala et al., 2009; Colvard, 2014; Dichiarante et al., 2015; Furlan et al., 2015).

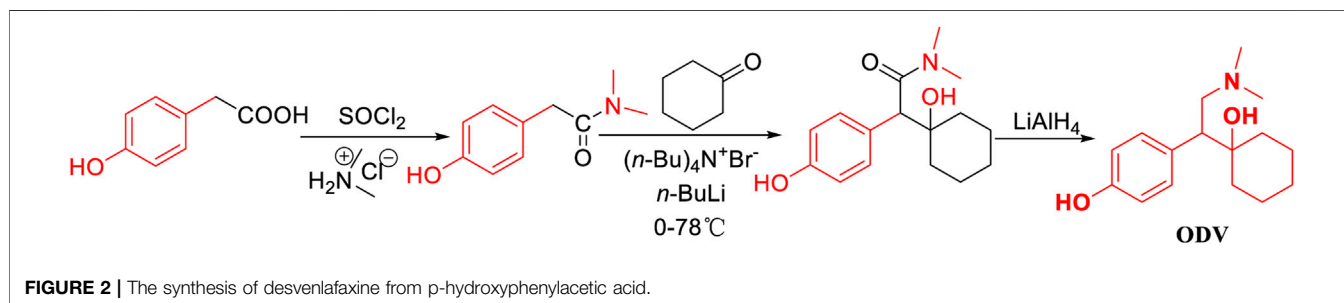
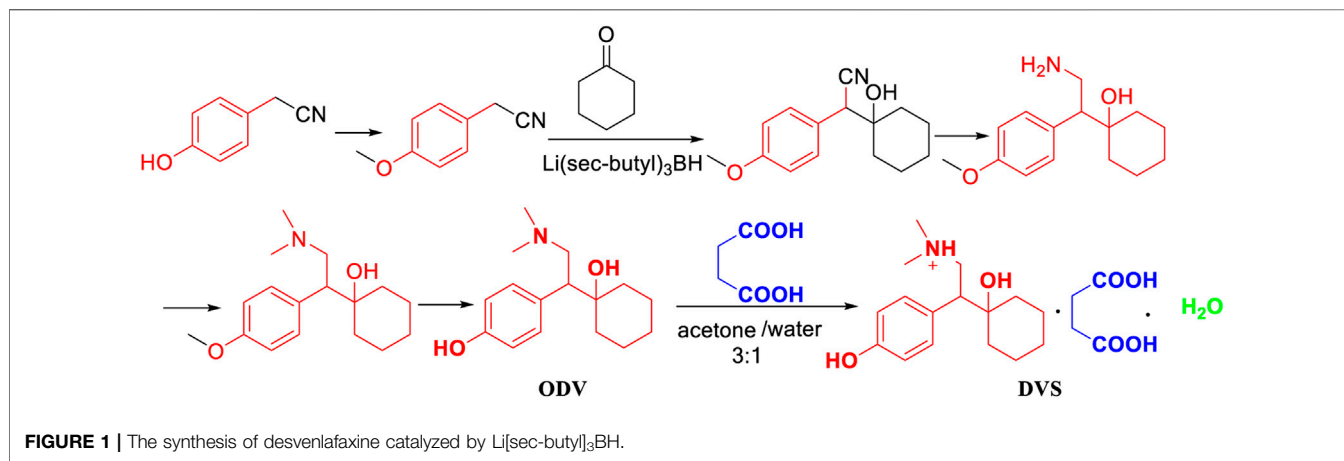
Hadfield, A. F. (Hadfield et al., 2009) reported that *p*-hydroxybenzene acetonitrile as the starting material was used to produce *p*-methoxybenzene acetonitrile with the action of methylating reagents (Figure 1). In addition, the flammable and irritating compound diphenylphosphine were used in relatively harsh conditions of the cyano group reduction,

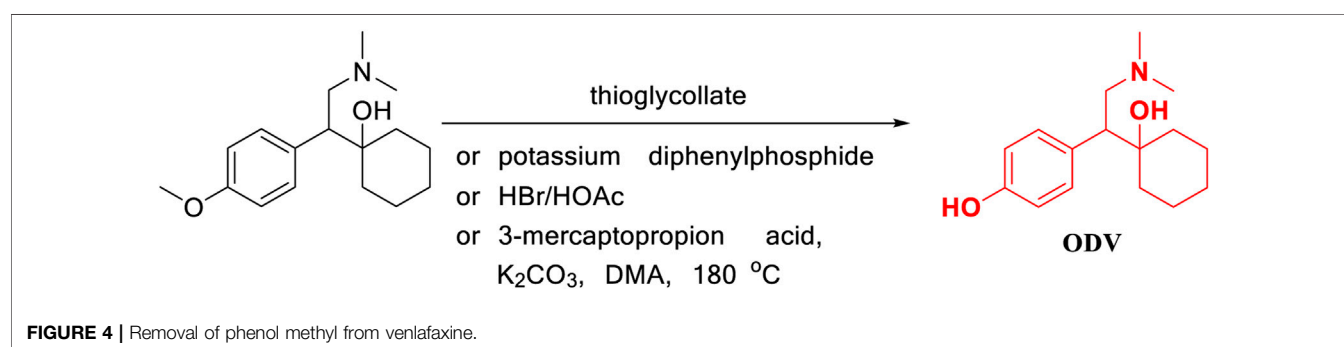
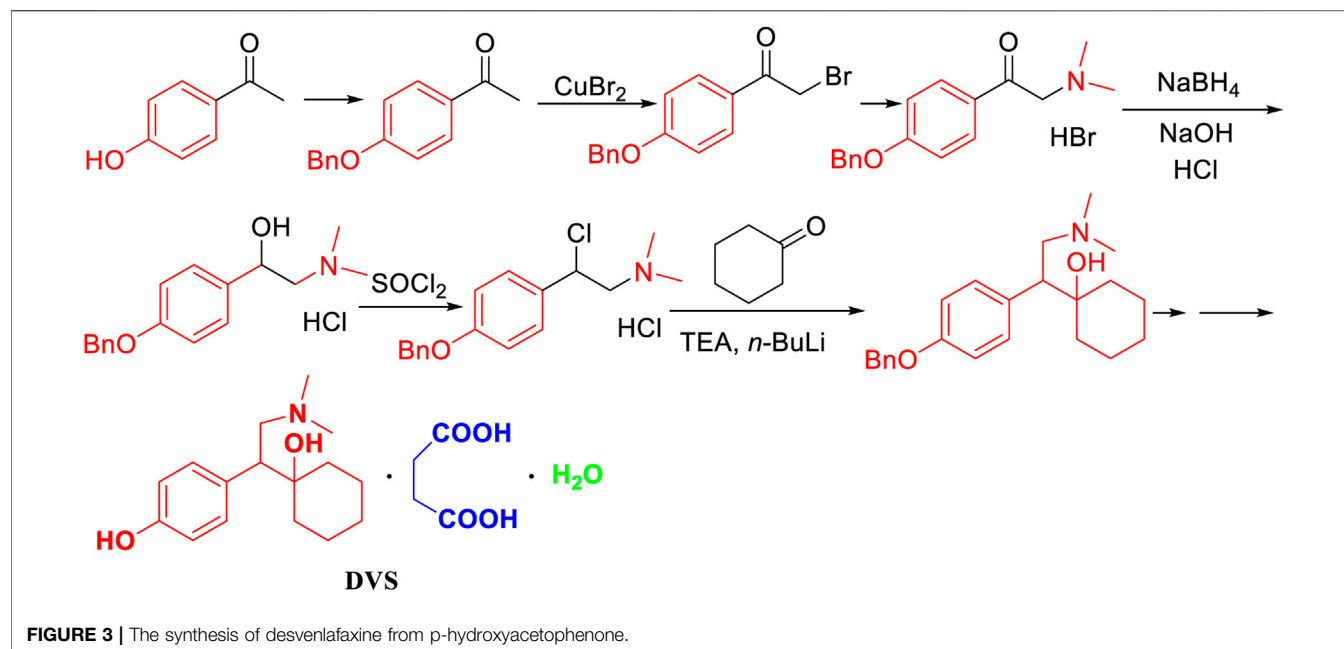
which does not meet the economic efficiency and is not suitable for industrial production.

Zuo, M. H. (Zuo et al., 2019) reported that the amide compound was prepared by acid halogenation and aminolysis and condensed with cyclohexanone from *p*-hydroxyphenylacetic acid as the starting material (Figure 2). In this method, the operation in the first two steps was complicated due to its use of acyl chloride reagent and dimethylamine aqueous solution in the condensation and amide reduction reaction steps.

Zhao, J. (Zhao et al., 2014) reported that benzyl-protected *p*-hydroxyacetophenone, which was synthesized by benzyl bromide under the existence of potassium carbonate, was halogenated under the action of copper dibromide and the dimethylation with 33% dimethylamine solution in bromine to prepared 1-(4-(benzyloxy)phenyl)-2-(dimethylamino)ethan-1-one hydrobromide (Figure 3). The method had long reaction steps and low yield. The dimethylamine aqueous solution and hydrogen bromide solution have a negative environmental impact. Moreover, the use of sodium borohydride greatly increases the risk factor of the reaction. The use of the *n*-butyl lithium and 10% Pd/C in the hydrogenation reaction of H₂ imposes higher requirements on the laboratory, which is not conducive to industrial production.

Jerussi, T. (Jerussi and Senanayake, 2005) reported that O-desmethylvenlafaxine was prepared using demethylation reagents such as mercaptan, diphenylphosphine, and HBr hydrobromide to remove phenol methyl from venlafaxine as





the starting material (**Figure 4**). In this method, the demethylation step uses toxic compounds that easily pollute the air, as well as mercaptans, flammable and irritating compounds such as diphenylphosphine, and a more corrosive compound HBr, which increases the difficulty of operation and subsequent production. The treatment process makes this type of reaction unsuitable for industrial production. In addition, Furlan, B. (Furlan et al., 2015) also reported a new strategy of 3-mercaptopropionic acid, which was introduced as a cheap new *O*-demethylating agent as exemplified by its application in the synthesis of antidepressant *O*-desmethylvenlafaxine from venlafaxine. The development of this method provides us with a new direction for the one-step synthesis of desvenlafaxine by venlafaxine.

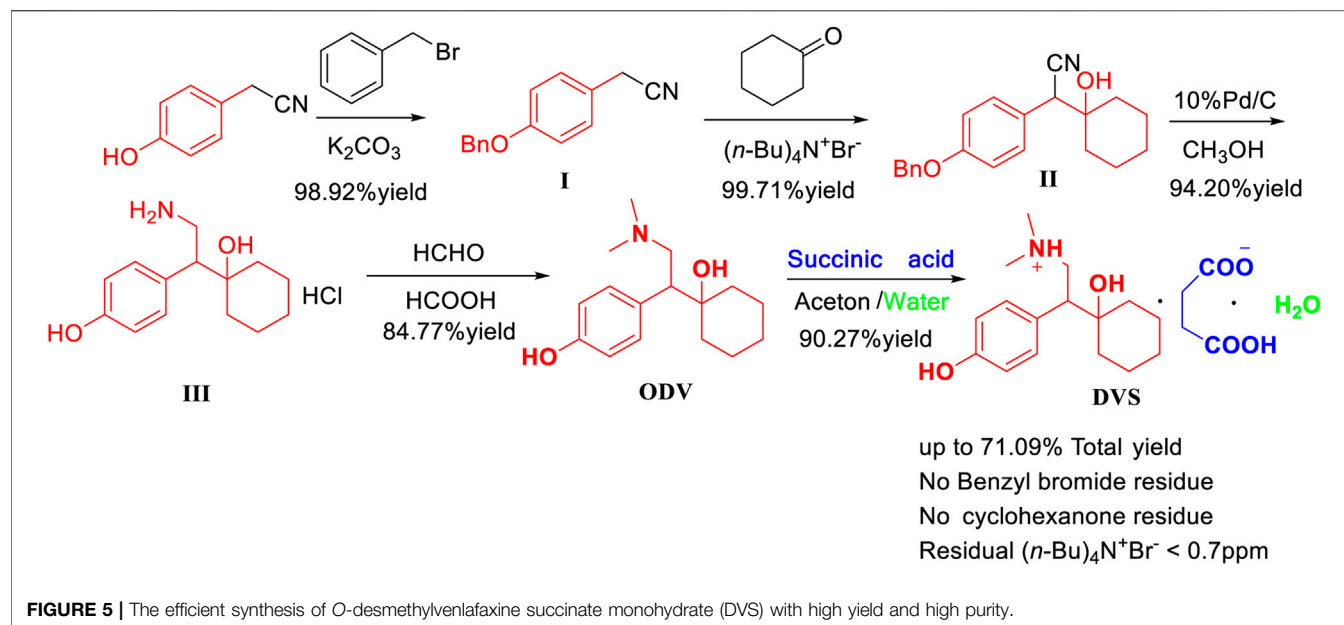
The process route method we designed overcomes the problem of cyclohexanone pollution in route five, and it uses *p*-hydroxyphenyl acetonitrile as the starting material to optimize the synthesis of desvenlafaxine with high yield. The yield of each step is high, and the raw materials are easily available. Reagent price is low, and no column

chromatography is needed, which is conducive to industrial production (**Figure 5**).

RESULTS AND DISCUSSION

Condition Optimization of Intermediate I

The synthesis of Intermediate I was based on *p*-hydroxybenzene acetonitrile as the starting material, under the action of an inorganic base to protect the hydroxyl group of benzyl bromide, wherein the molar equivalent ratio of *p*-hydroxybenzene acetonitrile to benzyl bromide had little effect on the purity of the product but much influence on the product yield. The more benzyl bromide equivalent, the more thorough the reaction. Under the premise of ensuring that the residual excess of benzyl bromide does not exceed the standard, 1.2 equivalent of benzyl bromide is selected for the reaction, and Intermediate I can be obtained with 99.83% purity and 90.10% yield (**Table 1**, I-2). The reaction time is optimized from 2 to 4 h. The reaction progress of different reaction times is tracked by

**TABLE 1 |** Condition optimization of Intermediate I.

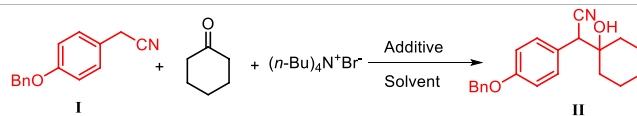
No.	n(Benzene acetonitrile)	n(Benzyl bromide)	Time/h	T/°C	Solvent	Additive	Purity/% ^a	Yield/% ^{b,e}
I-1	1	1.1	3	45	Acetone	K ₂ CO ₃	99.60	87.80
I-2	1	1.2	3	45	Acetone	K ₂ CO ₃	99.83	90.10
I-3	1	1.3	3	45	Acetone	K ₂ CO ₃	99.60	90.82
I-4	1	1.2	2	45	Acetone	K ₂ CO ₃	75.50 ^c	—
I-5	1	1.2	3	45	Acetone	K ₂ CO ₃	87.06 ^c	—
I-6	1	1.2	4	45	Acetone	K ₂ CO ₃	99.56^c	—
I-7	1	1.2	4	25	Acetone	K ₂ CO ₃	99.79	80.98
I-8	1	1.2	4	35	Acetone	K ₂ CO ₃	99.69	92.19
I-9	1	1.2	4	45	Acetone	K ₂ CO ₃	99.71	90.28
I-10	1	1.2	4	55	Acetone	K ₂ CO ₃	98.93	97.94
I-11	1	1.2	4	55	Acetone	K ₂ CO ₃	98.22	93.00
I-12	1	1.2	4	55	Methanol	K ₂ CO ₃	99.53	89.27
I-13	1	1.2	4	55	DCM	K ₂ CO ₃	0 ^d	0 ^d
I-14	1	1.2	4	55	Ethylacetate	K ₂ CO ₃	99.64	86.76
I-15	1	1.2	4	55	Acetone	K₂CO₃	99.42	98.92
I-16	1	1.2	4	55	Acetone	NaOH	99.04	83.96

^aDetected by HPLC.^bOne recrystallization without column chromatography separation.^cHPLC detects the reaction progress of the reaction solution.^dNo solid product is precipitated.^eIsolated yields % = (Actual isolated amount of product/Theoretical amount of product) × 100%.

The meaning of the bold values is to emphasize that this group of data with obvious advantages over other groups, and might be used as a potential optimal condition for further optimization.

high performance liquid chromatography. The results show that too short a time is not conducive to the formation of Intermediate I. The reaction time of 4 h reaches the highest reaction progress (Table 1, I-6). The reaction temperature mainly affects the yield of Intermediate I. The higher the temperature, the more favorable

the nucleophilic attack of the phenoxy anion on the benzyl methyl cation and the leaving of the bromide ion (Table 1, I-10). The reaction did not produce a solid product in dichloromethane. The purity of acetone, ethyl acetate, and methanol were similar, and the yield of ethyl acetate was not dominant (Table 1, I-14). Under

TABLE 2 | Condition optimization of Intermediate II.

No.	n(I)	n(Cyclohexanone)	n((n-Bu) ₄ N ⁺ Br ⁻)	n(NaOH)	Time/h	T/°C	Solvent	Purity/% ^a	Yield/% ^{b,g}
II-1	1	1.0	0.08	1.0	4	25	H ₂ O	94.42	90.00
II-2	1	2.0	0.08	1.0	4	25	H ₂ O	97.83	98.59
II-3	1	3.0	0.08	1.0	4	25	H ₂ O	95.62	94.64
II-4	1	2.0	0.06	1.0	4	25	H ₂ O	96.51	98.43
II-5	1	2.0	0.08	1.0	4	25	H ₂ O	93.15	99.71
II-6	1	2.0	1.00	1.0	4	25	H ₂ O	98.85	99.90
II-7	1	2.0	0.08	0.5	4	25	H ₂ O	93.50	93.00
II-8	1	2.0	0.08	1.0	4	25	H ₂ O	94.18	96.57
II-9	1	2.0	0.08	1.5	4	25	H ₂ O	94.72	92.15
II-10	1	2.0	0.08	1.0	2	25	H ₂ O	0.04 ^c	—
II-11	1	2.0	0.08	1.0	3	25	H ₂ O	72.92 ^c	—
II-12	1	2.0	0.08	1.0	4	25	H ₂ O	95.66^c	—
II-13	1	2.0	0.08	1.0	4	10	H ₂ O	96.97	95.57
II-14	1	2.0	0.08	1.0	4	25	H ₂ O	98.69	99.71
II-15	1	2.0	0.08	1.0	4	35	H ₂ O	96.97	94.86
II-16	1	2.0	0.08	1.0	4	25	H ₂ O	95.51	99.29
II-17	1	2.0	0.08	1.0	4	25	Acetone	5.71 ^d	30.01
II-18	1	2.0	0.08	1.0	4	25	CH ₃ OH	47.46 ^d	78.03
II-19	1	2.0	0.08	1.0	4	25	H₂O	99.13	95.44
II-20	1	2.0	0.08	1.0 ^e	4	25	H ₂ O	48.99	2.70
II-21	1	2.0	0.08	1.0 ^f	4	25	H ₂ O	99.42	95.86

^aDetected by HPLC.^bOne recrystallization without column chromatography separation.^cHPLC detects the reaction progress of the reaction solution.^dA small amount of solid product is precipitated.^eK₂CO₃.^fKOH.^gIsolated yields % = (Actual isolated amount of product / Theoretical amount of product) × 100%.

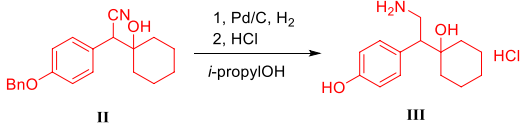
The meaning of the bold values is to emphasize that this group of data with obvious advantages over other groups, and might be used as a potential optimal condition for further optimization.

the conditions of similar yield and purity, acetone is the best reaction solvent (Table 1, I-11) from the perspective of atom economy and raw material production cost. Among them, the alkalinity of the inorganic base has a direct impact on the reaction. Too strong an alkalinity will increase by-products and affect the content of related substances and impurities in Intermediate I (Table 1, I-16). The alkalinity is too weak to prevent phenol. The H atom of the hydroxyl group undergoes anionization, thereby reducing the nucleophilic offensive activity of the oxygen anion on the benzyl methyl group of the benzyl bromide, which is not conducive to the departure of the bromide ion. Compared with other works, the synthesis process of Intermediate I has the advantages of higher yield and better purity, and the acetone solvent used can be continuously recovered by rotary evaporator, and has the advantage of continuous recycling after simple treatment.

Condition Optimization of Intermediate II

Intermediate I and cyclohexanone are condensed to synthesize Intermediate II under the condition of inorganic base catalysis.

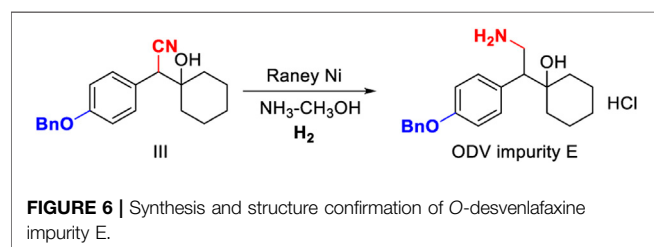
Under the action of phase transfer catalyst (n-Bu)₄N⁺Br⁻, the reaction solvent has good yield and purity in water. When the molar equivalent ratio of cyclohexanone to Intermediate I is 2.0, it is beneficial to the 1, 2-nucleophilic addition reaction of Intermediate I to the unsaturated carbonyl group on cyclohexanone. The yield is high, and the residual cyclohexanone is also removed in the subsequent process (Table 2, II-2). (n-Bu)₄N⁺Br⁻ is a genotoxic impurity, so the catalytic dosage is relatively strict. It ensures that the benzyl anion of Intermediate I undergoes a homogeneous reaction with cyclohexanone through phase transfer catalysis, and no more residues are allowed. To mitigate the risk of exceeding the standard, when the equivalent ratio of (n-Bu)₄N⁺Br⁻ to Intermediate I is 0.08, high yield and low residue results can be obtained (Table 2, II-5). Carbanionization of the benzyl methyl group of Intermediate I is also a crucial step, which directly determines the 1, 2-nucleophilic addition reaction activity to the unsaturated carbonyl group on cyclohexanone, so the choice of additives and additive equivalents is also very important. The condensation product was synthesized from

TABLE 3 | Condition optimization of Intermediate III.


No.	n(II)	10%Pd/C (m/m)	HCl (m/v)	Time/h	T/°C	Solvent	Purity/% ^a	Yield/% ^{b,e}
III-1	1	0.50	0.3	5	45	CH ₃ OH	0.07	33.97
III-2	1	0.40	0.3	5	45	CH ₃ OH	99.11	72.00
III-3	1	0.30	0.3	5	45	CH ₃ OH	98.82	87.00
III-4	1	0.30	0.3	5	45	CH ₃ OH	94.44	94.20
III-5	1	0.30	0.5	5	45	CH ₃ OH	91.31	85.13
III-6	1	0.30	1.0	5	45	CH ₃ OH	76.79	69.54
III-7	1	0.30	0.3	5	25	CH ₃ OH	90.42	77.32
III-8	1	0.30	0.3	5	35	CH ₃ OH	83.01	61.48
III-9	1	0.30	0.3	5	45	CH ₃ OH	90.82	86.75
III-10	1	0.30	0.3	5	45	CH₃OH	81.09	87.53
III-11	1	0.30	0.3	4	45	Ethanol	86.12	70.90
III-12	1	0.30	0.3	4	45	<i>i</i> -propanol	4.07 ^d	2.40 ^d
III-13	1	0.30	0.3	2	45	CH ₃ OH	66.93 ^c	—
III-14	1	0.30	0.3	3	45	CH ₃ OH	70.69 ^c	—
III-15	1	0.30	0.3	4	45	CH₃OH	74.15^c	—

^aDetected by HPLC.^bOne recrystallization without column chromatography separation.^cHPLC detects the reaction progress of the reaction solution.^dLittle amount of solid product is precipitated.^eIsolated yields % = (Actual isolated amount of product/Theoretical amount of product) × 100%.

The meaning of the bold values is to emphasize that this group of data with obvious advantages over other groups, and might be used as a potential optimal condition for further optimization.

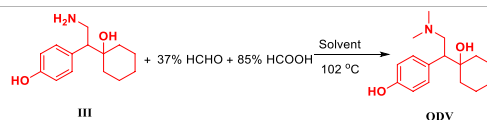


cyclohexanone and *p*-methoxybenzene acetonitrile catalyzed by Li[sec-butyl]₃BH. The cyanide was used as the raw material in this method, but at a slightly higher price. The reducing reagent of Li[sec-butyl]₃BH has a high risk factor for fire or explosion. The results show that when sodium hydroxide is used as an inorganic base, by-products increase at 1.5 equivalents (Table 2, II-9) and, at 0.5 equivalents, the reaction activity decreases and the reaction is incomplete (Table 2, II-7). In addition, the weak alkaline condition of the inorganic base is not conducive to the formation of benzyl methyl carbanion (Table 2, II-20). When the alkalinity is strong, the generated carbanion continues to produce intermediate 1, 2-nucleophilic addition to the unsaturated carbonyl group. Form II, the yield is higher (Table 2, II-21), the reaction is 4 h, the reaction is complete, and the reaction progress of the reaction solution is 95.66% (Table 2, II-12). The 1,2-nucleophilic addition reaction of the

carbanion to the unsaturated carbonyl group obtained by the action of sodium hydroxide with the benzyl methyl group of Intermediate I is relatively active, and the reaction temperature at the beginning of the condensation reaction should not be too high to reduce side effects. The formation of the product (Table 2, II-14) was compared with organic solvents as reaction solvents (Table 2, II-16, 17, 18), higher yield and purity could be obtained in water, with no organic waste liquid, and with the process being more green and economical. Moreover, the detection results of (*n*-Bu)₄N⁺Br⁻ and cyclohexanone showed that cyclohexanone was not detected, and the residual content of (*n*-Bu)₄N⁺Br⁻ was below the standard, with a minimum of 0.7 ppm, which is of great significance for improving the quality of APIs. Compared with other works, our synthesis process of intermediate II not only has the advantages of higher yield and better purity, but also does not involve the participation of organic solvents, which greatly reduces pollution and is environmentally friendly.

Condition Optimization of Intermediate III

The deprotection of the benzyl group and the reduction of the cyano group can be achieved by the palladium-carbon hydrogenation method at the same time. The harsh reaction conditions of a low temperature environment was used for the condensation step with *n*-butyl lithium, and used in the last step as the carbonyl reduction reagent reduced the convenience and safety of industrialized production. From

TABLE 4 | Condition optimization of ODV.

NO.	n(III)	37%HCHO	85%HCOOH	Solvent	Time/h	Purity/% ^a	Yield/% ^{b,e}
ODV-1	1	2.0	7.0	H ₂ O	24	94.87	64.28
ODV-2	1	2.5	7.0	H ₂ O	24	94.17	66.61
ODV-3	1	3.0	7.0	H ₂ O	24	94.38	69.64
ODV-4	1	4.0	7.0	H ₂ O	24	97.64	57.51
ODV-5	1	5.0	7.0	H ₂ O	24	98.77	56.33
ODV-6	1	6.0	7.0	H ₂ O	24	98.00	56.17
ODV-7	1	3.0	5.0	H ₂ O	24	98.13	68.74
ODV-8	1	3.0	7.0	H ₂ O	24	95.03	69.64
ODV-9	1	3.0	10.0	H ₂ O	24	98.11	67.04
ODV-10	1	3.0	5.0	CH ₃ OH	24	99.13	48.27
ODV-11	1	3.0	5.0	H ₂ O	24	95.12	70.24
ODV-12	1	3.0	5.0	<i>i</i>-propylOH	24	99.20	84.38
ODV-13	1	3.0	5.0	HCOOH	24	— ^d	—
ODV-14	1	3.0	5.0	<i>i</i> -propylOH	8	61.09 ^c	57.13
ODV-15	1	3.0	5.0	<i>i</i>-propylOH	24	84.18^c	83.04
ODV-16	1	3.0	5.0	<i>i</i>-propylOH	28	84.02^c	83.79
ODV-17	1	3.0	5.0	<i>i</i> -propylOH	30	85.19 ^c	84.62
ODV-18	1	3.0	5.0	<i>i</i> -propylOH	48	99.02	84.77

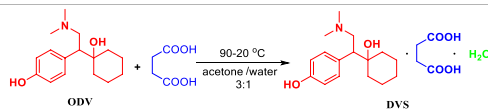
^aDetected by HPLC.^bOne recrystallization without column chromatography separation.^cHPLC detects the reaction progress of the reaction solution.^dA small amount of solid product is precipitated.^eIsolated yields % = (Actual isolated amount of product/Theoretical amount of product) × 100%.

The meaning of the bold values is to emphasize that this group of data with obvious advantages over other groups, and might be used as a potential optimal condition for further optimization.

the perspective of cost saving, we have optimized the process of palladium-carbon catalyst equivalent and recycling. The catalytic equivalent of 10% palladium-carbon reductant is 0.30, 87% yield (**Table 3**, III-3) can be obtained, and 0.60 equivalent of recovered palladium-carbon reducing agent has the same reducing effect. The addition of hydrochloric acid is beneficial to form a salt with the amine group in the product, so that the cyano group is continuously reduced to an amine group, and when the equivalent weight is 0.3, a yield of 94.20% and a purity of 94.44% (**Table 3**, III-4) are obtained. The increase in the equivalent of hydrochloric acid increases the by-products and causes the isomerization of *tertiary* alcohols in an unstable state under acidic conditions (**Table 3**, III-6). When the benzyl group is deprotected and the cyano group is reduced under pressure, the increase in temperature is favorable for the reaction to proceed (**Table 3**, III-7, 8, 9). When the protic solvent isopropanol is used as the reaction solvent, more raw materials remain (**Table 3**, III-12), and methanol has an advantage over ethanol in yield (**Table 3**, III-10, 11). The reaction time should not be less than 5 h. It can be seen from the results of HPLC tracking the reaction progress of the reaction solution (**Table 3**, III-13, 14, 15) that the reaction time is short to obtain the by-product desvenlafaxine impurity E, which is not sufficiently reduced (**Figure 6**).

Condition Optimization of ODV

The methylation reaction of the amine group is achieved by using formaldehyde solution and intermediate III to form an imine intermediate, and using formic acid as a hydrogen source to reduce the imine intermediate to an amine methyl. However, excess formaldehyde is unfavorable to the reaction, and the best equivalent range is 2.0–3.0 equivalents (**Table 4**, ODV-1,2,3). When the equivalent of formaldehyde exceeds 4 equivalents, the imine intermediate formed is more stable and not easily destroyed to obtain lower yield (**Table 4**, ODV-6). Similarly, the equivalent of formic acid is 5 equivalents. By continuing to increase the equivalent of formic acid, the product yield will not increase significantly, and the material cost will be increased at the same time (**Table 4**, ODV-7, 8, 9). We were surprised to find that the reaction obtained unexpectedly good results when isopropanol was used as the reaction solvent (**Table 4**, ODV-12, 18). The highest yield was 84.77%, and the highest purity was 99.20%. The liquid progress, product yield, and purity are far higher than the results of using water or methanol as the solvent (**Table 4**, ODV-10, 11). It is also a protic solvent. Methanol and water are more polar than isopropanol and are more likely to form a solvation effect with Intermediate III, which is not conducive to the formation of imine intermediates of formaldehyde. When formic acid is used as the reaction solvent and when the reaction is carried out under solvation-free conditions, few products are produced and the yield is very low. This also proves that

TABLE 5 | Condition optimization of DVS.

No.	n(ODV)	n(Succinic acid)	Time/h	Solvent (v/m)	Purity/% ^a	Yield/% ^{b,i}
DVS-1	1	0.90	4	10	99.79	51.72
DVS-2	1	0.95	4	10	99.72	59.47
DVS-3	1	1.00	4	10	99.69	58.00
DVS-4	1	0.95	2	10	99.90 (0918)	46.51
DVS-5	1	0.95	3	10	99.90 (0918)	53.97
DVS-6	1	0.95	4	10	99.92 (0918)	62.49
DVS-7	1	0.95	4	3	99.90 (0922)	68.74
DVS-8	1	0.95	4	5	99.90 (0922)	69.64
DVS-9	1	0.95	4	7	99.89 (0922)	67.04
DVS-10	1	0.95	4	5	99.90 (0924)	73.81
DVS-11	1	0.95	5	5	99.90 (0924)	85.95
DVS-12	1	0.95	6	5	99.90 (0924)	90.27
DVS-13 ^c	1	0.95	6	5	99.91 (0926)	89.46
DVS-14 ^d	1	0.95	6	5	99.90 (0926)	85.17
DVS-15 ^e	1	0.95	6	5	99.91 (0926)	82.39
DVS-16 ^f	1	0.95	6	5	99.92 (0927)	82.15
DVS-17 ^g	1	0.95	6	5	99.90 (0927)	80.62
DVS-18 ^h	1	0.95	6	5	99.90 (0927)	81.79

^aDetected by HPLC. (HPLC conditions: the filler is octadecylsilane-bonded silica gel; the mobile phase A is phosphate buffer (adjusted to pH 3.0 with phosphoric acid)-acetonitrile (90:10), and phosphate buffer (adjusted with phosphoric acid) is used as mobile phase A. pH to 3.0)-acetonitrile (40:60) as mobile phase B; detection wavelength at 225 nm; flow rate at 1.0 ml/min; column temperature at 35°C; injection volume at 10 µl).

^bOne recrystallization without column chromatography separation.

^cChange the cleaning solvent from acetone to ethyl acetate and isopropanol (1:1) (5 v/m).

^dChange the cleaning solvent from acetone to ethyl acetate and isopropanol (1:1) (10 v/m).

^eChange the cleaning solvent from acetone to ethyl acetate and isopropanol (1:1) (15 v/m).

^fCrystallization under complete solution conditions in ethyl acetate and isopropanol (1:1) (10 v/m).

^gBeating at 50 °C in ethyl acetate and isopropanol (1:1) (10 v/m).

^hBeating at room temperature in ethyl acetate and isopropanol (1:1) (10 v/m).

ⁱIsolated yields % = (Actual isolated amount of product/Theoretical amount of product) × 100%.

The meaning of the bold values is to emphasize that this group of data with obvious advantages over other groups, and might be used as a potential optimal condition for further optimization.

the greater the polarity of the protic solvent, the more unfavorable the progress of the reaction (Table 4, ODV -13).

Condition Optimization of DVS

The synthesis process of O-desmethylvenlafaxine succinate monohydrate crystalline form I is prepared by complete solution reaction and natural cooling and crystallization in a mixed solvent of acetone and water, and then purified by acetone cleaning to obtain qualified products. When the volume-to-mass ratio of the reaction solvent is 10 times the amount, 0.5 equivalent of succinic acid can obtain 99.72% purity and 59.47% yield (Table 5, DVS-2). The results of the reaction time of 2–4 h (Table 5, DVS-4, 5, 6) show that the longer the reaction time, the more conducive to crystallization, with a highest purity of 99.90% and a yield of 90.27% (Table 5, DVS-12) possible to obtain. Since O-desmethylvenlafaxine succinate monohydrate has a certain solubility in water, the more the amount of solvent, the less the product will be precipitated, and reducing the amount of solvent has a good effect on the product yield (Table 5, DVS-8). By changing the cleaning solvent acetone to a mixed solvent of ethyl acetate and isopropanol to achieve the maximum single impurity content control, it was found that as the

amount of mixed solvent increased, the purity of the product was 99.91%, and the yield was proportional to the amount of solvent. The inverse ratio shows that the refining effect of the mixed solvent at room temperature is not obvious (Table 5, DVS-13, 14, 15), and the highest refining effect of the mixed solvent under heating conditions is 99.92%, the single impurity content is 0.08%, and the yield is low (Table 5, DVS- 16, 17, 18), which has a greater impact on yield. XRD powder diffraction and DSC-TGA of the products prepared by mixed solvents have done XRD powder diffraction and DSC-TGA to detect the crystal form and crystal water of the product, showing that the crystal form has changed compared with the refining process of acetone (see SI).

EXPERIMENTAL SECTION

Synthesis of 4-Benzyloxyphenylacetonitrile

Add 200.0 g *p*-hydroxybenzene acetonitrile, 282.56 g benzyl bromide, and 1,000 ml acetone to a 3.0 L reaction flask. After the addition is complete, slowly add 320.28 g anhydrous potassium carbonate in batches, stir and react overnight at 55°C, and monitor the reaction by TLC (ethyl acetate: *n*-hexane = 5:1).

After the reaction is complete, the solvent is directly removed by rotary evaporation and a large amount of white solid precipitates out. Filter, rinse the filter cake with a large amount of water, and dry to obtain 331.19 g, 98.68% yield. $C_{15}H_{13}NO$, 1H NMR (400 MHz, Chloroform-*d*) δ 7.45–7.28 (m, 5H), 7.25–7.18 (m, 2H), 6.96 (d, J = 8.7 Hz, 2H), 5.05 (s, 2H), 3.65 (s, 2H). ^{13}C NMR (101 MHz, Chloroform-*d*) δ 158.57, 136.72, 129.17, 128.69, 128.13, 127.50, 122.14, 118.24, 115.53, 70.14, 22.85.

Synthesis of 1-[Cyano(4-benzyloxyphenyl)methyl]cyclohexanol

Add 250.0 g of Intermediate I and 500 ml of water to a 1.0 L three-necked reaction flask. Slowly add 176.02 g of cyclohexanone under stirring. After the addition is complete, add 22.0 g of $(n-Bu)_4N^+Br^-$, and then slowly add 100 ml of 36.0 g sodium hydroxide aqueous solution at the temperature of the reaction solution lower than 5°C, mechanically stir at lower than 20°C for 4 h after the addition is complete, and monitor the reaction by TLC (ethyl acetate: n-hexane = 5:1), a large amount of white solid precipitates, Filter, rinse the filter cake with a lot of water, and dry it to get 359.69g, the yield is 99.94%. $C_{21}H_{23}NO_2$, 1H NMR (400 MHz, Chloroform-*d*) δ 7.46–7.35 (m, 4H), 7.33 (dd, J = 8.3, 5.5 Hz, 1H), 7.26 (d, J = 8.7 Hz, 2H), 6.97 (d, J = 8.7 Hz, 2H), 5.06 (s, 2H), 3.72 (s, 1H), 1.71 (d, J = 13.1 Hz, 1H), 1.67–1.43 (m, 9H), 1.18 (dd, J = 12.7, 6.2 Hz, 1H). ^{13}C NMR (101 MHz, Chloroform-*d*) δ 158.97, 136.68, 130.72, 128.69, 128.15, 127.52, 123.98, 119.88, 115.00, 72.77, 70.14, 49.38, 34.98, 34.90, 25.22, 21.59, 21.51.

Synthesis of 1-[2-amino-1-(4-hydroxyphenyl)ethyl]cyclohexanol Hydrochloride

Add 300.0 g of Intermediate II, 3,000 ml of industrial methanol to a 5.0 L high pressure hydrogenation reactor, slowly add 99.99 g 10% Pd/C under stirring. Then slowly add 90.00 ml of concentrated hydrochloric acid, reacting at 45°C and 2.0 MPa pressure for 4 h, monitored by TLC (ethyl acetate: n-hexane = 2.5:1). After the reaction is complete, the solvent is directly removed by rotary evaporation and a large amount of white solid precipitates. The solid is recrystallized twice with ethyl acetate and dried to obtain 179.90 g. The yield is 82.52%. $C_{14}H_{22}NO_2Cl$, 1H NMR (400 MHz, DMSO-*d*₆) δ 9.43 (s, 1H), 7.78 (s, 3H), 7.06 (s, 2H), 6.75 (s, 2H), 4.46 (s, 1H), 3.06 (t, J = 11.8 Hz, 1H), 2.82 (s, 1H), 1.78–0.86 (m, 11H). ^{13}C NMR (101 MHz, DMSO-*d*₆) δ 157.00, 131.02, 128.53, 115.51, 72.24, 53.20, 36.80, 33.81, 25.81, 21.89, 21.57.

Synthesis of O-Desvenlafaxine

Add 150.0 g of Intermediate III and 1,500 ml of isopropanol to a 3,000 ml single-necked reaction flask. Slowly add 153.30 g of 37% formaldehyde solution with stirring, stir for 2 h at 20°C, and then slowly add 176.70 g of 85% formic acid solution, at 103°C. The reaction is monitored by TLC (dichloromethane: methanol: trimethylamine = 2.5:10:1.0 drop). After the reaction is complete, the solvent is removed by rotary evaporation to a syrupy state, 500 ml

of water is added, and filtered to remove floating insoluble matter. The filtrate is added for cleaning with 300 ml of toluene, liquid separation, and removal. Water layer is adjusted to pH 9.5 with 50% sodium hydroxide solution and filtered to obtain crude solids. Recrystallize once with 1,500 ml water at 90°C, filter the residue with 300 ml ethyl acetate, and then 300 ml isopropyl alcohol is recrystallized once at 70°C, recrystallized twice, and dried to obtain 146.47 g, with a yield of 87.70%. $C_{16}H_{25}NO_2$, 1H NMR (400 MHz, DMSO-*d*₆) δ 9.11 (s, 1H), 6.96 (d, J = 6.9 Hz, 2H), 6.64 (d, J = 6.9 Hz, 2H), 5.41 (s, 1H), 3.12–2.86 (m, 1H), 2.72 (s, 1H), 2.40–2.25 (m, 1H), 2.14 (s, 6H), 1.61–1.25 (m, 8H), 1.19–0.81 (m, 3H). ^{13}C NMR (101 MHz, DMSO-*d*₆) δ 156.04, 132.18, 130.55, 114.87, 73.03, 60.92, 52.10, 45.77, 37.64, 32.86, 26.18, 21.74, 21.69. ESI $[M + H]^+$ 264.10.

Synthesis of O-Desmethylvenlafaxine Succinate Monohydrate (DVS)

Add 64 g desvenlafaxine, 27.30 g succinic acid, 300 ml acetone, and 100 ml water to an 1,000 ml round bottom flask, and stir well. Slowly raise the temperature to 90°C and stir for 1 h to dissolve all into a colorless and transparent shape. Cool down to 60°C and filter to remove trace insoluble matter. Continue to lower the temperature to 35°C, stir for 6 h, and make the product fully discharged. Cool and filter in an ice-water bath, wash the filter cake with 100 ml ethyl acetate and 100 ml isopropanol, drain well, and dry at 60°C for 3 h to obtain the finished product of desvenlafaxine succinate monohydrate, a total of 82.40 g. The yield is 85.83%. $C_{20}H_{32}NO_7$, 1H NMR (400 MHz, D₂O) δ 7.19 (d, J = 8.3 Hz, 2H), 6.83 (d, J = 8.7 Hz, 2H), 3.64 (t, J = 12.5 Hz, 1H), 3.51 (dd, J = 13.1, 4.0 Hz, 1H), 2.97 (dd, J = 12.0, 4.0 Hz, 1H), 2.76 (s, 3H), 2.70 (s, 3H), 2.44 (s, 4H), 1.60 (d, J = 13.4 Hz, 1H), 1.48–1.38 (m, 3H), 1.35 (dt, J = 7.3, 4.2 Hz, 1H), 1.33–1.23 (m, 2H), 1.19 (dd, J = 10.3, 4.5 Hz, 2H), 1.06–0.98 (m, 1H). ^{13}C NMR (101 MHz, Deuterium Oxide) δ 179.65, 155.41, 127.44, 115.69, 73.31, 58.36, 50.32, 45.04, 41.37, 35.00, 33.87, 31.31, 24.85, 21.23, 20.99.

Synthesis and Structure Confirmation of O-Desvenlafaxine Impurity E

Add 1-[Cyano(4-benzyloxyphenyl)methyl]cyclohexanol 20.00 g, 15.00 g Raney nickel, and 18 g amine methanol solution to 1.0 L hydrogenation reactor, ventilate at 1.50 MPa, and react at 55°C and 2.0 Mpa pressure for 4 h. After the reaction, lower the temperature to below 30°C, remove the remaining gas, open the autoclave, and remove the reaction solution. Remove the solvent by rotary evaporation to a syrupy state, add ethyl acetate and stir uniformly. Slowly add concentrated hydrochloric acid under ice-water bath conditions, and a white solid precipitates. The white solid is filtered, the filter cake is washed twice with 100 ml ethyl acetate, and dried at 55°C for 2 h to obtain 16.77 g with a yield of 99.70%. $C_{21}H_{27}NO_2$, 1H NMR (400 MHz, DMSO-*d*₆) δ 7.84 (s, 3H), 7.50–7.44 (m, 2H), 7.44–7.38 (m, 2H), 7.38–7.28 (m, 1H), 7.22 (d, J = 8.5 Hz, 2H), 6.98 (d, J = 8.7 Hz, 2H), 5.08 (s, 2H), 3.15–3.05 (m, 1H), 2.99–2.82 (m, 1H), 1.57 (d, J = 10.5 Hz, 2H), 1.49–1.37 (m, 3H), 1.34–1.13 (m,

3H), 1.12–0.98 (m, 2H). ^{13}C NMR (101 MHz, DMSO- d_6) δ 157.98, 137.68, 131.24, 130.79, 128.93, 128.33, 128.22, 128.10, 114.77, 72.15, 69.66, 53.04, 36.76, 34.07, 25.78, 21.89, 21.57.

CONCLUSION

Through our continuous optimization of the existing process, the high yield and high purity synthetic preparation of Intermediate I and Intermediate II is obtained. The process of Intermediate II is more green, and there is no organic waste liquid to eliminate the pollution impact on the environment. At the same time, the residues of benzyl bromide and $(n\text{-Bu})_4\text{N}^+\text{Br}^-$ with genotoxic impurities are below the standard limit, which improves the quality of raw materials and makes the drug market safer. The preparation of Intermediate III adopts a low pressure, normal temperature, and dilute acid process conditions, which to a certain extent reduces the safety risk of high pressure and high temperatures in the reduction and hydrogenation of difunctional groups, simplifies post-processing and refining operations, and is more conducive to large-scale industrial production. The preparation process of O-desvenlafaxine was revealed that isopropanol, as a protic solvent, exhibits special advantages in the dimethylation step, and isopropanol can also be recycled and reused. The method can prepare desvenlafaxine succinate with high yield and high purity, and different new crystal forms can be obtained by using different refining conditions, which has important reference significance for formulation process development in formulation research and development.

DATA AVAILABILITY STATEMENT

The original contributions presented in the study are included in the article/**Supplementary Material**, further inquiries can be directed to the corresponding authors.

REFERENCES

- Agüera-Ortiz, L., Claver-Martín, M. D., Franco-Fernández, M. D., López-Álvarez, J., Martín-Carrasco, M., Ramos-García, M. I., et al. (2020). Depression in the elderly. Consensus statement of the Spanish psychogeriatric association. *Front. Psychiatry* 11, 380. doi:10.3389/fpsy.2020.00380
- Colvard, M. D. (2014). Key differences between Venlafaxine XR and Desvenlafaxine: An analysis of pharmacokinetic and clinical data. *Ment. Health Clin.* 4, 35–39. doi:10.9740/mhc.n186977
- Da Silva, J. D., de Sousa, V. P., Cabral, L. M., Davanço, M. G., Meulman, J., de Oliveira Carvalho, P., et al. (2020). *In vitro-in vivo* correlation for desvenlafaxine succinate monohydrate extended release tablets. *AAPS PharmSciTech* 21 (5), 195–199. doi:10.1208/s12249-020-01740-x
- Deecher, D. C., Beyer, C. E., Johnston, G., Bray, J., Shah, S., Abou-Gharbia, M., et al. (2006). Desvenlafaxine succinate: A new serotonin and norepinephrine reuptake inhibitor. *J. Pharmacol. Exp. Ther.* 318, 657–665. doi:10.1124/jpet.106.103382
- Dichiarante, E., Curzi, M., Giaffreda, S. L., Grepioni, F., Maini, L., and Braga, D. (2015). Crystal forms of the hydrogen oxalate salt of o-desmethylvenlafaxine. *J. Pharm. Pharmacol.* 67, 823–829. doi:10.1111/jphp.12378
- Duggirala, N. K., Kanniah, S. L., Muppidi, V. K., Thaimattam, R., and Devarakonda, S. (2009). Polymorphism in desvenlafaxine

AUTHOR CONTRIBUTIONS

YSW conceived the review. PFY and CSY collected the literatures. YXS collected the IR spectra. YSW wrote the manuscript. YSW and HY edited the manuscript. All authors read and approved the final version of the manuscript.

FUNDING

Hefei Normal University School-level Scientific Research Natural Science Key Project (2021KJZD0 4); Hefei Postdoctoral Fund Project (Grade A). The Key project of Anhui Provincial Department of Education, (KJ 2020A672); The Open Fund Project of Anhui Key Laboratory of Pharmaceutical Preparation Technology and Application (2021KFKT01, 2021KFKT08); Key Research Project of Natural Science in Universities in Anhui Province (KJ 2021A0932).

ACKNOWLEDGMENTS

The authors gratefully acknowledge the test service support provided by the University of Science and Technology of China and financial support provided by Hefei Normal University. We also gratefully acknowledge Professor Wu Zonghao from Hefei Huafang Pharmaceutical Technology Co., Ltd. for his guidance and support.

SUPPLEMENTARY MATERIAL

The Supplementary Material for this article can be found online at: <https://www.frontiersin.org/articles/10.3389/fchem.2022.860292/full#supplementary-material>

- succinate monohydrate. *CrystEngComm* 11 (6), 989–992. doi:10.1039/B821274K
- Furlan, B., Časar, Z., Šterk, D., and Fabris, J. (2015). 3-Mercaptopropionic acid as a new reagent for the industrially applicable synthesis of highly pure O-desmethylvenlafaxine from venlafaxine. *J. Sulfur Chem.* 36, 67–73. doi:10.1080/17415993.2014.964241
- Gahr, M., Hiemke, C., and Kölle, M. A. (2020). Development of obsessive-compulsive symptoms following abrupt discontinuation of venlafaxine. *Front. Psychiatry* 11, 32. doi:10.3389/fpsy.2020.00032
- Hadfield, A. F., Shah, S. M., Winkley, M. W., Sutherland, K. W., Provost, J. A., Park, A., et al. (2009). O-Desmethylvenlafaxine succinate salts. U.S. Patent Application No. 11/841, 638.
- Jerussi, T., and Senanayake, C. (2005). Methods of preparing O-desmethylvenlafaxine. U.S. Patent Application No. 11/091, 518.
- Kamath, J., and Handratta, V. (2008). Desvenlafaxine succinate for major depressive disorder: A critical review of the evidence. *Expert Rev. Neurother.* 8, 1787–1797. doi:10.1586/14737175.8.12.1787
- Khandpekar, M. (2014). Comparative studies on synthesis and structure of old and new polymorphs of desvenlafaxine-an antidepressant drug. *Indones. J. Pharm.* 25, 25. doi:10.14499/indonesianjpharm25iss1pp25
- Klamerus, K. J., Moloney, K., Rudolph, R. L., Sisenwine, S. F., Jusko, W. J., and Chiang, S. T. (1992). Introduction of a composite parameter to

- the pharmacokinetics of venlafaxine and its active O-desmethyl metabolite. *J. Clin. Pharmacol.* 32, 716–724. doi:10.1002/j.1552-4604.1992.tb03875.x
- Liu, M., Sun, Y., Zhao, S., Li, Y., Piao, R., Yang, Y., et al. (2016). A novel prodrug strategy to improve the oral absorption of O-desmethylvenlafaxine. *Exp. Ther. Med.* 12, 1611–1617. doi:10.3892/etm.2016.3453
- Llorca, M., Castellet-Rovira, F., Farré, M. J., Jaén-Gil, A., Martínez-Alonso, M., Rodríguez-Mozaz, S., et al. (2019). Fungal biodegradation of the N-nitrosodimethylamine precursors venlafaxine and O-desmethylvenlafaxine in water. *Environ. Pollut.* 246, 346–356. doi:10.1016/j.envpol.2018.12.008
- Safer, D. J., and Zito, J. M. (2019). Short-and long-term antidepressant clinical trials for major depressive disorder in youth: Findings and concerns. *Front. Psychiatry* 10, 705. doi:10.3389/fpsyt.2019.00705
- Sopko, M. A., Jr, Ehret, M. J., and Grgas, M. (2008). Desvenlafaxine: Another “me too” drug? *Ann. Pharmacother.* 42, 1439–1446. doi:10.1345/aph.1K563
- Venu, N., Sreekanth, B. R., Ram, T., and Devarakonda, S. (2008). Desvenlafaxine succinate monohydrate. *Acta Crystallogr. C* 64, o290–o292. doi:10.1107/S0108270108010019
- Zhang, Y., Bi, X., Adebisi, O., Wang, J., Mooshekhian, A., Cohen, J., et al. (2019). Venlafaxine improves the cognitive impairment and depression-like behaviors in a cuprizone mouse model by alleviating demyelination and neuroinflammation in the brain. *Front. Pharmacol.* 10, 332. doi:10.3389/fphar.2019.00332
- Zhao, J., Shang, W. D., and Xue, N. (2014). Synthesis of desvenlafaxine. *China Pharm. Industry J.* 45 (7), 601–603. CNKI:SUN:ZHOU.0.2014-07-001.
- Zuo, M. H., Shao, F., and He, Y. L. (2016). Progress in synthesis of desvenlafaxine. *Chem. Manag.* 20, 100. doi:10.3969/j.issn.1008-4800.2016.20.092

Conflict of Interest: The authors declare that the research was conducted in the absence of any commercial or financial relationships that could be construed as a potential conflict of interest.

Publisher’s Note: All claims expressed in this article are solely those of the authors and do not necessarily represent those of their affiliated organizations, or those of the publisher, the editors and the reviewers. Any product that may be evaluated in this article, or claim that may be made by its manufacturer, is not guaranteed or endorsed by the publisher.

Copyright © 2022 Yang, Chen, Wang, Zhang, Li, Yuan, Peng and He. This is an open-access article distributed under the terms of the Creative Commons Attribution License (CC BY). The use, distribution or reproduction in other forums is permitted, provided the original author(s) and the copyright owner(s) are credited and that the original publication in this journal is cited, in accordance with accepted academic practice. No use, distribution or reproduction is permitted which does not comply with these terms.



OPEN ACCESS

EDITED BY
Djalal Trache,
Ecole Militaire Polytechnique, Algeria

REVIEWED BY
Pal Perjesi,
University of Pécs, Hungary
Vipan Kumar,
Guru Nanak Dev University, India

*CORRESPONDENCE
Simone Brogi,
simone.brogi@unipi.it
Giuseppe Campiani,
campiani@unisi.it

SPECIALTY SECTION
This article was submitted to Green and Sustainable Chemistry, a section of the journal Frontiers in Chemistry

RECEIVED 07 July 2022
ACCEPTED 12 August 2022
PUBLISHED 12 September 2022

CITATION
Marotta L, Rossi S, Ibba R, Brogi S, Calderone V, Butini S, Campiani G and Gemma S (2022), The green chemistry of chalcones: Valuable sources of privileged core structures for drug discovery.
Front. Chem. 10:988376.
doi: 10.3389/fchem.2022.988376

COPYRIGHT
© 2022 Marotta, Rossi, Ibba, Brogi, Calderone, Butini, Campiani and Gemma. This is an open-access article distributed under the terms of the [Creative Commons Attribution License \(CC BY\)](#). The use, distribution or reproduction in other forums is permitted, provided the original author(s) and the copyright owner(s) are credited and that the original publication in this journal is cited, in accordance with accepted academic practice. No use, distribution or reproduction is permitted which does not comply with these terms.

The green chemistry of chalcones: Valuable sources of privileged core structures for drug discovery

Ludovica Marotta¹, Sara Rossi¹, Roberta Ibba¹, Simone Brogi^{2*}, Vincenzo Calderone², Stefania Butini¹, Giuseppe Campiani^{1*} and Sandra Gemma¹

¹Department of Biotechnology, Chemistry and Pharmacy, University of Siena, Siena, Italy, ²Department of Pharmacy, University of Pisa, Pisa, Italy

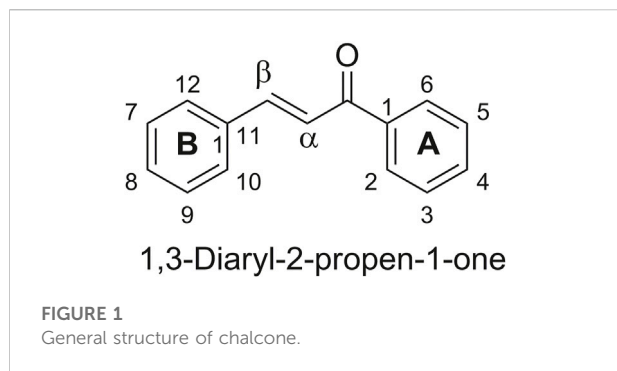
The sustainable use of resources is essential in all production areas, including pharmaceuticals. However, the aspect of sustainability needs to be taken into consideration not only in the production phase, but during the whole medicinal chemistry drug discovery trajectory. The continuous progress in the fields of green chemistry and the use of artificial intelligence are contributing to the speed and effectiveness of a more sustainable drug discovery pipeline. In this light, here we review the most recent sustainable and green synthetic approaches used for the preparation and derivatization of chalcones, an important class of privileged structures and building blocks used for the preparation of new biologically active compounds with a broad spectrum of potential therapeutic applications. The literature here reported has been retrieved from the SciFinder database using the term “chalcone” as a keyword and filtering the results applying the concept: “green chemistry”, and from the Reaxys database using the keywords “chalcone” and “green”. For both databases the time-frame was 2017–2022. References were manually selected based on relevance.

KEYWORDS

chalcones, green chemistry, pharmaceuticals, drug discovery, green synthetic techniques, privileged structures, artificial intelligence

1 Introduction

Since many years, the pharma industry has realized that the production of medicines and pharmaceutical products needs to be accomplished by taking into account the sustainability of the manufacturing pipeline. This requisite has prompted the investigation and design of greener approaches for the production of active pharmaceutical ingredients (APIs). In particular, the “12 principles of green chemistry” should be applied not only during the manufacturing of APIs and related products, but also in all phases of the drug discovery and development workflow, starting



from the early investigation of the chemical scaffolds suitable for the synthesis through green and sustainable approaches.

The use of privileged structures, defined as molecular scaffolds endowed with drug-like properties and characterized by versatile binding modes, is a design strategy massively and successfully exploited at the lead optimization stages of the drug discovery pipeline. Among the plethora of privileged structures identified so far, the chalcone framework, defined as a α,β -unsaturated carbonyl moiety substituted by two aromatic rings at both ends (general structure in Figure 1) is particularly interesting due to its widespread diffusion in the plant kingdom, food and nutraceuticals coupled to its interesting biological properties. The pharmacological profile of chalcones (Salehi et al., 2021) is wide and interesting and they are potentially useful for the development of therapeutic agents against cancer (Ouyang et al., 2021), infectious diseases (Mahapatra et al., 2015; Duran et al., 2021; Pozzetti et al., 2022), obesity, neurological/neurodegenerative disorders (Cho et al., 2011; Thapa et al., 2021), inflammatory-related syndromes (Mahapatra et al., 2017), allergic illnesses (Yamamoto et al., 2004; Iwamura et al., 2010) etc. In addition, antioxidant effects of chalcones have been demonstrated (Janković et al., 2020) conferring to them the status of privileged scaffolds. In fact, chalcone-based molecules such as metochalcone and sofalcone are used in clinical practice as choleric drugs and anti-ulcer agents, respectively, also establishing gastroprotection in patients suffering from *Helicobacter pylori* (Higuchi et al., 2010; Gomes et al., 2017c).

Moreover, the chalcone structure represents a versatile starting material suitable for further derivatization and conversion into structurally diverse molecular entities, such as pyrrole and pyrazoles, pyridines, pyrimidines, as well as bicyclic derivatives such as indoles, quinolines and coumarins, all characterized by drug-like properties. In this scenario, green synthetic approaches for the preparation and derivatization of natural and synthetic chalcones could represent the starting point for greener and more sustainable drug discovery pipelines.

A number of reviews have focused on synthetic methodologies for the preparation and derivatization of

chalcones using green approaches, often compared to standard ones, or focused on their most relevant biological activities (Rosa et al., 2017; Taresh, 2022; Wilhelm et al., 2022). Herein, we review the most recent literature (2017-to date) describing green approaches for the synthesis and derivatization of chalcone with a focus on methodologies aimed at optimizing solvent and energy consumption. The application of important green processes such as one-pot syntheses, click-chemistry, biocatalysis, and green enabling technologies such as flow chemistry and photochemistry will also be discussed in the field of chalcone synthesis and derivatization. Finally, artificial intelligence (AI) as a powerful tool for the prioritization of compound libraries will also be briefly outlined.

2 Green solvents for the synthesis and derivatization of chalcones

The first principle of green chemistry is to prevent waste, the fifth is the reduction of auxiliary substances as solvents and the decrease in their toxicity. However, as often reported, the greenest option for solvent is to avoid solvent. Though it is not always an easy task in the managing of organic reactions, many researchers have investigated the use of eco-friendly solvents that owe this definition to environmental reasons, low cost, time and energy waste. Amongst the many techniques encompassing procedures or devices where solvents are not necessary, several may be applied to the formation of chalcones or their derivatives. The use of ionic liquids as the catalyst allows to carry out solvent-free reactions, increasing yield products, regioselectivity, minimizing the production of chemical wastes, decreasing reaction time and simplifying operational procedures (Mahato et al., 2017; Aegurla and Peddinti, 2018; Bahrami et al., 2019; Das et al., 2020; Karimi-Jaberi et al., 2020; Karimi-Jaberi et al., 2020). Solvent-free conditions can be applied to microwave-assisted synthesis of chalcones, speeding up the reaction time. A common association is between solvent-free reactions and mechanochemical techniques, which include grinding and high-speed ball milling. These techniques are frequently used in the synthesis of chalcones and chalcone derivatives in academic research as well as in industrial applications allowing to reduce the consumption of high cost catalysts and shortening the reaction times (Praveena et al., 2019; Zangade and Patil, 2020).

2.1 Mechanochemistry and solvent-free synthesis

In the recent years, mechanochemistry has combined the principles of chemistry and mechanical engineering, assuming that to get a chemical transformation, energy is needed. This

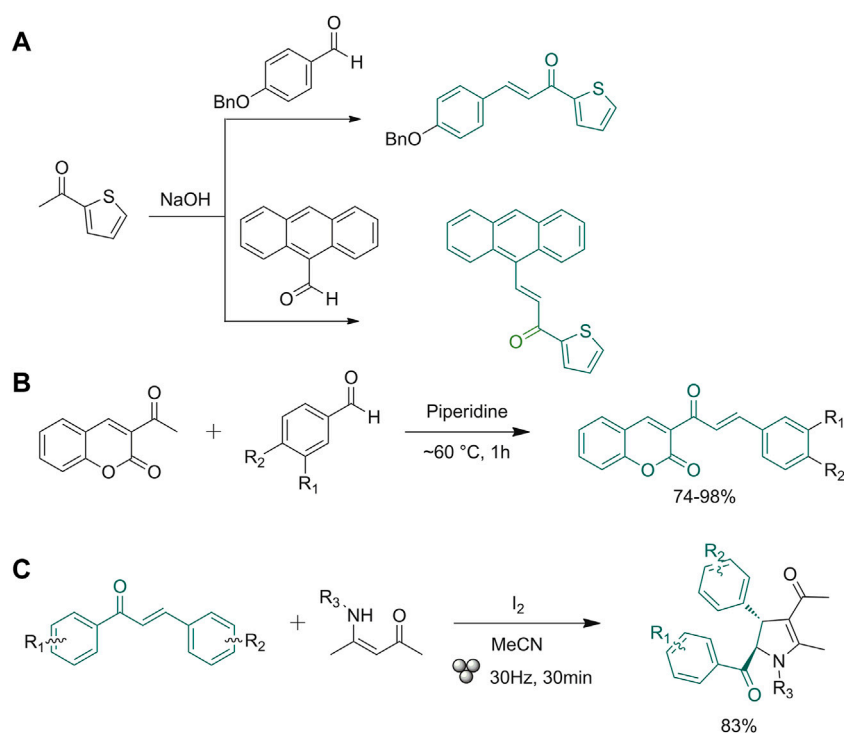


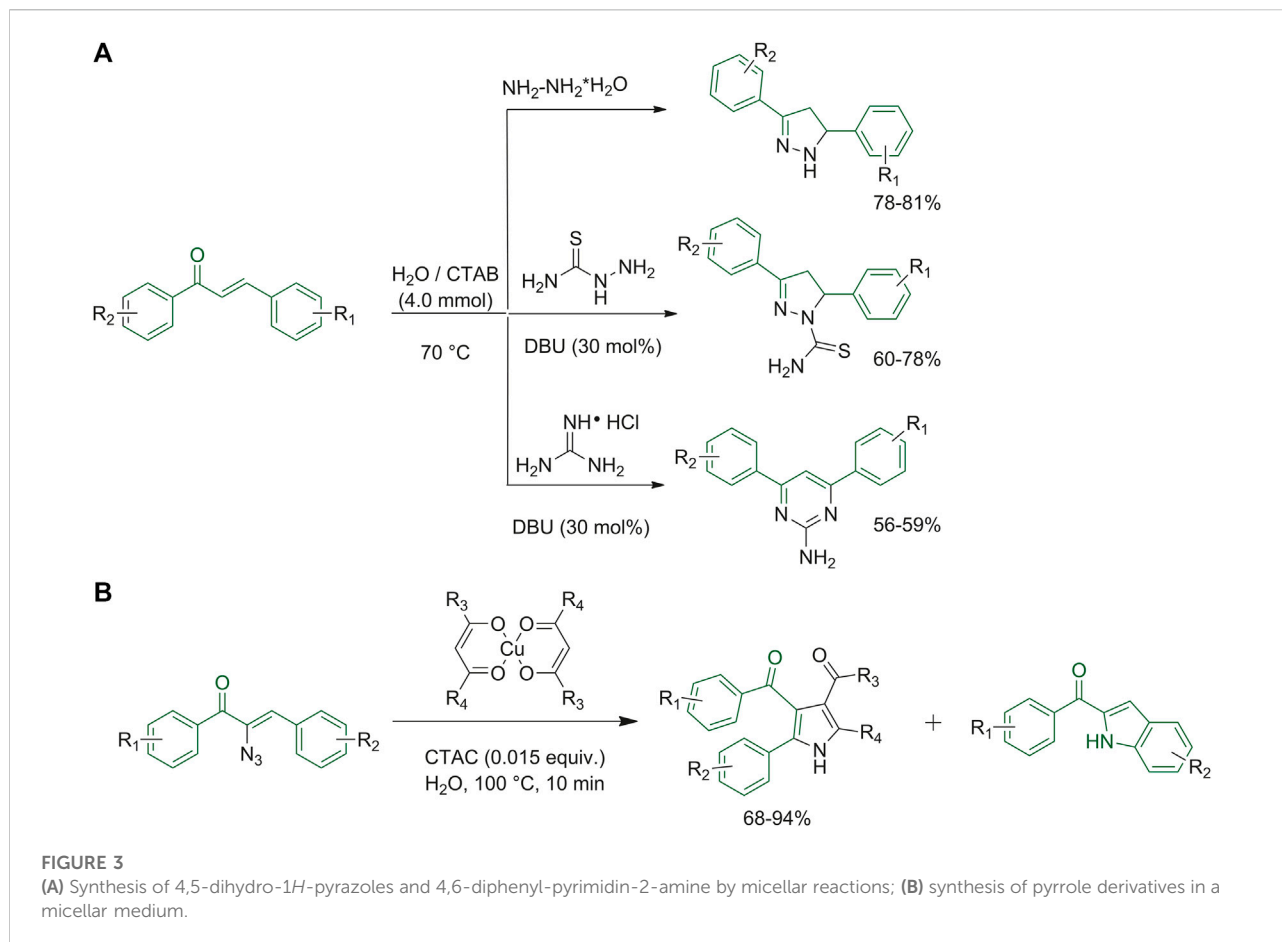
FIGURE 2

(A) Synthesis of anthracene- and 4-benzyloxy-based chalcones; (B) Claisen-Schmidt condensation between 3-acetyl-2H-chromen-2-one mono- and disubstituted benzaldehydes; (C) synthesis of polysubstituted 2,3-dihydropyrroles (relative stereochemistry is shown).

goal can be achieved either by using simple tools such as mortar and pestle or by more costly instruments as a ball mill (Gomes et al., 2020). The former is an easy-to-find tool but significant variations may occur depending on the operator; the latter is an automatic instrument, which leads to good reproducibility thanks to the automatic control of many parameters such as milling frequency, material and size of the milling balls and jars, the number of balls and the type of rotation (Gomes et al., 2020). Many research groups are investigating this new technology for implementing new devices which are based on the simple principle of applying a mechanical force during the reaction. Examples from recent literature are reported below where chalcone formation and chalcone derivatization reactions have been performed using the principle of mechanical chemistry.

Praveena et al. described two examples of reactions carried out through the use of pestle and mortar (Praveena et al., 2019). As exemplified in Figure 2A, 4-(benzyloxy) benzaldehyde or 9-anthracenecarbaldehyde were mixed with 1-(thiophen-2-yl)ethanone and NaOH and then grinded with mortar and pestle for 10 min. The formed solid chalcones were filtered off and re-crystallized from ethanol (Praveena et al., 2019). Gomes et al. used a laboratory device consisting of a single-screw drill (SSD)

placed on top of a steel cylinder with a central hole, where the drill screw penetrates once operated. A friction force is generated using this technique, resulting in an intense shear stress able to reduce the powders down to 1 μm in 1 min and create a properly mixed reaction, subjecting the system to high pressure. This technique has been tested on the classical Claisen-Schmidt condensation reaction using various aldehydes and methyl ketones as starting materials (Gomes et al., 2020). The same experiment was carried out using the ball milling technique. The SSD tool, which uses the shear force instead of shock pressure, allows a higher availability of the molecular surface, increasing the reaction yields (Gomes et al., 2020). The SSD method provided chalcones in high yields regardless of the physical state (solid or liquid) or the presence of functional groups (electron-donating, electron-withdrawing) on the starting material scaffolds. The aim of the research group of Cuellar and co-workers was to synthesize active pharmacological coumaro-chalcone compounds by a sustainable route (Figure 2B). They applied a classic Claisen-Schmidt condensation without solvent, obtaining high yields (75.2–99.4%) with the selective formation of the trans isomer in the chalconoid system (Cuellar et al., 2022). Exploiting the mechanochemistry technique, another research group performed reactions using nitrones as a replacement for



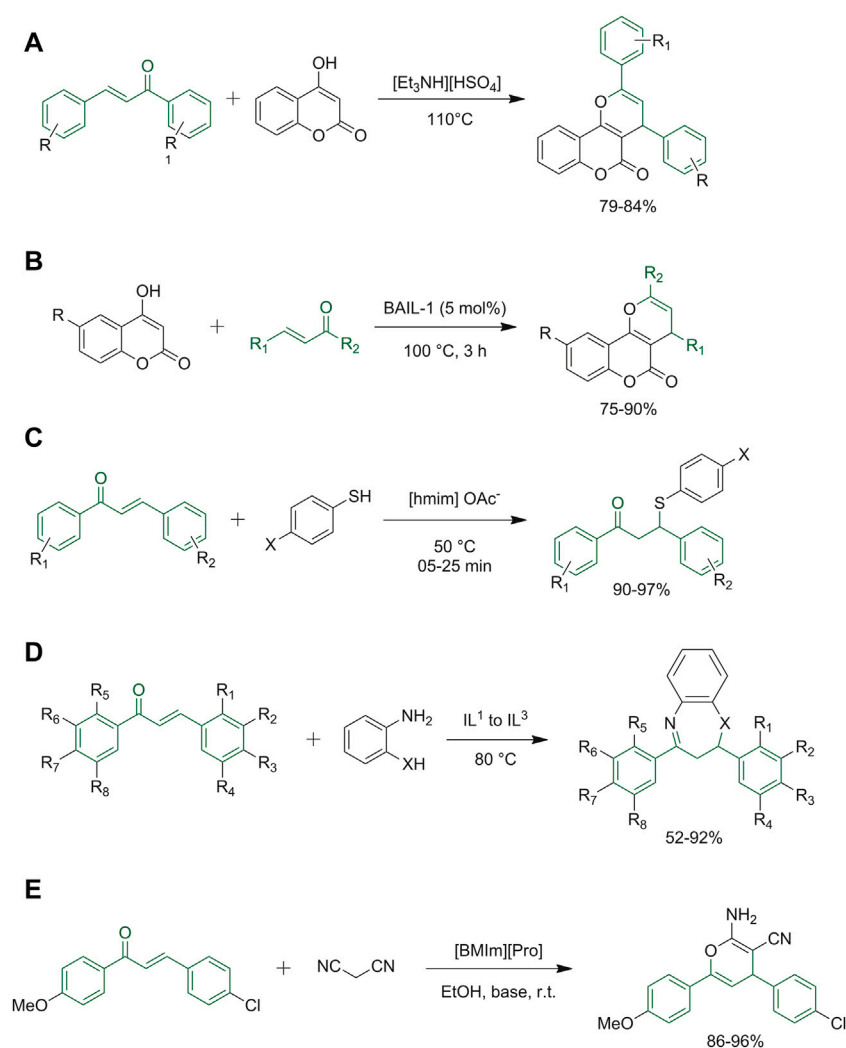
aldehydes. In the experiments, they verified that the reaction yield with nitron derivatives and acetophenone does not change as compared to the use of aldehydes. They also tested the addition of small amounts of xylene, a high boiling non-polar solvent, for facilitating the grinding mechanism (Antony et al., 2021).

Being able to facilitate reaction conditions in the presence of a small amount of solvent (or any), ball milling devices have several applications in green organic synthetic approaches. Weng et al. (Weng et al., 2021) exploited this technique for derivatizing the scaffold of chalcones. Starting from a simple condensation reaction, they developed a protocol for preparing a library of polysubstituted 2,3-dihydropyrrole derivatives (Figure 2C). This reaction was performed via iodine-promoted cyclization with the use of additives such as liquid-assisted grinding solvents (LAGs). Different solvents were tested, with different starting material equivalents and different time rates, until the reaction was optimized, and high yields were obtained. The optimization of the above-described protocol allowed to create a consistent library of 2,3-dihydropyrroles, and to study the effects of substitution patterns on reactivity.

2.2 Micellar chemistry

Water may be considered as the greenest solvent due to several inherent properties (i.e., water is neither toxic, flammable or carcinogenic, it is readily available and inexpensive). Unfortunately, the use of water as a solvent for organic chemistry reactions presents many limitations, the most important being the poor solubility of most reagents. To overcome this problem, surfactants are used to increase the miscibility among hydrophobic substances and water. Due to their amphiphilic nature, in the presence of a large amount of water, surfactants form micelles, defined as spherical supramolecules with a colloidal size (Wei and Cue, 2018). The “supramolecule” term indicates that cohesion forces are not covalent and even if the micelles appear as a homogeneous phase, they consist of a micro-heterogeneous two-phase system. Tensides are used in many industrial applications, in chemical synthesis they are used as micellar catalysts able to accelerate or inhibit a reaction process (La Sorella et al., 2015).

Starting from appropriately substituted chalcones, Mishra et al. studied a new procedure to synthesize the 4,5-dihydro-

**FIGURE 4**

(A) Synthesis of pyrano [3,2-c]coumarins; (B) synthesis of pyrano [3,2-c]coumarin using BAIL-1 as liquid ionic; (C) synthetic route for 1,3-diphenyl-3-(phenyl thio) propan-1-one derivatives; (D) Michael addition followed by cyclo-condensation to give 1,5-benzodiazepines and 1,5-benzothiazepines; (E) formation of the 2-amino-3-cyano-4H-pyran.

1H-pyrazole and 4,6-diphenylpyrimidin-2-amine to prevent environmental pollution and reduce the extensive use of organic solvents. They chose cetyltrimethylammonium bromide (CTAB) as the cationic surfactant for the micelles formation and added 1,5-diazabicyclo(5.4.0)undec-7-ene (DBU) as the base catalyst. They screened different molar concentrations and several bases, gaining the best yields when they used the conditions reported in Figure 3A (Mishra et al., 2017). Rajaguru *et al.* aimed at synthesizing indoles by reacting α -azidochalcones in the presence of metal β -diketonates using cetyl trimethyl ammonium chloride (CTAC) in water as the micellar medium. During their experiments they could obtain substituted pyrroles, and for this reason they extended the study of reaction conditions in

order to improve the yields of the pyrrole derivatives, as depicted in Figure 3B (Rajaguru et al., 2017).

Kothandapani and co-workers started with the synthesis of the non-ionic surfactant stearyl methoxyPEGglycol succinate (SMPS). This compound emerged as an interesting option due to its non-toxic nature. Non-ionic surfactants SMPS can be modified by changing the length of the hydrophilic tail to improve their aqueous miscibility, while the substitution of different alcohols to 1-octadecanol gave different degrees of lipophilia (Kothandapani et al., 2017). To test the efficacy of the surfactant that they synthesized, the research group applied the reduction reaction of nitrochalcone derivatives to the classical approach employing palladium/diphenyl sulfide complex catalyst, which is expensive and toxic. Consequently,

Kothandapani *et al.* performed the reduction by SMPS surfactant in aqueous medium with zinc and ammonium chloride. The efficiency of SMPS was verified by carrying out the reaction under the same conditions without the surfactants (Kothandapani *et al.*, 2017).

2.3 Ionic-liquid synthesis

In chemical processes, organic solvents are used in enormous amounts because they are needed during reaction, separation, and formulation and, depending on an appropriate selection, they can lead to good yields and bring a quality product. The use of less toxic solvents would have an important impact on the sustainability of the API manufacturing process. In the last few years, ionic liquids have emerged as a green alternative to common organic solvents. By definition, ionic liquids are salts with a low melting point and are characterized by physicochemical properties such as negligible vapor pressure, high thermal stability, and wide liquid range; moreover, these features can be modulated by combining two ILs or by modifying the length and flexibility of the organic cation. This accounts for their high adaptability to different specific applications. On the other hand, the lack of data about endpoints and toxicity profiles, their tendency to combustion, high cost and low potential biodegradability led to the conclusion that ILs still need to be studied and optimized (Wei and Cue, 2018).

Triethylammonium hydrogen sulfate is considered an environmentally safe and cheap ionic liquid catalyst, which is easily prepared by an acid-base neutralization reaction. This catalyst has been successfully employed in the synthesis of pyrano[3,2-*c*]coumarins by the reaction of 4-hydroxycoumarin with differently substituted chalcones (Figure 4A) (Karimi-Jaberi *et al.*, 2020). Pyrano[3,2-*c*]coumarins were synthesized by Mahato *et al.* using Brønsted acidic ionic liquids (BAILs) (Figure 4B). Firstly, the authors applied solvent-free conditions coupled to heating at high temperatures, obtaining satisfactory yields. Then they also investigated different *ad hoc* synthesized ILs, and the best result was obtained by BAIL-1, a recyclable IL that can be easily purified with water being the only byproduct (Mahato *et al.*, 2017). 1,4-Addition of mercaptans to chalcones was obtained under a variety of reaction conditions, characterized by heating at high temperatures, the need of expensive catalysts, and long reaction times. Shreyas S. Mahurkar and co-workers developed a green method for the synthesis of 1,3-diphenyl-3-(phenylthio)propan-1-one derivatives using [hmim]OAc-ionic liquid for the thia-Michael addition reaction (Figure 4C). This ionic liquid was effective as a reaction medium and a good catalyst. The authors hypothesized that the dissociation constant of thiophenol, which is higher in ionic liquids than in organic solvents, could be responsible for the improved reaction outcomes (Mahurkar *et al.*, 2019). Sakirolla *et al.* employed imidazolium salt ionic liquids to synthesize 1,5-

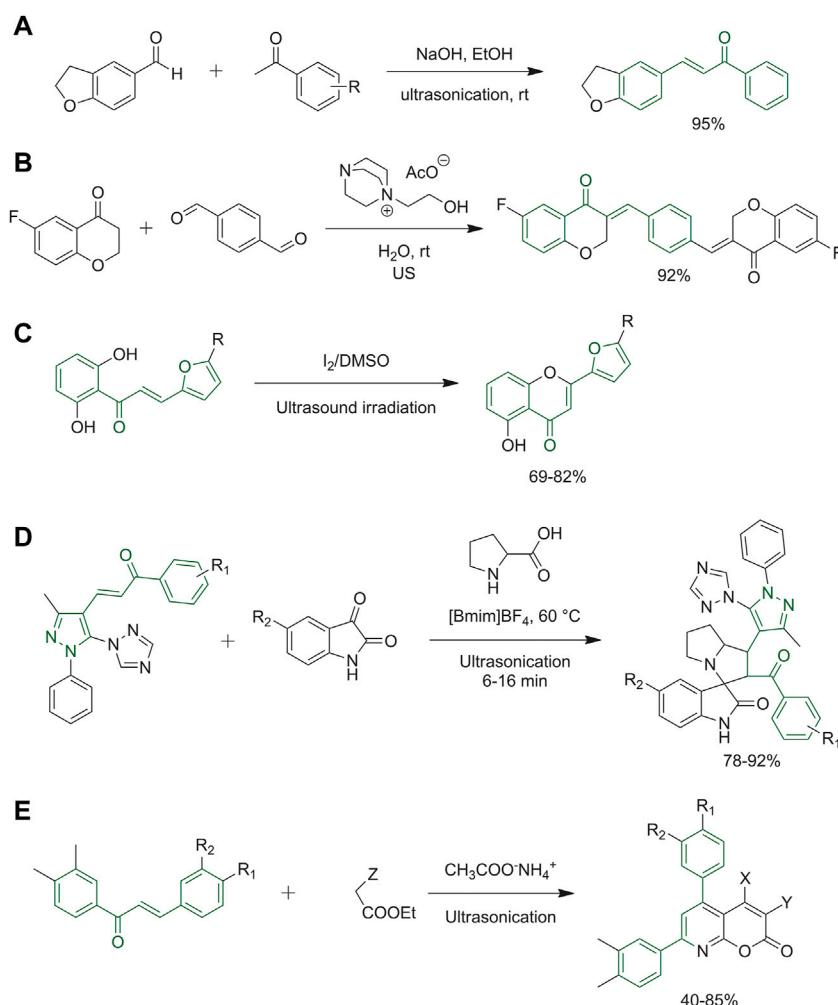
benzothiazepine starting from α,β -unsaturated carbonyl systems typified by chalcones (Figure 4D). These ILs have proven to be environmentally friendly since they can be recycled for three cycles, IL-C is the most efficient reaction medium among the others because it allowed to reduce the time reaction and increase the final yield (Sakirolla *et al.*, 2018). Recently, the research group of Dhadda, has applied together with the use of ionic liquids with the technique of sonication and managed to create a scheme for different synthetic heterocyclic compounds, including 2-amino-3,4-pyrimidine, pyrazole, oxazole, and pyridine derivatives. The basic ionic liquid [DBUH]OAc has proven to be the best IL since it leads to obtaining good yield of the desired result and it can also be reused for up to five catalytic cycles (Dhadda *et al.*, 2022).

Besides being used as solvents, ILs have also been used purely as catalysts. Amino acidic-based ionic liquids such as *L*-proline nitrate and [BMIm]-proline have been used as green and biodegradable catalysts in conjugate addition reactions with chalcones (Bahekar *et al.*, 2017). In this case, the use of a *L*-proline nitrate avoids the need of long reaction times and high-temperature, which are typical reaction conditions required for thia-Michael reactions; at the same time, high yields and environmental sustainability were attained [BMIm]-proline proved to be an efficient ionic liquid catalyst allowing the synthesis of various 2-amino-4*H*-chromene-3-carbonitrile derivatives in high yields. The catalyst can be recycled up to five times still giving good yields, though the recovery process can be time-consuming (Figure 4E) (Hajipour and Khorsandi, 2017).

3 Synthesis of chalcones using green sources of energy

In the last 30 years, ultrasound technique has encountered increasing interest in the field of drug synthesis as an advantageous methodology for more sustainable manufacturing approaches. Indeed, the mechanism of the ultrasound system, also called sonochemistry, consists of the generation of a high amount of energy released by the collapse of microbubbles. Microbubbles are formed by piezoelectrical materials subjected to electrical potential, these materials convert electrical energy to mechanical vibration energy letting it spread through the liquid medium to form microbubbles (Wei and Cue, 2018; Draye *et al.*, 2020). These microbubbles absorb energy from the waves generated by piezoelectrical materials and grow until they implode. This localized explosion with extreme conditions of temperature and pressure allows the reaction to take place (Draye *et al.*, 2020).

In the last decades, the microwave technique has proven to be effective in increasing reaction yields and reducing both reaction times and the formation of side products. In contrast to conventional heating, microwave irradiation warms up the solution homogeneously and rapidly. Microwave frequencies

**FIGURE 5**

(A) Synthesis of (E)-3-(2,3-dihydrobenzofuran-5-yl)-1-(aryl)prop-2-en-1-one derivatives; (B) 6-fluorochroman-4-one and terephthalaldehyde are used for a Claisen–Schmidt condensation to obtain bischalcone by ultrasound method and DABCO-based IL; (C) the last synthetic step to obtain 2-(5-substituted-furan-2-yl)-4H-chromen-4-ones; (D) final step of ultrasonication-ionic liquid synergy to obtain 1,2,4-triazol-1-yl-pyrazole based spirooxindolopyrrolizidine derivatives; (E) ultrasonication reaction between chalcone derivative and ethyl-substituted acetate obtaining pyran [2,3-b]pyridine.

work as electric fields that generate heat when they encounter materials with dielectric properties. Indeed, the selectivity of the reaction can be enhanced by the knowledge that polar molecules are more affected by microwave irradiation than apolar ones. This technique falls into the sixth principle of green chemistry since the energy efficiency is increased. Despite this, the microwave is still considered ambiguous as a green process because only 65% of electrical energy is converted into electromagnetic radiation, and the radiation heat can be slow when the mixture reaction is apolar. Nonetheless, microwave chemistry is widely used for solvent-free reactions or with the support of other devices such as flow chemistry devices (De La Hoz et al., 2016).

3.1 Ultrasound chemistry

Adole and co-workers reported the first synthetic route to obtain (E)-3-(2,3-dihydrobenzofuran-5-yl)-1-(aryl)prop-2-en-1-one derivatives under ultrasound irradiation. Their goal was to simplify the work-up procedures. The best identified reaction conditions consisted in reacting 2,3-dihydrobenzofuran-5-carbaldehyde with substituted acetophenones in ethanol, in the presence of sodium hydroxide, under ultrasound irradiation at room temperature (Figure 5A) (Adole et al., 2020). Sharma and co-workers developed an approach to get coumarin hybrids with other molecules such as maleimide, α -lipoic acid and resveratrol, thus combining two biologically active structures and also synthesized a set of chalcones presenting

coumarin heterocycle as the ring B (Sharma et al., 2018). Arafa et al. had the goal of finely-tune a new green protocol to synthesize bis-chalcones through a Claisen-Schmidt condensation. Based on their knowledge of ILs as sustainable solvents and the ultrasound techniques, they optimized the reaction between 6-fluorochroman-4-one and terephthalaldehyde, which occurred with poor yields when using conventional methods, using ethanol as the solvent, at room temperature, and using sodium hydroxide as the base. A slight improvement was attained using the ultrasound method. Subsequently, both the solvent and the base catalysts were changed, and the best yields were obtained with DABCO-based IL [DABCO-EtOH][AcO] coupled to ultrasonication, as reported in Figure 5B. By using these optimized reaction conditions, several bis-chalcone derivatives have been obtained (Arafa, 2018). Kakade et al. synthesized 2-(5-substituted-furan-2-yl)-4H-chromen-4-ones from furan-substituted chalcones, in dimethyl sulfoxide in the presence of a catalytic amount of iodine under ultrasound irradiation at room temperature conditions (Kakade and Vedpathak, 2020). The products depicted in Figure 5C were obtained within a few minutes in good yields. Pogaku et al. developed a green procedure joining together the IL 1-butyl-3-methylimidazoliumtetrafluoroborate ([Bmim]BF₄) and ultrasonication. Figure 5D represents the one-pot reaction among a chalcone intermediate, isatin and L-proline to obtain the final product 1,2,4-triazol-1-yl-pyrazole-based spirooxindolopyrrolizidine derivatives. The identified optimal conditions exploited [Bmim]BF₄ with ultrasonication at 60°C. The use of classical solvents such as methanol at room temperature or under reflux resulted in no reaction or a very low yield of the spirocyclic heterocycles (Pogaku et al., 2019). The reaction reported in Figure 5E represents the synthesis of a series of pyrano [2,3-b]pyridines elaborated by Rizk group. This procedure allowed to achieve high yields under mild conditions, starting from chalcone derivatives and reacting them with ethyl-substituted acetate under ultrasonic radiation. The ethyl-substituted acetates used were diethylmalonate, ethylacetoacetate or ethylcyanoacetate. The final pyrano [2,3-b]pyridines obtained differ in the substitution of substituents X and Y depending on the nature of the ethyl-substituted acetate used and the number of reactants such as via three- or four-component reactions. The same reaction was performed by grindstone technology providing equally high yields (Rizk et al., 2017).

Oxyprenylated chalcones of natural origin, such as cordoin and 4-hydroxycordoin, have interesting biological properties. Villena et al. have recently investigated the synthesis of oxyprenylated derivatives through alkylation of 2',4'-dihydroxychalcone with different alkyl bromides as the first step of the synthesis in the presence of a slightly basic medium and under ultrasound conditions. The reaction mixture was irradiated in a water bath by an ultrasonic cleaner. The ultrasonic system allowed to reduce reaction

time, improving the overall alkylation yields (Villena et al., 2021). Several aryl/indolyl substituted 4,5-dihydro-1H-pyrazole derivatives were synthesized by Kannan and co-workers. Chalcones exposed to aryl hydrazides undergo a Michael addition-cyclization reaction, forming the corresponding pyrazole scaffolds. This reaction was carried out both by conventional method and ultrasonic irradiation, the latter allowed to decrease the reaction time with a comparable yield (Kannan et al., 2019). Thanks to the success of the previous reaction, Kannan and co-workers extended the synthetic process to indole-based chalcones by reacting them with different carbohydrazides following the same ultrasonication conditions reported above (Kannan et al., 2019). Finally, a one-pot cyclo condensation reaction was performed between chalcone derivatives and o-aminothiophenol by Devkate et al. In their approach, several solvents were tested and PEG-400 was identified as the best choice providing a shorter reaction time and straightforward separation procedures for the target 1,5-benzothiazepines (Devkate et al., 2018).

3.2 Microwave chemistry

Microwave irradiation is widely used for the synthesis of chalcones and their derivatives. Chalcone synthesis is commonly realized through conventional Claisen-Schmidt condensation at high temperatures. With conventional heating, the reaction times can rise to 24 h depending on the general structure of the starting materials; moreover, the reaction yields are often not satisfactory. For these reasons, new and green synthetic strategies using microwave irradiation are more and more popular among researchers.

Prabhakar and co-workers developed a green protocol for the synthesis of 9-anthracenyl chalcone derivatives, which were tested as anti-bacterial compounds against *Staphylococcus aureus* and *Bacillus subtilis*. The reaction was carried out under solvent-free conditions, using KOH as the catalyst and under microwave irradiation, giving excellent yields in 5 min (Prabhakar et al., 2017). This protocol can be applied to scaffolds bearing different functional groups as reported by Sahoo and co-workers (Sahoo et al., 2019; Tupare and Pawar, 2020). Comparative studies to prove the effectiveness of microwave-assisted synthesis over conventional methods for chalcone synthesis showed that the conventional synthesis of chalcones starting from o-hydroxyacetophenones requires longer reaction times, higher solvent amounts and provides lower yields when compared to microwave-assisted protocols (Shntaif, 2016; Sahoo et al., 2017; Rahim et al., 2018).

Wang et al. applied an original one-pot synthesis, made of two steps, to obtain quinolinyl chalcones (Figure 6A). They used Nafion NR50 as the catalyst in EtOH; it is a reusable synthetic polymer with ionic properties that acts as an acidic catalyst enhancing the yield rate and allowing a more sustainable

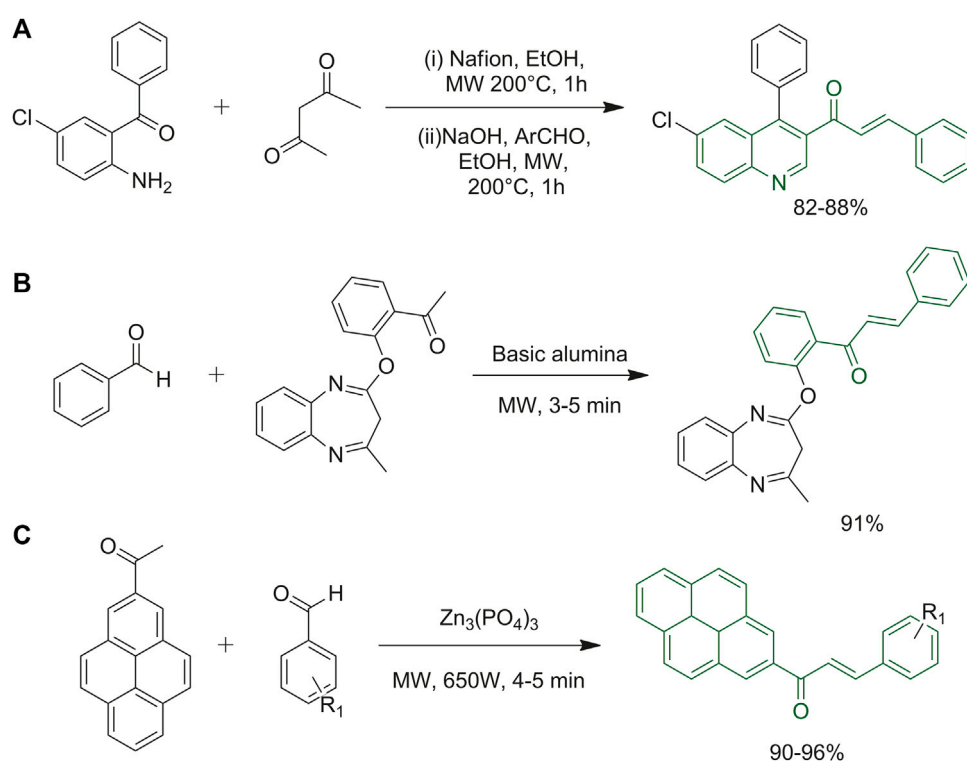


FIGURE 6

(A) One-pot synthesis of quinolinyl chalcones; (B) synthesis of 3H-benzo [b][1-4]diazepine derivatives; (C) synthesis of styryl 2-pyrenylketones using zinc phosphate as the coupling reagent.

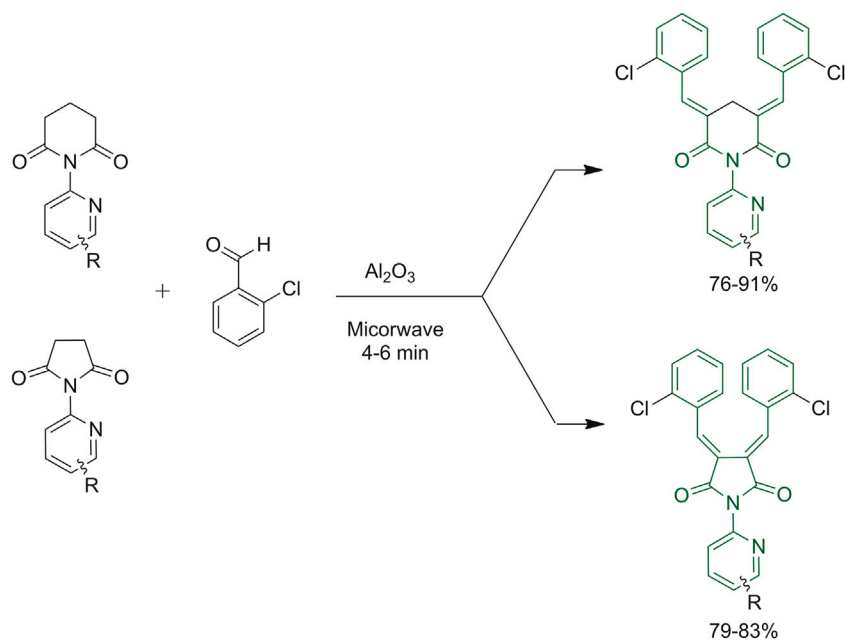


FIGURE 7

Routes to synthesize bischalcone derivatives.

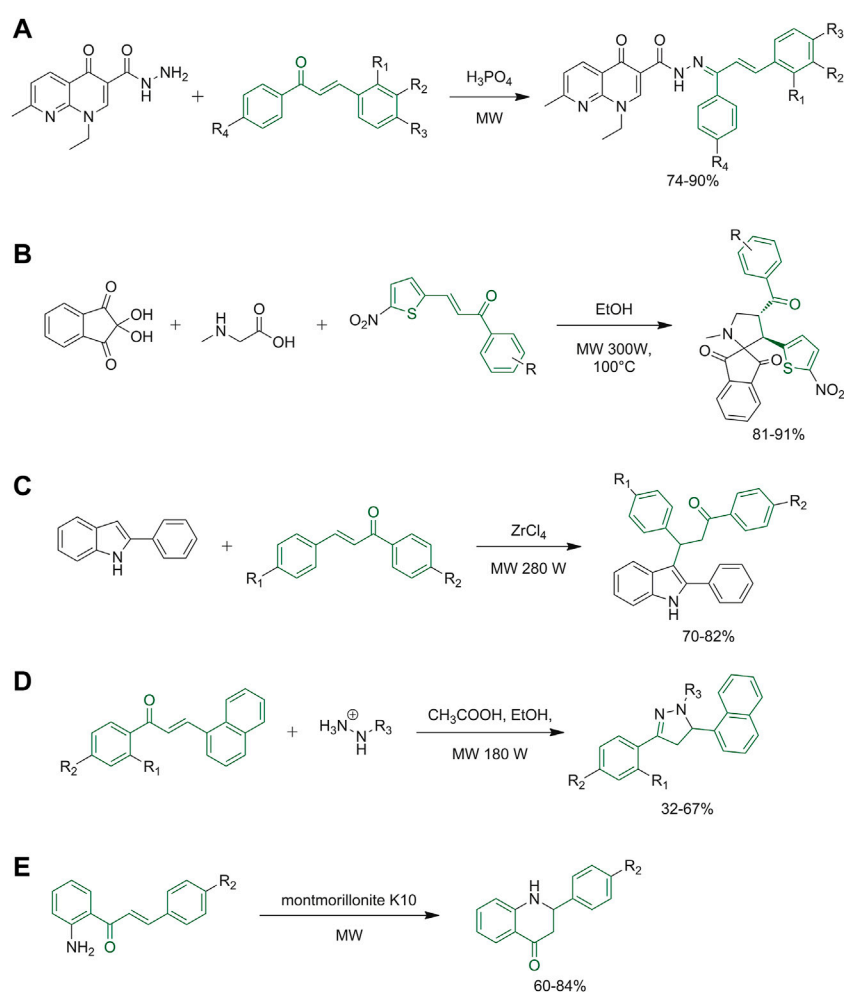


FIGURE 8

(A) Synthetic step of *N'*-(1,3-diphenylallylidene)-1-ethyl-7-methyl-4-oxo-1,4-dihydro-1,8-naphthyridine-3-carbohydrazide derivatives; (B) synthesis of novel spiropyrrolidine derivatives; (C) synthesis of 3-(3-oxoaryl) indole derivatives; (D) synthesis of pyrazoline derivatives; (E) the final step to synthesize 2-aryl-2,3-dihydroquinolin-4(1*H*)-ones by microwave technique.

synthesis of this important scaffold (Chan et al., 2020). Chalcones were combined with the well-known 1,5-benzodiazepine moiety to evaluate the biological activity of these complex poly-functionalized heterocyclic scaffolds (Figure 6B). This one-pot microwave-assisted synthetic strategy avoided the use of toxic solvents and provided good yields and avoided the need of purification by column chromatography. The desired starting materials and basic alumina were grinded in a mortar with the minimum quantity of solvent, and then the reaction mixture was irradiated with microwaves until reaction completion (Balyan et al., 2020). Muthuvel and co-workers used microwave irradiation to synthesize styryl-2-pyrenylketones using zinc phosphate (Figure 6C). The solvent-free procedure was carried out with various benzaldehydes, the ones with electron-donating groups gave better yields than the ones with electron-withdrawing functional groups. The synthetic route was tested

up to 6 times to verify the reusability of the catalyst and the efficiency was not affected until the fifth reuse (Muthuvel et al., 2021).

A solvent-free protocol was also tested by Chaudhari et al. as reported in Figure 7. The routes to obtain the bis-chalcones started with the reaction of an aromatic aldehyde with *N*-phenylpyrrolidine-2,5-dione and *N*-phenyl piperidine-2,6-dione (Chaudhari and Rajput, 2018).

Li et al. studied the use of eco-friendly catalysts in the classical Claisen-Schmidt condensation synthesis of chalcones. Reduced graphene oxide (RGO) is widely used and studied for many industrial applications due to its chemical-physical properties, likewise, ZnO nanoparticles have received a greater interest as a catalyst in chemical reactions. The mixture of ZnO nanoparticles dispersed on RGO (Zn/RGO) results in good catalytic activity. This is often used during photocatalysts or

photodegradation reactions, but Li *et al.* evaluated its efficacy in the Claisen-Schmidt condensation using different aryl aldehydes and aryl ketones with a mixture of ethanol and water as sustainable solvents under microwave heating. Further research reported that the electronic and steric hindrance effects of functional groups and electron-withdrawing groups were the most effective (Li *et al.*, 2017). The synthesis of 4-piperidinophenylene derivatives was carried out by Ranganathan *et al.* The reaction was performed by a microwave-assisted protocol with solid Cu^{2+} /Zeolite catalyst under solvent-free conditions. This approach highlighted that benzaldehydes with electron-donating substituents gave higher yields than those with electron-withdrawing substituents; the best concentration of catalyst was also assessed (Ranganathan *et al.*, 2020).

As previously mentioned, chalcones are not only important biological scaffolds, but they are also useful synthons. The growing interest in the synthesis of hybrid molecules led Mubarak *et al.* to study a new scaffold obtained by the condensation of nalidixic acid and chalcones to obtain several N' -(1,3-diphenylallylidene)-1-ethyl-7-methyl-4-oxo-1,4-dihydro-1,8-naphthyridine-3-carbohydrazides.

Figure 8A reports the green synthetic step used for the preparation of the product, where microwave irradiation was used to increase the yield and decrease the reaction time. To assess the sustainability of the protocol, metrics of atom economy, carbon efficiencies and reaction mass efficiency were calculated, as well as energy consumption data (Mubarak *et al.*, 2019). Kalluraya and co-workers reported a regioselective synthesis of spiropyrrolidine derivatives in a comparative study in which microwave-assisted reactions afforded the best results in facilitating the condensation of starting materials and afterwards in the formation of the final regioselective cycloadducts (Figure 8B). The reactions were tested with and without the use of solvent, obtaining comparable results (Kalluraya *et al.*, 2018). In the same way, a new protocol, for the synthesis of 3-(3-oxoaryl)indole derivatives, was developed through a microwave-assisted Michael addition of the appropriate chalcone derivatives using commercially available and non-toxic catalyst under solvent-free conditions (Figure 8C) (Patel *et al.*, 2019). 1,5-Benzodiazepine derivatives were synthesized with good yields and without the need for column chromatography purification, starting from differently substituted chalcones and 2-aminoaniline dissolved in piperidine and ethanol with the aid of a domestic microwave (Shetye and Pawar, 2017). Similarly, pyrazoline derivatives were synthesized from the appropriate chalcones and hydrazine hydrate derivatives with the addition of a catalyst in ethanol under microwave irradiation (Figure 8D) (Jasril *et al.*, 2019). Rocha and co-workers synthesized the 2'-aminochalcones derivatives using a green protocol employing microwave radiations. After that, they submitted the chalcone

derivatives to a cyclization reaction to obtain 2-aryl-2,3-dihydroquinolin-4(1H)-ones (Figure 8E) (Rocha *et al.*, 2019).

4 Tools and strategies for improving the efficiency of chalcone synthesis and derivatization

4.1 Click chemistry

Click chemistry has been well known since 2001, when Prof. Barry Sharpless conceived its definition. Click reactions must be modular and versatile, give high yields, be stereospecific, easy to perform and must create only harmless by-products (Shankaraiah *et al.*, 2020). This methodology is regarded as a powerful tool for green chemistry applications due to properties such as no or few by-products, atom economy, use of catalysts (re-usable), compatibility with water and benign reaction conditions (Gupta *et al.*, 2020). Chalcones containing alkyne-based substituents at the A or B rings were found to be compatible with the azide-alkyne Huisgen cycloaddition leading to the 1,2,3-triazole conjugates. Some examples are reported below.

The research group of Yadav reacted 4-O-propargylated chalcone derivatives with organic azides and various benzyl bromides. Importantly, the reaction was performed in the presence of cellulose-supported copper nanoparticles (Figure 9A), which proved stable (reusable without losing any significant activity) and chemoselective for Huisgen cycloaddition, justifying their increasingly widespread use (Yadav *et al.*, 2017). Yadav *et al.* also tested the same reaction on different scaffolds. As reported in Figure 9B, a click reaction between propargylated chalcones and azides using cellulose-supported copper nanoparticles was performed using two different reaction conditions. In the first method, chalcone conjugates were reacted with sodium azides and various benzyl bromides ($\text{R}_2\text{-Br}$), while in the second method, the previously functionalized azides ($\text{R}_2\text{-N}_3$) were used. Both methods gave 1,2,3-triazoles in good yields (Yadav *et al.*, 2018). Pereira *et al.* also reported the preparation of chalcone derivatives bearing a 1,2,3-triazole moiety. These compounds were obtained, as represented in Figure 9C, using a click reaction carried out with assisted copper(I)-catalyzed azide-alkyne cycloaddition (CuCAA). O-propargyl intermediates and azide sugar derivatives were the elected reagents (Pereira *et al.*, 2021). Similarly, Om and co-workers synthesized chalcone-triazole hybrids, which showed a synergetic biological activity when compared to the two pharmacophoric moieties taken separately. The one-pot synthesis of the azide and subsequently of the triazole is carried out in DMF using an aqueous solution of sodium azide, 2-bromo-N-arylacetamides, and the propargylated chalcone, using copper sulfate pentahydrate and sodium ascorbate as catalysts (Figure 9D)

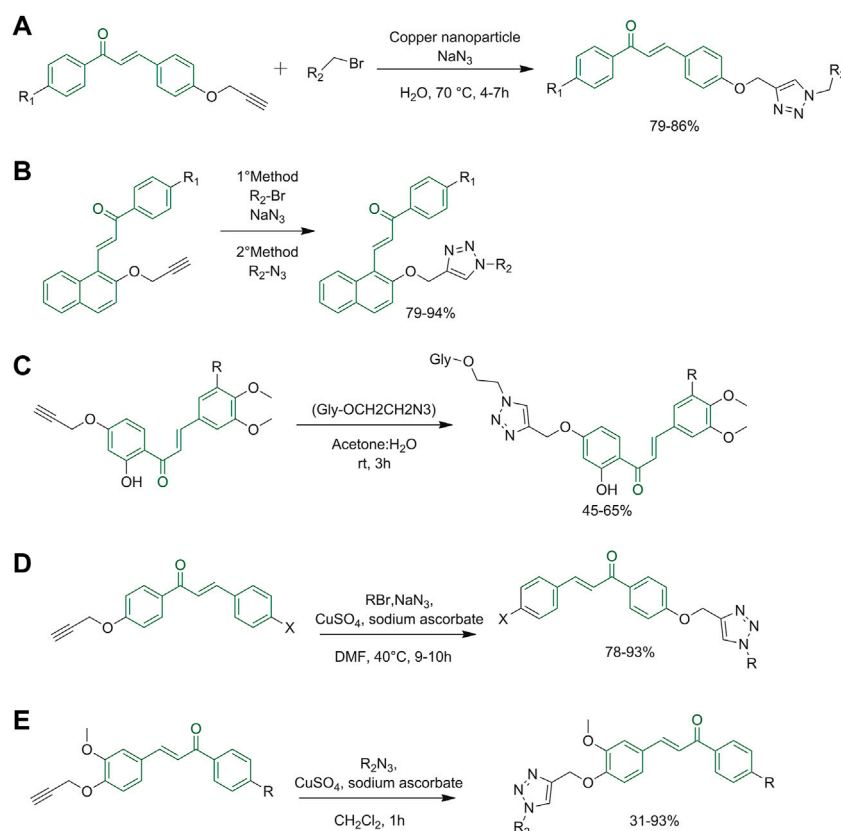


FIGURE 9

(A) Synthesis of chalcone derivatives starting with 4-O-propargylated benzaldehyde; (B) synthesis of 1,2,3-triazole derivatives using propargylated chalcones and azides; (C) click reaction copper(II)-catalyzed azide-alkyne cycloaddition (CuCAA) to obtain flavonoid glycosides with triazole moieties; (D) triazole synthesis through one-pot click reaction; (E) triazole synthesis through one pot click reaction catalyzed by CuSO_4 and Na-Asc.

(Sharma et al., 2022). The click reaction can be carried out under ultrasonication to enhance the reaction rate as reported by Kaur, the reaction was performed with variably substituted aromatic azides and terminal alkynes (Figure 9E) (Kaur et al., 2022).

4.2 One-pot synthesis

One-pot reactions consist of a sequence of several synthetic transformations carried out in a single pot avoiding purification steps of intermediate compounds. A one-pot procedure can form several chemical bonds in one-row synthesis also allowing the formation of very complex molecules. It can be considered a green approach since the use of solvents and chemical waste is minimal, harsh reaction conditions are avoided and the simplification of the synthetic routes is maximized (Sydnes, 2014).

The chalcone chemical scaffold may be synthesized by classical one-pot Claisen-Schmidt condensation, where the desired aldehyde and ketone mixed under basic conditions

render final chalcones. (Murugesan et al., 2017a; Murugesan et al., 2017b). They may also be obtained from alternative one-pot synthetic approaches. Soozani et al. reported the synthesis of quinoxaline chalcones via a one-step reaction of 3-substituted-2-chloroquinoxalines, and aromatic aldehydes with calcium carbide, in acetonitrile using diethylamine as the base and Pd/Cu as the catalyst (Figure 10A) (Soozani et al., 2017). The use of calcium carbide, to avoid protection and deprotection steps, results in an efficient and green one-pot procedure (Soozani et al., 2017). Dasari and collaborators developed a one-pot synthesis of variously functionalized indole-condensed benzimidazole chalcones. Several solvents, catalysts, and temperatures were evaluated to tune the best conditions to obtain the desired compounds with good yields, as reported in Figure 10B. The chalcone is formed as the first step of the proposed mechanism and then it reacts as an intermediate with the indole-derivative to produce the final compounds (Dasari et al., 2020).

Several examples of chalcone derivatization have also been developed. De Aquino et al. reported the synthesis of various

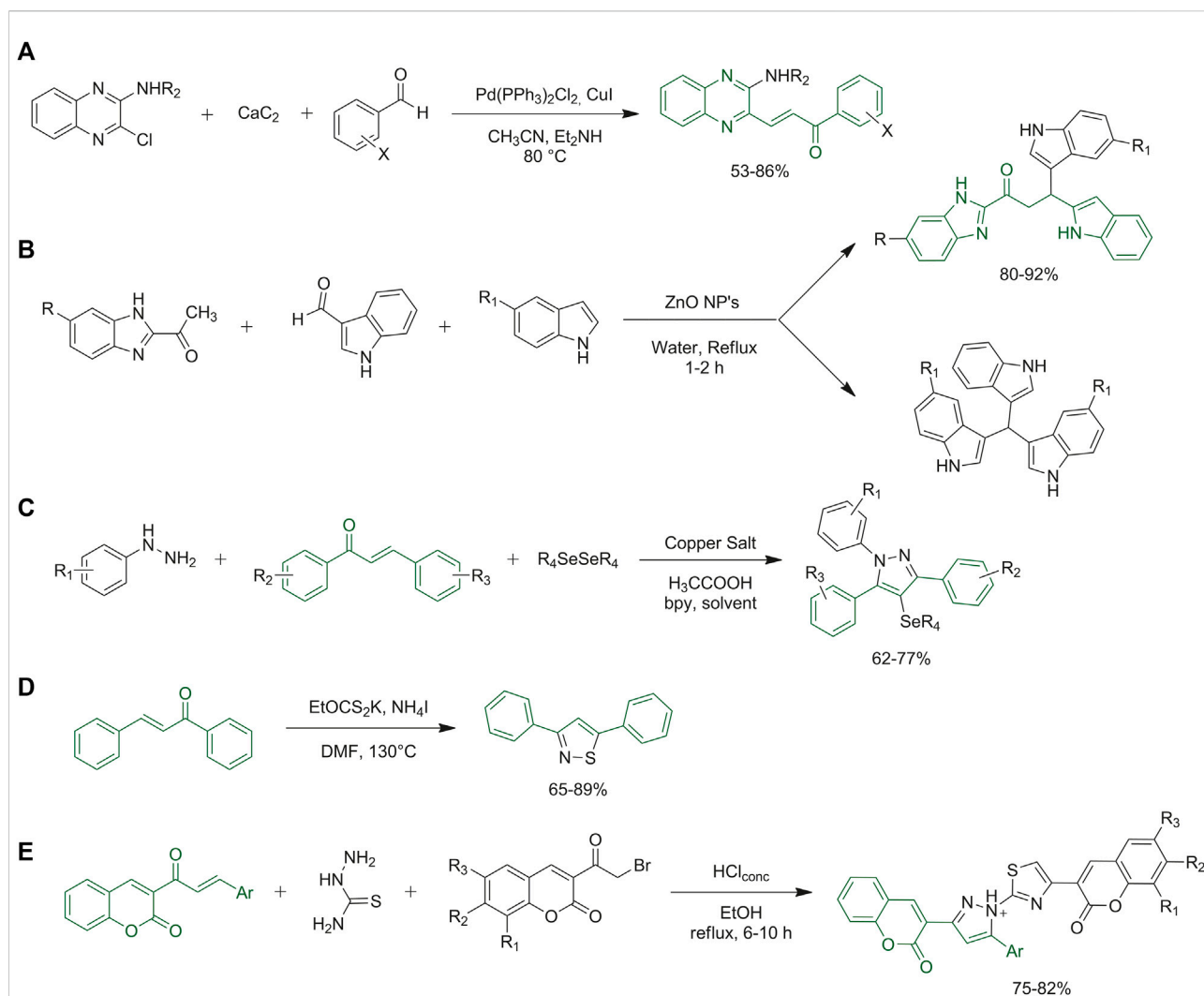


FIGURE 10

(A) Synthesis of (E)-3-(2-aminoquinoxalin-3-yl)-1-arylprop-2-en-1-one derivatives from 2-amino-substituted-3-chloroquinoxalines, calcium carbide, and aromatic aldehydes; (B) synthesis of indole-condensed benzimidazole chalcones via one-pot synthesis; (C) synthetic strategies for the synthesis of 1,3,5-triaryl-4-(arylselanyl)-pyrazoles through one-pot synthesis; (D) metal-free approach to get off various isothiazoles via three-component one-pot route: general synthesis; (E) synthetic strategy to obtain designed thiazolyl-pyrazole-biscoumarin via eco-friendly one-pot synthetic approach.

1,3,5-triaryl-4-(arylselanyl)-pyrazoles via a one-pot approach starting from properly designed chalcones and phenylhydrazines with the addition of acetic acid, diphenyl diselenide, CuBr , 2,2'-bipyridine (bpy) and solvent. 1,3,5-Triaryl-4-(arylselanyl)-pyrazoles were obtained with good yields via the optimized conditions, as reported in Figure 10C (de Aquino et al., 2018). Several syntheses of substituted isothiazoles are reported in the literature, starting from different building blocks. Li and collaborators proposed the synthesis of various isothiazoles through a one-step synthetic route starting from, among others, chalcone derivatives. They optimized the following procedure: NH_4I , EtOCS_2K and water

were added to the desired chalcone in DMF , and the reaction was carried out at 130°C for 12 h (Figure 10D). Isothiazoles were obtained in high yields (Li et al., 2021). Mahmoodi and Ghodsi reported the synthesis of thiazolyl-pyrazole-biscoumarin derivatives by a one-pot three-component green cyclocondensation of variously substituted coumarin chalcones, with thiosemicarbazide and 2-bromocoumarin in ethanol and a catalytic amount of HCl . Details are reported in Figure 10E (Mahmoodi and Ghodsi, 2017).

Tran et al. reported a rare example of the synthesis of 4,5-disubstituted thiazoles in a one-pot reaction assembling chalcones, glycine ethyl ester hydrochloride and elemental

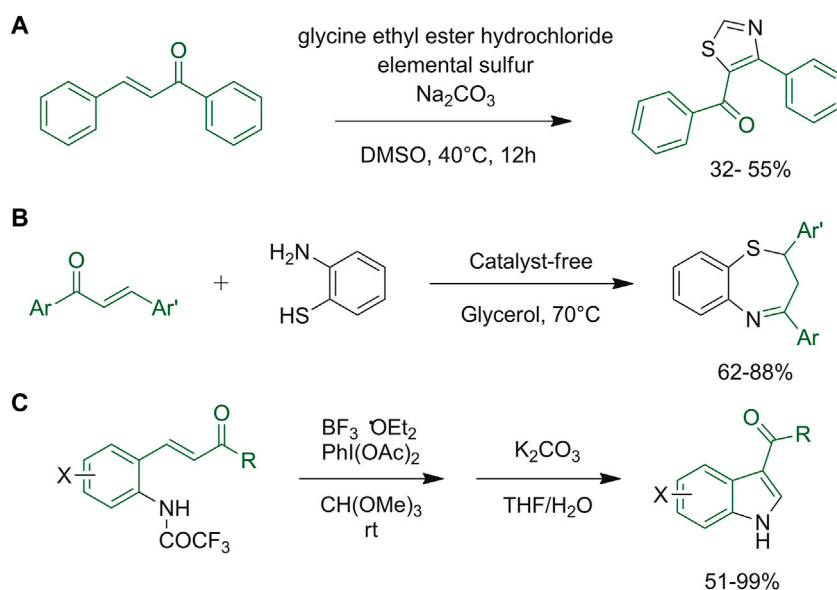


FIGURE 11

(A) Synthesis of 4,5-disubstituted thiazoles; (B) general synthetic protocol for the preparation of benzothiazepines via catalyst-free one-pot method using green glycerol medium; (C) one-pot synthesis of functionalized 3-acylindoles starting from properly selected chalcones.

sulfur (Tran et al., 2022). The research group also reported a plausible reaction mechanism, in which a trisulfur radical-anion, which is formed *in situ*, attacks the chalcone of interest, allowing the formation of a thiirane intermediate. Subsequently, the key enaminone intermediate is formed upon nucleophilic ring opening of the thiirane intermediate, at which point, the sulfuration of the activated alkene by excess elemental sulfur at high temperatures, rapid sequential aerobic oxidation and the final dealkoxycarbonylation induced by NaCl at high temperatures afford the final thiazole (Figure 11A). Yadav and collaborators synthesized benzothiazepines via a clean and efficient one-pot approach from chalcones and ortho-aminothiophenol (Yadav et al., 2019). Glycerol was selected as the medium to perform the synthesis under acid, base, or metal-free conditions. It resulted in a green synthesis with reusable media, short reaction time, catalyst-free conditions, easily available starting materials, broad substrate panel, easy process and work-up and final high yields (Yadav et al., 2019) (Figure 11B). 3-Acylindoles were obtained through oxidative rearrangement of 2-aminochalcone using a hypervalent iodine reagent optimizing one-pot conditions. The chalcone moiety is firstly functionalized as desired, and then cyclization of the indole scaffold is carried out under basic conditions in the same synthetic vessel. Optimized conditions (Figure 11C) afforded the desired products in quantitative yields (Nakamura et al., 2017).

Other examples of one-pot chalcone derivatizations are those reported by Ahmed et al., which were aimed at synthesizing novel

pyrimidine-based compounds. They developed a one-pot procedure where ketones and aldehydes were allowed to react to form the intermediate chalcone, then the properly functionalized guanidine was added to finalize the one-pot reaction, catalyzed in water media by green bio-organic $\text{Zn}(\text{L-proline})_2$ catalyst complex (Ahmed et al., 2021). Khalili and colleagues proposed graphene oxide (GO) as a catalyst for the sequential formation of chalcone and derivatization thereof by aza-Michael addition of the desired amines to form β -amino ketones (Khalili et al., 2020).

5 Green enabling technologies applied to the synthesis and derivatization of chalcones

5.1 Flow chemistry

Flow chemistry exploits a continuous flow reactor in which two pumps push the reagents, generating a continuous flowing stream where the reaction takes place. Different transformations can be achieved using different reactors such as coil, microchip, column, microspheres and tube-in-tube (TIT) (de Souza et al., 2018). The use of a flow reactor has several advantages, for instance, it is safer than the synthesis in round-bottomed flasks and reaction time is reduced, therefore, less energy is used. Moreover, gas substances can be used in flow reactions while being safely managed. Thanks to the capability

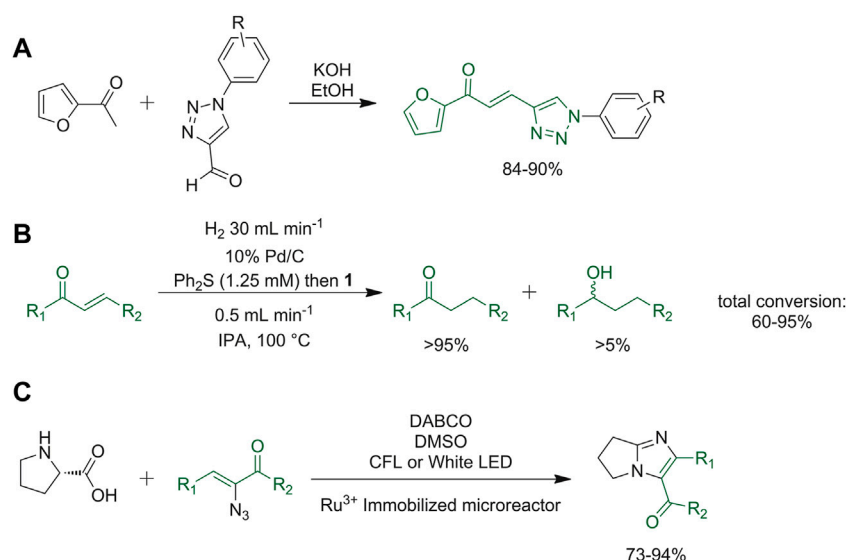


FIGURE 12

(A) Synthesis of 1,2,3-triazole-furan hybrid chalcone derivatives; (B) Pd/C-catalyzed reduction of chalcone moiety with diphenyl sulfide; (C) decarboxylation and a denitrogenation reaction to obtain imidazole derivatives.

of modifying and controlling parameters such as temperature, pressure and reactant concentration, it can be considered as a high-performance device to build up rapid, efficient and greener organic synthesis (de Souza et al., 2018). As detailed below, the flow chemistry technique has been recently applied to both the synthesis of heterocyclic chalcones and to the derivatization of chalcones into further functionalized analogues.

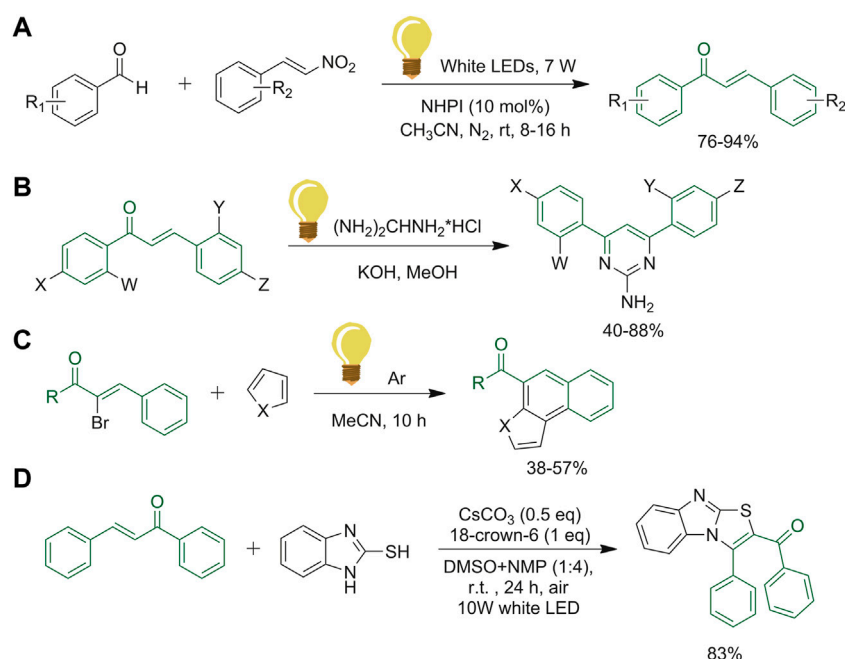
Kumar *et al.* described the synthesis of 1,2,3-triazole-furan hybrid chalcone derivatives. The reaction depicted in Figure 12A was firstly carried out in batch, optimizing the best basic conditions. Then, the reaction was performed under microwave irradiation or in a flow reactor, thus attaining a shortening of the reaction time, and an improvement of the yield. The flow reactor device is favorable since it allows larger scale processes than microwave irradiation (Kumar et al., 2020). Moore and co-workers described a Pd/C-catalyzed reduction of chalcone moiety based on the addition of diphenyl sulfide that confers selectivity in conjugate reduction (Moore et al., 2019). This reduction reaction was adapted into a continuous hydrogenation method, based on the *in situ* constant production of hydrogen by water hydrolysis (Figure 12B). In order to avoid the poisoning of the catalyst caused by continuous pumping of sulfide additive that reduces the reactivity, pretreatment of the catalyst bed with a solution of diphenyl sulfide was performed (Moore et al., 2019). Adiyala *et al.* developed a novel synthetic strategy starting from *L*-proline and α -azido chalcones to obtain imidazole derivatives through decarboxylation and a denitrogenation reaction, respectively. A

Ru^{3+} -immobilized polydimethylsiloxane (PDMS) microreactor under fluorescent or white LED light was used for the continuous flow procedure. In this way, time was reduced under 2 min and yield increased up to 70–94% when compared to the reactions run in batch (Figure 12C) (Adiyala et al., 2020).

5.2 Photochemistry

In the last decades, photochemistry techniques had an exponential growth. The possibility of using visible light to activate photocatalysts or substrate-catalyst complexes makes this method an innovative and promising green approach. The growth in interest in its potential use is due to the need of mild reaction conditions. (Rehm, 2020). Photochemical chemistry uses photons as a reagent to generate radical intermediates during a reaction. Photons are the greenest reagents since no residues are left at the end of the reaction, even if the photon is either absorbed (and the reaction is activated) or not (and moves out of the vessel). Despite the described advantages, nowadays photochemistry finds poor applications both in academia and industries. Several reasons limit the integration of this technique in synthetic schemes, among which we can find the formation of undesired mixtures of products and the unpredictable course of the reactions together with the expensive devices (Wei and Cue, 2018).

Solar radiation is a green and renewable source of energy, useful for both photochemical and thermal reactions. CSR (concentrated solar radiation) can be obtained through the Fresnel lens and allows rapid organic synthesis, eventually

**FIGURE 13**

(A) Synthesis of chalcones with NHPI catalysts, an efficient visible light organophotocatalyst; (B) UV-radiation reaction procedure to afford pyrimidine derivatives; (C) photo-induced tandem vinyl radical cyclization with α -bromo-chalcone and pyrrole derivatives; (D) visible-light induced imidazo [2,1-*b*]thiazoles synthesis with photocatalysts-, oxidants- and transition metal-free technique.

reaching high temperatures and gaining final compounds in high yields. Jadhav and colleagues tested this new method by reacting 4-methoxyacetophenone with 4-fluorobenzaldehyde in the presence of potassium hydroxide (Jadhav et al., 2017). The advantage of using CSR instead of a classical reaction method is a short-term reaction with a higher yield. The solar radiations include infrared waves that allow the molecules to vibrate and rotate faster. Interestingly, Jadhav group proposed a possible explanation based on the bombardment radiations, giving an increment of energy, that speed up the reaction itself (Jadhav et al., 2017).

The synthesis of substituted chalcones reported in Figure 13A was carried out by Tripathi et al. making the new and re-usable organo-photocatalyst, *N*-hydroxyphthalimide (NHPI), able to replace the metal-based visible light photocatalysts. These latter are efficient and productive, but could not be considered green catalysts (Tripathi et al., 2018). After the optimization of the reaction conditions, the compatibility of the synthetic methodology with different electron-donating and electron-withdrawing groups in the aromatic rings was assessed. Both gave high yields of the desired products, although the electron-withdrawing substituent allowed to achieve a faster reaction and afforded slightly higher yields (Tripathi et al., 2018). Saleem et al. conducted studies on pyrimidine scaffolds obtained from chalcone derivatives. They

initiated with a conventional method, which includes the solubilization of the chalcone, guanidine HCl and the selected base in methanol. Subsequently, they performed the same reaction with UV-radiation instead of conventional heating (Saleem et al., 2018). The method illustrated in Figure 13B has been compared to the classic one, which showed an increment of yield and time reduction, giving the chance to perform the reaction in a more sustainable way (Saleem et al., 2018). In the last few years, many research groups have investigated the synthesis of polycyclic xanthenes by photo-induced tandem vinyl radical cyclization. Yang and co-workers explored this reaction with α -bromo-chalcone and the respective pyrrole, as represented in Figure 13C (Yang et al., 2017). Under these conditions, the products of this one-pot reaction were obtained in a reasonable amount, and without the use of transition-metal complexes or high boiling solvent, making the procedure environment-friendly (Yang et al., 2017). Several imidazo [2,1-*b*]thiazoles were constructed by Chen and colleagues via electron-donor-acceptor (EDA) complex by performing a cyclization of chalcones and 2-mercaptobenzoimidazoles (Figure 13D). The aminothioloation reaction was performed through only visible-light irradiation. With this new technique, Chen et al. avoided the use of transition metals, external photocatalysts and oxidants (Chen et al., 2022).

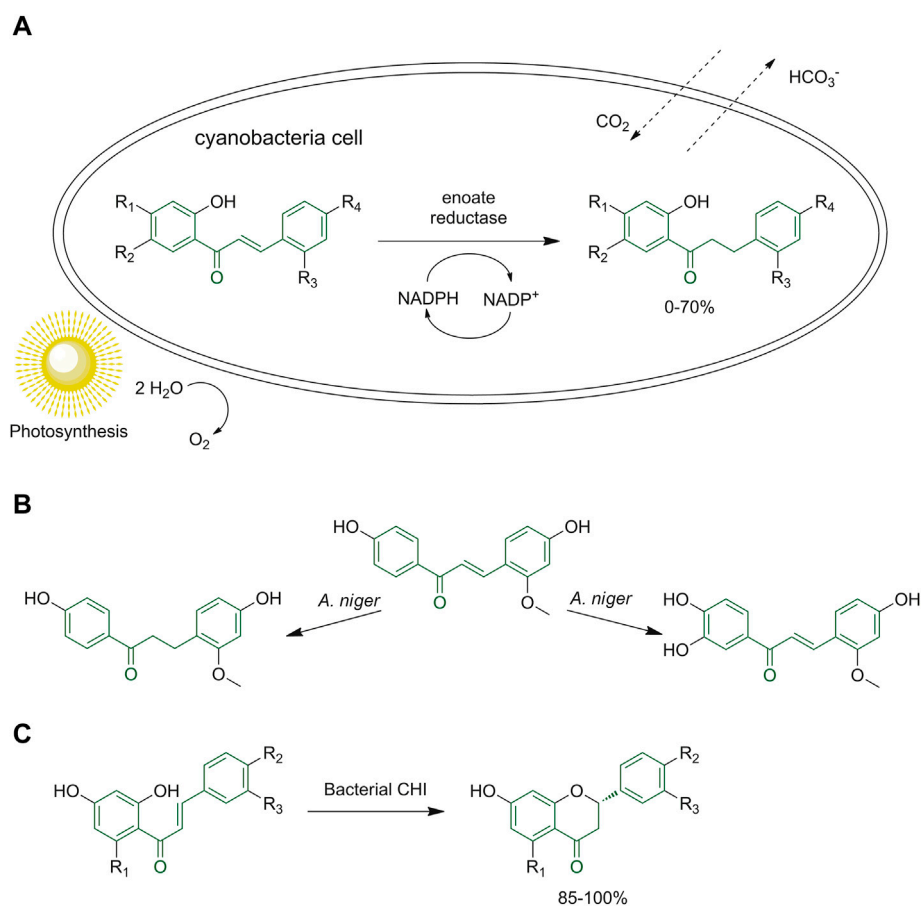


FIGURE 14

(A) General scheme of the biotransformation of methoxylated and methylated derivatives of 2'-hydroxychalcone in halophilic and freshwater cyanobacterial cells; (B) chalcone biotransformation by *A. niger*; (C) reaction performed by bacterial CHI to obtain (S)-flavones.

6 Biocatalysis

Biocatalysis is considered a promising process in which enzymes are used to obtain pharmaceutical compounds. Among the main features of biocatalysis, selectivity, recyclability, an increase in atom economy, and safety are the most relevant. At the beginning, lipases and ketoreductases were the only available enzymes, now thanks to the development of technology for the production of new enzymes, it is possible to design an artificial “enzyme cascade” that allows to choose the desired proteins for the production of the target compounds (Carullo et al., 2019; Carullo et al., 2020; Mazzotta et al., 2021). Synthesis and modification of chalcones can be obtained using different biocatalytic approaches, whole-cell biocatalysts, free enzymes, or agro-food wastes (Bell et al., 2021).

An example of biocatalysis in the preparation of the chalcone scaffold is the one reported by Tamuli *et al.*, in which the use of fruit peel ash, as a green, easily available, and biodegradable catalyst for the Claisen-Schmidt condensation reaction allowed

the formation of various chalcones and flavone derivatives. This reaction protocol can be carried out at room temperature with a reaction time that ranges from 10 min to 1 h, more importantly, is the possibility of carrying out the reaction with the use of green solvents or neat (Tamuli et al., 2020).

Żyszka-Haberecht *et al.* tested the introduction of methoxylated and methylated derivatives of 2'-hydroxychalcone in a culture of halophilic and freshwater cyanobacteria to verify the conditions of cells to the exposure of these molecules and the reactions occurring within the organism. They determined that the methoxylated chalcone derivatives were converted into the corresponding dihydroderivatives as the only product (Figure 14A); instead, the methylated starting compounds gave dihydro- and hydroxy-, also ethoxy derivatives, highlighting how the methyl group can affect these biotransformations (Żyszka-Haberecht et al., 2019).

The ene-reductase (ER) enzyme is used to obtain pure enantiomers using asymmetric bioreduction of activated C=C double bonds when the stereogenic center is produced.

Magallanes-Noguera and co-workers tried to expand the applications of ene-reductase enzymes, studying three axenic plant tissue cultures. *Tessaria absinthioides calli* demonstrated to have high selectivity for the C=C double bonds, *Medicago sativa* and *Capsicum annuum* were capable of hydrogenating also the carbonyl group (Magallanes-Noguera et al., 2017). Non-Conventional Yeasts (NCYs) were recently proven to express ER activities, thanks to the presence of cofactor-recycling systems for NAD(P)H useful for their cell metabolism. These ER activities can be exploited for whole-cells biotransformations in NCYs and have proven to be a cheap and useful alternative to purified enzymes to reduce the α,β -unsaturated chalcones. Dihydrochalcones were obtained from corresponding chalcones using a number of NCYs, such *Cyberlindnera amylophila*, *Kazachstania spencerorum*, *Naganishia diffluens*, *Kluyveromyces lactis*, among others, as reported by Filippucci et al. From the latter study, several lyophilized NCYs turned out as great alternatives with good reproducibility bioconversions, low deviations and high yields were also obtained (Filippucci et al., 2020).

Different biotransformation reactions can be achieved by *A. niger*, including hydroxylation, hydrogenation, epoxidation, hydrolysis, reduction, cyclization and alkylation, depending on the starting materials and the reaction conditions (Figure 14B). (Mohamed et al., 2022). Through the Sequence-Structure-Function-Evolution (SSFE) strategy the research group of Meinert and coworkers discovered 66 novel bacterial chalcone isomerase enzymes (CHIs) using the GenBank database. These enzymes have been investigated because they can be used as a sustainable synthetic route to obtain (S)-flavones starting from different hydroxylated and methoxylated (S)-chalcones (Figure 14C) (Meinert et al., 2021).

6.1 Artificial intelligence to design chalcone derivatives

Due to their broad spectrum of biological activities and therapeutic potential applications, the generation of focused libraries based on the chalcone scaffold related to different drug targets is a challenging task. To this end, in the new era of drug discovery, computational approaches are highly valuable, and not dispensable also for organic chemistry applications, thanks to the improvements in computing capacity, algorithms, and data availability. In fact, in silico methods based on AI could assist the synthesis of *ad hoc* compounds saving time, and money, and preventing damage to the environment (de Almeida et al., 2019; Jiménez-Luna et al., 2021). Considering the growing interest in the chalcone structural core, AI methods have been applied to prioritize derivatives to be synthesized, and here we report some successful approaches in this field of chalcones and derivatization products.

In the field of anti-infective agents, some studies have exploited AI to select and prioritize chalcone scaffolds. Gomes and coworkers employed these scaffolds to develop antitubercular agents. In particular, they developed a computational tool using matched molecular pair analysis (MMPA), starting from 604 chalcone derivatives with inhibition data against *Mycobacterium tuberculosis* strain H37Rv, for establishing and validating binary QSAR models. Fifteen different binary QSAR models were developed using several key descriptors such as MACCS, AtomPairs, Morgan, FeatMorgan, and Avalon fingerprints combined with machine learning methods (SVM, gradient boosting machine (GBM), and random forest (RF)). After that, they united all these models in a consensus ensemble model with significant statistical parameters (CCR = 0.77; Kappa = 0.53; Se = 0.79; Sp = 0.74; Coverage = 1.00), that was used in a screening of chalcone-based dataset, prioritizing 33 compounds for the synthesis. The synthesized compounds were evaluated for their antitubercular activity. Among them, 10 heteroaryl chalcone derivatives were found to exhibit nanomolar activities against replicating mycobacteria, low micromolar activity against nonreplicating bacteria, and nanomolar and micromolar activity against rifampicin- and isoniazid-resistant strains (Gomes et al., 2017b). The same research group, adopting a different computer-based approach, prioritized some compounds for the synthesis with potential anti-leishmanial activity. Starting from a chalcone-based library previously designed, they developed a target fishing protocol to identify possible activities against some leishmania drug targets. Using this computational protocol, nine most promising compounds and three potentially inactive compounds were experimentally evaluated against *Leishmania infantum* amastigotes and mammalian cells. Four synthesized compounds exhibited EC₅₀ in the micromolar range, potentially acting as procathepsin L inhibitors. Furthermore, two chalcone-based derivatives, LabMol-65 and LabMol-73, showed low cytotoxicity and high selectivity toward Vero cells (Gomes et al., 2017a). Le and coworkers used a designed library containing chalcone-based molecules to identify, using ligand- and structure-based methods, possible molecules able to inhibit efflux pumps such as P-glycoprotein and NorA. In particular, by using machine learning techniques, they implemented a computational model using a total of 184 MOE 2D descriptors and 1,444 PaDEL 1D and 2D descriptors representing 63 different types of molecular properties, along with 166 MACCS (Molecular ACCess System) fingerprints, 881 PubChem fingerprints, and 307 substructure fingerprints to feature the compounds for the subsequent construction of classification, regression, and cognitive map models, respectively. Successively, molecular docking studies employing the 3D structures of the efflux pumps provided the most performing compounds to synthesize. Based on this computer-based analysis, the authors identified four compounds (F29, F88, F90, and F91) potentially able to inhibit the selected efflux

pumps. After the synthesis, the authors performed the validation of the identified hit compounds by *in vitro* tests, showing that F88 and F90 showed inhibitory potency against both transporters, with effectiveness against different *Staphylococcus aureus* strains overexpressing NorA and resistant to ciprofloxacin (Le et al., 2022).

Dong and collaborators described the synthesis of five chalcone-based derivatives endowed with a vasorelaxant profile using AI-based methods such as the support vector machine (SVM). This technique was used to generate a robust classification model employing 111 vasodilators and 232 non-vasodilators. The developed computational tool showed predictive accuracy of 93.0, 82.6, and 89.5% considering the training set, the test set and a validation set, respectively. Accordingly, they used the model for exploring the structure-activity relationship (SAR), identifying five promising chalcone-based derivatives classified as active as vasorelaxants. The selected target compounds were synthesized and evaluated for their vasorelaxant activity. Gratifyingly, all compounds showed a vasorelaxant profile in agreement with the prediction obtained employing the AI-based model (Dong et al., 2009).

Hwang and collaborators applied a computational protocol, mainly based on QSAR techniques and molecular docking, to perform a field-based rational design to synthesize a focused library of histone acetyltransferase inhibitor (HAT). In particular, starting from a previously developed HAT inhibitor, applying the *in silico* protocol, they found that the replacement of a moiety of the original inhibitor with a chalcone core improved the *in silico* performance of the conceived inhibitors. Accordingly, they synthesized some chalcone-based derivatives and among them, one compound showed the best inhibitory profile against p300 HAT in the submicromolar range. Because of the significant inhibitory potency, they performed a preliminary characterization of this chalcone derivative as an anti-fibrotic agent in both TGF- β 1-stimulated lung fibroblasts and bleomycin-induced *in vivo* lung fibrosis mice. Delightfully, based on the obtained findings, the chalcone derivative should represent a good starting point for developing anti-fibrotic drugs (Hwang et al., 2020).

7 Conclusion

In the earlier phases of drug discovery, the hit and lead optimization cycles are extremely important and need to be accomplished in a timely fashion and in a highly efficient way in order to explore ample chemical space around selected scaffolds and/or privileged structures. For these and other reasons, metal-based C–C and C–X formation reactions represent a typical toolkit for medicinal chemists since the last 20 years. However, with the strong need of a paradigm shift toward the development of greener and more sustainable

toolboxes, medicinal chemists are facing new challenges and bottlenecks in chemistry. Therefore, it is important to widen the range of green chemistry tools that could be useful for the preparation of biologically relevant structures. In this regard, seminal and recent literature reports prove that a growing interest is taking place in the development of sustainable chemistry applied to the chalcone scaffold. In particular, in the last few years, chalcones have been increasingly used as starting materials for further transformations to afford novel heterocyclic scaffolds endowed with potentially interesting biological activities and contributing to increasing the sustainable access to diverse scaffolds. Flow chemistry and biocatalysis are the most interesting techniques so far developed and show great potential for chalcones preparation and derivatization, but also photochemistry, despite some limitations such formation of complex mixtures or standardization of the reaction conditions could be a powerful technique that should be more in-depth investigated. Finally, the potential of AI for prioritizing compounds for the synthesis is another important aspect and from the examples reported in this review and considering the improvements that are expected in computational methods in the next future, we can anticipate that the *in silico* techniques will be necessary also for guiding the synthesis of focused libraries as in the presented cases of chalcone-based compounds. This will speed up the research on drug discovery, paying attention to the environment, reducing the experimental need.

Author contributions

All authors listed have made a substantial, direct, and intellectual contribution to the work and approved it for publication.

Conflict of interest

The authors declare that the research was conducted in the absence of any commercial or financial relationships that could be construed as a potential conflict of interest.

Publisher's note

All claims expressed in this article are solely those of the authors and do not necessarily represent those of their affiliated organizations, or those of the publisher, the editors and the reviewers. Any product that may be evaluated in this article, or claim that may be made by its manufacturer, is not guaranteed or endorsed by the publisher.

References

- Adiyala, P. R., Jang, S., Vishwakarma, N. K., Hwang, Y.-H., and Kim, D.-P. (2020). Continuous-flow photo-induced decarboxylative annulative access to fused imidazole derivatives via a microreactor containing immobilized ruthenium. *Green Chem.* 22, 1565–1571. doi:10.1039/c9gc03496j
- Adole, V. A., Jagdale, B. S., Pawar, T. B., and Sagane, A. A. (2020). Ultrasound promoted stereoselective synthesis of 2, 3-dihydrobenzofuran appended chalcones at ambient temperature. *S. Afr. J. Chem.* 73, 35–43. doi:10.17159/0379-4350/2020/v73a6
- Aegurla, B., and Peddinti, R. K. (2018). Metal-free sulfonylation of α , β -conjugated systems by using sulfonyl hydrazides. *Asian J. Org. Chem.* 7, 946–954. doi:10.1002/ajoc.201700696
- Ahmed, E. A., Soliman, A. M. M., Ali, A. M., and Ali El-Remaily, M. A. E. A. A. (2021). Boosting the catalytic performance of zinc linked amino acid complex as an eco-friendly for synthesis of novel pyrimidines in aqueous medium. *Appl. Organomet. Chem.* 35, e6197. doi:10.1002/aoc.6197
- Antony, J., Rappai, J. P., Ramakrishnan, K., and Natarajan, R. (2021). Aldonitrones as aldehyde surrogates in solvent free synthesis of chalcones under mechanochemical activation. *Results Chem.* 3, 100224. doi:10.1016/j.rechem.2021.100224
- Arafa, W. A. A. (2018). Sustainable catalytic process with a high eco-scale score for the synthesis of novel series of bischalcones through claisen-schmidt condensation. *J. Heterocycl. Chem.* 55, 456–464. doi:10.1002/jhet.3063
- Bahekar, S. P., Agrawal, N. R., Sarode, P. B., Agrawal, A. R., and Chandak, H. S. (2017). L-proline nitrate: An amino acid ionic liquid for green and efficient conjugate addition of thiols to sulfonamide chalcones. *ChemistrySelect* 2, 9326–9329. doi:10.1002/slct.201701891
- Bahrami, K., Khodaei, M. M., Batooei, N., Hosseinzadeh, N., and Foroumadi, A. (2019). Hexyltriphenylphosphonium bromide as an absolutely chemoselective ionic liquid catalyst in the three-component reaction of aryl aldehydes, acetophenones and malononitrile. *ChemistrySelect* 4, 6190–6193. doi:10.1002/slct.201901076
- Balyan, S., Sharma, R., and Lal, J. (2020). Microwave-assisted, efficient and eco-friendly synthesis of novel 3H-Benzo[b] [1, 4]diazepine derivatives using basic alumina as a reusable catalyst. *Chem. Afr.* 3, 35–44. doi:10.1007/s42250-019-00110-w
- Bell, E. L., Finnigan, W., France, S. P., Hepworth, L. J., Lovelock, S. L., Hayes, M. A., et al. (2021). Biocatalysis. *Nat. Rev. Methods Prim.* 1, 46–21. doi:10.1038/s43586-021-00044-z
- Carullo, G., Governa, P., Leo, A., Gallelli, L., Citraro, R., Cione, E., et al. (2019). Quercetin-3-Oleate contributes to skin wound healing targeting FFA1/GPR40. *ChemistrySelect* 4 (29), 8429–8433. doi:10.1002/slct.201902572
- Carullo, G., Mazzotta, S., Koch, A., Hartmann, K. M., Friedrich, O., Gilbert, D. F., et al. (2020). New oleoyl hybrids of natural antioxidants: Synthesis and *in vitro* evaluation as inducers of apoptosis in colorectal cancer cells. *Antioxidants* 9, 1077. doi:10.3390/antiox9111077
- Chan, C.-K., Lai, C.-Y., and Wang, C.-C. (2020). Environmentally friendly nafion-mediated friedlander quinoline synthesis under microwave irradiation: Application to one-pot synthesis of substituted quinolinyl chalcones. *Synth. (Stuttg)* 52, 1779–1794. doi:10.1055/s-0039-1690088
- Chaudhari, P. P., and Rajput, S. S. (2018). Clean synthesis and antimicrobial interpretation of azo (dipyrano) and bis- chalcones derivatives from n-phenyl pyrrolidine-2, 5-dione and n-phenyl piperidine-2, 6-dione. *Heterocycl. Lett.* 8, 133–144.
- Chen, Z., Xue, F., Zhang, Y., Jin, W., Wang, B., Xia, Y., et al. (2022). Visible-light-promoted [3 + 2] cyclization of chalcones with 2-mercaptobenzimidazoles: A protocol for the synthesis of imidazo[2, 1- b]thiazoles. *Org. Lett.* 24, 3149–3154. doi:10.1021/acs.orglett.2c00867
- Cho, S., Kim, S., Jin, Z., Yang, H., Han, D., Baek, N. I., et al. (2011). Isoliquiritigenin, a chalcone compound, is a positive allosteric modulator of GABA A receptors and shows hypnotic effects. *Biochem. Biophys. Res. Commun.* 413, 637–642. doi:10.1016/j.bbrc.2011.09.026
- Cuellar, J. E., Quiñones, W., Robledo, S., Gil, J., and Durango, D. (2022). Coumaro-chalcones synthesized under solvent-free conditions as potential agents against malaria, leishmania and trypanosomiasis. *Heliyon* 8, e08939. doi:10.1016/j.heliyon.2022.e08939
- Das, S., Porashar, B., Saikia, S., and Borah, R. (2020). Bronsted acidic ionic liquids catalysed sequential michael-like addition of indole with chalcones via claisen-schmidt condensation. *ChemistrySelect* 5, 3041–3047. doi:10.1002/slct.201904851
- Dasari, G. K., Sunkara, S., and Gadupudi, P. C. R. (2020). Green and ecofriendly synthesis of indole-condensed benzimidazole chalcones in water and their antimicrobial evaluations. *J. Heterocycl. Chem.* 57, 1201–1210. doi:10.1002/jhet.3856
- de Almeida, A. F., Moreira, R., and Rodrigues, T. (2019). Synthetic organic chemistry driven by artificial intelligence. *Nat. Rev. Chem.* 3, 589–604. doi:10.1038/s41570-019-0124-0
- de Aquino, T. F. B., Seidel, J. P., de Oliveira, D. H., do Nascimento, J. E. R., Alves, D., Perin, G., et al. (2018). Copper-catalyzed synthesis of 1, 3, 5-triaryl-4-(organylselanyl)-1H-pyrazoles by one-pot multicomponent reactions. *Tetrahedron Lett.* 59, 4090–4095. doi:10.1016/j.tetlet.2018.10.008
- De La Hoz, A., Díaz-Ortiz, A., and Prieto, P. (2016). “Microwave-assisted green organic synthesis,” in *Alternative energy sources for green chemistry* (The Royal Society of Chemistry). doi:10.1039/9781782623632-00001
- de Souza, J. M., Galaverna, R., de Souza, A. A. N., Brocksom, T. J., Pastre, J. C., de Souza, R. O. M. A., et al. (2018). Impact of continuous flow chemistry in the synthesis of natural products and active pharmaceutical ingredients. *An. Acad. Bras. Cienc.* 90, 1131–1174. doi:10.1590/0001-3765201820170778
- Devkate, C. G., Kola, S. S., Gaikwad, D. D., and Siddique, M. I. M. (2018). Ultrasound promoted one pot synthesis of 1, 5-benzothiazepines using polyethylene glycol (PEG-400). *Int. Res. J. Pharm.* 9, 182–185. doi:10.7897/2230-8407.0911280
- Dhadda, S., Goswami, P. G., and Sharma, H. (2022). “Green synthesis of chalcone derivatives using chalcones as precursor,” in *Green chemistry - new perspectives* (London: IntechOpen). doi:10.5772/intechopen.103959
- Dong, X., Chen, J., Jiang, C., Liu, T., and Hu, Y. (2009). Design, synthesis, and biological evaluation of prenylated chalcones as vasorelaxant agents. *Arch. Pharm. Wein.* 342, 428–432. doi:10.1002/ardp.200800229
- Draye, M., Chatel, G., and Duwald, R. (2020). Ultrasound for drug synthesis: A green approach. *Pharmaceuticals* 13, 23. doi:10.3390/ph13020023
- Duran, N., Polat, M. F., Aktas, D. A., Alagoz, M. A., Ay, E., Cimen, F., et al. (2021). New chalcone derivatives as effective against SARS-CoV-2 agent. *Int. J. Clin. Pract.* 75 (12), e14846. doi:10.1111/ijcp.14846
- Filippucci, S., Tasselli, G., Kenza Labbani, F.-Z., Turchetti, B., Cramarossa, M. R., Buzzini, P., et al. (2020). Non-conventional Yeasts as sources of ene-reductases for the bioreduction of chalcones. *Fermentation* 6, 29. doi:10.3390/fermentation6010029
- Gomes, C., Vinagreiro, C. S., Damas, L., Aquino, G., Quaresma, J., Chaves, C., et al. (2020). Advanced mechanochemistry device for sustainable synthetic processes. *ACS Omega* 5, 10868–10877. doi:10.1021/acsomega.0c00521
- Gomes, M. N., Alcántara, L. M., Neves, B. J., Melo-Filho, C. C., Freitas-Junior, L. H., Moraes, C. B., et al. (2017a). Computer-aided discovery of two novel chalcone-like compounds active and selective against Leishmania infantum. *Bioorg. Med. Chem. Lett.* 27, 2459–2464. doi:10.1016/j.bmcl.2017.04.010
- Gomes, M. N., Braga, R. C., Grzelak, E. M., Neves, B. J., Muratov, E., Ma, R., et al. (2017b). QSAR-driven design, synthesis and discovery of potent chalcone derivatives with antitubercular activity. *Eur. J. Med. Chem.* 137, 126–138. doi:10.1016/j.ejmech.2017.05.026
- Gomes, M. N., Muratov, E. N., Pereira, M., Peixoto, J. C., Rosseto, L. P., Cravo, P. V. L., et al. (2017c). Chalcone derivatives: Promising starting points for drug design. *Molecules* 22, 1210. doi:10.3390/molecules22081210
- Gupta, S., Ameta, C., Ameta, R., and Punjabi, P. B. (2020). “Click chemistry: A tool for green chemical organic synthesis,” in *Green sustainable process for chemical and environmental engineering and science* (Elsevier), 13–48. doi:10.1016/B978-0-12-819539-0.00002-6
- Hajipour, A. R., and Khorsandi, Z. (2017). Application of immobilized proline on CNTs and proline ionic liquid as novel organocatalysts in the synthesis of 2-amino-4H-pyran derivatives: A comparative study between their catalytic activities. *ChemistrySelect* 2, 8976–8982. doi:10.1002/slct.201700847
- Higuchi, K., Watanabe, T., Tanigawa, T., Tominaga, K., Fujiwara, Y., and Arakawa, T. (2010). Sofalcone, a gastroprotective drug, promotes gastric ulcer healing following eradication therapy for *Helicobacter pylori*: A randomized controlled comparative trial with cimetidine, an H2-receptor antagonist. *J. Gastroenterol. Hepatol.* 25, 155–160. doi:10.1111/j.1440-1746.2010.06232.x
- Hwang, S. Y., Park, S. Y., Hong, J. Y., Lee, S. Y., Shin, J. H., Na, Y., et al. (2020). Field-based rational design of p300 histone acetyltransferase inhibitor and systematic evaluation as an anti-fibrotic agent. *Chem. Commun.* 56, 9795–9798. doi:10.1039/d0cc03553j
- Iwamura, C., Shinoda, K., Yoshimura, M., Watanabe, Y., Obata, A., and Nakayama, T. (2010). Naringenin chalcone suppresses allergic asthma by inhibiting the type-2 function of CD4 T cells. *Allergol. Int.* 59, 67–73. doi:10.2332/allergolint.09-OA-0118

- Jadhav, N. L., Pandit, A. B., and Pinjari, D. V. (2017). Green approach for the synthesis of chalcone (3-(4-fluorophenyl)-1-(4-methoxyphenyl)prop-2-en-1-one) using concentrated solar radiation. *Sol. Energy* 147, 232–239. doi:10.1016/j.solener.2017.03.047
- Janković, T., Turković, N., Kotur-Stevuljević, J., Vujić, Z., and Ivković, B. (2020). Differences in antioxidant potential of chalcones in human serum: *In vitro* study. *Chem. Biol. Interact.* 324, 109084. doi:10.1016/j.cbi.2020.109084
- Jasril, J., Teruna, H. Y., Aisyah, A., Nurlaili, N., and Hendra, R. (2019). Microwave assisted synthesis and evaluation of toxicity and antioxidant activity of pyrazoline derivatives. *Indones. J. Chem.* 19, 583–591. doi:10.22146/ijc.34285
- Jiménez-Luna, J., Grisoni, F., Weskamp, N., and Schneider, G. (2021). Artificial intelligence in drug discovery: Recent advances and future perspectives. *Expert Opin. Drug Discov.* 16, 949–959. doi:10.1080/17460441.2021.1909567
- Kakade, G. K., and Vedpathak, S. G. (2020). Ultrasound assisted green synthesis of 2-furan-2-yl-4H-chromen-4-ones from chalcones. *Int. J. Curr. Pharm. Res.* 12, 84–86. doi:10.22159/ijcpr.2020v12i3.38312
- Kalluraya, B., Mallya, S., and Kumar K, A. (2018). Microwave assisted neat synthesis of spiropyrrolidine library. *J. Heterocycl. Chem.* 55, 2075–2081. doi:10.1002/jhet.3247
- Kannan, D., Naveen, S., Jagadeesan, G., Lokanath, N. K., and Thennarasu, S. (2019). Ultrasonic cavitation facilitates rapid synthesis of trisubstituted pyrazole scaffolds through Michael addition/domino cyclization. *ChemistrySelect* 4, 9807–9810. doi:10.1002/slct.201902126
- Karimi-Jaberi, Z., Masoudi, B., Rahmani, A., and Alborzi, K. (2020). Triethylammonium hydrogen sulfate [Et₃NH][HSO₄] as an efficient ionic liquid catalyst for the synthesis of coumarin derivatives. *Polycycl. Aromat. Compd.* 40, 99–107. doi:10.1080/10406638.2017.1363061
- Kaur, H., Singh, R., and Kant, R. (2022). Synthesis, molecular docking, and antitubercular evaluation of triazole–chalcone conjugates. *Russ. J. Org. Chem.* 58, 518–525. doi:10.1134/S107042802204008X
- Khalili, D., Lavian, S., and Moayyed, M. (2020). Graphene oxide as a catalyst for one-pot sequential aldol coupling/aza-Michael addition of amines to chalcones through *in situ* generation of Michael acceptors under neat conditions. *Tetrahedron Lett.* 61, 151470. doi:10.1016/j.tetlet.2019.151470
- Kothandapani, J., Megarajan, S., Ayaz Ahmed, K. B., Priyanka, M., Anbazhagan, V., and Selva Ganesan, S. (2017). Stearyl MethoxyPEGglycol succinate-A designer micellar medium for diverse aniline derivatives synthesis. *ACS Sustain. Chem. Eng.* 5, 5740–5745. doi:10.1021/acssuschemeng.7b00317
- Kumar, K. S., Siddaiah, V., Lilakar, J. D., and Ganesh, A. (2020). An efficient continuous-flow synthesis and evaluation of antimicrobial activity of novel 1, 2, 3-Triazole-Furan hybrid chalcone derivatives. *Chem. Data Collect.* 28, 100457. doi:10.1016/j.cdc.2020.100457
- La Sorella, G., Strukul, G., and Scarso, A. (2015). Recent advances in catalysis in micellar media. *Green Chem.* 17, 644–683. doi:10.1039/C4GC01368A
- Le, M. T., Trinh, D. T. T., Ngo, T. Du, Tran-Nguyen, V. K., Nguyen, D. N., Hoang, T., et al. (2022). Chalcone derivatives as potential inhibitors of P-glycoprotein and NorA: An *in silico* and *in vitro* study. *Biomed. Res. Int.* 2022, 1–9. doi:10.1155/2022/9982453
- Li, J., Li, J., Ji, X., Liu, Q., Chen, L., Huang, Y., et al. (2021). Transition metal-free synthesis of substituted isothiazoles via three-component annulation of alkynes, xanthate and NH₄I. *Adv. Synth. Catal.* 363, 1059–1068. doi:10.1002/adsc.202001179
- Li, Z., Zhao, H., Han, H., Liu, Y., Song, J., Guo, W., et al. (2017). Graphene-supported ZnO nanoparticles: An efficient heterogeneous catalyst for the Claisen-Schmidt condensation reaction without additional base. *Tetrahedron Lett.* 58, 3984–3988. doi:10.1016/j.tetlet.2017.09.011
- Magallanes-Noguera, C., Cecati, F. M., Mascotti, M. L., Reta, G. F., Agostini, E., Orden, A. A., et al. (2017). Plant tissue cultures as sources of new ene- and ketoreductase activities. *J. Biotechnol.* 251, 14–20. doi:10.1016/j.jbiotec.2017.03.023
- Mahapatra, D., Bharti, S., and Asati, V. (2017). Chalcone derivatives: Anti-inflammatory potential and molecular targets perspectives. *Curr. Top. Med. Chem.* 17, 3146–3169. doi:10.2174/1568026617666170914160446
- Mahapatra, D. K., Bharti, S. K., and Asati, V. (2015). Chalcone scaffolds as anti-infective agents: Structural and molecular target perspectives. *Eur. J. Med. Chem.* 101, 496–524. doi:10.1016/j.ejmech.2015.06.052
- Mahato, S., Santra, S., Chatterjee, R., Zyryanov, G. V., Hajra, A., and Majee, A. (2017). Bronsted acidic ionic liquid-catalyzed tandem reaction: An efficient approach towards regioselective synthesis of pyrano[3, 2-c]coumarins under solvent-free conditions bearing lower E-factors. *Green Chem.* 19, 3282–3295. doi:10.1039/c7gc01158j
- Mahmoodi, N. O., and Ghodsi, S. (2017). Thiazolyl-pyrazole-biscoumarin synthesis and evaluation of their antibacterial and antioxidant activities. *Res. Chem. Intermed.* 43, 661–678. doi:10.1007/s11164-016-2644-2
- Mahurkar, S. S., Makone, S. S., and More, R. A. (2019). An efficient and recyclable catalyst for synthesis of 1, 3-diphenyl-3-(phenyl thio). *Chem. Biol. Interface* 9, 277–284.
- Mazzotta, S., Governa, P., Borgonetti, V., Marcolongo, P., Nanni, C., Gamberucci, A., et al. (2021). Pinocembrin and its linolenol ester derivative induce wound healing activity in HaCaT cell line potentially involving a GPR120/FFA4 mediated pathway. *Bioorg. Chem.* 108, 104657. doi:10.1016/j.bioorg.2021.104657
- Meinert, H., Yi, D., Zirpel, B., Schuiten, E., Geißler, T., Gross, E., et al. (2021). Discovery of novel bacterial chalcone isomerases by a sequence-structure-function-evolution strategy for enzymatic synthesis of (S)-Flavanones. *Angew. Chem. Int. Ed.* 60, 16874–16879. doi:10.1002/anie.202107182
- Mishra, A., Rai, P., Pandey, Y. K., Singh, J., and Singh, J. (2017). An eco-sustainable synthetic approach for 4, 5-dihydro-1H-pyrazoles via DBU catalysis in micellar medium. *ChemistrySelect* 2, 10979–10983. doi:10.1002/slct.201702400
- Mohamed, T. A., Ali, S. K., Elshamy, A. I., Saleh, I. A., Ibrahim, M. A. A., Atia, M. A. M., et al. (2022). Plant cell cultures: An enzymatic tool for polyphenolic and flavonoid transformations. *Phytomedicine* 100, 154019. doi:10.1016/j.phymed.2022.154019
- Moore, J. C., Howie, R. A., Bourne, S. L., Jenkins, G. N., Licence, P., Poliakoff, M., et al. (2019). *In situ* sulfidation of Pd/C: A straightforward method for chemoselective conjugate reduction by continuous hydrogenation. *ACS Sustain. Chem. Eng.* 7, 16814–16819. doi:10.1021/acssuschemeng.9b04347
- Mubarak, S., Zia-Ur-Rehman, M., Jamil, N., Zaheer, M., Arshad, M. N., and Asiri, A. M. (2019). Environment friendly synthesis of N'-(1, 3-diphenylallylidene)-1-ethyl-7-methyl-4-oxo-1, 4-dihydro-1, 8-naphthyridine-3-carbohydrazides: Crystal structure and their anti-oxidant potential. *Chem. Pharm. Bull.* 67, 1191–1200. doi:10.1248/cpb.c19-00478
- Murugesan, A., Gengan, R. M., and Lin, C.-H. (2017a). Efficient synthesis of ethyl-piperazinyl quinolinyl-(E)-chalcone derivatives via Claisen-Schmidt reaction by using TiO₂-BPTETSA catalyst. *J. Taiwan Inst. Chem. Eng.* 80, 852–866. doi:10.1016/j.jtice.2017.07.014
- Murugesan, A., Gengan, R. M., Rajamanikandan, R., Ilanchelian, M., and Lin, C.-H. (2017b). One-pot synthesis of Claisen-Schmidt reaction through (E)-chalcone derivatives: Spectral studies in human serum albumin protein binding and molecular docking investigation. *Synth. Commun.* 47, 1884–1904. doi:10.1080/00397911.2017.1355466
- Muthuvel, I., Thirunaranayan, G., Thangaraj, V., Sundaramurthy, N., Rajalakshmi, S., and Usha, V. (2021). Study of catalytic activity of Zn₃(PO₄)₂ on the synthesis of some pyrenyl enones. *Mater. Today Proc.* 43, 2203–2207. doi:10.1016/j.matpr.2020.12.169
- Nakamura, A., Tanaka, S., Imamiya, A., Takane, R., Ohta, C., Fujimura, K., et al. (2017). Synthesis of 3-acylindoles by oxidative rearrangement of 2-aminochalcones using a hypervalent iodine reagent and cyclization sequence. *Org. Biomol. Chem.* 15, 6702–6705. doi:10.1039/c7ob01536d
- Ouyang, Y., Li, J., Chen, X., Fu, X., Sun, S., and Wu, Q. (2021). Chalcone derivatives: Role in anticancer therapy. *Biomolecules* 11, 894. doi:10.3390/biom11060894
- Patel, T., Gaikwad, R., Jain, K., Ganesh, R., Bobde, Y., Ghosh, B., et al. (2019). First report on 3-(3-oxoaryl) indole derivatives as anticancer agents: Microwave assisted synthesis, *in vitro* screening and molecular docking studies. *ChemistrySelect* 4, 4478–4482. doi:10.1002/slct.201900088
- Pereira, D., Gonçalves, C., Martins, B. T., Palmeira, A., Vasconcelos, V., Pinto, M., et al. (2021). Flavonoid glycosides with a triazole moiety for marine antifouling applications: Synthesis and biological activity evaluation. *Mar. Drugs* 19, 5. doi:10.3390/md19010005
- Pogaku, V., Krishna, V. S., Sriram, D., Rangan, K., and Basavoju, S. (2019). Ultrasonication-ionic liquid synergy for the synthesis of new potent anti-tuberculosis 1, 2, 4-triazol-1-yl-pyrazole based spirooxindolopyrrolizidines. *Bioorg. Med. Chem. Lett.* 29, 1682–1687. doi:10.1016/j.bmcl.2019.04.026
- Pozzetti, L., Ibba, R., Rossi, S., Tagliatela-Scafati, O., Taramelli, D., Basilio, N., et al. (2022). Total synthesis of the natural chalcone lophirone E, synthetic studies toward benzofuran and indole-based analogues, and investigation of anti-leishmanial activity. *Molecules* 27, 463. doi:10.3390/molecules27020463
- Prabhakar, M., Merry, T., Zatsu, R., Tsurho, S., and Merugu, R. (2017). Microwave-assisted fast and efficient green synthesis of 9-anthracenyl chalcones and their anti-bacterial activity. *IOSR J. Pharm.* 7, 24–32.
- Praveena, P., Sarojini, B. K., and Madan Kumar, S. (2019). Mechanochemical synthesis and characterizations of chalcone derivatives: (2E)-3-[4-(Benzyloxy)phenyl]-1-(thiophen-2-yl)prop-2-en-1-one and (2E)-3-(anthracen-9-yl)-1-(thiophen-2-yl)prop-2-en-1-one. *Chem. Data Collect.* 24, 100298. doi:10.1016/j.cdc.2019.100298

- Rahim, A., Bhuiyan, M. M. H., Matin, M. M., Ali, R., and Kabir, E. (2018). Synthesis of 2-Phenylchromen-4-one derivatives by conventional and microwave: Assisted techniques, and their antimicrobial evaluation. *Int. J. Chem. Stud.* 6, 1–4.
- Rajaguru, K., Mariappan, A., Muthusubramanian, S., and Bhuvanesh, N. (2017). Divergent reactivity of α -azidochalcones with metal β -diketonates: Tunable synthesis of substituted pyrroles and indoles. *Org. Chem. Front.* 4, 124–129. doi:10.1039/c6qo00541a
- Ranganathan, K., Kamalakannan, D., Suresh, R., Sakthinathan, S. P., Arulkumaran, R., Sundararajan, R., et al. (2020). Cu²⁺/Zeolite catalyzed aldol condensation: Greener synthesis of 4'-piperidinophenyl enones. *Mater. Today Proc.* 22, 1196–1199. doi:10.1016/j.matpr.2019.12.120
- Rehm, T. H. (2020). Flow photochemistry as a tool in organic synthesis. *Chem. Eur. J.* 26, 16952–16974. doi:10.1002/chem.202000381
- Rizk, S. A., El-Hashash, M. A., and El-Badawy, A. A. (2017). Ultrasonic and grinding aptitudes of one-pot synthesis of 5-(4-chlorophenyl)-7-(3, 4-dimethyl phenyl)-2-oxo-2H-Pyrano[2, 3-b]Pyridine derivatives as antibacterial agents. *J. Heterocycl. Chem.* 54, 2003–2011. doi:10.1002/jhet.2797
- Rocha, D. H. A., Vaz, P. A. A. M., Pinto, D. C. G. A., and Silva, A. M. S. (2019). Synthesis chalcones and their isomerization into flavanones and azaflavanones. *Methods Protoc.* 2, 70. doi:10.3390/mps2030070
- Rosa, G. P., Seca, A. M. L., Barreto, M. D. C., and Pinto, D. C. G. A. (2017). Chalcone: A valuable scaffold upgrading by green methods. *ACS Sustain. Chem. Eng.* 5, 7467–7480. doi:10.1021/acssuschemeng.7b01687
- Sahoo, B. M., Banik, B. K., MazaharunnisaRao, N. S., and Raju, B. (2019). Microwave assisted green synthesis of benzimidazole derivatives and evaluation of their anticonvulsant activity. *Curr. Microw. Chem.* 6, 23–29. doi:10.2174/2213335606666190429124745
- Sahoo, B. M., Sahoo, B., Panda, J., and Kumar, A. (2017). Microwave-induced synthesis of substituted isoxazoles as potential antimicrobial agents. *Curr. Microw. Chem.* 4, 146–151. doi:10.2174/2213335603666160926101734
- Sakirolla, R., Tadiparthi, K., Yaeghoobi, M., and Abd Rahman, N. (2018). Dicationic ionic liquid catalyzed synthesis of 1, 5-benzothiazepines. *Asian J. Chem.* 30, 107–115. doi:10.14233/ajchem.2018.20920
- Saleem, S., Nazli, Z.-H., Saleem, N., Bashir, M. S., Hussain, S., and Parveen, B. (2018). Synthesis, spectroscopy and biological studies of chalcone derived pyrimidines. *Pharma Chem.* 10, 110–117.
- Salehi, B., Quispe, C., Chamkhi, I., El Omari, N., Balahbib, A., Sharifi-Rad, J., et al. (2021). Pharmacological properties of chalcones: A review of preclinical including molecular mechanisms and clinical evidence. *Front. Pharmacol.* 11, 592654. doi:10.3389/fphar.2020.592654
- Shankaraiah, N., Sakla, A. P., Laxmikeslav, K., and Tokala, R. (2020). Reliability of click chemistry on drug discovery: A personal account. *Chem. Rec.* 20, 253–272. doi:10.1002/tcr.201900027
- Sharma, M. K., Parashar, S., Chahal, M., Lal, K., Pandya, N. U., and Om, H. (2022). Antimicrobial and *in-silico* evaluation of novel chalcone and amide-linked 1, 4-disubstituted 1, 2, 3 triazoles. *J. Mol. Struct.* 1257, 132632. doi:10.1016/j.molstruc.2022.132632
- Sharma, S. P., Vashisht, N., Kumar, S., and Kritika (2018). Ultrasound promoted green synthesis of chalcones of 3-acetyl coumarin. *Chem. Sci. Trans.* 7, 396–401. doi:10.7598/cst2018.1502
- Shetye, A. P., and Pawar, M. G. (2017). Microwave assisted synthesis of some new 1, 5-benzodiazepines from chalcones. *Pharma Chem.* 9, 50–52.
- Shntaif, A. H. (2016). Green synthesis of chalcones under microwave irradiation. *Int. J. ChemTech Res.* 9, 36–39.
- Soozani, A., Keivanloo, A., and Bakherad, M. (2017). One-pot synthesis of quinoxaline chalcones from commercially available calcium carbide through palladium-catalyzed coupling reactions. *ChemistrySelect* 2, 9701–9705. doi:10.1002/slct.201701803
- Sydes, M. (2014). One-pot reactions: A step towards greener chemistry. *Curr. Green Chem.* 1, 216–226. doi:10.2174/2213346101666140221225404
- Tamuli, K. J., Sahoo, R. K., and Bordoloi, M. (2020). Biocatalytic green alternative to existing hazardous reaction media: Synthesis of chalcone and flavone derivatives via the Claisen-Schmidt reaction at room temperature. *New J. Chem.* 44, 20956–20965. doi:10.1039/d0nj03839c
- Tareh, B. (2022). Synthesis, pharmacological activity and uses of chalcone compounds: A review. *Sci. J. Med. Res.* 6, 43–46. doi:10.37623/sjomr.v06i21.9
- Thapa, P., Upadhyay, S. P., Suo, W. Z., Singh, V., Gurung, P., Lee, E. S., et al. (2021). Chalcone and its analogs: Therapeutic and diagnostic applications in Alzheimer's disease. *Bioorg. Chem.* 108, 104681. doi:10.1016/j.bioorg.2021.104681
- Tran, C. T. H., Tran, Q. D., Ly, D., Nguyen, T. T., Nguyen, K. X., Nguyen, T. T., et al. (2022). A one-pot synthesis of disubstituted thiazoles from chalcone C-H bonds, elemental sulfur, and Glycine ethyl ester. *Synlett* 33, 555–558. doi:10.1055/s-0041-1737899
- Tripathi, S., Kapoor, R., and Yadav, L. D. S. (2018). Visible light activated radical denitrative benzylation of β -nitrostyrenes: A photocatalytic approach to chalcones. *Adv. Synth. Catal.* 360, 1407–1413. doi:10.1002/adsc.201701559
- Tupare, S. D., and Pawar, R. P. (2020). Synthesis, characterization and biological evaluation of newer chalcones by microwave irradiation. *Chem. J.* 7, 150–162.
- Villena, J., Montenegro, I., Said, B., Werner, E., Flores, S., and Madrid, A. (2021). Ultrasound assisted synthesis and cytotoxicity evaluation of known 2', 4'-dihydroxychalcone derivatives against cancer cell lines. *Food Chem. Toxicol.* 148, 111969. doi:10.1016/j.fct.2021.111969
- Wei, Z., and Cue, B. W. (2018). *Green techniques for organic synthesis and medicinal chemistry*. Wiley.
- Weng, M.-Y., Xu, H., Chen, H., and Zhang, Z. (2021). Liquid-assisted mechanosynthesis of trans-2, 3-dihydropyrroles from chalcones and enamines. *Heterocycles* 102, 114–121. doi:10.3987/com-20-14365
- Wilhelm, A., Bonnet, S. L., Twigg, L., Rarova, L., Stenclova, T., Visser, H. G., et al. (2022). Synthesis, characterization and cytotoxicity evaluation of chalcone derivatives. *J. Mol. Struct.* 1251, 132001. doi:10.1016/j.molstruc.2021.132001
- Yadav, N., Yadav, V. B., Ansari, M. D., Sagir, H., Verma, A., and Siddiqui, I. R. (2019). Catalyst-free synthesis of 2, 3-dihydro-1, 5-benzothiazepines in a renewable and biodegradable reaction medium. *New J. Chem.* 43, 7011–7014. doi:10.1039/c8nj05611k
- Yadav, P., Lal, K., Kumar, A., Guru, S. K., Jaglan, S., and Bhushan, S. (2017). Green synthesis and anticancer potential of chalcone linked-1, 2, 3-triazoles. *Eur. J. Med. Chem.* 126, 944–953. doi:10.1016/j.ejmech.2016.11.030
- Yadav, P., Lal, K., Kumar, L., Kumar, A., Kumar, A., Paul, A. K., et al. (2018). Synthesis, crystal structure and antimicrobial potential of some fluorinated chalcone-1, 2, 3-triazole conjugates. *Eur. J. Med. Chem.* 155, 263–274. doi:10.1016/j.ejmech.2018.05.055
- Yamamoto, T., Yoshimura, M., Yamaguchi, F., Kouchi, T., Tsuji, R., Saito, M., et al. (2004). Anti-allergic activity of naringenin chalcone from a tomato skin extract. *Biosci. Biotechnol. Biochem.* 68, 1706–1711. doi:10.1271/bbb.68.1706
- Yang, Q., Wang, R., Han, J., Li, C., Wang, T., Liang, Y., et al. (2017). Photo-induced tandem cyclization of 3-iodoflavones with electron rich five-membered heteroarenes. *RSC Adv.* 7, 43206–43211. doi:10.1039/c7ra07793a
- Zangade, S., and Patil, P. (2020). A review on solvent-free methods in organic synthesis. *Curr. Org. Chem.* 23, 2295–2318. doi:10.2174/1385272823666191016165532
- Żyszka-Haberecht, B., Poliwoda, A., and Lipok, J. (2019). 'Structural constraints in cyanobacteria-mediated whole-cell biotransformation of methoxylated and methylated derivatives of 2'-hydroxychalcone. *J. Biotechnol.* 293, 36–46. doi:10.1016/j.jbiotec.2019.01.005

Frontiers in Chemistry

Explores all fields of chemical science across the periodic table

Advances our understanding of how atoms, ions, and molecules come together and come apart. It explores the role of chemistry in our everyday lives - from electronic devices to health and wellbeing.

Discover the latest Research Topics

[See more →](#)

Frontiers

Avenue du Tribunal-Fédéral 34
1005 Lausanne, Switzerland
frontiersin.org

Contact us

+41 (0)21 510 17 00
frontiersin.org/about/contact

